The Dissertation Committee for Jorge Luis Varela Rivera certifies that

this is the approved version of the following dissertation:

DEVELOPMENT OF R AND C$_d$ FACTORS FOR THE SEISMIC

DESIGN OF AAC STRUCTURES

Committee:

_____

Richard E. Klingner, Supervisor

_____

Eric B. Becker

_____

James O. Jirsa

_____

Michael E. Kreger

_____

Sharon L. Wood

DEVELOPMENT OF R AND C_d FACTORS FOR THE SEISMIC

DESIGN OF AAC STRUCTURES

by

Jorge Luis Varela Rivera, M.E., B.S.

Dissertation

Presented to the Faculty of the Graduate School of

The University of Texas at Austin

in Partial Fulfillment

of the Requirements

for the Degree of

Doctor of Philosophy

The University of Texas at Austin

May 2003

DEDICATION

To my wife, Guadalupe, for her love, patience and support. To my daughter, Judith,

for all her love. To my parents, for their love and guidance.

ACKNOWLEDGEMENTS

DEVELOPMENT OF R AND C_d FACTORS FOR THE SEISMIC DESIGN OF AAC STRUCTURES

Publication No. _____

Jorge Luis Varela Rivera, Ph.D.

The University of Texas at Austin, 2003

Supervisor: Richard E. Klingner

The seismic force-reduction factor (R) specified in seismic design codes is intended to account for energy dissipation through inelastic deformation (ductility) and for structural over-strength. The factor (R) is based on observation of the performance of different structural systems in previous strong earthquakes, on technical justification, and on tradition. For structures of autoclaved aerated concrete (AAC), the force-reduction factor (R) and the corresponding displacement-amplification factor (C_d) must be based on laboratory test results and numerical simulation of the response of AAC structures subjected to earthquake ground motions. The proposed factors must then be verified against the observed response of AAC structures in strong earthquakes. The objectives of this dissertation were: (1) to present a general procedure for selecting values of the factors (R) and (C_d) for use in the seismic design of structures; and (2) using

that procedure, to propose preliminary values of the factors (R) and (C_d) for the seismic design of AAC shear-wall structures. The general procedure is based on comparing the predicted ductility and drift demands in AAC structures, as functions of the factors (R) and (C_d), with the ductility and drift capacities of AAC shear walls, as observed in quasi-static testing under reversed cyclic loads. Nonlinear numerical simulations are carried out using hysteretic load-displacement behavior based on test results, and using suites of natural and synthetic ground motions from different seismically active regions of the United States.

Table of Contents

List of Tables

List of Figures

CHAPTER 1
Introduction

1.1 GENERAL

The seismic design philosophy of current United States building codes allows most structures to undergo inelastic deformations in the event of strong earthquake ground motions. As a result, the design lateral strength can be lower than that required to maintain the structure in the elastic range. In the International Building Code 2000 (IBC 2000) the seismic force-reduction factor and the displacement-amplification factor are expressed as a response modification coefficient (R) and a deflection amplification factor (C_d) respectively. The factor R is used to calculate the reduced design seismic forces of a structural system, and the factor C_d to estimate the corresponding maximum displacement that is likely to occur under an earthquake representing the design seismic forces. The values of the factors R and C_d prescribed in the IBC 2000 are based on observations of the performance of different structural systems in previous strong earthquakes, on technical justification, and on tradition.

The selection of an appropriate seismic force-reduction factor (R) for a structural system is important not only to define the required lateral strength of the structure but also to predict its probable performance during a strong earthquake ground motion. As the factor R increases, the design seismic forces and the corresponding lateral strength of the structure decrease. This reduction in capacity is usually associated with an increase in the inelastic deformation demand of the structure, which is related to damage in the structure. The amount of damage to critical structural elements can define the behavior of the structure under a severe earthquake ground motion. The selection of the displacement-

amplification factor (C_d) is important to predict an appropriate value of the maximum expected displacement of the structure, which is used to limit the amount of differential movement in the structure during a strong earthquake.

For new structural systems like autoclaved aerated concrete (AAC) shear-wall structures, the seismic force-reduction factor (R) and the corresponding displacement-amplification factor (C_d) cannot be based on the observed performance of structures during previous earthquakes. Therefore, alternative means have to be found to develop R and C_d factors for this and other potential new structural systems in current United States seismic codes. That is one of the objectives of the research presented here.

The research described in this dissertation forms part of a research program supported by the Autoclaved Aerated Concrete Products Association (AACPA). The program was carried out at the Phil M. Ferguson Structural Engineering Laboratory of The University of Texas at Austin.

1.2 SCOPE OF STUDY

The goal of the research described here was to produce draft design provisions for autoclaved aerated concrete to be used in the United States, and a comprehensive technical justification for those provisions. Results of experimental and analytical studies at The University of Texas at Austin, together with studies completed at other institutions, formed the basis for design equations for different AAC elements. Values of the force-reduction factor (R) and corresponding displacement-amplification factor (C_d) for the seismic design of AAC shear wall structures in the United States were proposed as part of this study.

The experimental study at The University of Texas at Austin (UT Austin) consisted of two phases. Phase I consisted of a series of fourteen AAC shear wall

specimens with aspect ratios ranging from 0.64 (shear-dominated walls) to 3.17 (flexure-dominated walls). The specimens were designed and tested using a variety of panel and block orientations, reinforcement layouts, and axial loads. Results from those tests were used to develop design provisions for AAC shear walls and pier elements. Results of this phase also provided experimental information necessary to develop analytical models, and to define appropriate values of maximum drift ratio and displacement ductility capacities for AAC shear walls. These values, in turn, were used to select the factors R and C_d for the seismic design of AAC shear wall structures.

Phase II of the study involved testing a full-scale, two-story AAC assemblage specimen. The assemblage, consisting of two flanged AAC shear walls connected by AAC diaphragms at each level, was subjected to reversed cyclic loads. Results of the assemblage specimen were used to validate the design equations developed during Phase I, to verify the integrity of different connection details similar to those used in concrete and masonry construction, and to validate the observed behavior of the flexure-dominated specimens tested during Phase I.

1.3   OBJECTIVES OF STUDY

The objectives of the study carried out at The University of Texas at Austin were to:

- determine fundamental material properties of AAC used in the United States, including synthesis of data from other sources;

- verify basic procedures to predict the behavior of AAC shear wall specimens. This includes the shear wall capacity based on flexural cracking, web-shear cracking, flexure-shear cracking, sliding shear, crushing of the diagonal strut, and flexural behavior;

3

- determine the differences in behavior of AAC shear walls with the same overall geometry, but with different arrangements and amounts of reinforcement;

- determine the differences in behavior of AAC shear walls with the same overall geometry, reinforcement, and axial load, but with different orientations of panel and block elements;

- evaluate the behavior of different AAC flexure-dominated specimens to verify the use of AAC shear wall structures in seismic zones;

- test an assemblage specimen to verify that the walls designed to fail in flexure will actually fail in flexure, verify proposed design equations for AAC shear walls, and verify the proposed analytical models and the observed behavior of the flexure-dominated specimens;

- determine if load can be transferred through an AAC floor diaphragm, and that current connection details for conventional pre-cast concrete and masonry are applicable in AAC construction;

- define appropriate values of drift ratio and displacement ductility capacities for AAC shear walls;

- develop analytical models that represent the flexural and shear behavior of AAC shear walls under lateral loads;

- predict the performance of AAC shear wall structures subjected to earthquake ground motions;

- develop a procedure to propose values of the force-reduction factor (R) and displacement-amplification factor (C_d) for the seismic design of AAC shear wall structures in the United States; and

- synthesize data on tests on reinforced AAC panels at UT Austin and other sources to produce draft code language for those elements.

1.4   ORGANIZATION OF STUDY

The completed work is described in several references. Development of the test setup and results of tests on pilot specimens are presented in Brightman (2000). Material from that reference has been used for Chapters 1, 2, and 3 of this dissertation, with appropriate modifications to include developments since 2000. Development of general design provisions is presented in Tanner (2003). Development of the force-reduction factor (R) and a displacement-amplification factor (C_d) are presented in this dissertation. Proposed design provisions for reinforced AAC panels and a synthesis of data from the University of Alabama at Birmingham are presented in Argudo (2003). A study of low-strength AAC shear wall specimens will be presented in Cancino (2003). Table 1.1 shows the study elements done by each graduate student.

Table 1.1 Study elements done by each graduate student

Study Element	Student
development of test setup and results of tests on pilot specimens	Brightman, Tanner, and Varela
development of general design provisions	Tanner and Argudo
development of R and C_d factors	Varela
synthesis of data	Argudo and Tanner
study of low-strength AAC shear walls	Cancino and Varela

1.5   SCOPE OF DISSERTATION

The goal of this dissertation was to develop a rational procedure to propose values of the force-reduction factor (R) and corresponding displacement-amplification factor (C_d) for the seismic design of AAC shear wall structures in the United States. The selection of the factors R and C_d for those AAC structures involved fourteen AAC shear wall specimens, a two-story assemblage specimen

tested under quasi-static reversed cyclic loads, and the simulation of the performance of different AAC structures under suites of earthquakes representative of different seismic zones of the United Sates.

Results from eight shear-dominated and six flexure-dominated wall specimens were used to select values of drift ratio and displacement ductility capacities for AAC shear wall structures, and to develop analytical models that represent the flexural and shear behavior of AAC shear walls subjected to lateral loads. Results from the assemblage were used to verify the proposed analytical models and the observed behavior of the flexure-dominated specimens.

1.6 OBJECTIVES OF DISSERTATION

The objectives of this dissertation were to:

- evaluate the behavior of different AAC flexure-dominated specimens to verify the use of AAC shear wall structures in seismic zones;
- test an assemblage specimen to verify the proposed analytical models and the observed behavior of the flexure-dominated specimens;
- define appropriate values of drift ratio and displacement ductility capacities for AAC shear walls;
- develop analytical models that represent the flexural and shear behavior of AAC shear walls under lateral loads;
- predict the performance of AAC shear wall structures subjected to earthquake ground motions; and
- develop a procedure to propose values of the force-reduction factor (R) and displacement-amplification factor (C_d) for the seismic design of AAC shear wall structures in the United States.

1.7   ORGANIZATION OF DISSERTATION

This dissertation describes a combination of experimental and analytical research used to propose values of the factors R and C_d for the seismic design of AAC shear wall structures in the United States. Chapter 2 describes AAC and use of AAC panels, and presents a literature review on the behavior of AAC, and on the factors R and C_d.   The testing programs for AAC shear walls and the two-story assemblage specimen are presented in Chapters 3 and 4 respectively. Results for the shear-dominated wall specimens are presented in Chapter 5. Results of the flexure-dominated specimens together with those for the two-story assemblage are presented in Chapter 6. The procedure to select the factor R_d, selection of AAC structures, selection of suites of earthquakes, selection and maximum drift ratio and displacement ductility capacities, and description of analytical models are described in Chapter 7. Values of the factors R and C_d for AAC shear wall structures are proposed in Chapter 8. The summary, major conclusions, and recommendations for future research are presented in Chapter 9.

CHAPTER 2

Background

2.1 DESCRIPTION OF AUTOCLAVED AERATED CONCRETE

Autoclaved Aerated Concrete (AAC), also known as cellular concrete, is a lightweight cellular material, most commonly composed of portland cement, quicklime, and finely ground sand. Some or all of the sand and cement can be replaced by fly ash. In the most common method of production, the dry materials are mixed with water to form a slurry, which is poured into large open molds. As the slurry is poured, it is mixed with a small amount of gas-forming agent, usually finely powdered aluminum. The aluminum powder reacts with the alkaline cement, forming many microscopic bubbles of hydrogen gas, which cause the slurry to increase in volume. At the same time, the quicklime reacts with the water to form hydrated lime, giving off considerable heat in the process. This heat is sufficient to produce an accelerated initial set in the portland cement within a few hours. The resulting "cake" is strong enough to support its own weight, and retains the cellular structure produced by the hydrogen bubbles. The cake is then de-molded, and cut into the desired shapes. At this stage of curing, the cake can be cut relatively easily, using steel wires. The cut shapes are then cured in an autoclave, producing a final material with about the same density as wood and which can be easily cut and shaped with hand tools (RILEM 1993, Argudo 2003, and Tanner 2003). The cellular structure of AAC is shown in Figure 2.1.

Figure 2.1 Cellular structure of AAC

2.2   TYPICAL MECHANICAL AND THERMAL CHARACTERISTICS OF AAC

In Table 2.1, typical mechanical and thermal characteristics of AAC are compared with those of conventional concrete, including conventional concrete made with lightweight aggregates. AAC typically has one-sixth to one-third the density of conventional concrete, and about the same ratio of compressive strength. Its thermal conductivity is one-sixth or less than that of concrete, making it potentially energy-efficient. Its fire rating is slightly longer than that of conventional concrete of the same thickness, making it potentially useful in applications where fire resistance is important. Because of its internal porosity, AAC has very low sound transmission, making it potentially useful acoustically.

2.3   AAC STRENGTH CLASSES

AAC is produced in different densities and corresponding compressive strengths, in accordance with ASTM C1386 (Precast Autoclaved Aerated Concrete Wall Construction Units) and ASTM C 1452 (Standard Specification for Reinforced Autoclaved Aerated Concrete Elements).   Densities and corresponding strengths are described in terms of "strength classes." In each case,

9

the strength class corresponds to the specified compressive strength in MPa (Table 2.2).

Table 2.1 Typical mechanical and thermal characteristics of AAC

Characteristic	AAC	Conventional Concrete
density, lb/ft^3 (kg/m^3)	25 - 50 (400 - 800)	80 - 150 (1280 - 2400)
compressive strength, lb/in^2 (MPa)	360 - 1090 (2.5 - 7.5)	1000 - 10000 (6.9 - 69)
thermal conductivity, Btu-in/ft^2-hr-F	0.75 - 1.20	6.0 – 10.0
fire rating, hours	≤ 8	≤ 6

Table 2.2 Material characteristics of AAC in different strength classes

Strength Class	Specified Compressive Strength lb/in^2 (MPa)	Average Compressive Strength lb/in^2 (MPa)	Nominal Dry Bulk Density lb/ft^3 (kg/m^3)	Density Limits lb/ft^3 (kg/m^3)
AAC 2.0	290 (2.0)	360 (2.5)	25 (400)	22 (350) - 28 (450)
			31 (500)	28 (450) - 34 (550)
AAC 3.3	478 (3.3)		31 (500)	28 (450) - 34 (550)
			37 (600)	34 (550) - 41 (650)
AAC 4.0	580 (4.0)	720 (5.0)	31 (500)	28 (450) - 34 (550)
			37 (600)	34 (550) - 41 (650)
			44 (700)	41 (650) - 47 (750)
			50 (800)	47 (750) - 53 (850)
AAC 4.4	638 (4.4)		37 (600)	34 (550) - 41 (650)
			44 (700)	41 (650) - 47 (750)
AAC 6.0	870 (6.0)	1090 (7.5)	44 (700)	41 (650) - 47 (750)
			50 (800)	47 (750) - 53 (850)

2.4   USE OF AAC TO FORM STRUCTURAL ELEMENTS

AAC can be used to make a variety of structural elements: unreinforced masonry-type units (blocks), factory-reinforced floor panels, roof panels, wall panels, lintels, beams, and other special shapes (Figure 2.2). These elements can be used in a variety of applications including residential, commercial and industrial construction. Reinforced wall panels can be used as cladding systems as well as loadbearing and non-loadbearing exterior and interior wall systems. Reinforced floor and roof panels can be efficiently used to provide the horizontal diaphragm system while supporting the necessary gravity loads.

Figure 2.2 Examples of AAC elements

The typical thickness of the blocks and panels ranges from 4 in. (102 mm) to 12 in. (305 mm). The modular blocks are usually 8 in. (203 mm) tall and 24 in. (610 mm) long. Floor, roof, and wall panels are typically 24 inches tall (610 mm) and have a maximum length of 240 inches (6.10 m), but can be easily cut to shorter lengths.

11

Shear walls are the major structural elements resisting lateral forces in AAC structures under earthquake ground motions. Those AAC walls can be made out of blocks, horizontal, and vertical panels. Flexural reinforcement is typically placed in vertical grouted cores at the ends of the wall.

Design provisions for AAC panels are under discussion by American Concrete Institute (ACI) Subcommittee 523A, and corresponding design provisions for field-reinforced masonry are being considered by the AAC Masonry Subcommittee of the Masonry Standards Joint Committee (MSJC) (Argudo 2003 and Tanner 2003).

2.4.1 Thin-Bed-Mortar

The thin-bed mortar used to bond the AAC panels is more like a structural adhesive than a conventional masonry mortar. It is typically laid only in joints that are approximately 1/32 in. to 1/8 in. (1 mm to 3 mm) thick. It is made from a mix of portland cement, fine silica sand, polymers such as latex or vinylester, and admixtures such as water-retention admixtures. The compressive strength of the thin-bed mortar is greater than that of the AAC itself. For example, the average compressive strength of twelve 2 in. (5 mm) by 2 in. (5 mm) thin-bed mortar cubes tested at FSEL as part of this study was 2100 psi (14.5 MPa), which is greater than the maximum compressive strength of the AAC. The measured tensile bond strength between AAC and thin-bed mortar is equal to the modulus of rupture of AAC for material with a compressive strength of the AAC less than 450 psi (3.1 MPa), and is limited to about 94 psi for material with compressive strength above 450 psi (3.1 MPa) (Argudo 2003 and Tanner 2003).

2.4.2 Construction Process for AAC Walls

The general construction process for AAC walls is independent of whether horizontal panels, vertical panels or blocks are used. First, the top of the concrete

base or foundation is roughened by light bush-hammering, and shims are placed on top, and leveled to within a tolerance of ±1/32 inch (0.8 mm). Next, an ASTM C270, Type S mortar by proportion is placed on top of the concrete base between the shims (Figure 2.3). The shims and mortar provide a surface on which to level the first course of panels.

Figure 2.3 Placing Type S mortar by proportion on concrete foundation

Once the first course is leveled, it is not necessary to level subsequent courses because the panels are manufactured to close tolerances, and the mortar joints are quite thin. Subsequent courses are laid over the preceding one with only a layer of thin-bed mortar separating them (Figure 2.4 and Figure 2.5).

Figure 2.4 Placing a layer of thin-bed mortar on AAC panel

Figure 2.5 Placing second course of AAC panels

2.5 LITERATURE REVIEW

The literature review presented in the following two sections focused on previous research carried out on the behavior of AAC walls, and on procedures to select the factors R and C_d for the seismic design of structures.

2.5.1 Previous Research on AAC Walls

Prior research on AAC walls has focused primarily on the behavior of walls constructed using AAC masonry-type units. For example, one research project (de Vekey *et al*. 1986) studied the performance of AAC wallettes and walls under lateral loads to study the effect of thickness, moisture content, and specimen size on the flexural strength. That study concluded that the flexural strength of the specimens decreased as the thickness of the specimen increased, the flexural strength decreased as the moisture content increased, and the flexural strength increased as the size of the unit decreased when the load was applied perpendicular to the bed joints, and it was about the same when the load was applied parallel to the bed joints. In another research project, the out-of-plane flexural behavior of non-load bearing AAC walls constructed with blocks in running bond was studied, to investigate the flexural strength of the walls parallel or perpendicular to the bed joints (Al-Shaleh and Attiogbe 1997). That study concluded that the out-of-plane flexural strength of the AAC walls was the same parallel or perpendicular to the bed joints.

Based on this part of the literature review, insufficient prior research exists on the seismic performance of AAC structures to develop seismic design provisions or analytical models to predict the behavior of AAC shear-wall structures under earthquake ground motions. Sufficient information, however, has been acquired to permit the development of design provisions in areas with low seismic risk, such as Florida and Texas. The insufficient research on AAC

structures clearly indicates the need for more experimental data, mainly on the in-plane behavior of AAC shear walls subjected to lateral loads.

2.5.2   Previous Research on R and C_d Factors

Several research studies have been conducted on the selection of force-reduction factors (R) for the seismic design of structures. For example, Miranda and Bertero (1994) present a summary of different investigations on the factor R, described in that study as a strength reduction factor (R_μ). Results from those different investigations were reviewed by Miranda and Bertero (1994), who presented the existing equations for R_μ in a common format for a better comparison among them. Four of those proposed equations are presented below:

Lai and Biggs (1980) proposed a strength reduction factor (R_μ) that can be expressed in the form of Equation 2.1:

$$R_\mu = \alpha + \beta \left(\log T \right) \qquad\qquad \textbf{\textit{(2.1)}}$$

In the above equation, α and β are parameters that depend on the natural period of the structure (T) and the displacement ductility ratio (μ). Some values of the parameters α and β as a function of T and μ are shown in Table 2.3. Equation (2.1) was based on the response of elasto-plastic, single-degree-of-freedom systems subjected to 20 synthetic earthquake ground motions whose elastic response spectra represented the Newmark and Hall elastic design spectrum.

***Table 2.3 Values of the parameters α and β as a function of T and μ (Lai and
Biggs 1980, as reported by Miranda and Bertero 1994)***

Period Range	Coefficient	μ = 2	μ = 3	μ = 4
$0.1 \leq T < 0.5$ sec	α	1.6791	2.2296	2.6587
	β	0.3291	0.7296	1.0587
$0.5 \leq T \leq 0.7$ sec	α	2.0332	2.7722	3.3700
	β	1.5055	2.5320	3.4217

Riddell *et al*. (1989) developed Equations (2.2) and (2.3) to estimate the factor
(R_μ) as a function of the parameters R^* and T^*, which depend on the ductility
ratio (μ).

$$\text{for } 0 \leq T \leq T^* \qquad R_\mu = 1 + \frac{R^* - 1}{T^*} T \qquad\qquad \textbf{\textit{(2.2)}}$$

$$\text{for } T \geq T^* \qquad\qquad R_\mu = R^* \qquad\qquad \textbf{\textit{(2.3)}}$$

Some values of the parameters R^* and T^* as a function of ductility ratios are
shown in Table 2.4. Equations (2.2) and (2.3) were developed using the response
of elasto-plastic, single-degree-of-freedom systems subjected to four different
suites of earthquake ground motions. The first suite was a combination of
earthquakes from United States (specifically California), Peru, Chile, Nicaragua,
and Argentina; the second and third suites included earthquakes from Chile only;
and the fourth suite, from Peru only.

17

Table 2.4 Values of the parameters R* and T* as a function of ductility ratios
(Riddell et al. 1989, as reported by Miranda and Bertero 1994)

Parameter	$\mu = 2$	$\mu = 3$	$\mu = 4$
R^*	2.0	3.0	4.0
T^*	0.1	0.2	0.3

Nassar and Krawinkler (1991) proposed Equation (2.4) to calculate the factor (R_μ) as a function of the ductility ratio (μ) and the parameter (c), which is calculated using Equation (2.5):

$$R_\mu = \left[c\left(\mu - 1\right) + 1 \right]^{1/c} \qquad (2.4)$$

$$c\left(T, \alpha\right) = \frac{T^a}{1 + T^a} + \frac{b}{T} \qquad (2.5)$$

In Equation (2.5), T is the natural period of the structure, α is the post-yielding stiffness as percentage of the initial stiffness, and (a) and (b) are parameters given as a function of α as shown in Table 2.5. Equations (2.4) and (2.5) were based on the response of single-degree-of-freedom systems (bilinear and stiffness degrading) subjected to fifteen earthquake ground motions recorded in the western United States.

Table 2.5 Values of the parameters a and b as a function of α (Nassar and Krawinkler 1991, as reported by Miranda and Bertero 1994)

α	a	b
0.00	1.00	0.42
0.02	1.00	0.37
0.10	0.80	0.29

Miranda (1988) proposed the following expression to estimate the factor (R_μ) as a function of the ductility ratio (μ) and the parameter Φ:

$$R_\mu = \frac{\mu - 1}{\Phi} + 1 \geq 1 \qquad (2.6)$$

In Equation (2.6), Φ is a function of the ductility ratio (μ), the natural period of the structure (T), and the soil conditions; for rock sites, Φ is given by the following equation:

$$\Phi = 1 + \frac{1}{10\,T - \mu\,T} - \frac{1}{2\,T} \exp\left[-\frac{3}{2}\left(\ln T - \frac{3}{5} \right)^2 \right] \qquad (2.7)$$

Equations (2.6) and (2.7) were developed using the response of single-degree-of-freedom systems subjected to real earthquake ground motions from United States (specifically California), Rumania, Japan, Chile, Mexico, and El Salvador.

Equations (2.1) to (2.7) were in general based on the response of nonlinear single-degree-of-freedom systems subjected to real and synthetic earthquake ground motions. The extrapolation of these results to multi-degree-of freedom

19

systems required a relationship between local and global ductilities. The proposed equations suggested that the factor (R_μ) is mainly a function of the displacement ductility (μ), the natural period of the structure (T) and the soil conditions.

One conclusion of the study by Miranda and Bertero (1994) is that the use of strength reduction factors based on ductility, period and soil conditions together with the evaluation of structural overstrength factors, and relationships between local and global ductility demands are needed to establish rational seismic design approaches. Even though Equations (2.1) to (2.7) seem reasonable and may be incorporated in future United States seismic codes, the reality is that today single values of the factor (R) are still proposed in those seismic codes to design different structural systems. Therefore, given this limitation, a rational procedure should be developed to select a single value of the factor R for the seismic design of AAC shear wall structures in the United States. This procedure should address the behavior of AAC structures modeled as multi-degree-of-freedom systems, using a large number of real and synthetic suites of earthquake ground motions representative of different seismic regions of the United States.

In another study, Uang (1991) derived explicit equations to establish the seismic force-reduction factor (R) and the displacement amplification factor (C_d) as a function of two parameters: the structural ductility factor (μ_s); and the structural overstrength factor denoted as Ω_o by Uang (1991). The factor (R) is defined by Equation (2.8) and the factor (C_d) by Equation (2.9).

$$R = R_\mu \, \Omega_o \qquad\qquad\qquad\qquad (2.8)$$

$$C_d = \mu_s \, \Omega_o \qquad\qquad\qquad (2.9)$$

In Equation (2.8), R_μ is the ductility reduction factor, which is a function of the structural ductility factor (μ_s), and a corresponding equivalent viscous damping ratio. For a single-degree-of-freedom system the relationship between the factors (μ_s) and (R_μ) is known (Lai and Biggs 1980; Riddell *et al*. 1989). For structures with more than one degree of freedom, however, that study suggested that the structural ductility factor (μ_s) depends on the parameter used to define ductility; for example, story drift can be used to define structural ductility. Equation (2.8) is identified by the 2000 NEHRP (NEHRP 2000) as an appropriate equation to establish factors (R) for the seismic design of different structural systems.

The structural overstrength factor (Ω_o), defined in Equations (2.8) and (2.9), is a function of the structural redundancy, story drift limitations, multiple load combinations, strain hardening, participation of nonstructural elements, and variation of lateral force profiles. The factor (Ω_o) is therefore calculated as the product of a number of overstrength factors, which should be evaluated independently for each particular structural system.

One conclusion presented in the study of Uang (1991) was that values of the factors (R) and (C_d) proposed in NEHRP are not consistent for various structural systems; that is, they do not give a uniform margin of safety against collapse. That study also suggested that it is difficult to justify the relative values of the factors (R) and (C_d) proposed in NEHRP, and that the factor R would be smaller than the factor C_d for various structural systems.

Equations (2.8) and (2.9) indicate that the seismic force-reduction factor R is the product of two independent parameters: the ductility reduction factor (R_μ) and the structural overstrength factor (Ω_o). Similarly, the displacement

amplification factor (C_d) depends on the structural ductility factor (μ_s) and the structural overstrength (Ω_o). The values of R_μ, Ω_o, and μ_s should therefore be evaluated independently to establish values of the factors R and C_d.

In this dissertation, Equation (2.8) was used to define the seismic force reduction factor (R) because is consistent with that presented in NEHRP (2000) for different structural systems, and also with that proposed in Uang (1991). The ductility reduction factor was defined using the variable R_d to be consistent with that equation presented in NEHRP 2000. The structural overstrength factor that represents the system overstrength factor (denoted by Uang as Ω_o) was denoted by the variable Ω_{system} to avoid possible confusion with the use of that same variable, Ω_o, to refer to element overstrength in the IBC 2000 and ASCE 7-98.

CHAPTER 3

Test Program

The experimental part of this dissertation consisted of two phases. Phase I involved testing 14 AAC shear wall specimens; and Phase II, testing a two-story assemblage specimen. This chapter describes the test setup for those AAC shear wall specimens, the objectives and fundamental characteristics of each test specimen, the loading equipment, instrumentation, and loading history. The test setup used in this test program was verified through two initial tests, AAC Shear Wall Pilot Specimen 1 and AAC Shear Wall Pilot Specimen 2 (Brightman 2000).

The test setup, objectives, loading equipment, instrumentation, and loading history of the assemblage specimen are described in Appendix A. A summary of the test setup and objectives of the assemblage specimen is presented in Chapter 4.

The first eight shear wall specimens described here were intended to represent AAC shear walls whose behavior is controlled by shear and the remaining six specimens by flexure. The specimen geometry, reinforcement, and axial loads were selected based on those objectives.

Eight shear-dominated walls were designed and tested to verify proposed design formulas for web-shear cracking, sliding shear, and crushing of the diagonal strut for AAC shear walls. Those specimens were also intended to provide experimental data to develop analytical models that represent the behavior of shear-dominated AAC walls subject to earthquake ground motions. The first four AAC shear-dominated wall specimens were also tested to determine the differences in behavior of AAC shear-dominated walls with the same overall geometry, but constructed with different orientations of panel and block elements.

The geometry, flexural reinforcement, and axial force for each of the shear-dominated specimens were selected to force shear behavior. The geometry of the AAC shear-dominated specimens was selected to represent potential walls of AAC structures. The height of the shear-dominated specimens was 12 ft (3.6 m), and the length of the first shear dominated-specimens was 20 ft (6.1 m). This length was reduced in some specimens to study the effect of change in wall length in the capacity of the AAC walls as governed by web-shear cracking (Tanner 2003). The axial load was varied in some cases among the shear-dominated specimens to determine the influence of the axial force in the capacity of the AAC walls as governed by web shear cracking (Tanner 2003).

Six flexure-dominated walls were designed and tested to verify proposed design formulas for flexural shear cracking, flexural capacity, and to provide experimental data to develop analytical models to predict the behavior of flexure-dominated AAC shear walls under earthquake ground motions, and to define appropriate values of drift ratio and displacement ductility capacities for AAC shear walls.

The geometry, flexural reinforcement, and axial force for each of the flexure-dominated specimens were selected to force flexural behavior. The wall geometry for the flexure-dominated specimen was selected to represent the aspect ratio (height divided by plan length) of walls of potential AAC structures whose behavior is dominated by flexure. The axial force in those specimens was varied to represent the range of compressive stresses found in shear walls located in the first story of potential AAC structures up to five stories high.

3.1   SUMMARY OF DETAILS OF SHEAR WALL SPECIMENS

For each of the fourteen shear wall specimens, the intended failure mode, AAC units used in construction, material supplier, and test date is summarized in

Table 3.1. The geometry, amount and location of exterior and interior flexural reinforcement for each shear wall specimen are summarized in Table 3.2. Details of the axial load applied to each of the shear wall specimens are presented in Table 3.3. The measured average compressive strengths of AAC for the different AAC units used in the shear wall specimens are presented in Table 3.4. Detailed description for each of the shear wall specimens is presented in Section 3.2.

Table 3.1 Intended failure mode, AAC units used in construction, and material supplier for each AAC shear wall specimen

Specimen	Intended Failure Mode	AAC units	Material Supplier	Test Date
1	Shear	Horizontal Panels	Contec 1	6/15/2000
2	Shear	Vertical Panels	Ytong 1	7/26/2000
3	Shear	Blocks	Ytong 2	12/11/2000
4	Shear	Horizontal Panels	Matrix 1	10/21/2000
5	Shear	Blocks	Contec 2	5/15/2001
7	Shear	Blocks	Ytong 2	11/18/2000
9	Shear	Horizontal Panels	Matrix 1	2/6/2001
11	Shear	Blocks	Contec 2	4/10/2001
13	Flexure	Horizontal Panels	Ytong 1	07/03/2001
14a	Flexure	Horizontal Panels	Babb 1	12/10/2001
14b	Flexure	Horizontal Panels	Babb 1	03/07/02
15a	Flexure	Vertical Panels with Blocks	Babb 1	11/29/01
15b	Flexure	Vertical Panels with Blocks	Babb 1	03/28/02
16	Flexure	Vertical Panels with U-Blocks	Babb 1	1/17/02

In Table 3.1 the number following the material supplier refers to the shipment number of the material. For example, Babb-1 is the first shipment of AAC units received at the FSEL from Babb.

Table 3.2 Geometry, amount and location of exterior and interior flexural

reinforcement for each shear wall specimen

Specimen	Length in. (m)	Height in. (m)	Thickness in. (m)	Exterior Reinforcement	Interior Reinforcement
1	240 (6.1)	154 (3.9)	8 (0.2)	2-B7 1 in. (25 mm) 24 in.(0.6 m) from ends	No
2	240 (6.1)	154 (3.9)	8 (0.2)	2-B7 1 in. (25 mm) 24 in.(0.6 m) from ends	No
3	240 (6.1)	152 (3.8)	8 (0.2)	2-B7 1 in. (25 mm) 24 in.(0.6 m) from ends	No
4	240 (6.1)	154 (3.9)	8 (0.2)	2-B7 1 in. (25 mm) 24 in.(0.6 m) from ends	#5 (16 mm) at 48 in. (1.2 m)
5	240 (6.1)	152 (3.8)	8 (0.2)	2-B7 1 in. (25 mm) 24 in.(0.6 m) from ends	No
7	144 (3.7)	152 (3.8)	8 (0.2)	2-B7 1 in. (25 mm) 24 in.(0.6 m) from ends	No
9	96 (2.4)	154 (3.9)	8 (0.2)	2-B7 1 in. (25 mm) right at wall ends	No
11	48 (1.2)	152 (3.8)	8 (0.2)	2-B7 1 in. (25 mm) right at wall ends	No
13	72 (2.1)	154 (3.9)	8 (0.2)	No	# 5 (16 mm) 12 in. (0.3 m) from ends
14a	56 (1.4)	154 (3.9)	10 (0.25)	No	# 5 (16 mm) 4 in. (0.1 m) from ends
14b	56 (1.4)	154 (3.9)	10 (0.25)	No	# 5 (16 mm) 4 in. (0.1 m) from ends
15a	112 (2.8)	154 (3.9)	10 (0.25)	No	# 5 (16 mm) 8 in. (0.2 m) from ends
15b	112 (2.8)	154 (3.9)	10 (0.25)	No	# 5 (16 mm) 8 in. (0.2 m) from ends
16	112 (2.8)	154 (3.9)	10 (0.25)	No	# 5 (16 mm) 8 in. (0.2 m) from ends

Table 3.3 Details of axial load applied to each shear wall specimen

Specimen	Axial Load (Exterior Reinforcement) kips (kN)	Axial Load (Load Maintainer) kips (kN)	Self Weight Loading Beam kips (kN)	Total Axial Load kips (kN)
1	32 (142.3)	116 (516.0)	8 (35.6)	156 (693.9)
2	40 (177.9)	108 (480.4)	8 (35.6)	156 (693.9)
3	48 (213.5)	64 (284.7)	8 (35.6)	120 (533.8)
4	48 (213.5)	64 (284.7)	8 (35.6)	120 (533.8)
5	36 (160.1)	16 (71.2)	8 (35.6)	60 (266.9)
7	40 (177.9)	35 (155.7)	5 (22.2)	80 (355.8)
9	50 (222.4)	5 (22.2)	5 (22.2)	60 (266.9)
11	20 (89.0)	0 (0.0)	5 (22.2)	25 (111.2)
13	0 (0.0)	20 (89)	5 (22.2)	25 (111.2)
14a	0 (0.0)	0 (0.0)	5 (22.2)	5 (22.2)
14b	0 (0.0)	0 (0.0)	5 (22.2)	5 (22.2)
15a	0 (0.0)	20 (90.0)	5 (22.2)	25 (111.2)
15b	0 (0.0)	20 (90.0)	5 (22.2)	25 (111.2)
16	0 (0.0)	20 (90.0)	5 (22.2)	25 (111.2)

Table 3.4 Measured compressive strength for different units used in shear wall specimens

Material	Measured Compressive Strength f_{AAC} psi (MPa)
Contec 1	781 (5.4)
Contec 2	1040 (7.2)
Babb 1	1140 (7.9)
Matrix 1	133 0(9.2)
Ytong 1	NA
Ytong 2	650 (4.5)

3.2 SHEAR WALL SPECIMENS

In the following sections, the geometry, type of AAC units used in construction, reinforcement, and axial force is presented in detail for each of the shear wall specimens.

3.2.1 Shear Wall Specimen 1

Shear Wall Specimen 1 was constructed with horizontal AAC panels placed in running bond (Figure 3.1). The wall measured 240 in. (6.1 m) long by 154 in. (3.91 m) high (top of base to line of load application) by 8 in. (203.2 mm) thick. The aspect ratio of the wall (height divided by plan length) was 0.64. An axial load of 80 kips (355.8 kN) was applied at the beginning of the test, and was increased throughout the test to a final axial load of 156 kips (693.9 kN). The axial load was increased during the test because sliding of the wall with respect to its base was observed. The increase in the axial load provided additional sliding shear capacity in the wall, to force web shear cracking in the specimen (Tanner 2003). The first four panels of this specimen were previously used in AAC Shear Wall Pilot Specimen 2 (Brightman 2000); since the damage in that specimen was concentrated to the top two panels, these panels were replaced. The damaged panels were removed and the bed joint was carefully sanded and leveled to allow for full contact of the thin-bed mortar across the joint. The exterior flexural reinforcement of this wall consisted of two ASTM A193-B7 threaded rods 1 in. (25.4 mm) in diameter, placed 24 in. (0.6 m) from each wall end. This reinforcement was selected to force shear- rather than flexure-dominated behavior. Steel buttresses were attached to the base and to the loading beam at the ends of the wall to avoid slip for Shear Wall Specimen 1 (Brightman 2000). Steel buttresses were used in this shear wall specimen only. The AAC panels in Shear Wall Pilot Specimen 2 were supplied by Contec Mexicana (Monterrey, Mexico) and the thin-bed mortar was supplied by Ytong Florida, Ltd. (Haines City, Florida).

28

Figure 3.1 Text labels in figure:
- 20 in. (0.5 m)
- 144 in. (3.7 m)
- 20 in. (0.5 m)
- Threaded Rods Used as Exterior Flexural Reinforcement and to Apply Axial Load
- Threaded Rods Used to Apply Constant Axial Load
- Steel Buttresses
- 24 in. (0.6 m)
- 48 in. (1.2 m)
- 96 in. (2.4 m)
- 48 in. (1.2 m)
- 24 in. (0.6 m)
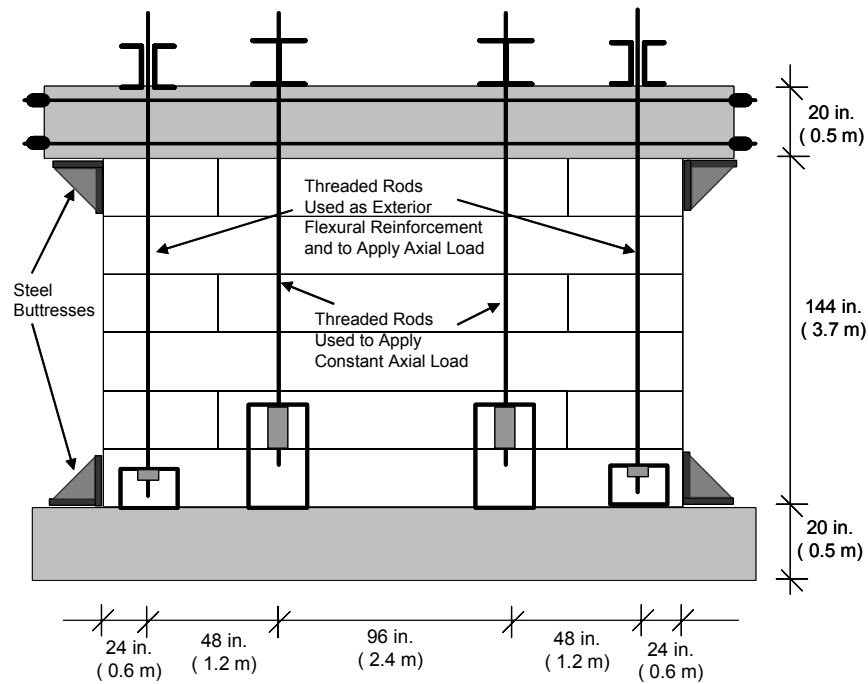
Figure 3.1 Layout of Shear Wall Specimens 1

3.2.2   Shear Wall Specimen 2

Shear Wall Specimen 2 was constructed with vertical AAC panels (Figure 3.2). The wall measured 240 in. (6.1 m) long by 154 in. (3.91 m) high (top of base to line of load application) by 8 in. (203.2 mm) thick. The aspect ratio of the wall was 0.64.   A constant axial load of 156 kips (693.9 kN) was applied throughout the test. The exterior flexural reinforcement consisted of two ASTM A193-B7 threaded rods 1 in. (25.4 mm) in diameter, placed 24 in. (0.6 m) from each wall end. The AAC panels and the thin-bed mortar were supplied by Ytong Florida, Ltd. (Haines City, Florida).

29
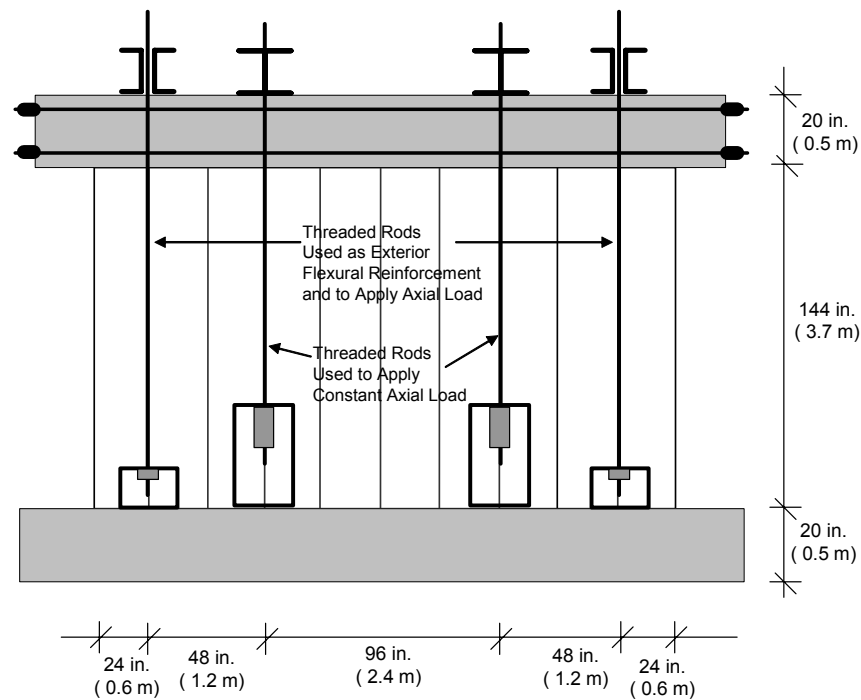
Figure 3.2 Layout of Shear Wall Specimen 2

3.2.3 Shear Wall Specimen 3

Shear Wall Specimen 3 was constructed with AAC masonry units placed in running bond (Figure 3.3). The wall measured 240 in. (6.1 m) long by 152 in. (3.86 m) high by 8 in. (203.2 mm) thick. The aspect ratio of the wall was 0.63, and a constant axial load of 120 kips (533.8 kN) was applied throughout the test. The exterior flexural reinforcement consisted of two ASTM A193-B7 threaded rods 1 in. (25.4 mm) in diameter, placed 24 in. (0.6 m) from each wall end. The AAC blocks and the thin-bed mortar were supplied by Ytong Florida, Ltd. (Haines City, Florida).
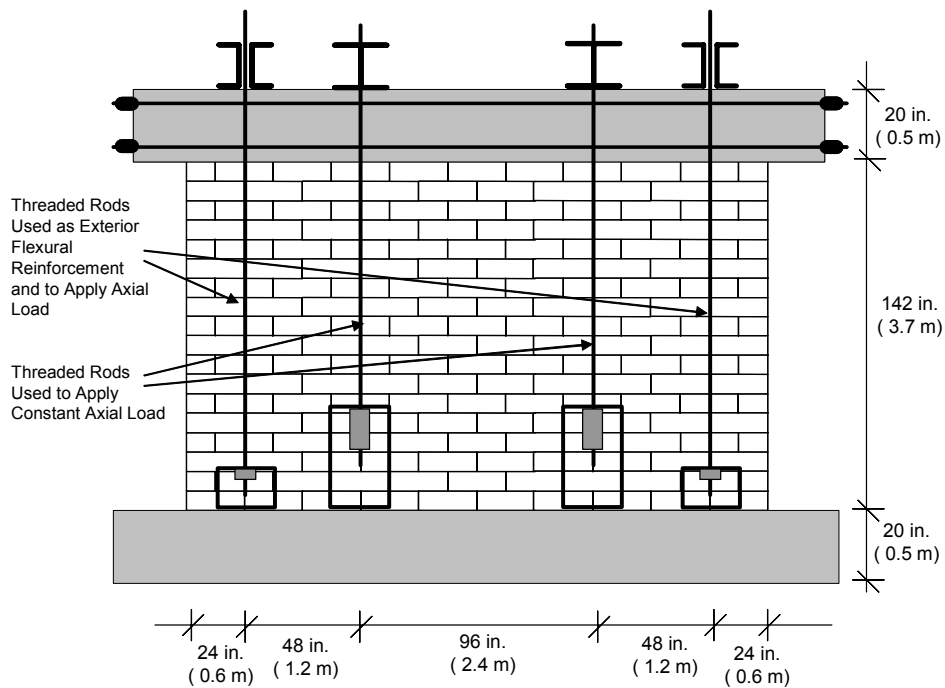
Figure 3.3 Layout of Shear Wall Specimens 3

3.2.4   Shear Wall Specimen 4

Shear Wall Specimen 4 was constructed with horizontal AAC panels placed in running bond (Figure 3.4). The geometry of the wall was the same as that of Shear Wall Specimen 1. An axial load of 120 kips (533.8 kN) was applied throughout the test. This specimen consisted of both exterior and interior flexural reinforcement. The exterior flexural reinforcement consisted of two A193-B7 threaded rods 1 in. (25.4 mm) in diameter, placed 24 in. (0.6 m) from each wall end, and the internal flexural reinforcement consisted of 1 # 5 (16 mm) bar spaced at every 48 in. (1.22 m) starting 24 in. (0.6 m) from the end of the wall. This internal flexural reinforcement was placed in 3 in. (76.2 mm) grouted cores. ASTM C 476 coarse grout by proportion was used to fill the grouted cores in this

specimen. The AAC panels and the thin-bed mortar were supplied by Hebel / Matrix (now Babb International, Inc.).
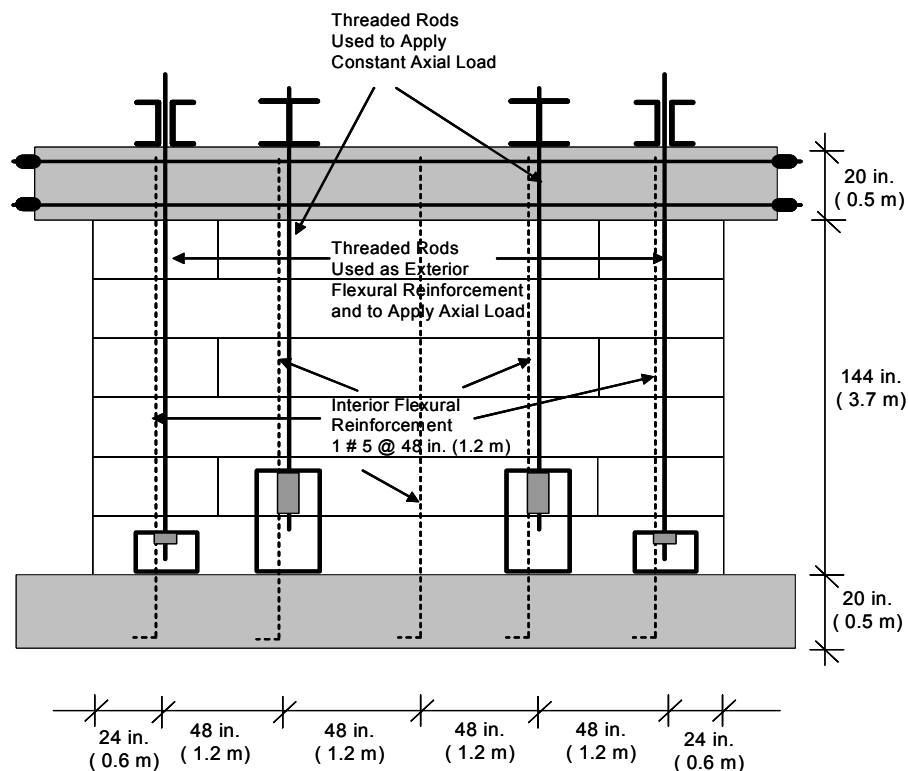
Figure 3.4 Layout of Shear Wall Specimens 4

3.2.5 Shear Wall Specimen 5

Shear Wall Specimen 5 was constructed with AAC blocks placed in running bond (Figure 3.3). The layout of the wall was the same as that of Shear Wall Specimen 3, except that 20 in. (0.51 m) #5 dowels were placed at the base of the wall and between the loading beam and the top of the wall. A total of 9 dowels were spaced at 24 in (0.6 m) starting 24 in. (0.6 m) from the end of the wall. The dowels were grouted in 3 in. (76 mm) cores fabricated at the Ferguson Structural Engineering Laboratory (FSEL). ASTM C476 coarse grout by proportion was used to fill the grouted cores in this specimen. Dowels provided

32

additional sliding shear resistance to reduce the axial load to 60 kips (266.9 kN). The exterior flexural reinforcement consisted of two ASTM A193-B7 threaded rods 1 in. (25.4 mm) in diameter, placed 24 in. (0.6 m) from each wall end. The AAC blocks and the thin-bed mortar were supplied by Contec Mexicana (Monterrey, Mexico).
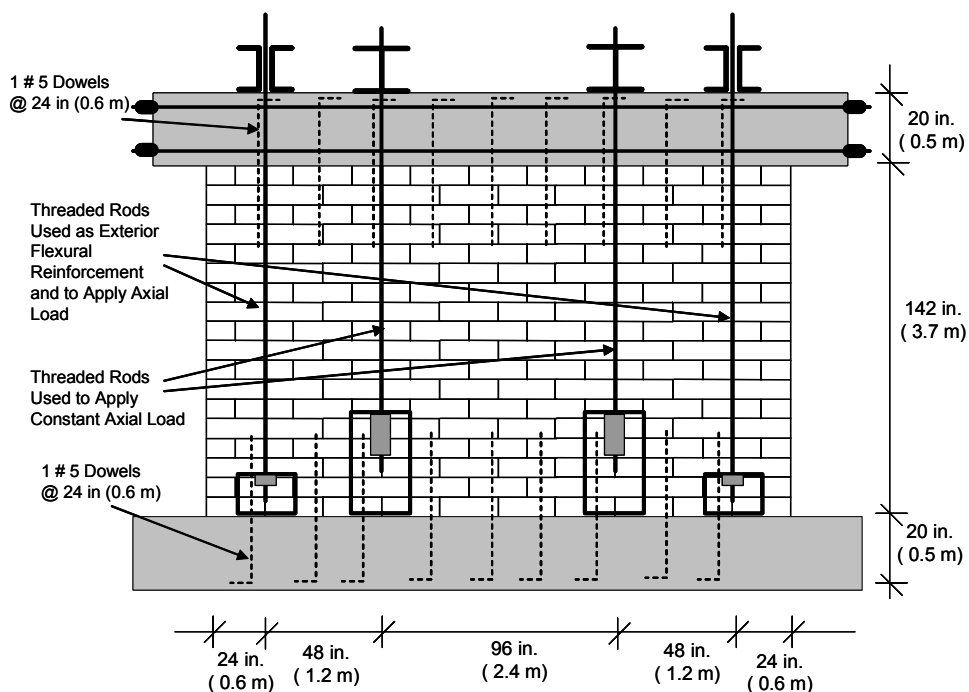
Figure 3.5 Layout of Shear Wall Specimens 5

3.2.6   Shear Wall Specimen 7

Shear Wall Specimen 7 was constructed with AAC masonry units placed in running bond (Figure 3.6). The wall measured 144 in. (3.66 m) long by 152 in. (3.86 m) high by 8 in. (203.2 mm) thick. The aspect ratio of the wall was 1.05. An axial load of 80 kips (355.8 kN) was applied throughout the test. The exterior flexural reinforcement consisted of two ASTM A193-B7 threaded rods 1 in. (25.4

mm) in diameter, placed 24 in. (0.6 m) from each wall end. The AAC blocks and the thin-bed mortar were supplied by Ytong Florida, Ltd. (Haines City, Florida).
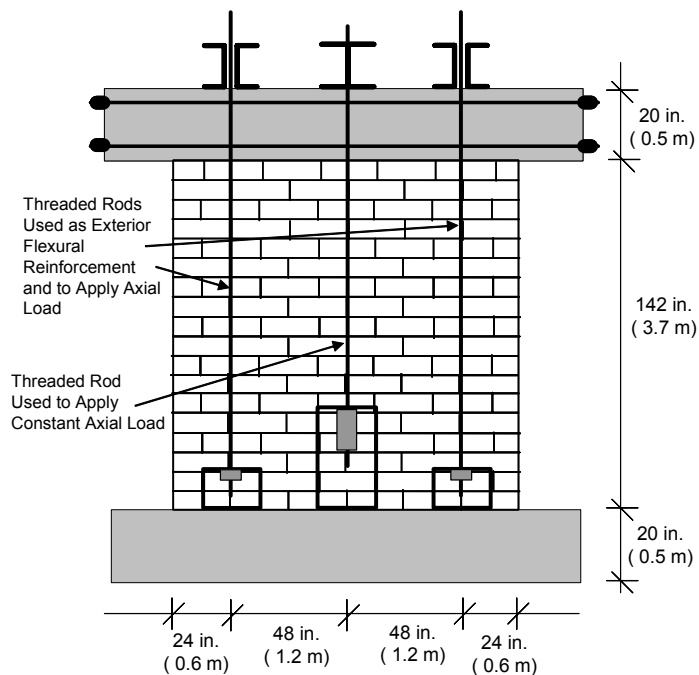
Figure 3.6 Layout of Shear Wall Specimen 7

3.2.7   Shear Wall Specimen 9

Shear Wall Specimen 9 was constructed with horizontal AAC panels placed in running bond (Figure 3.7). The wall measured 96 in. (2.43 m) long by 154 in. (3.91 m) high by 8 in. (203.2 mm) thick. The aspect ratio of the wall was 1.6, and an axial load of 60 kips (266.9 kN) was applied throughout the test. The exterior flexural reinforcement consisted of two ASTM A193-B7 threaded rods 1 in. (25.4 mm) in diameter, placed just outside the ends of the wall. The AAC panels and the thin-bed mortar were supplied by Hebel / Matrix (now Babb International, Inc.).
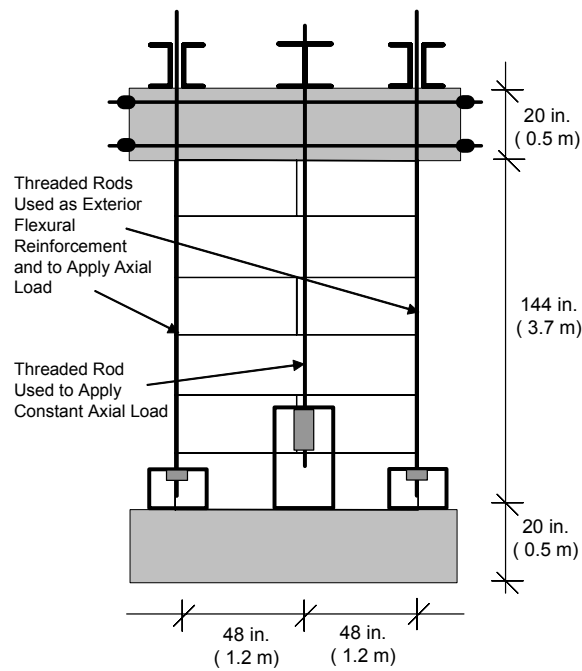
Figure 3.7 Layout of Shear Wall Specimen 9

3.2.8   Shear Wall Specimen 11

Shear Wall Specimen 11 was constructed with AAC masonry units placed in running bond (Figure 3.8). The wall measured 48 in. (1.22 m) long by 152 in. (3.86 m) high by 8 in. (203.2 mm) thick. The aspect ratio of the wall was 3.17, and an axial load of 25 kips (111.2 kN) was applied throughout the test. The exterior flexural reinforcement consisted of two ASTM A193-B7 threaded rods 1 in. (25.4 mm) in diameter, placed just outside each wall end. The AAC blocks and the thin-bed mortar were supplied by Contec Mexicana (Monterrey, Mexico).

35
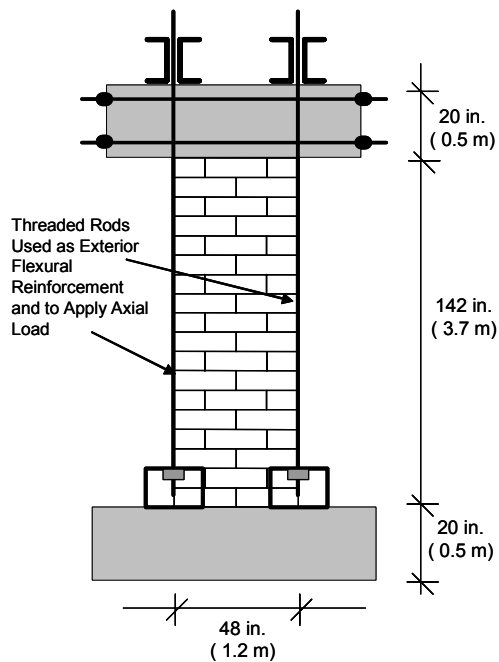
Figure 3.8 Layout of Shear Wall Specimen 11

3.2.9   Shear Wall Specimen 13

Shear Wall Specimen 13 was constructed with horizontal AAC panels placed in stack bond (Figure 3.9). The wall measured 72 in. (1.83 m) long by 154 in. (3.91 m) high by 8 in. (203.2 mm) thick with a corresponding aspect ratio of 2.14. An axial of load 25 kips (111.2 kN) was applied at the beginning of the test. This specimen was created out of surplus 144 in. (3.7 m) panels used in the construction of Shear Wall Specimen 2, which were cut and cored at FSEL. The flexural reinforcement of this wall consisted of 1 # 5 (16 mm) bar placed 12 in. (0.3 m) from each wall end. The reinforcement was placed in a 3 in. (76.2 mm) grouted cell. ASTM C476 coarse grout by proportion was used to fill the grouted cores.

36
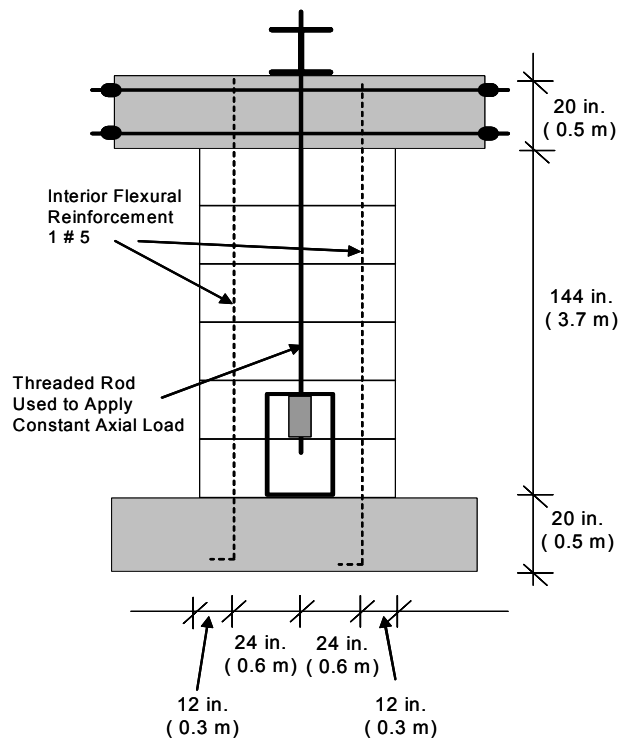
Figure 3.9 Layout of Shear Wall Specimen 13

3.2.10 Shear Wall specimen 14a

Shear Wall Specimen 14a was constructed with horizontal AAC panels placed in running bond (Figure 3.10). The wall measured 56 in. (1.42 m) long by 154 in. (3.91 m) high by 10 in. (254 mm) thick with a corresponding aspect ratio of 2.75. A constant axial of load 5 kips (22.2 kN) was applied throughout the test. The original specimen was longer than anticipated so the panels were cut to the adjusted length at FSEL. The centerline of the cores was not aligned with the longitudinal centerline of the panels. The maximum offset was 1 in. (25 mm) in both the transverse and longitudinal axes of the wall panel. Therefore, 3 in. (76 mm) diameter cores were drilled at the correct location at FSEL. ASTM C476 coarse grout by proportion was used to fill the grouted cores. The AAC panels

and the thin-bed mortar were supplied by Babb International, Inc. (Smyrna, Georgia). The flexural reinforcement of this wall consisted of one # 5 (16 mm) bar placed 4 in. (101.6 mm) from each wall end.
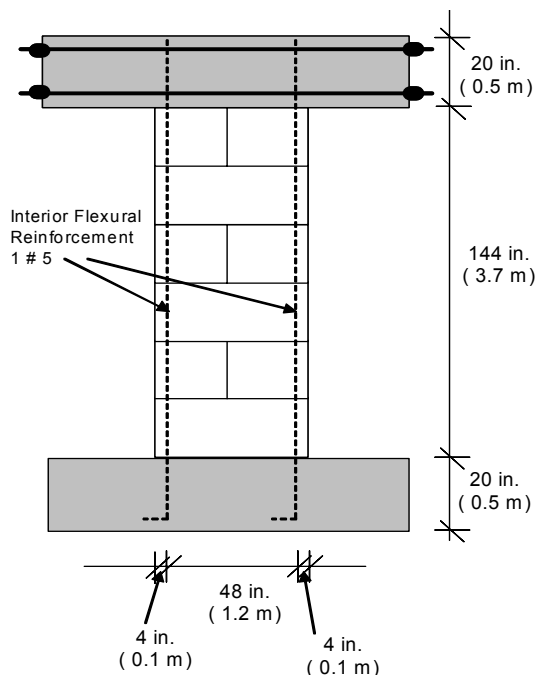
Figure 3.10 Layout of Shear Wall Specimen 14a and 14b

3.2.11 Shear Wall Specimen 14b

Shear Wall Specimen 14b was a replicate of Shear Wall Specimen 14a. The AAC panels and thin-bed mortar for Shear Wall Specimen 14b arrived in the same shipment as the material for Shear Wall Specimen 14a.

3.2.12 Shear Wall specimen 15a

Shear Wall Specimen 15a was made of vertical AAC panels with AAC blocks at the ends (Figure 3.11). The wall measured 112 in. (2.84 m) long by 154 in. (3.91 m) high by 10 in. (254 mm) thick with a corresponding aspect ratio of 1.38. A constant axial of load 25 kips (111.2 kN) was applied throughout the test.

The flexural reinforcement of this wall consisted of 1 # 5 (16 mm) bar placed 8 in. (203.2 mm) from each wall end. The reinforcement was placed in a 3 in. (76.2 mm) grouted core that was shared between the end vertical panels and AAC blocks oriented vertically (Figure 3.12). The half-cores in the AAC blocks were made at FSEL. ASTM C476 coarse grout by proportion was used to fill the cores in the AAC blocks and the vertical panels. The AAC panels and the thin-bed mortar were supplied by Babb International, Inc. (Smyrna, Georgia).
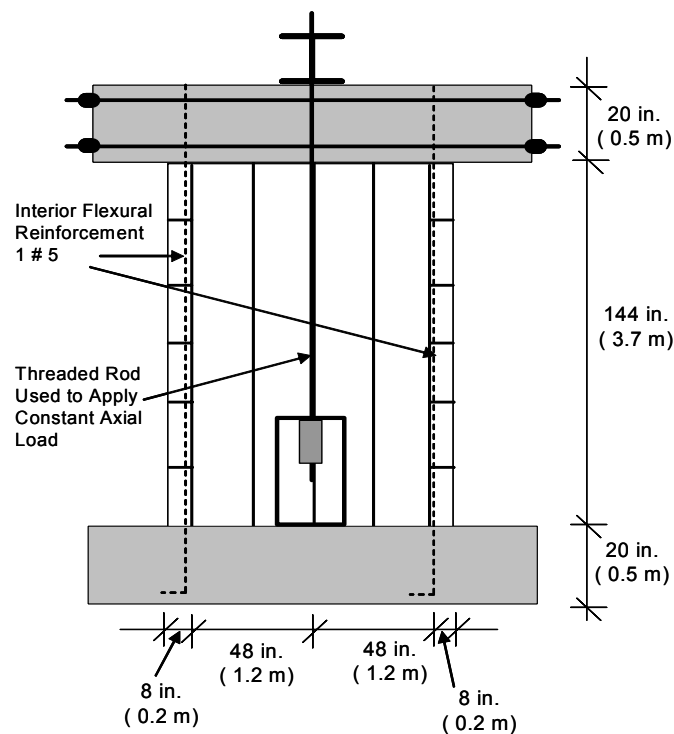
Figure 3.11 Layout of Shear Wall Specimens 15a, 15b and 16
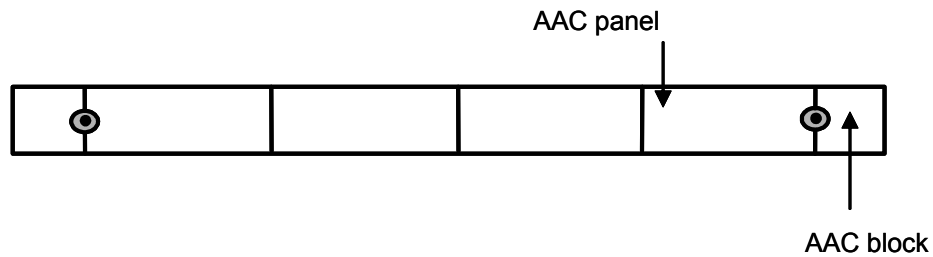
Figure 3.12 Plan View of Shear Wall Specimens 15a and 15b

3.2.13 Shear Wall Specimen 15b

Shear Wall Specimen 15b was a replicate of Shear Wall Specimen 15a. The AAC material and thin-bed mortar arrived in the same shipment as the material for Shear Wall Specimen 15a.

3.2.14 Shear Wall Specimen 16

Shear Wall Specimen 16 was made of vertical AAC panels with AAC U-blocks at the ends (Figure 3.11). The wall measured 112 in. (2.84 m) long by 154 in. (3.91 m) high by 10 in. (254 mm) thick with a corresponding aspect ratio of 1.38. An axial of load 25 kips (111.2 kN) was applied at the beginning of the test. The flexural reinforcement of this wall consisted of 1 # 5 (16 mm) bar placed 8 in. (203.2 mm) from each wall end. The reinforcement was placed in a grouted cell that was shared between the vertical panels and an AAC U-block oriented vertically (Figure 3.13). ASTM C476 coarse grout by proportion was used to fill the half-cores in the vertical panels and the U-blocks. The AAC panels and the thin-bed mortar were supplied by Babb International, Inc. (Smyrna, Georgia).

40
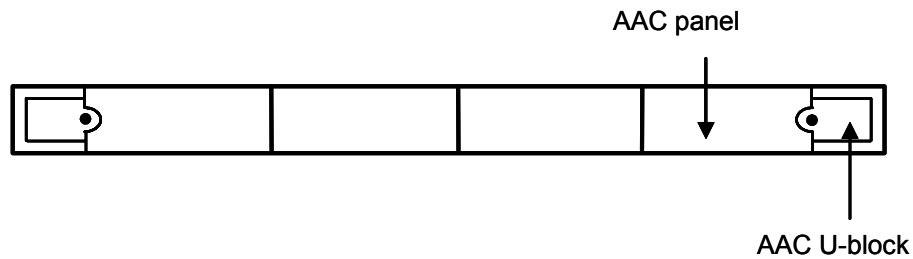
Figure 3.13 Plan view of Shear Wall Specimen 16

3.3 TEST SETUP

3.3.1 Lateral Loading System

The lateral load was applied using a pair of horizontal actuators mounted side by side for most specimens, and a single actuator for Shear Wall Specimen 14b and Shear Wall Specimen 15b (Figure 3.14). Each actuator was bolted at one end to a reinforced concrete loading beam connected to the specimen, and at the other end to a steel beam attached to the biaxial reaction wall of FSEL. The loading beam was connected along the top of each specimen using conventional portland cement-lime masonry mortar conforming to ASTM C270, Type S by proportion.

41
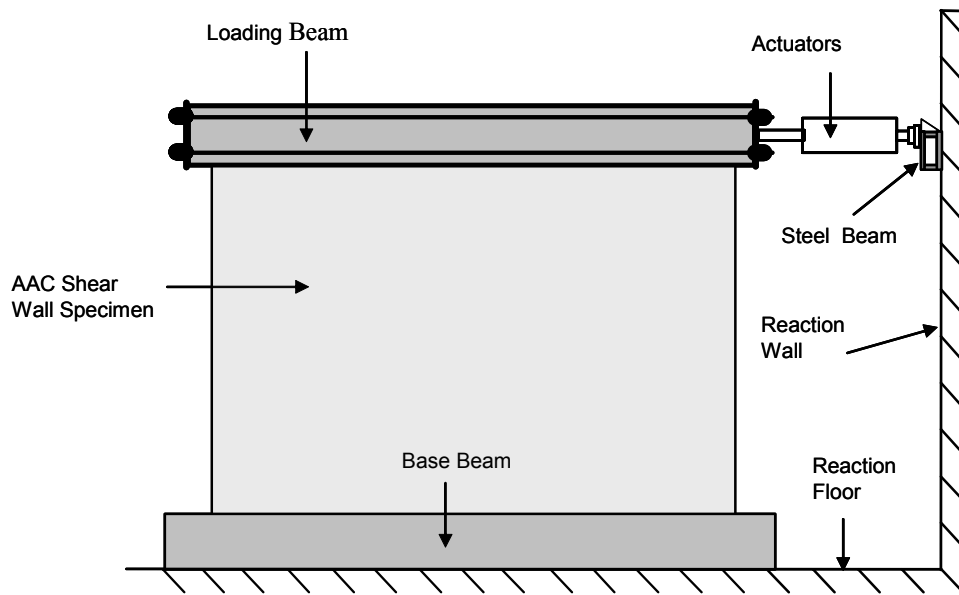
Figure 3.14 Setup for applying lateral load

3.3.2   Axial Load System

Axial load was applied to the shear-dominated specimens using 1 in. (25.4 mm) threaded rods pos-tensioned manually, and by hydraulic actuators controlled by a load maintainer (Figure 3.15). The tops of the threaded rods were connected to a transverse beam consisting of two steel channels, while the bottoms were connected to a steel box bolted to the base beam. These threaded rods located close to the wall ends were also used as external flexural reinforcement for the shear-dominated specimens.

At the beginning of each test the axial load was applied to the specimen. The exterior threaded rods were post-tensioned by tightening the nuts located inside the steel boxes connected to the base beam. The interior threaded rods were loaded by applying pressure in the actuators. The total axial load of each shear-dominated specimen was the sum of the axial load applied in the exterior

threaded rods, the axial load applied using the hydraulic actuators, and the self-weight of the concrete loading beam.
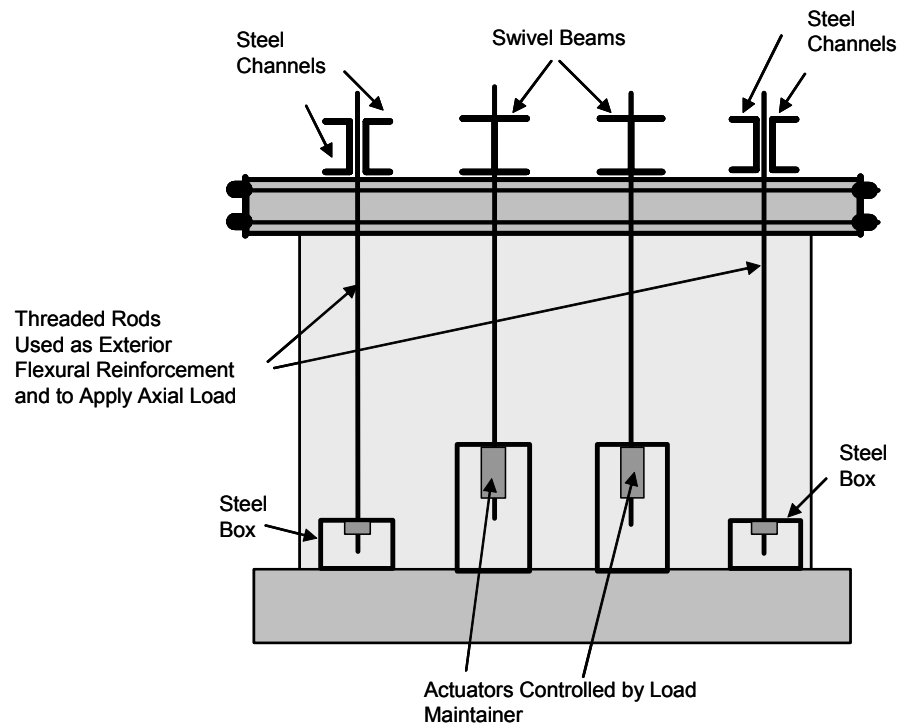
Figure 3.15 Axial load setup for shear-dominated specimens

Figure 3.16 shows a detail of the axial load setup used together with the actuators to apply constant axial load during the tests. In this figure, two threaded rods are connected at one end to a steel swivel beam connected to a steel spreader beam, and at the other end to a swivel steel box bolted to the base beam. The top swivel beam and the bottom swivel box allowed both horizontal and vertical displacements in the wall. The goal of the load maintainer was to ensure constant axial load during the tests.

43
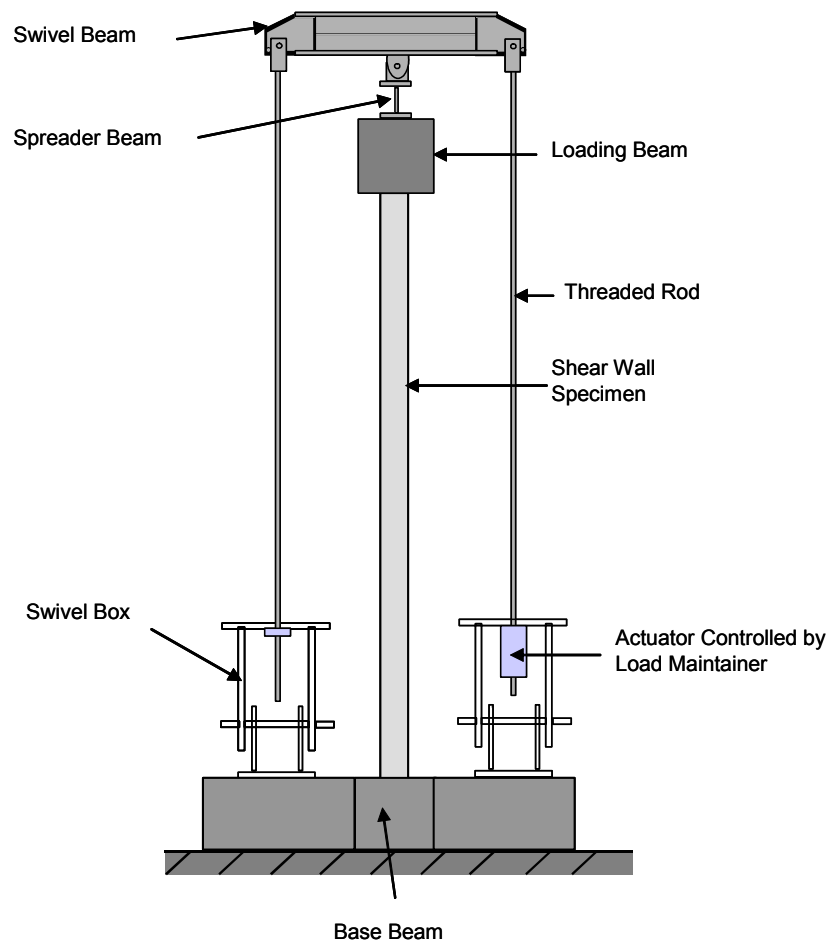
Figure 3.16 Detail of axial load setup used with actuators

Axial load was applied to the flexure-dominated specimens using only hydraulic actuators controlled by a load maintainer (Figure 3.17). The total axial load for each of those specimens was defined by the sum of the axial load applied using the hydraulic actuators and the self weight of the concrete loading beam. Details of the axial load applied to each of the shear wall specimens are presented in Table 3.3.
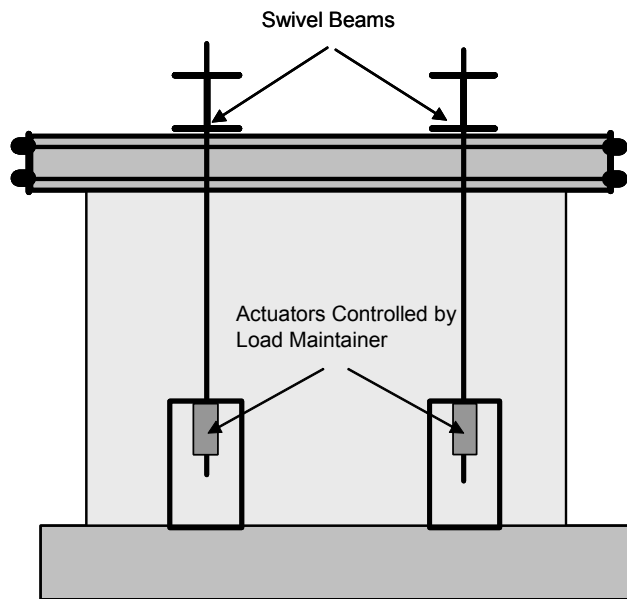
Figure 3.17 Axial load setup for flexure-dominated specimens

3.3.3 Base Beam

The specimens were built on a precast, post-tensioned concrete base beam representing a concrete foundation (Figure 3.18). Each specimen was constructed on a leveling bed of conventional portland cement-lime masonry mortar conforming to ASTM C270, Type S by proportion. To prevent the foundation from sliding or uplifting, the base beam was tied to the reaction floor using post-tensioned rods (Figure 3.18).
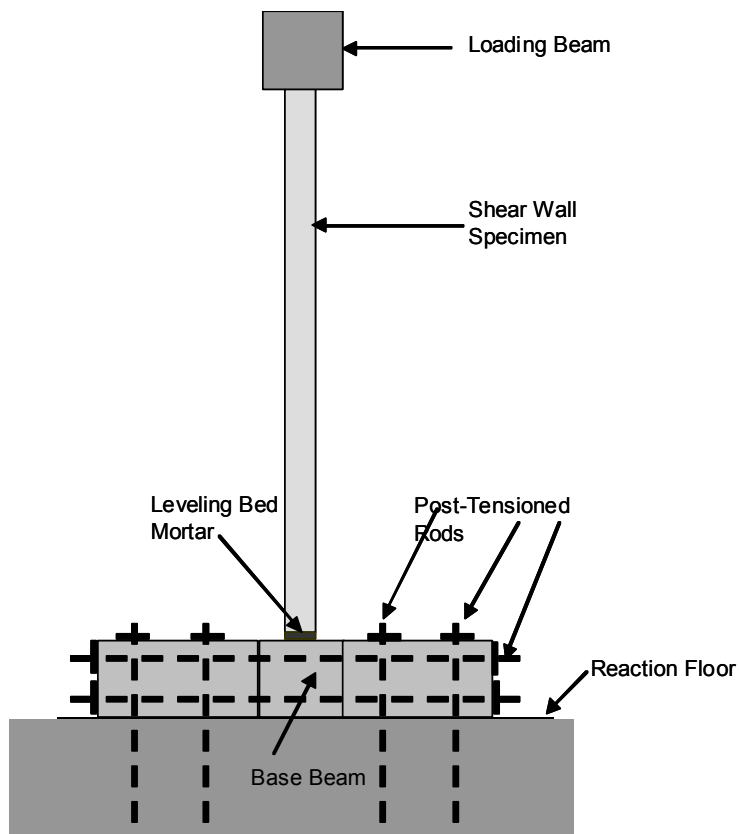
Figure 3.18 Precast concrete base beam used as foundation

Because the concrete base beams were used for construction of more than one AAC shear wall specimen, #5 grade 60 dowel bar splicers (Figure 3.19) were cast into that concrete base beam to provide a mechanical anchorage for the #5 grade 60 internal vertical reinforcement. The vertical reinforcement is upset-threaded at one end as shown in Figure 3.19.

Figure 3.19 Dowel bar splicer and reinforcement enlarged and threaded at end

3.3.4 Lateral Bracing System

The specimens were braced against out-of-plane displacements by cables (Figure 3.20), one end was attached to vertically oriented steel plates attached to the loading beam at two points on both sides of the wall, and the other end to horizontally oriented rods bolted through holes in the flanges of W-shape columns positioned alongside the specimen, and bolted to the reaction floor.
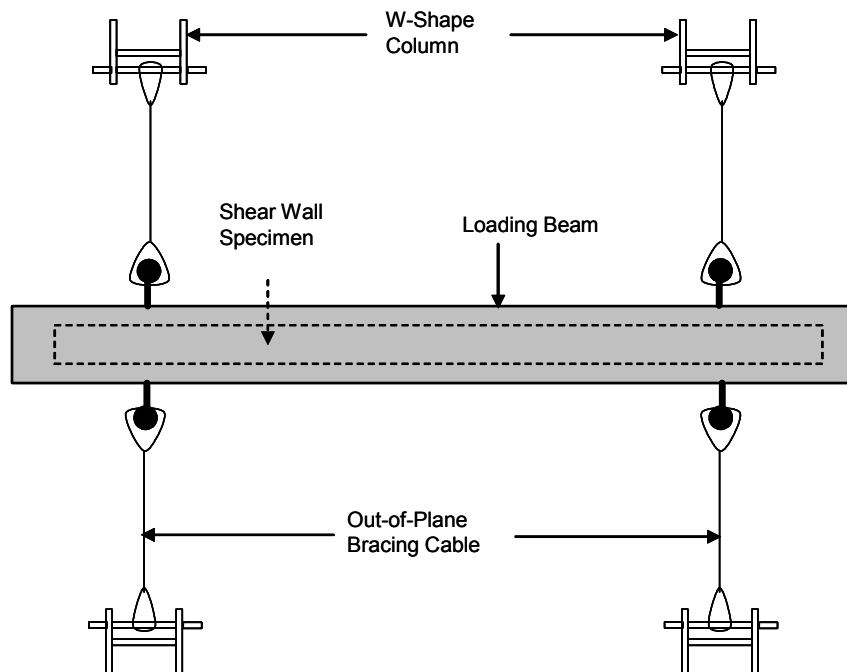
Figure 3.20 Lateral bracing system (plan view)

An elevation view of the test setup used for the shear-dominated specimens is presented in Figure 3.21. An elevation view of the test setup used for the flexure-dominated specimens is presented in Figure 3.22, and a cross-section view of that setup is presented in Figure 3.23. A detail of the connection between the actuators and the loading beam is presented in Figure 3.24.

Figure 3.21 Elevation view of test setup used for the shear-dominated specimens

Figure 3.22 Elevation view of test setup used for the flexure-dominated specimens

49

Figure 3.23 Cross-section view of test setup used for the flexure-dominated specimens

Figure 3.24 Detail of connection between actuators and loading beam

3.4 INSTRUMENTATION AND DATA ACQUISITION

3.4.1 Overall Behavior

The instrumentation used to measure overall hysteretic behavior is shown in Figure 3.25, and included the following:

- load cells to measure the applied horizontal force;

- pressure transducers to measure the pressure in the jacks that applied the horizontal force. This pressure value was converted to an applied force and was used as a check on the load cells;

- linear potentiometers to measure the horizontal displacement at the top of the wall; and

- linear potentiometers to measure the full-height vertical displacement at the ends of the wall.
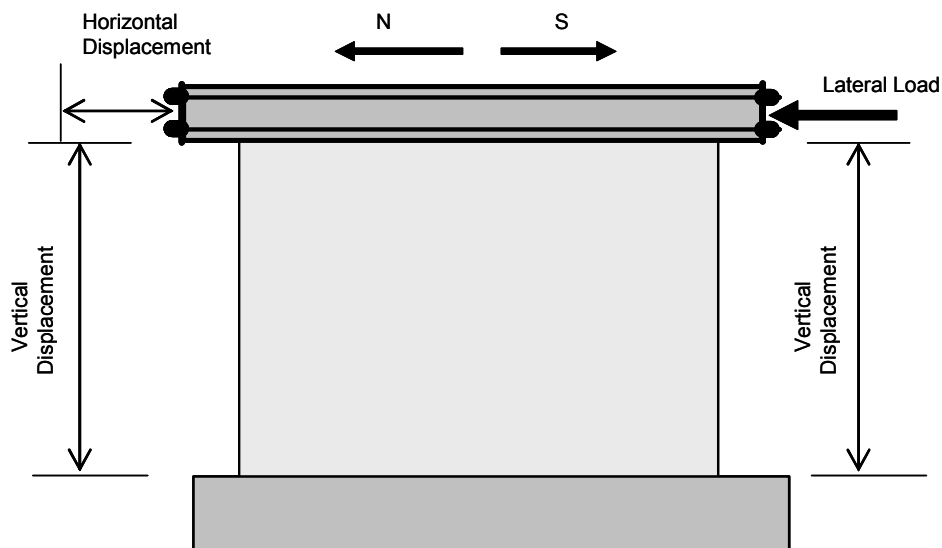
Figure 3.25 Instrumentation for measuring overall behavior (linear
potentiometers)

3.4.2 Local Behavior

The instrumentation used to measure local behavior is shown in Figure 3.26 and Figure 3.27, and included the following:

- linear potentiometers to measure:
    - deformation along the diagonals of the specimen;
    - incremental vertical deformations at the ends of the specimen;
    - slip between the specimen and its base;
    - slip between the base and the floor;
    - slip between the loading beam and the top of the wall;
- a dial gage to measure the pressure in the hydraulic actuators controlled by the load maintainer;
- force washers to measure force in exterior reinforcement; and
- strain gages to measure the lateral force that caused yielding of the internal flexural reinforcement. The strain gages were mounted only on the flexural reinforcement of the flexure-dominated specimens.
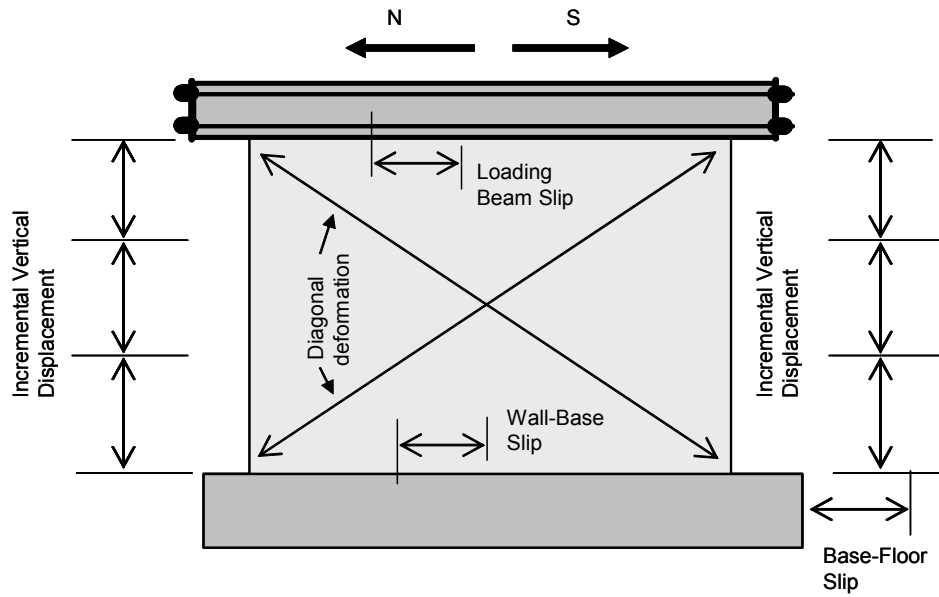
Figure 3.26 Instrumentation to measure local behavior
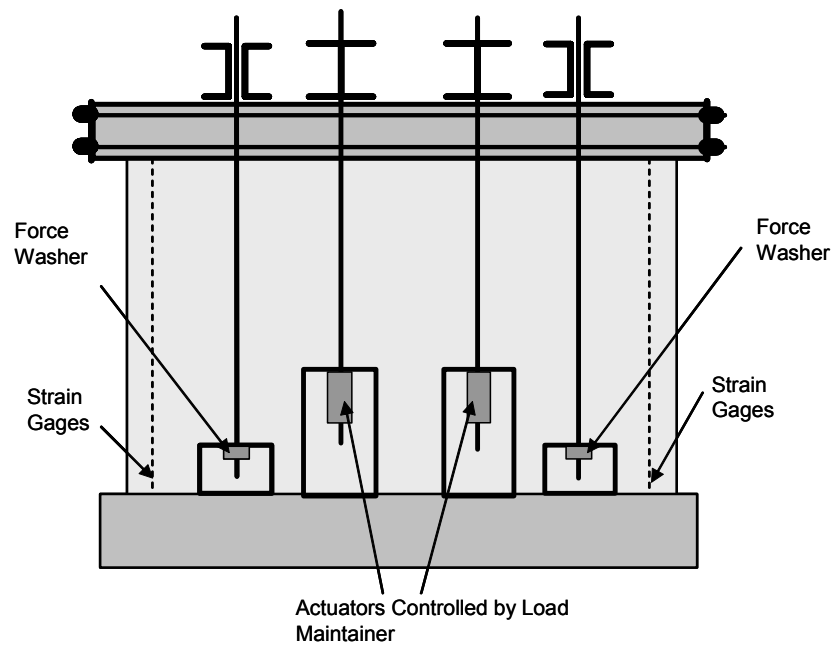
Figure 3.27 Instrumentation to measure local behavior (forces)

53

3.4.3 Data Acquisition

Data were acquired through a Hewlett-Packard 3852 scanner. Analog-to-digital conversion was carried out by a National Instruments card in a Windows-based microcomputer, running under Measure, a National Instruments add-on for the Microsoft Excel® spreadsheet program. Once in Excel format, data were plotted conventionally.

3.5 LOADING HISTORY

The planned in-plane loading history for the shear wall specimens, shown in Figure 3.28, consisted of a series of reversed cycles to monotonically increasing maximum load or displacement amplitudes. At the beginning of the test, target load values were used; after web-shear cracking or yielding of the flexural reinforcement target displacement values were used. The predetermined target values (PV) were based on the loads that were calculated to produce significant changes in the behavior of the specimen (for example, flexural cracking or web-shear cracking). The planned loading history for shear-dominated specimens involved three increments between each target force. Since the predetermined target values for the flexure dominated specimens were smaller than the corresponding values for the shear-dominated specimens were two increments between each target force level were used. After web-shear cracking or yielding of the flexural reinforcement the test was controlled by displacements; a minimum of one cycle at each displacement level was applied.

54
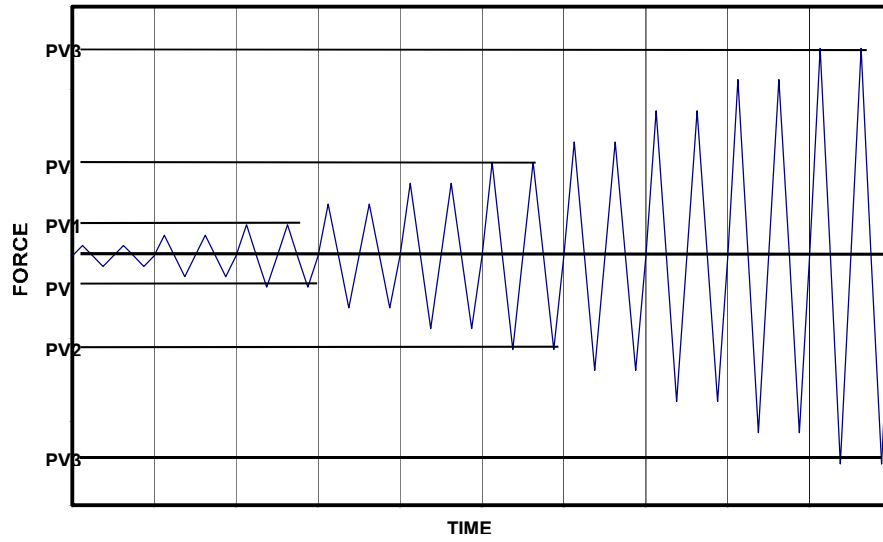
Figure 3.28 Planned loading history for shear wall specimens

CHAPTER 4

Testing Program for Two-story AAC Assemblage Specimen

Phase II of the experimental program consisted of testing a two-story, full-scale assemblage specimen with AAC shear walls and untopped AAC floor diaphragms. The specimen was subjected to reversed cyclic loads applied at each floor level. In Appendix A, the objectives, test setup, loading equipment, loading history and instrumentation of that assemblage are presented.

4.1 OBJECTIVES OF TESTING PROGRAM (PHASE II)

The objectives of the assemblage were: to verify that a system of squat walls designed to fail in a flexure-dominated mode would indeed fail in flexure; to verify proposed design provisions for AAC shear walls; to verify that lateral load could be transferred through AAC floor diaphragms; to verify proposed design procedures for such diaphragms; and to verify the proposed analytical models for the flexure-dominated specimens.

4.2 DESCRIPTION OF SPECIMEN

The Two-Story AAC Assemblage Specimen consisted of two flanged walls connected by floor slabs. The walls were constructed with vertical AAC panels, and the floor slabs were constructed with untopped AAC floor panels. Details of the Two-Story AAC Assemblage Specimen and decisions made in its construction are presented in Appendix A.

CHAPTER 5

Test Results for Shear-Dominated Shear Wall Specimens

This chapter presents the test results and behavior of the eight shear-dominated shear wall specimens. In the following sections, the response of those specimens is discussed with respect to their recorded load-displacement curves, focusing on changes in the in-plane lateral stiffness and strength of the walls as the specimens were loaded and unloaded during the tests. Maximum drift ratios are presented for each of those shear-dominated specimens. The experimental data presented in this chapter, together with that presented in Chapter 6, were used to develop analytical models representing the behavior of AAC shear walls subjected to earthquake ground motions. Response of the shear wall specimens with respect to load history and with regard to the observed cracking patterns, are presented in Tanner (2003). A complete list of the data collected during those tests is presented in Section 3.4. Only those data necessary to describe the above results are presented here.

The load-displacement curves presented in this chapter show applied in-plane shear versus horizontal displacement at the level of load application, or applied in-plane shear versus lateral drift ratio, expressed as a percentage. The lateral drift ratio was calculated as the horizontal displacement at the level of load application, divided by its height (distance between the top of the base and the line of load application). For Shear Wall Specimen 1, the horizontal displacement was corrected for sliding at the base of the wall by subtracting the sliding from the lateral displacement measured at the top of the wall. Expressing the wall behavior without considering slip isolates the effect that other mechanisms, such as web

shear cracking, have on the hysteretic behavior. Even though sliding was observed between two horizontal AAC panels in Shear Wall Specimen 4, the corresponding load-displacement curve was not corrected because no instruments were mounted on that wall to measure the relative movement between those AAC panels. Detailed information on sliding of Shear Wall Specimens 1 and 4 is presented in Tanner (2003). Each figure in this chapter and in Chapter 6 will specify if it has been corrected for sliding.

5.1   BEHAVIOR OF SHEAR-DOMINATED SHEAR WALL SPECIMENS

The changes in the hysteretic load-displacement response of the eight shear-dominated shear wall specimens were in general described by the following:

- initial stiffness;
- stiffness after flexural cracking;
- unloading stiffness after web shear cracking; and
- strength degradation after web shear cracking.

Initial tangent and backbone stiffnesses were calculated for each shear-dominated shear wall specimen. The initial tangent stiffness (K_{ot-o}) was calculated using the slope of the first half load cycle of the load-displacement curve and the initial backbone stiffness (K_{ob-o}) using data from the first load cycles of that load-displacement curve (Figure 5.1). The secant stiffness after flexural cracking was calculated as the applied load at which web-shear cracking was first observed, divided by the corresponding horizontal displacement at that load. F_{ws1} and D_{ws1} are the load and displacement when web shear cracking was first observed in the south direction, and F_{wn1} and D_{wn1} in the north direction respectively. Two secant stiffnesses were calculated for each shear-dominated specimen; one in the south direction (K_{cr-os}) and the other in the north direction

(K_{cr-on}) as shown respectively in Figure 5.2. The unloading stiffness after web shear cracking was calculated using the slope of the unloading branch of the load-displacement curve right after web shear cracking was first observed during the test. Two unloading stiffnesses were calculated for each shear-dominated specimen, one corresponding to loading the specimen in the south direction (K_{u-os}) and the other in the north direction (K_{u-on}) respectively (Figure 5.3). D_{u-os} and D_{u-on} are the maximum observed displacements in the load cycles at which those unloading stiffnesses were calculated in the south and north directions respectively. The strength ratio after web shear cracking was calculated as the maximum applied load in the corresponding next cycle after web shear cracking divided by the applied load at which web shear cracking was first observed during the test. F_{ws2} and F_{wn2} are the maximum loads in the following cycle after web shear cracking was first observed in the south and north directions respectively, and D_{ws2} and D_{wn2} the corresponding displacements at those loads. Two strength ratios were calculated for each shear-dominated specimen, one corresponding to loading the specimen in the south, and the other to the north.

5.1.1 Shear Wall Specimen 1

The initial tangent stiffness and the initial backbone stiffness of Shear Wall Specimen 1 were 678.6 kips/in. (119 kN/mm) and 667 kips/in. (117 kN/mm) respectively (Figure 5.1).
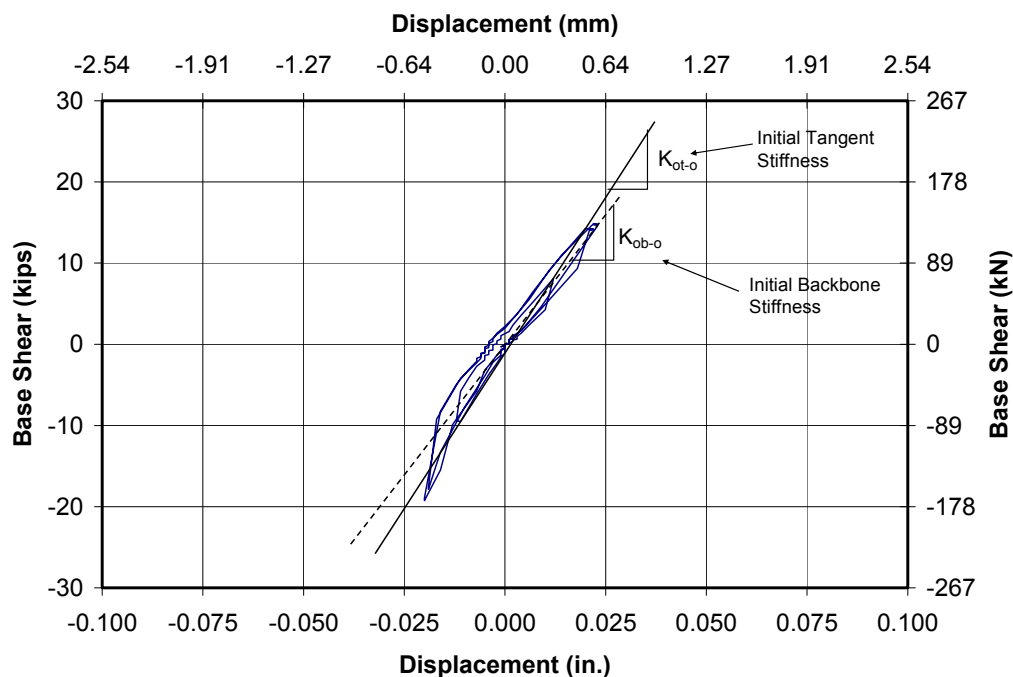
Figure 5.1 Initial tangent and backbone stiffnesses for Shear Wall Specimen 1

Web shear cracking was first observed in this specimen when the wall was loaded in the north direction. The observed load at which web shear cracking was observed in the north direction was 164.2 kips (730.4 kN), and the corresponding horizontal displacement at that load was 0.85 in (21.6 mm). This displacement was not totally corrected for sliding because the instrument used to measure slip between the wall and the concrete base exceeded its stroke. A proposed displacement of 0.65 in. (16.5 mm) equal to that observed when web shear cracking was first observed in the south direction was selected. The corresponding stiffness after flexural cracking calculated using that proposed displacement was 252.6 kips/in. (44.2 kN/mm). The observed load at which web shear cracking was first observed in the south direction was 135.7 kips (603.6 kN), the horizontal displacement was 0.65 in. (16.5 mm), and the corresponding stiffness after

60

flexural cracking was 208.8 kips/in. (36.6 kN/mm). Figure 5.2 shows both secant stiffnesses after flexural cracking for Shear Wall Specimen 1.
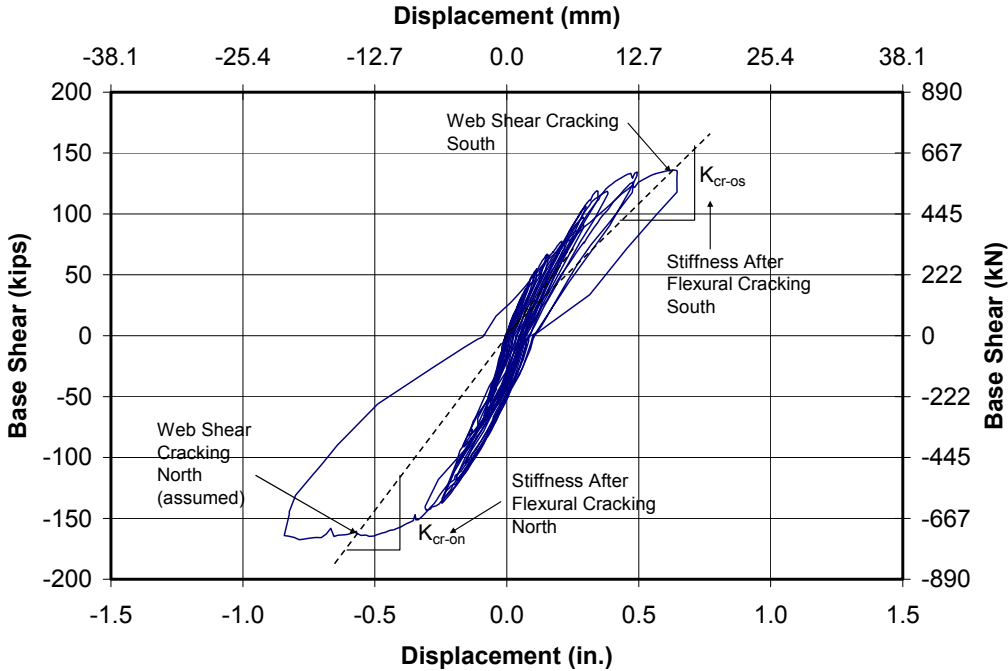
Figure 5.2 Secant stiffnesses after flexural cracking for Shear Wall Specimen 1 (north direction not corrected for sliding)

The unloading stiffnesses after web shear cracking was first observed in the south and north directions were 175.3 kips/in. (30.7 kN/mm) and 209.4 kips/in. (36.7 kN/mm) respectively (Figure 5.3).
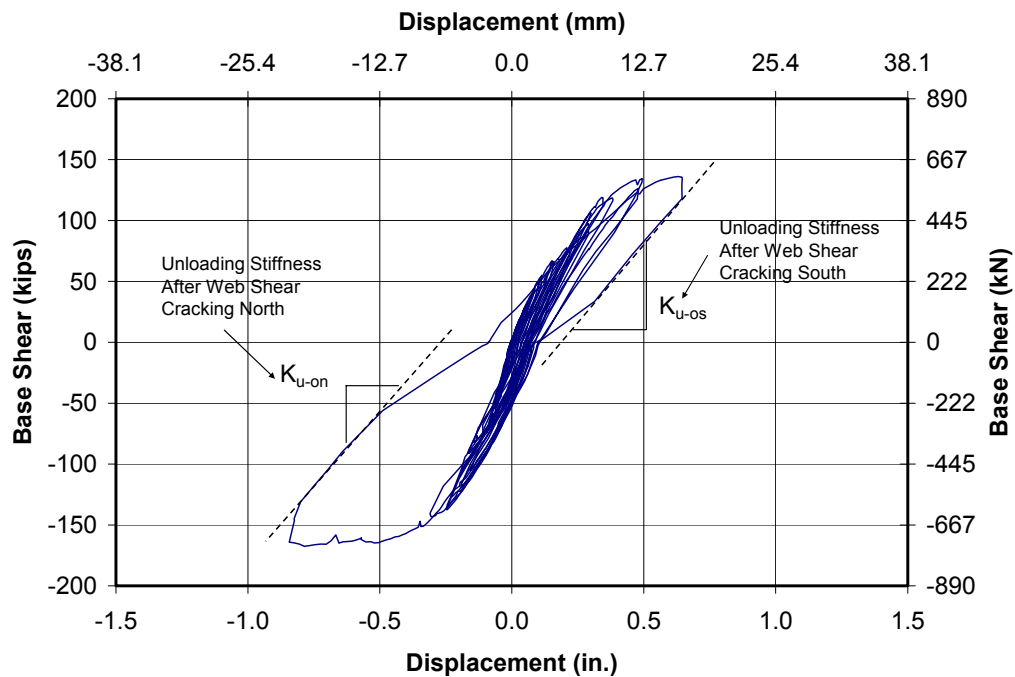
Figure 5.3 Unloading stiffnesses after web shear cracking for Shear Wall Specimen 1 (north direction not corrected for sliding)

The maximum applied load in the corresponding next cycle after web shear cracking was first observed in the south direction was 67 kips (298 kN). The horizontal displacement at that load was 0.78 in. (19.8 mm), and the corresponding strength ratio was 0.49. The maximum applied load in the corresponding next cycle after web shear cracking was first observed in the north direction was 134.4 kips (597.8 kN). The horizontal displacement at that load was 1.06 in. (26.9 mm), and the corresponding strength ratio was 0.81. Both maximum applied loads in the next corresponding cycles after web shear cracking are shown in Figure 5.4 for Shear Wall Specimen 1. The complete hysteretic load-displacement response of Shear Wall Specimen 1 at the end of the test is presented in Figure 5.5.

Figure 5.4 Maximum applied load after web shear cracking in the south and north directions for Shear Wall Specimen 1 (north direction not corrected for sliding)
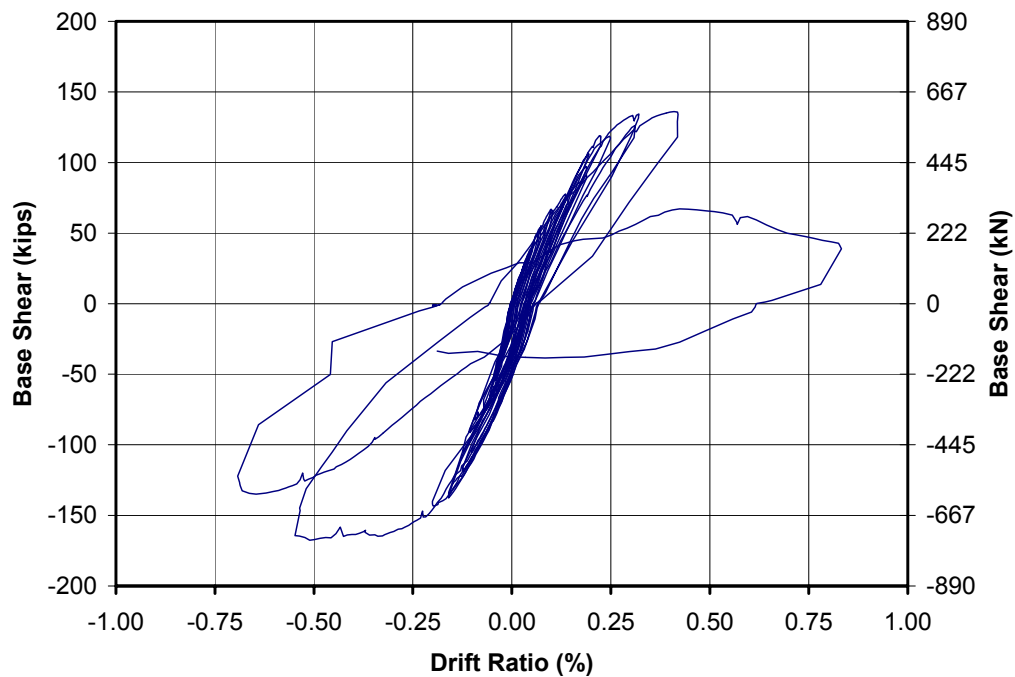
Figure 5.5 Load-displacement response of Shear Wall Specimen 1 at the end of the test (north direction not corrected for sliding)

5.1.2   Shear Wall Specimen 2

In this specimen, two shrinkage cracks had already formed along the height of the wall prior to testing. Shortly after flexural cracking was observed, two new vertical cracks formed, separating the wall into a number of individual walls of different sections. The behavior of this specimen was controlled by the behavior of those individual walls. Because the behavior of this specimen was not the behavior of a single monolithic wall, the load-displacement response is not included in this dissertation.   Detailed information on the behavior of this specimen is presented in Tanner (2003).

5.1.3 Shear Wall Specimen 3

The initial tangent and backbone stiffnesses for Shear Wall Specimen 3 were 732.1 kips/in. (128.2 kN/mm) and 704.8 kips/in. (123.4 kN/mm) respectively. Web shear cracking was first observed in this specimen when it was loaded in the north direction. The load at which web shear cracking was first observed in the north direction was 81.3 kips (361.6 kN). The horizontal displacement at that load was 0.14 in. (3.56 mm), and the corresponding stiffness after flexural cracking was 580.7 kips/in. (101.7 kN/mm). The load at which web shear cracking was first observed in the south direction was 98.7 kips (439 kN). The horizontal displacement at that load was 0.19 in. (4.8 mm), and the corresponding stiffness after flexural cracking was 519.5 kips/in. (91 kN/mm). Figure 5.6 shows the points at which web shear cracking was first observed in the south and north directions. The unloading stiffnesses after web shear cracking for this specimen corresponding to the south and north directions were 534.4 kips/in. (93.6 kN/mm) and 546.7 kips/in. (95.7 kN/mm) respectively (Figure 5.6). The maximum displacements before unloading the specimen in the south and north directions were 0.22 in. (5.6 mm) and 0.15 in. (3.8 mm) respectively.
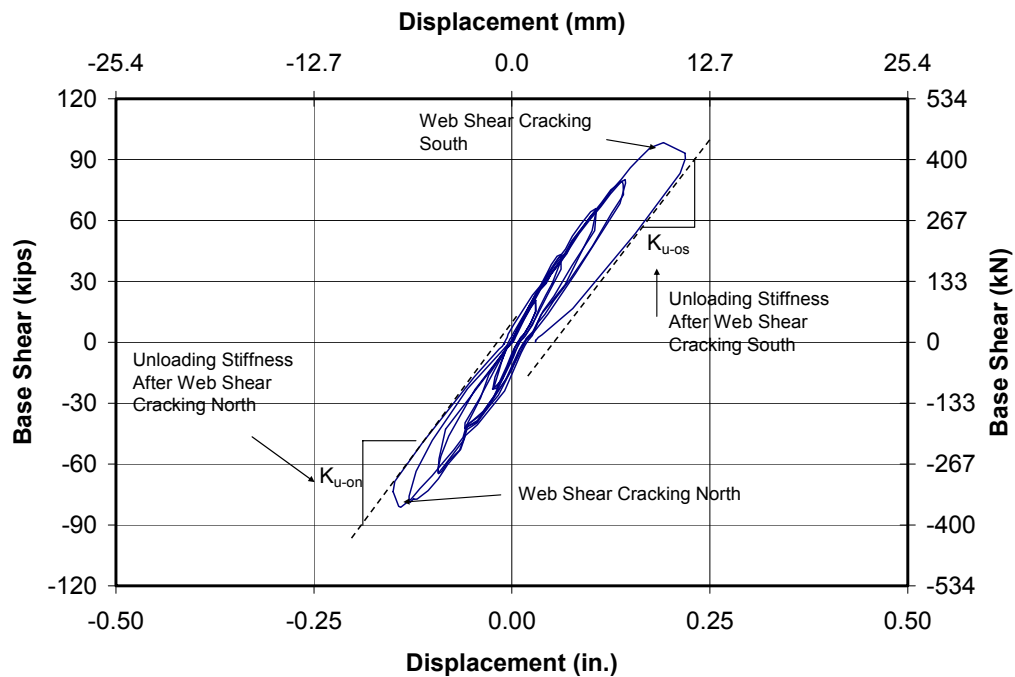
***Figure 5.6 Points at which web shear cracking was first observed and
unloading stiffnesses after web shear cracking for Shear Wall Specimen 3***

The maximum applied load in the corresponding next cycle after web shear cracking was first observed in the south direction was 101 kips (449.2 kN). The horizontal displacement at that load was 0.26 in. (6.6 mm), and the corresponding strength ratio was 1.02. The maximum applied load in the corresponding cycle after web shear cracking was first observed in the north direction was 99.5 kips (442.6 kN). The horizontal displacement was 0.28 in. (7.1 mm), and the corresponding strength ratio was 1.22. Both maximum applied loads in the corresponding next cycles after web shear cracking for Shear Wall Specimen 3 are shown in Figure 5.7. The complete hysteretic load-displacement response of Shear Wall Specimen 3 at the end of the test is presented in Figure 5.8.
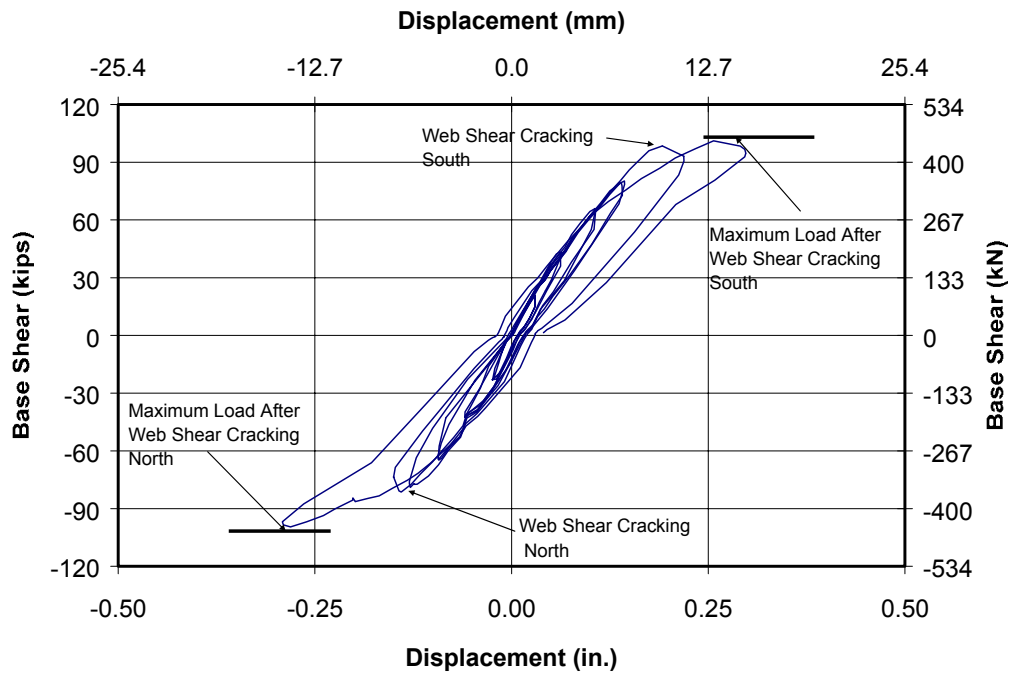
Figure 5.7 Maximum applied load after web shear cracking was first observed in the south and north directions for Shear Wall Specimen 3
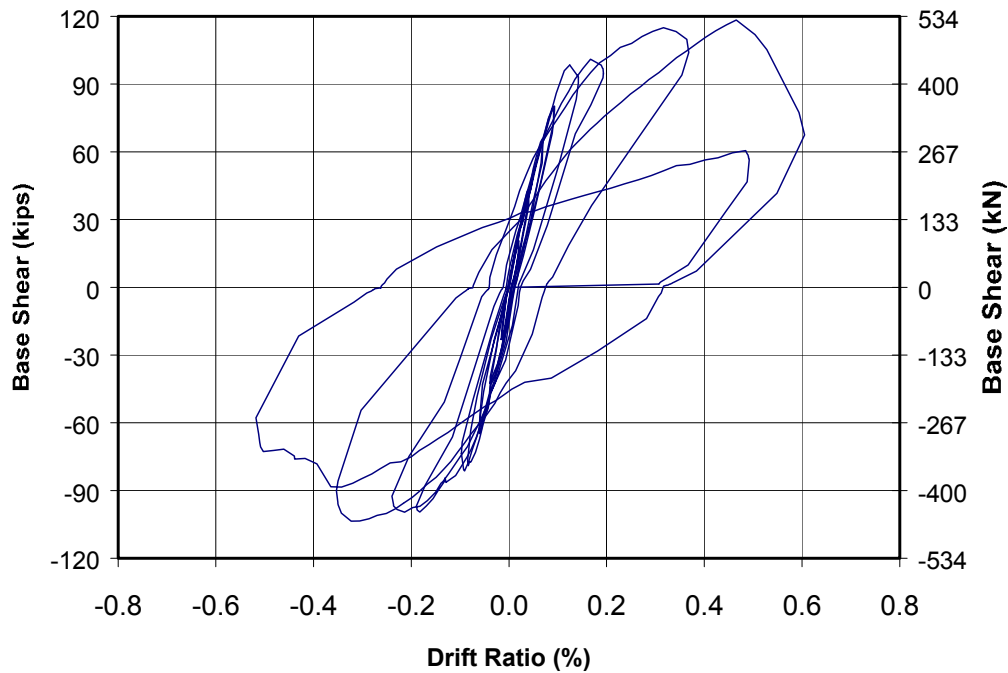
Figure 5.8 Load-displacement response at the end of the test for Shear Wall Specimen 3

5.1.4 Shear Wall Specimen 4

The initial tangent and backbone stiffness for Shear Wall Specimen 4 were 591.8 kips/in. (103.6 kN/mm) and 559.5 kips/in. (98 kN/mm) respectively. Web shear cracking was first observed in this specimen when it was loaded in the south direction. The load at which web shear cracking was first observed in the south direction was 110.5 kips (491.5 kN). The horizontal displacement at that load was 0.27 in. (6.9 mm), and the corresponding stiffness after flexural cracking was 409.3 kips/in. (71.7 kN/mm). The load at which web shear cracking was first observed in the north direction was 107.7 kips (479 kN). The horizontal displacement at that load was 0.25 in. (6.4 mm), and the corresponding stiffness after flexural cracking was 430.8 kips/in. (75.4 kN/mm). Figure 5.9 shows the

points at which web shear cracking was first observed in the south and north directions. The unloading stiffnesses after web shear cracking of this specimen in the south and north directions were 377.7 kips/in. (66.1 kN/mm) and 359.4 kips/in. (62.9 kN/mm) respectively (Figure 5.9). The maximum displacements before unloading the specimen in the south and north directions were 0.28 in. (7.1) and 0.26 in (6.6 mm) respectively.
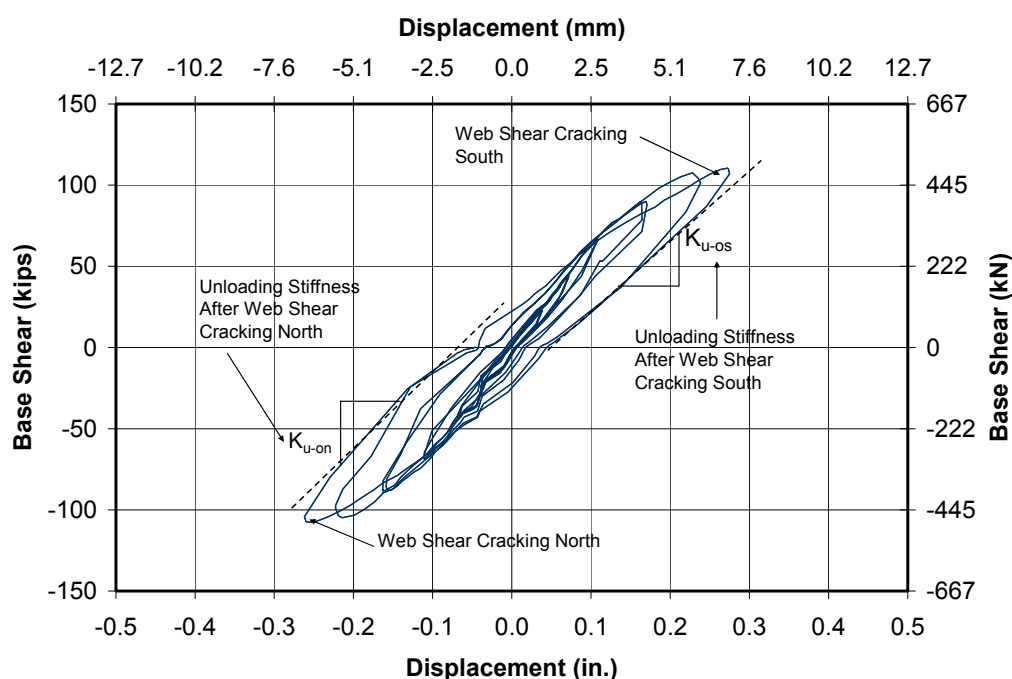
Figure 5.9 Points at which web shear cracking was first observed and unloading stiffnesses after web shear cracking for Shear Wall Specimen 4

The maximum applied load in the corresponding next cycle after web shear cracking was first observed in the south direction was 126.2 kips (561.3 kN). The horizontal displacement at that load was 0.38 in. (9.7 mm), and the corresponding strength ratio was 1.14. The maximum applied load in the corresponding cycle after web shear cracking was first observed in the north

direction was 109.3 kips (486.2 kN), the horizontal displacement was 0.32 in. (8.13 mm), and the corresponding strength ratio was 1.01. Both maximum applied loads in the corresponding next cycles after web shear cracking for Shear Wall Specimen 4 are shown in Figure 5.10. The complete hysteretic load-displacement response of Shear Wall Specimen 4 at the end of the test is presented in Figure 5.11
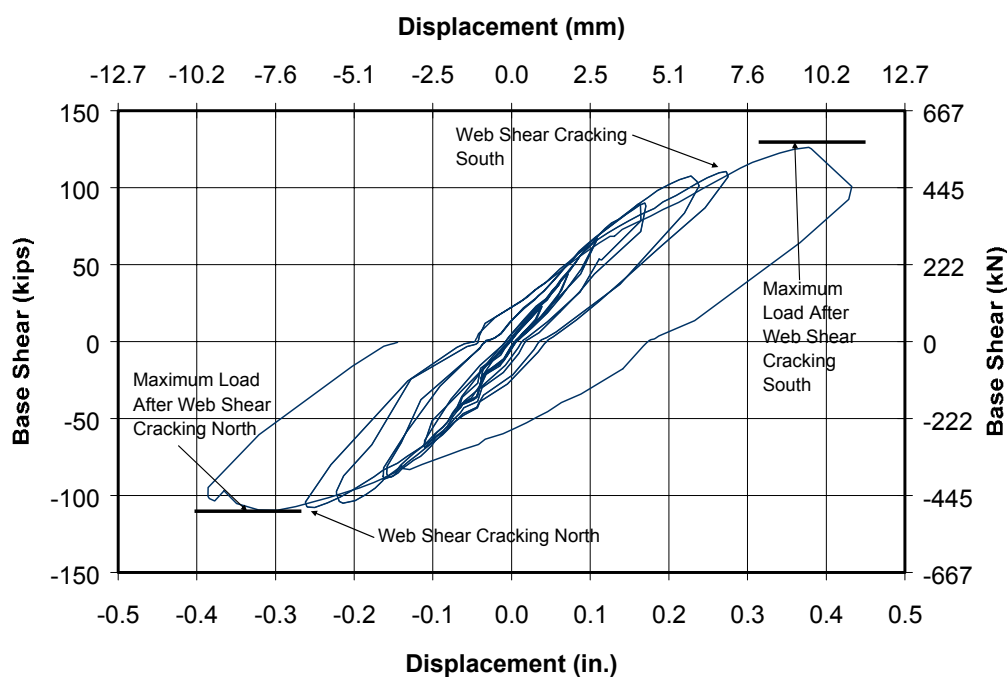
Figure 5.10 Maximum applied load after web shear cracking was first observed in the south and north directions for Shear Wall Specimen 4
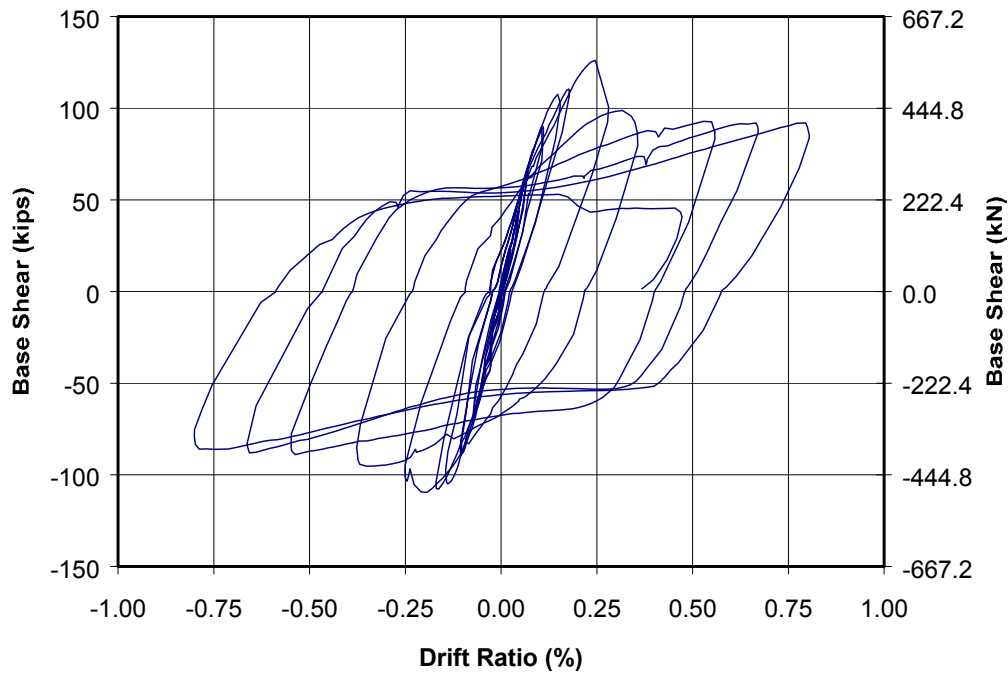
Figure 5.11 Load-displacement response at the end of the test for Shear Wall Specimen 4 (including sliding)

5.1.5 Shear Wall Specimen 5

The initial tangent stiffness and the initial backbone stiffness for Shear Wall Specimen 5 were 771.8 kips/in. (135.1 kN/mm) and 805.8 kips/in. (141.1 kN/mm) respectively. Web shear cracking was first observed in this specimen when it was loaded in the south direction. The load at which web shear cracking was first observed in the south direction was 62.2 kips (276.7 kN). The horizontal displacement at that load was 0.11 in. (2.8 mm), and the corresponding stiffness after flexural cracking was 564.5 kips/in. (98.8 kN/mm). The load at which web shear cracking was first observed in the north direction was 64.1 kips (285.1 kN). The horizontal displacement at that load was 0.095 in. (2.4 mm), and the

corresponding stiffness after flexural cracking was 674.7 kips/in. (118.1 kN/mm). Figure 5.12 shows the points at which web shear cracking was first observed in the south and north directions. The unloading stiffnesses after web shear cracking of this specimen corresponding to the south and north directions were 460.2 kips/in. (80.6 kN/mm) and 546.8 kips/in. (95.7 kN/mm) respectively. The maximum displacements before unloading the specimen in the south and north directions were 0.16 in. (4.1 mm) and 0.14 in. (3.6 mm) respectively.
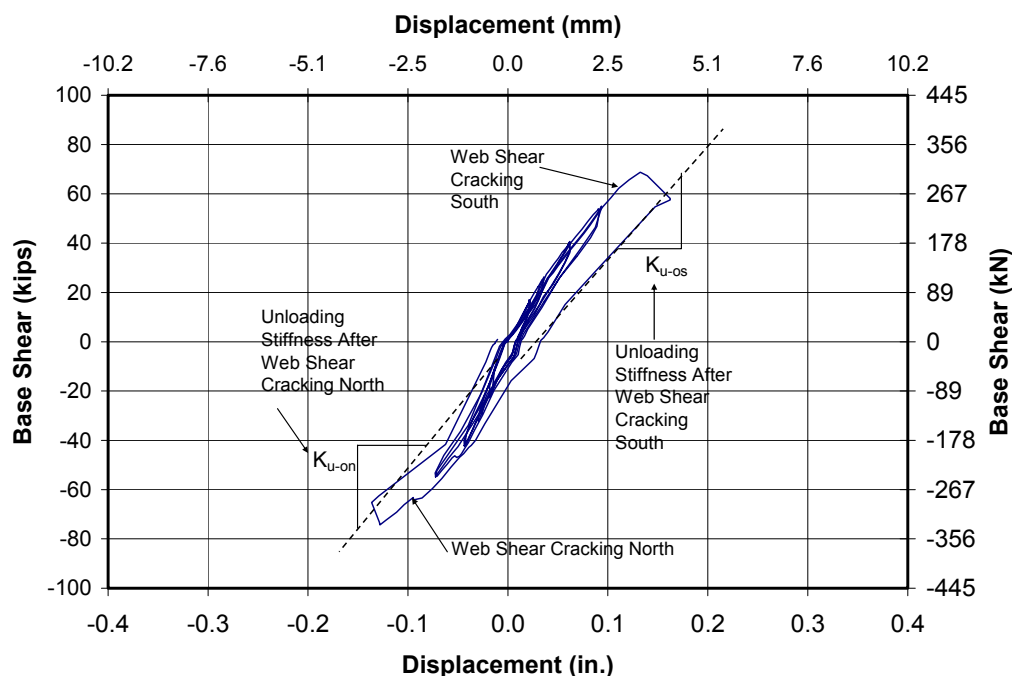
Figure 5.12 Points at which web shear cracking was first observed and unloading stiffnesses after web shear cracking for Shear Wall Specimen 5

The maximum applied load in the corresponding next cycle after web shear cracking was first observed in the south direction was 71.8 kips (319.4 kN). The horizontal displacement at that load was 0.26 in. (6.6 mm), and the corresponding strength ratio was 1.15. The maximum applied load in the

72

corresponding cycle after web shear cracking was first observed in the north direction was 73.7 kips (327.8 kN). The horizontal displacement was 0.22 in. (5.6 mm), and the corresponding strength ratio was 1.15. Both maximum applied loads in the corresponding next cycles after web shear cracking for Shear Wall Specimen 5 are shown in Figure 5.13.
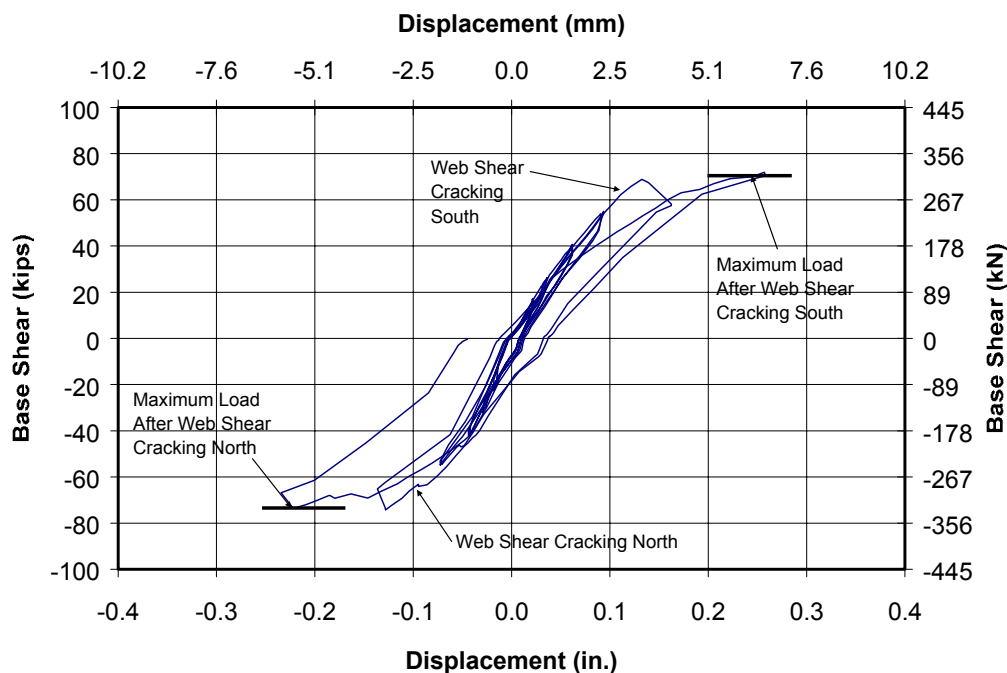
Figure 5.13 Maximum applied load after web shear cracking was first observed in the south and north directions for Shear Wall Specimen 5

The complete hysteretic load-displacement response of Shear Wall Specimen 5 at the end of the test is presented in Figure 5.14.
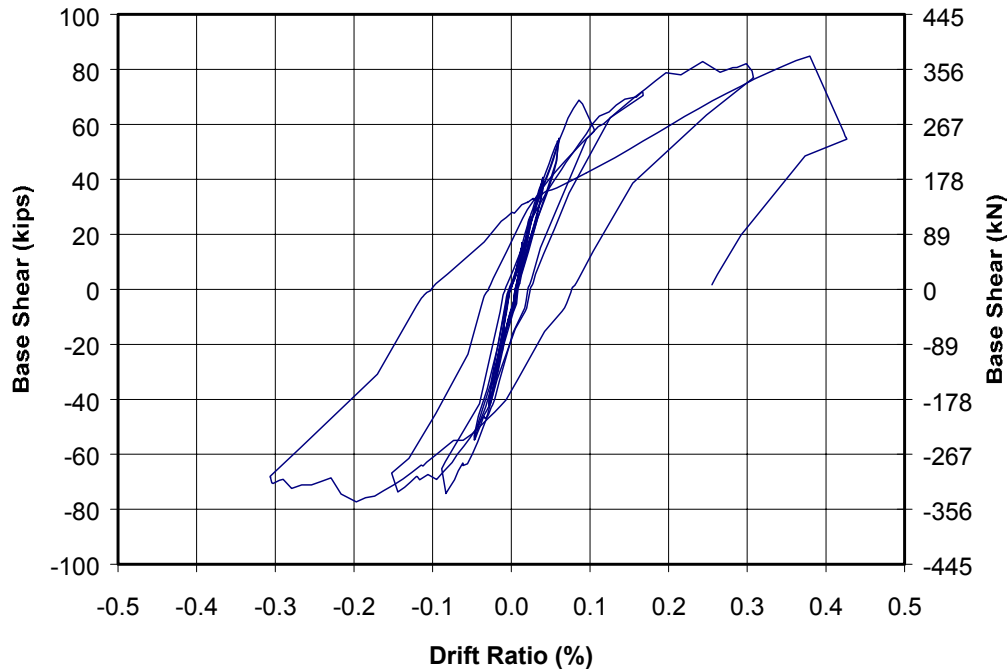
Figure 5.14 Load-displacement response at the end of the test for Shear Wall Specimen 5

5.1.6   Shear Wall Specimen 7

The initial tangent and backbone stiffnesses for Shear Wall Specimen 7 were 300 kips/in. (52.5 kN/mm) and 308.4 kips/in. (54 kN/mm) respectively. Web shear cracking was first observed in this specimen when it was loaded in the south direction. The load at which web shear cracking was first observed in the south direction was 57.4 kips (255.3 kN). The horizontal displacement at that load was 0.59 in. (15 mm), and the corresponding stiffness after flexural cracking was 94 kips/in. (16.5 kN/mm). The load at which web shear cracking was first observed in the north direction was 59.2 kips (263.3 kN).   The horizontal displacement was 0.63 in. (16 mm), and the corresponding stiffness after flexural cracking was 97.8 kips/in. (17.1 kN/mm). Figure 5.15 shows the points at which

74

web shear cracking was first observed in the south and north directions. The unloading stiffnesses after web shear cracking of this specimen corresponding to the south and north directions were 98.8 kips/in. (17.3 kN/mm) and 99.9 kips/in. (17.5 kN/mm) respectively (Figure 5.15). The maximum displacements before unloading the specimen in the south and north directions were 0.65 in. (16.5 mm) and 0.65 in. (16.5 mm) respectively.
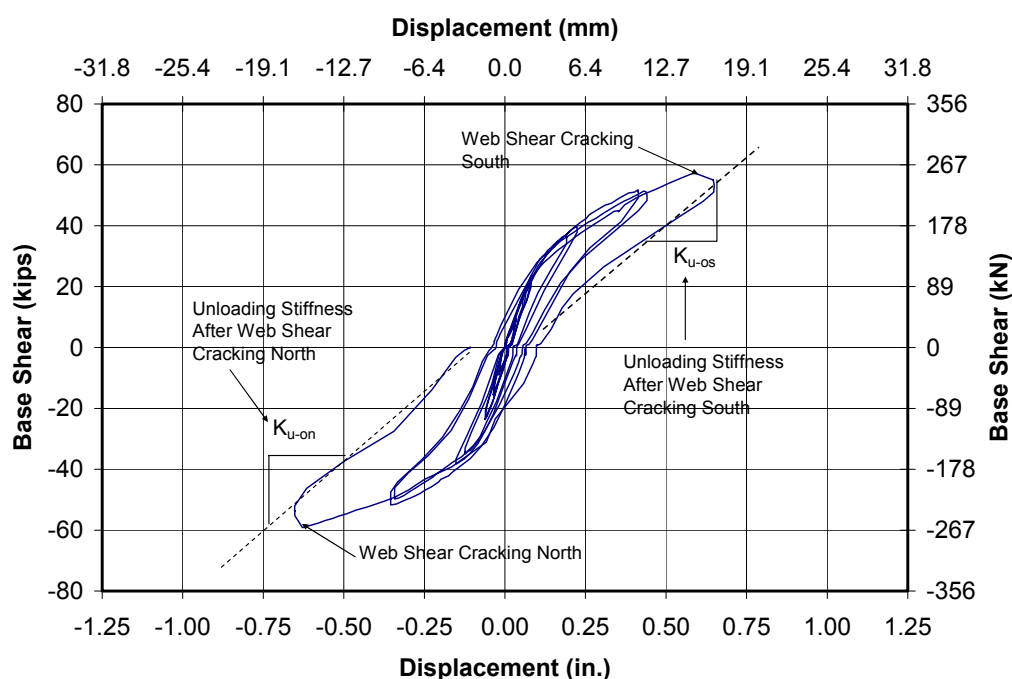
Figure 5.15 Points at which web shear cracking was first observed and unloading stiffnesses after web shear cracking for Shear Wall Specimen 7

The maximum applied load in the corresponding next cycle after web shear cracking was first observed in the south direction was 59.2 kips (263.3 kN). The horizontal displacement at that load was 0.85 in. (21.6 mm), and the corresponding strength ratio was 1.03. The maximum applied load in the corresponding cycle after web shear cracking was first observed in the north

direction was 52.9 kips (235.3 kN). The horizontal displacement was 0.92 in. (23.4 mm), and the corresponding strength ratio was 0.89. Both maximum applied loads in the corresponding next cycles after web shear cracking for Shear Wall Specimen 7 are shown in Figure 5.16.
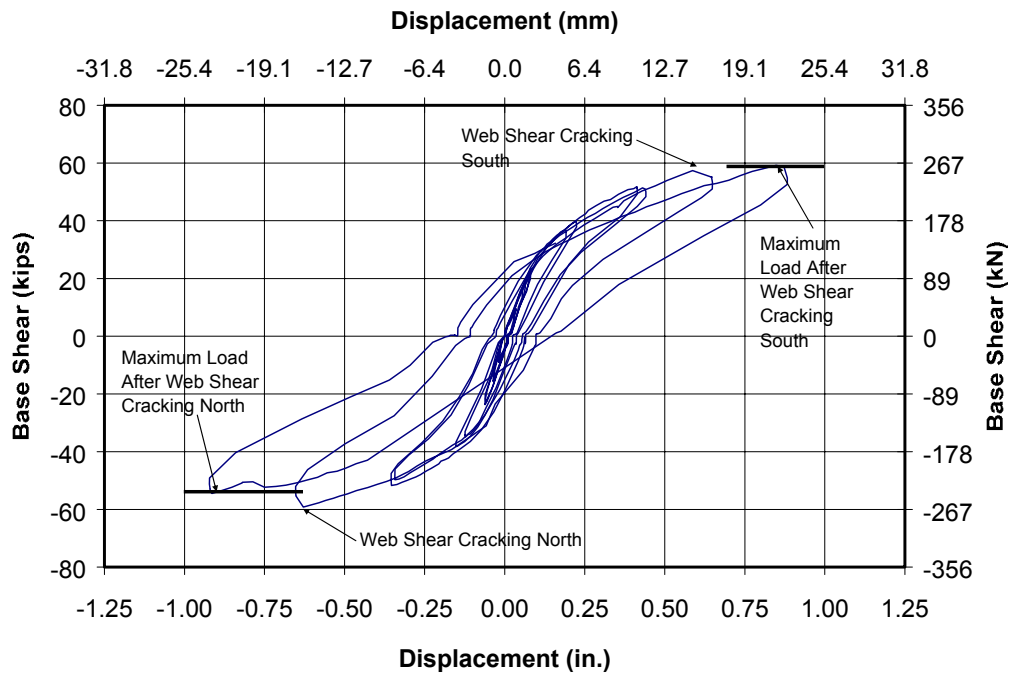
Figure 5.16 Maximum applied load after web shear cracking was first observed in the south and north directions for Shear Wall Specimen 7

The complete hysteretic load-displacement response of Shear Wall Specimen 7 at the end of the test is presented in Figure 5.17.

76
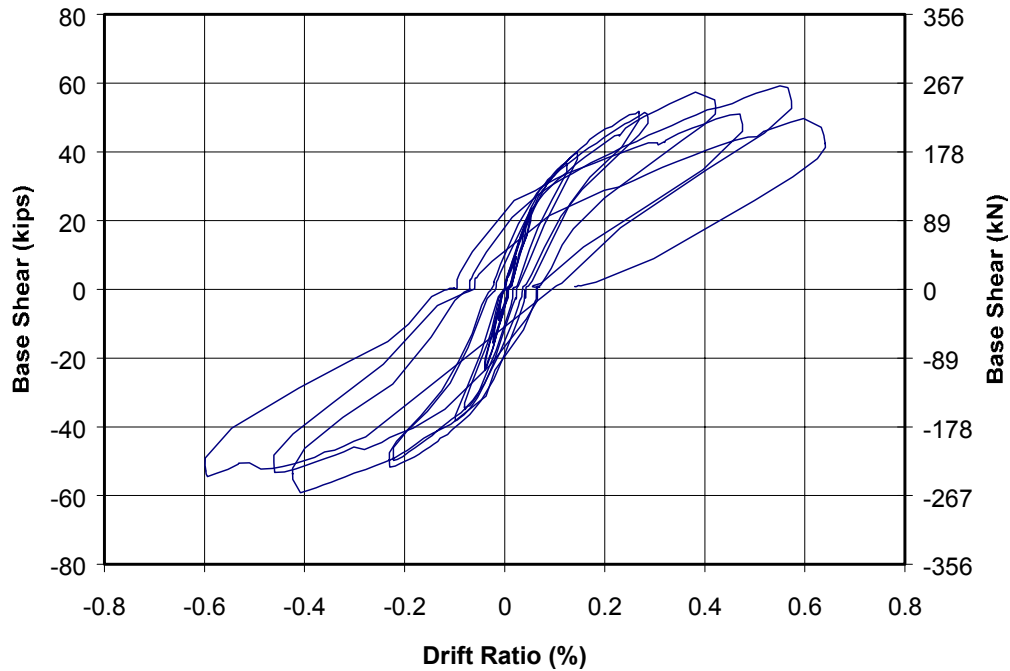
***Figure 5.17 Load-displacement response at the end of the test for Shear Wall
Specimen 7***

5.1.7   Shear Wall Specimen 9

The initial tangent stiffness and the initial backbone stiffness for Shear
Wall Specimen 9 were 143 kips/in. (25 kN/mm) and 138.2 kips/in. (24.2 kN/mm)
respectively. Web shear cracking was first observed in this specimen when it was
loaded in the south direction. The load at which web shear cracking was first
observed in the south direction was 37.4 kips (166.4 kN).   The horizontal
displacement at that load was 1.12 in. (28.4 mm), and the corresponding stiffness
after flexural cracking was 33.4 kips/in. (5.8 kN/mm). The load at which web
shear cracking was first observed in the north direction was 42.2 kips (187.7 kN).
The horizontal displacement at that load was 0.84 in. (21.3 mm), and the
corresponding stiffness after flexural cracking was 50.2 kips/in. (8.8 kN/mm).

77

Figure 5.18 shows the points at which web shear cracking was first observed in the south and north directions. The unloading stiffnesses after web shear cracking of this specimen corresponding to the south and north directions were 33.9 kips/in. (5.9 kN/mm) and 26.2 kips/in. (4.6 kN/mm) respectively. The maximum displacements before unloading the specimen in the south and north directions were 1.14 in. (29 mm) and 1.21 in. (30.7 mm) respectively (Figure 5.18).
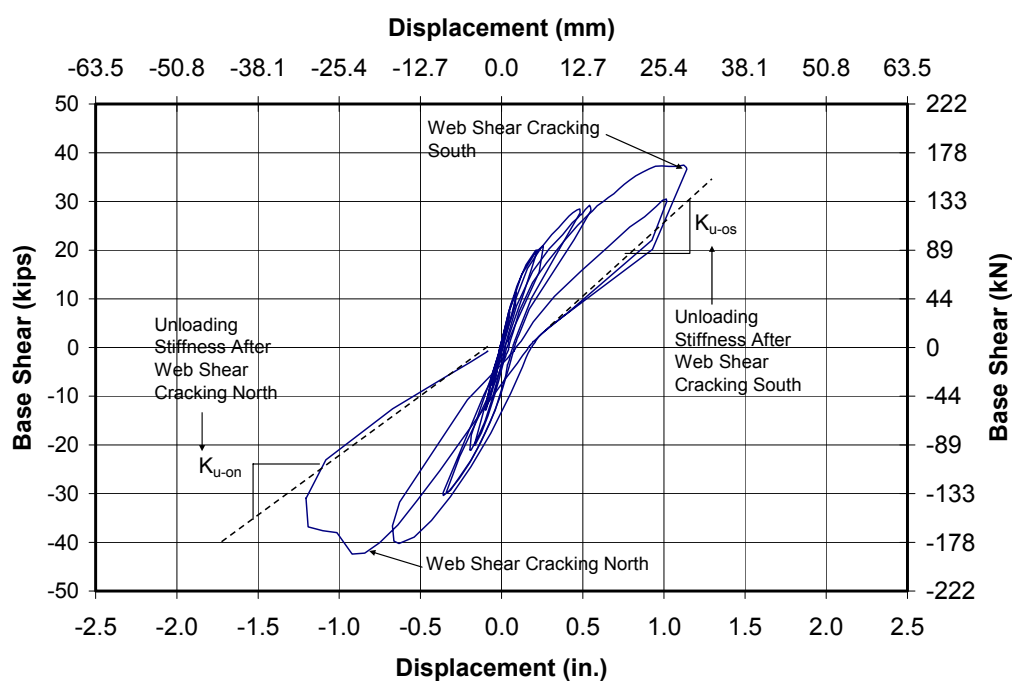
Figure 5.18 Points at which web shear cracking was first observed and unloading stiffnesses after web shear cracking for Shear Wall Specimen 9

The maximum applied load in the corresponding next cycle after web shear cracking was first observed in the south direction was 30.3 kips (134.8 kN), the horizontal displacement at that load was 1.47 in. (37.3 mm), and the corresponding strength ratio was 0.81. The maximum applied load in the corresponding next cycle after web shear cracking was first observed in the north

direction was 15.3 kips (68.1 kN). The horizontal displacement at that load was 1.2 in. (30.5 mm), and the corresponding strength ratio was 0.36. The maximum applied load in the corresponding next cycle after web shear cracking in the south and north directions for Shear Wall Specimen 7 are shown in Figure 5.19.
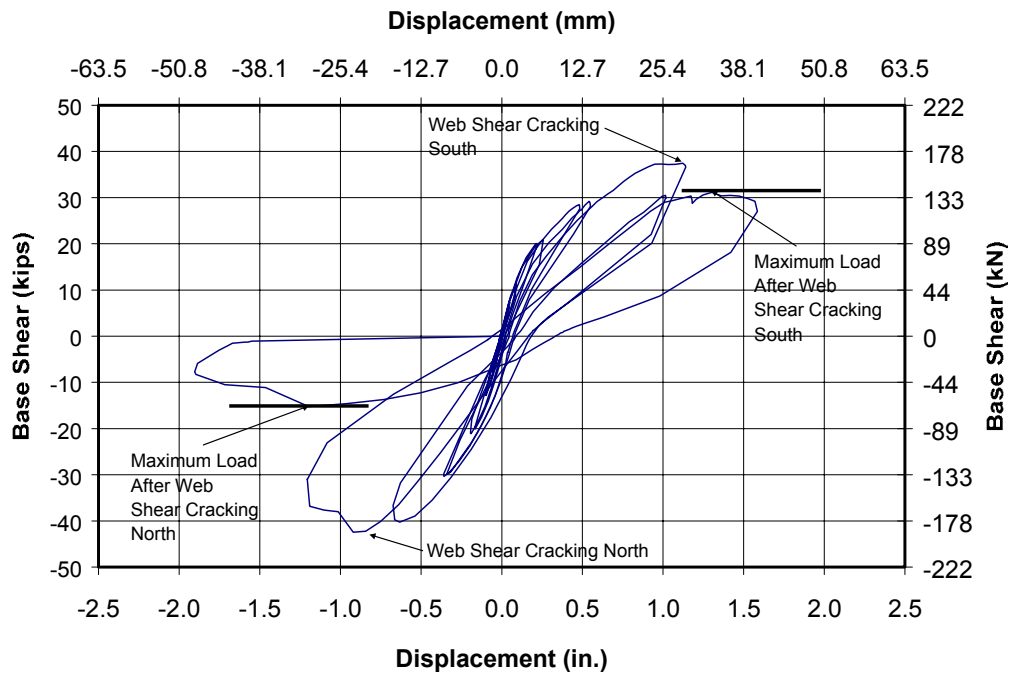
Figure 5.19 Maximum applied load after web shear cracking was first observed in the south and north direction for Shear Wall Specimen 9

The complete hysteretic load-displacement response of Shear Wall specimen 9 at the end of the test is presented in Figure 5.20.
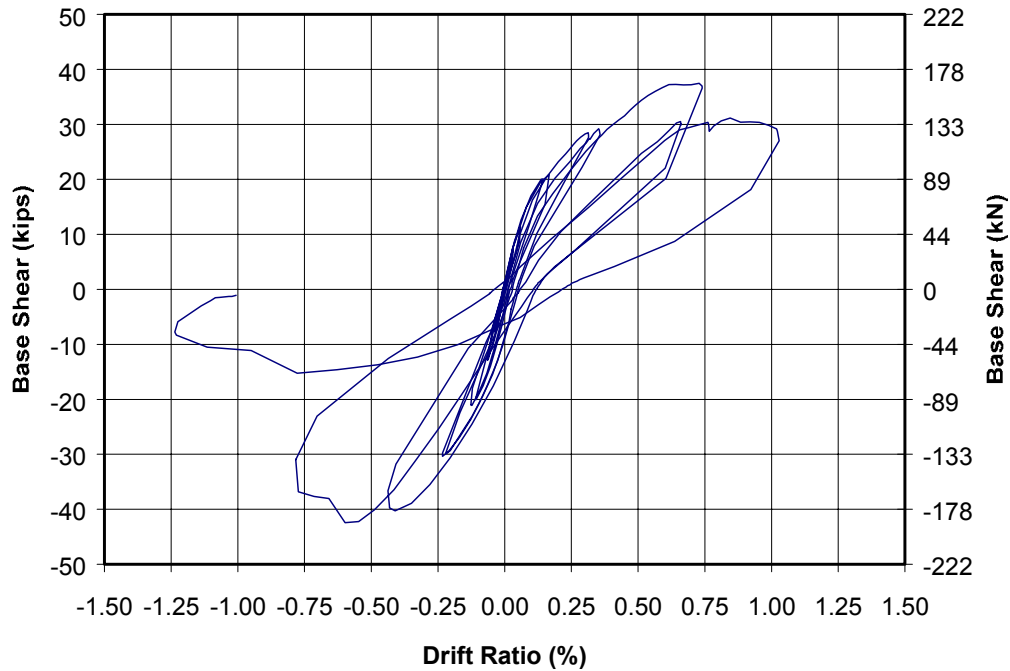
Figure 5.20 Load-displacement response at the end of the test for Shear Wall Specimen 9

5.1.8 Shear Wall Specimen 11

The initial tangent stiffness and the initial backbone stiffness for Shear Wall Specimen 11 were 34.9 kips/in. (6.1 kN/mm) and 32.3 kips/in. (5.7 kN/mm) respectively. Web shear cracking was observed in this specimen only when the wall was loaded in the south direction. The load at which web shear cracking was observed in the south direction was 15.6 kips (69.4 kN).   The horizontal displacement at that load was 1.93 in. (49 mm), and the corresponding stiffness after flexural cracking was 8.1 kips/in. (1.4 kN/mm). No additional information was obtained from this specimen because the wall failed immediately after web shear cracking was first observed in the south direction. Figure 5.21 shows the point at which web shear cracking was observed in the south direction.   The

complete hysteretic load-displacement response of Shear Wall Specimen 11 at the
end of the test is presented in Figure 5.22.

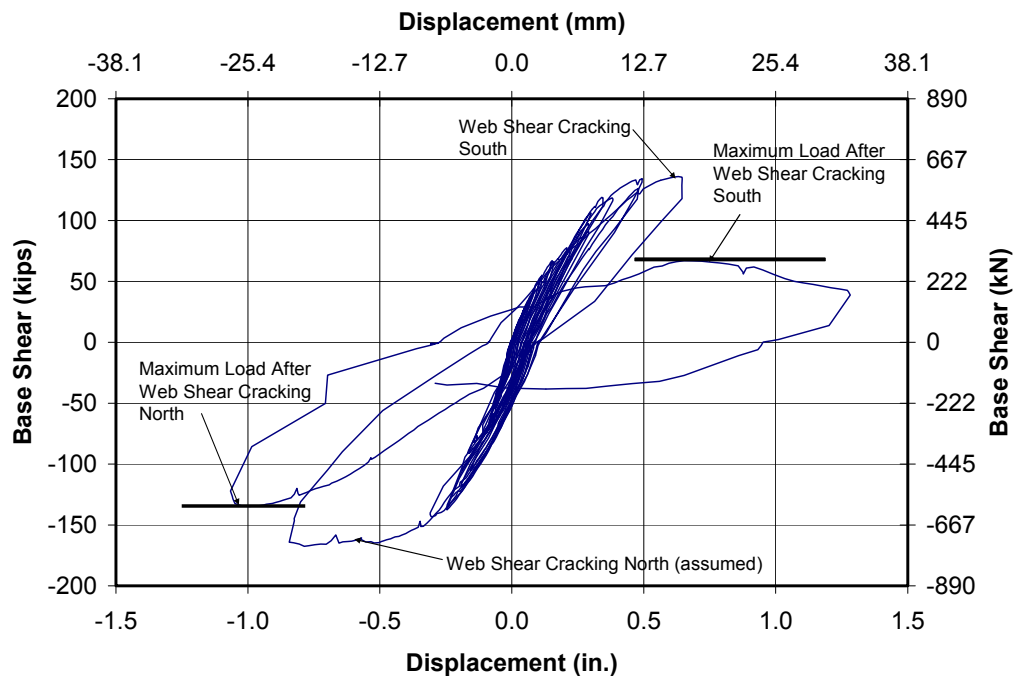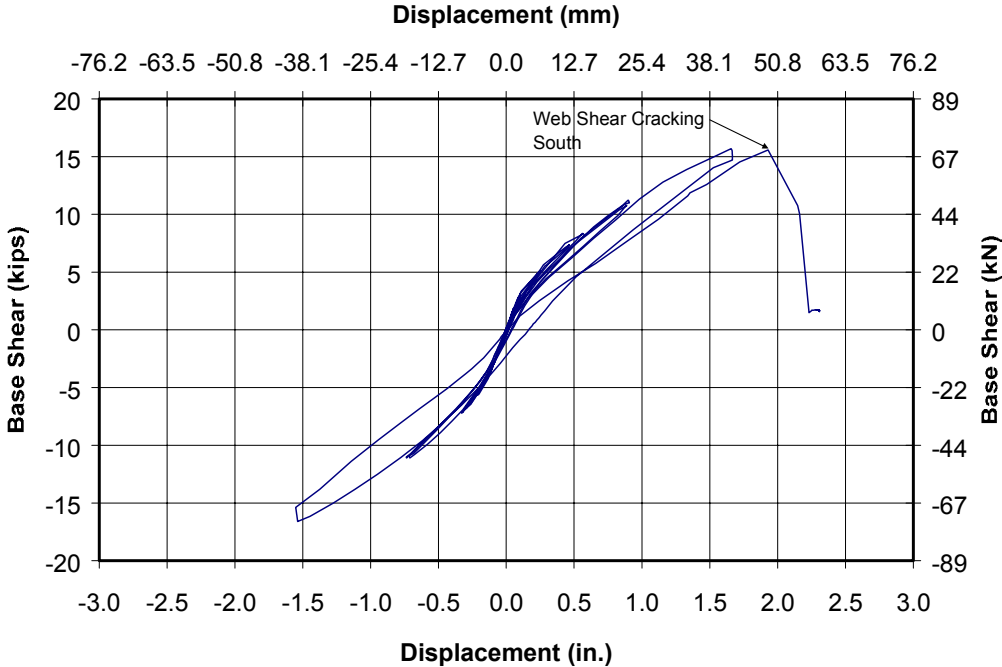*Figure 5.21 Point at which web shear cracking was observed in the south
direction for Shear Wall Specimen 11*
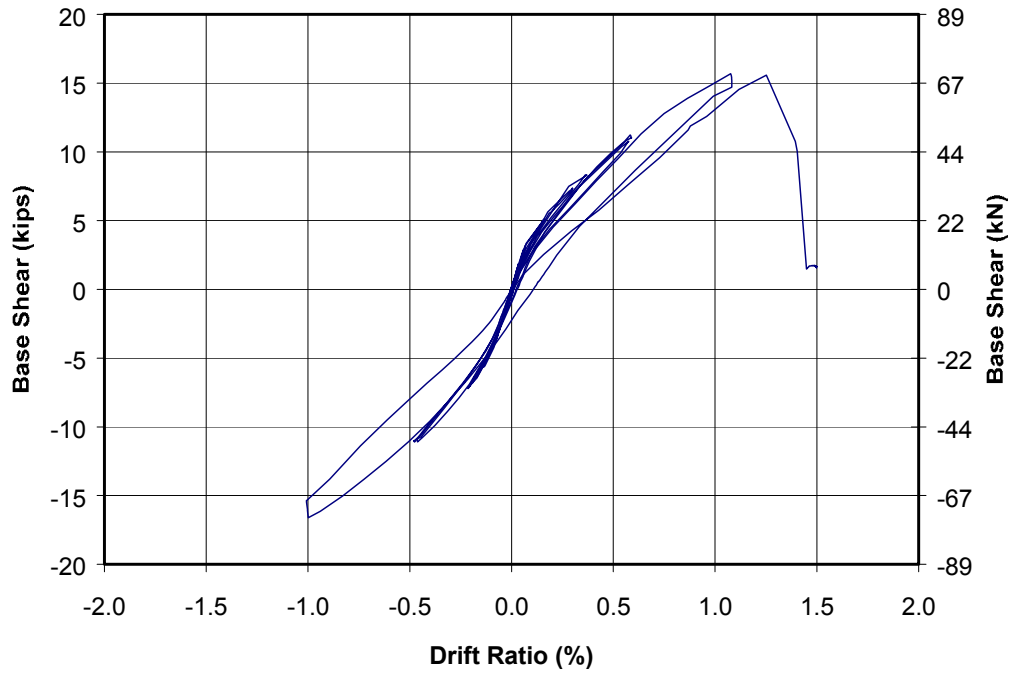
Figure 5.22 Load-displacement response at the end of the test for Shear Wall Specimen 11

5.2 SUMMARY OF RESULTS FOR SHEAR-DOMINATED WALL SPECIMENS

The observed initial tangent stiffness (K_{ot-o}), initial backbone stiffness (K_{ob-o}), and the ratio of the initial backbone stiffness to initial tangent stiffness for each of the shear-dominated specimens are presented in Table 5.1.

Table 5.1 Observed initial tangent and backbone stiffnesses for each shear-dominated specimen

Specimen Number	K_{ot-o} Kips/in. (kN/mm)	K_{ob-o} Kips/in. (kN/mm)	K_{ob-o}/K_{ot-o}
1	678.6 (118.8)	667.0 (116.8)	0.98
3	732.1 (128.2)	704.8 (123.4)	0.96
4	591.8 (103.6)	559.5 (98.0)	0.95
5	771.8 (135.1)	805.8 (141.1)	1.04
7	300.0 (52.5)	308.4 (54.0)	1.03
9	143.0 (25.0)	138.2 (24.2)	0.97
11	34.9 (6.1)	32.3 (5.7)	0.92

Table 5.1 shows a good agreement between the observed initial stiffness and the backbone initial stiffness for each of the shear-dominated specimens. The observed initial stiffnesses presented in Table 5.1 can be affected by potential shrinkage cracks in the leveling bed mortar between the concrete base and the AAC wall, and by variation in the properties of the Type S leveling bed mortar in each wall. The observed secant stiffnesses after flexural cracking in the south (K_{cr-os}) and north (K_{cr-on}) directions, and the ratio of those observed secant stiffness after flexural cracking to initial tangent stiffness for each shear-dominated specimen, are presented in Table 5.2.

Table 5.2 Secant stiffnesses after flexural cracking for each shear-dominated specimen

Specimen Number	K_{cr-os} Kips/in (kN/mm)	K_{cr-os}/K_{ot-o}	K_{cr-on} Kips/in (kN/mm)	K_{cr-on}/K_{ot-o}
1	208.8 (36.6)	0.31	252.6 (44.2)	0.37
3	519.5 (91.0)	0.71	580.7 (101.7)	0.79
4	409.3 (71.7)	0.69	430.8 (75.4)	0.73
5	564.5 (98.8)	0.73	674.4 (118.1)	0.87
7	97.8 (17.1)	0.33	94.0 (16.5)	0.31
9	33.4 (5.8)	0.23	50.2 (8.8)	0.35
11	8.08 (1.4)	0.23	--	--

Table 5.2 shows that the ratio of observed secant stiffness after flexural cracking to initial tangent stiffness varied from 0.23 to 0.73 when the specimens were loaded in the south direction, and from 0.35 to 0.79 when the specimens were loaded in the north direction. The unloading stiffness after web shear cracking in the south direction (K_{u-os}), and the ratio of that unloading stiffness to the initial tangent stiffness for each shear-dominated specimen, are presented in Table 5.3. The unloading stiffness after web shear cracking in the north direction (K_{u-on}) and the ratio of that unloading stiffness to the initial tangent stiffness for each shear-dominated specimen, are presented in Table 5.4.

Table 5.3 Unloading stiffnesses after web shear cracking in the south direction for each shear-dominated specimen

Specimen Number	K_{u-os} Kips/in (kN/mm)	K_{u-os}/K_{ot-o}	D_{u-os}/D_{ws1}
1	175.3 (30.7)	0.26	--
3	534.4 (93.6)	0.73	1.16
4	377.7 (66.1)	0.64	1.04
5	460.2 (80.6)	0.60	1.45
7	98.8 (17.3)	0.33	1.10
9	33.9 (5.9)	0.24	1.02
11	--	--	--

Table 5.4 Unloading stiffnesses after web shear cracking in the north direction for each shear-dominated specimen

Specimen Number	K_{u-on} Kips/in (kN/mm)	K_{u-on}/K_{ot-o}	D_{u-on}/D_{wn1}
1	209.4 (36.7)	0.31	--
3	546.7 (95.7)	0.75	1.07
4	359.4 (62.9)	0.61	1.04
5	546.8 (95.7)	0.71	1.40
7	99.9 (17.5)	0.33	1.03
9	26.2 (4.6)	0.18	1.44
11	--	--	--

Table 5.3 shows that the ratio of the unloading stiffness after web shear cracking to initial tangent stiffness varied from 0.24 to 0.73 when the wall was loaded in the south direction, and

Table 5.4 shows that the ratio varied from 0.18 to 0.75 when loaded in the north direction. The low values of the ratio of the unloading stiffness after web shear cracking to initial tangent stiffness in both south and north directions for Shear Wall Specimens 1, 7 and 9 were related to the presence of crushing of the compressive toe, together with web shear cracking in those specimens (Figure 5.23 though Figure 5.25).

Figure 5.23 Crushing of the compressive toes of Shear Wall Specimen 1

Figure 5.24 Crushing of the north compressive toe of Shear Wall Specimen 7
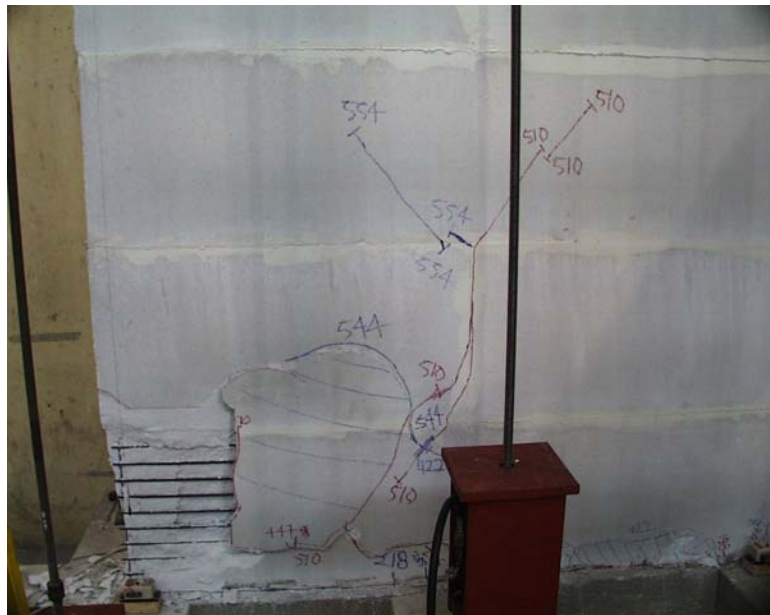
Figure 5.25 Crushing of the north compressive toe of Shear Wall Specimen 9

The strength ratio after web shear cracking and the ratio of the horizontal displacement at the maximum applied load in the corresponding next cycle after web shear cracking, to the horizontal displacement at web shear cracking in the south and north directions for each shear-dominated specimen, are presented in Table 5.5.

Table 5.5 Strength ratios after web shear cracking and corresponding displacement ratios for each shear-dominated specimen

Specimen Number	F_{ws2}/F_{ws1}	D_{ws2}/D_{ws1}	F_{wn2}/F_{wn1}	D_{wn2}/D_{wn1}
1	0.49	1.20	0.82	1.63
3	1.02	1.37	1.22	2.00
4	1.14	1.41	1.01	1.28
5	1.15	2.36	1.15	2.20
7	1.03	1.44	0.89	1.46
9	0.81	1.31	0.36	1.43
11	--	--	--	--

Table 5.5 shows that the strength ratios varied from 0.49 to 1.15 when the specimens were loaded in the south direction, and from 0.36 to 1.22 when the specimens were loaded in the north direction. The observed variation in the strength ratios after web shear cracking in both south and north directions can be related to the number, length and width of the shear cracks observed at web shear cracking. As the number, length and width of those observed shear cracks increased the corresponding stiffness and strength ratios decreased. The low values of the strength ratio of 0.49 and 0.36 observed for Shear Wall Specimen 1 and 9 respectively can also be related to the presence of crushing of the compressive toe together with web shear cracking in those specimens.

Elevation views of Shear wall Specimens 3, 4, 5 and 11 at the end of the test are presented in Figure 5.26, though Figure 5.29 respectively.
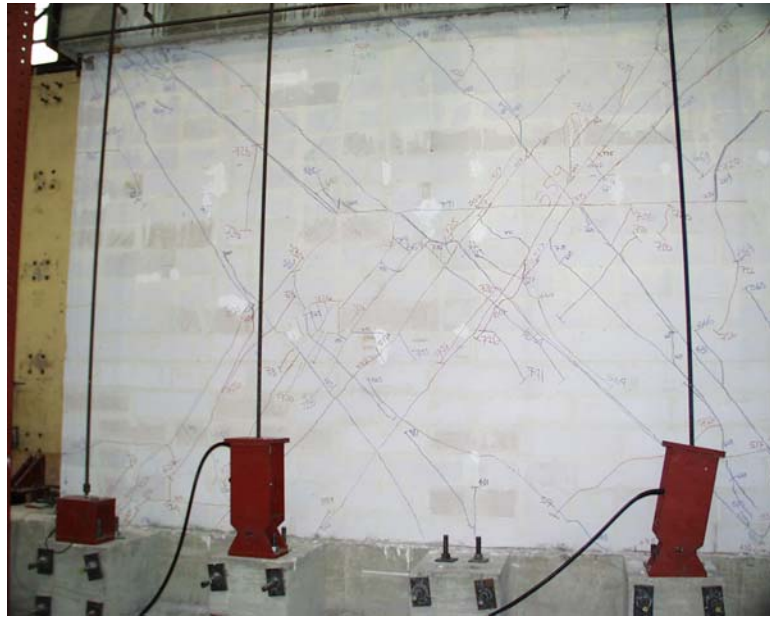
Figure 5.26 Elevation view of Shear Wall Specimen 3 at the end of the test

Figure 5.27 Elevation view of Shear Wall Specimen 4 at the end of the test
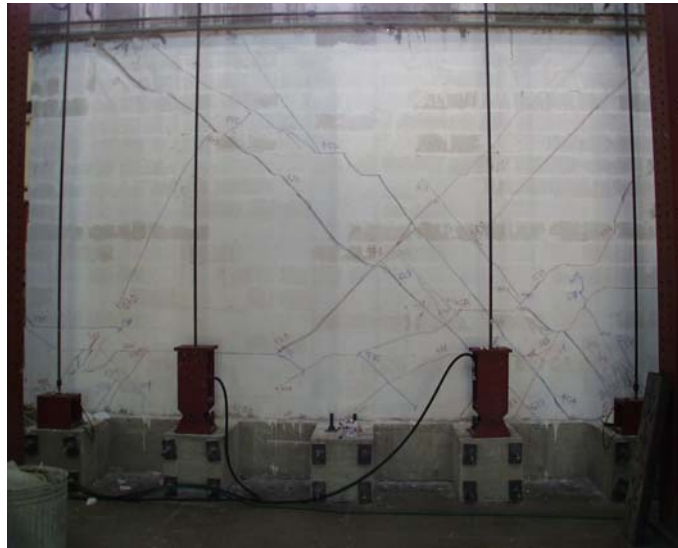
Figure 5.28 Elevation view of Shear Wall specimen 5 at the end of the test

Figure 5.29 Elevation view of Shear Wall Specimen 11 at the end of the test

89

CHAPTER 6

Test Results for Flexure-Dominated Shear Wall Specimens and Two-Story Assemblage Specimen

This chapter presents the test results and behavior of six flexure-dominated shear wall specimens and a two-story assemblage specimen. In the following sections, the response of those specimens is discussed with respect to their recorded load-displacement curves, focusing on changes in the in-plane lateral stiffness and strength of the walls as the specimens were loaded and unloaded during the tests. Maximum drift ratios and displacement ductilities are presented for each of those specimens. The experimental data presented in this chapter, together with that presented in Chapter 5, were used not only to develop analytical models that represent the behavior of AAC shear walls subjected to earthquake ground motions, but also to define appropriate values of drift ratio and displacement ductility capacities for those AAC shear walls. The response of the two-story assemblage specimen with respect to the load history and with regard to the observed cracking patterns is presented in Tanner (2003). The load-displacement curves presented in this chapter for the flexure-dominated specimens are similar to those presented for the shear-dominated specimens. Those for the assemblage specimen show total base shear versus displacement at the second level of load application or drift ratio, expressed as a percentage. The total base shear was calculated as the summation of the equal loads applied in each story of the assemblage. The drift ratio for each wall of the assemblage specimens was calculated as the horizontal displacement at the second level of load application, divided by its height.

6.1 BEHAVIOR OF FLEXURE-DOMINATED SHEAR WALL SPECIMENS

The changes in the hysteretic load-displacement response of the flexure-dominated shear wall specimens were in general described by the following:

- initial stiffness;
- stiffness after flexural cracking;
- stiffness after yielding of the flexural reinforcement; and
- unloading stiffness after yielding of the flexural reinforcement.

Initial tangent and backbone stiffnesses were calculated for each flexure-dominated wall specimen similar to those calculated for each shear-dominated wall specimen. The secant stiffness after flexural cracking was calculated as the applied load in the wall at which yielding of the flexural reinforcement was observed during the test divided by the corresponding horizontal displacement. D_{ys} and D_{yn} are the displacement at yielding of the flexural reinforcement in the south and north directions respectively. Two secant stiffnesses were calculated for each flexure-dominated specimen, one corresponding to loading the specimen in the south direction (K_{cr-os}) and the other in the north direction (K_{cr-on}). Yielding of the flexural reinforcement was in general based on the readings of the strain gages mounted on the flexural reinforcement of each of the flexure-dominated specimens. The unloading stiffness after yielding of the flexural reinforcement was calculated using the slope of the unloading branch of the load-displacement curve right after yielding of the flexural reinforcement was observed during the test. Two unloading stiffnesses were calculated for each flexure-dominated specimen, one corresponding to loading the specimen in the south direction (K_{u-os}) and the other in the north direction (K_{u-on}) respectively. The stiffness after yielding of the flexural reinforcement was calculated using the slope of the load-displacement curve after yielding of the flexural reinforcement was observed in a number of consecutive cycles. Two stiffnesses after yielding of the flexural

reinforcement were calculated for each flexure-dominated specimen, one corresponding to loading the specimen in the south direction (K_{y-os}) and the other in the north direction (K_{y-on}). The displacement ductility was calculated as a maximum selected horizontal displacement divided by the corresponding displacement at yielding of the flexural reinforcement. The selected horizontal displacement was based on the following criteria:

- a degradation in the capacity of the AAC wall of more than 10%; or
- a change in the shape of the hysteretic loop from the corresponding previous load cycle, for example, a large reduction in the energy dissipated.

Degradation in capacity is defined in this dissertation as a reduction in the maximum observed strength of the specimen in a given load cycle with respect to the maximum observed strength in the previous corresponding load cycle, as exemplified by Figure 6.1. Two displacement ductilities were calculated for each flexure-dominated specimen, one corresponding to loading the specimen in the south direction ($\mu_{\Delta-os}$) and the other in the north direction ($\mu_{\Delta-on}$). The maximum global drift ratio was also based on the selected horizontal displacement. Two maximum global drift ratios were calculated for each flexural-dominated specimen, one corresponding to loading the specimen in the south direction (δ_{os}) and the other in the north direction (δ_{on}). Although specimens were subjected to the same drifts in each direction during the displacement-controlled portion of each test, the selected maximum horizontal displacement capacity in each direction could be limited by strength degradation as noted above, and therefore could be different in each direction.
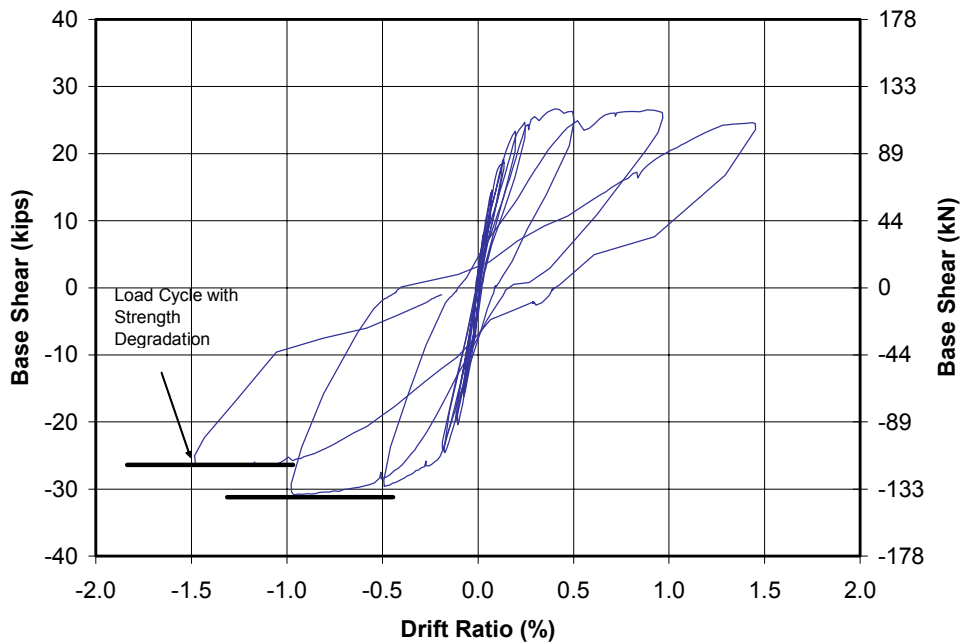
Figure 6.1 Example of strength degradation

6.1.1 Shear Wall Specimen 13

The initial tangent stiffness and the initial backbone stiffness for Shear Wall Specimen 13 were 61.6 kips/in. (10.8 kN/mm) and 63.4 kips/in. (11.1 kN/mm) respectively. Because none of the strain gages of this specimen worked, the force at yielding of the flexural reinforcement in both south and north directions was assumed equal to the predicted force at yielding of the flexural reinforcement of 11.2 kips (49.8 kN). The predicted force at yielding was calculated using a yield strength of 75 ksi (517 MPa), based on mill report tests for the vertical reinforcement used in this specimen, assuming a linear distribution between stress and strain of the AAC, and a linear strain distribution. The yielding strength of 75 ksi (517 MPa) was later verified with the average observed yielding strength of 77 ksi (530 MPa)) of three bars tested at FSEL. The

93

predicted force at yielding of the flexural reinforcement was also verified using the observed load-displacement curve of this specimen. The displacement at yielding of the flexural reinforcement was assumed equal to that observed displacement corresponding to the predicted force at yielding of the flexural reinforcement of 11.2 kips (49.8 kN). In the south direction, the assumed horizontal displacement at yielding was 0.45 in. (11.4 mm) and the corresponding stiffness after flexural cracking was 24.9 kips/in. (4.4 kN/mm). In the north direction, the assumed displacement at yielding was 0.43 in. (10.9 mm) and the corresponding stiffness after flexural cracking was 26 kips/in. (4.6 kN/mm). Figure 6.2 shows the assumed points at yielding of the flexural reinforcement and the stiffnesses after flexural cracking in the south and north directions for Shear Wall Specimen 13.
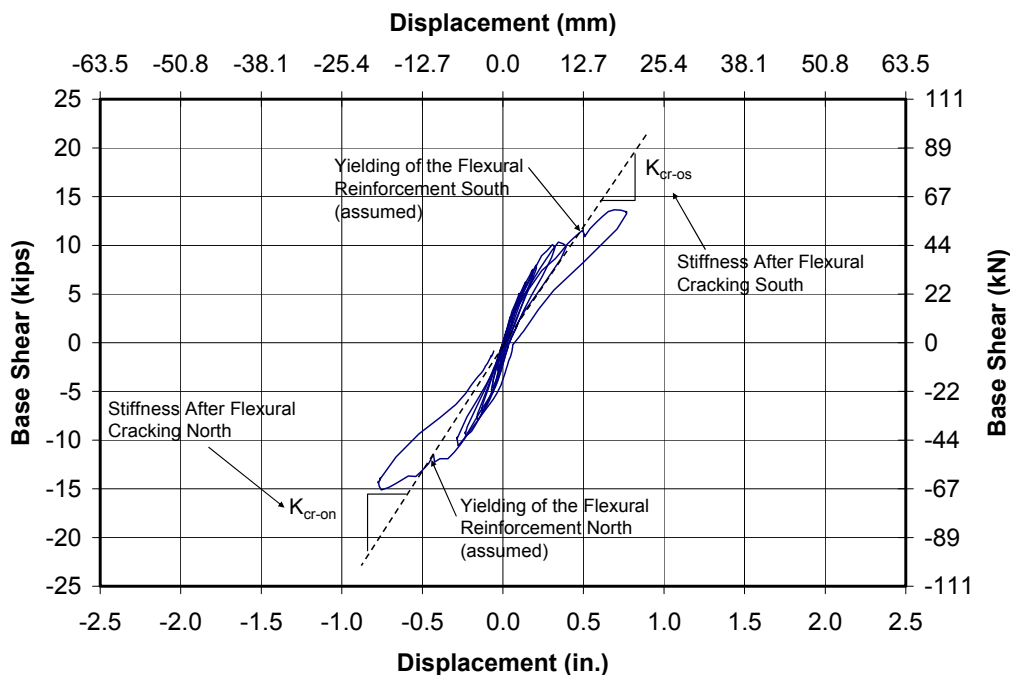
Figure 6.2 Assumed points at yielding of the flexural reinforcement and stiffnesses after flexural cracking for Shear Wall Specimen 13

94

The unloading stiffnesses after yielding of the flexural reinforcement of this specimen in the south and north directions were 18.6 kips/in. (3.3 kN/mm) and 17.5 kips/in. (3.1 kN/mm) respectively (Figure 6.3). The maximum displacements before unloading the specimen in the south and north directions were 0.76 in. (19.3 mm) and 0.77 in. (19.6 mm) respectively.
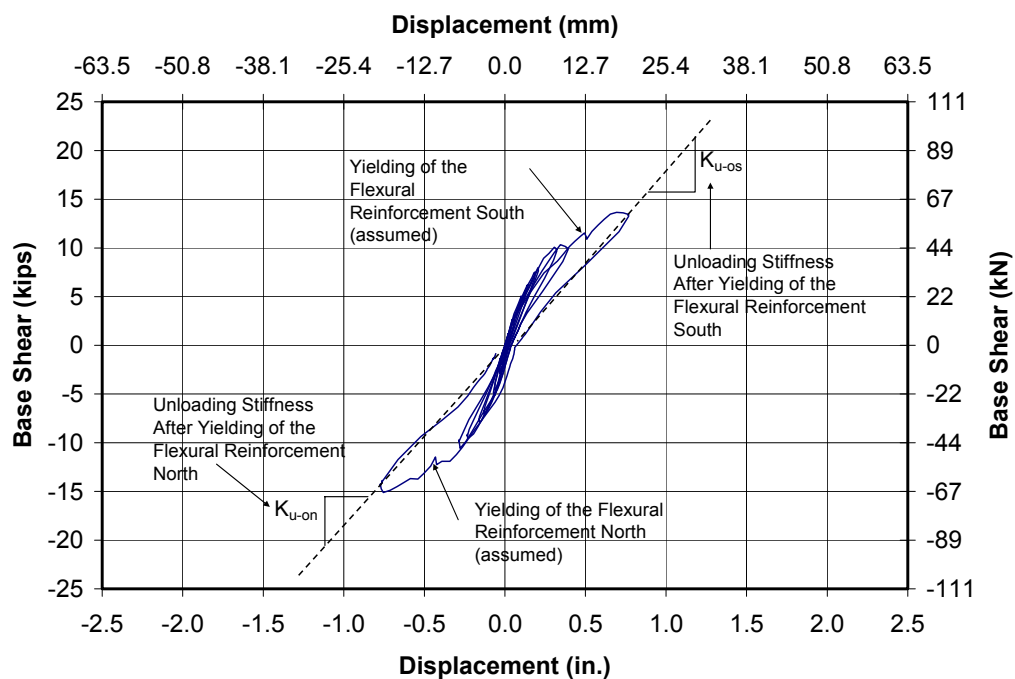
Figure 6.3 Unloading stiffnesses after yielding of the flexural reinforcement for Shear Wall Specimen 13

The stiffnesses after yielding of the flexural reinforcement in the south and north directions were calculated using the slope of the dashed lines shown in Figure 6.4. The observed loads higher than 15.5 kips (68.9 kN) shown in that figure were not considered in calculating the stiffness after yielding of the flexural reinforcement in the south direction, because that increment in the applied load was related to an inadvertent increase in the axial load in the specimen caused

when the hydraulic ram used with the load maintainer bottomed out (reached its minimum extension and could not retract further). This is discussed in Tanner (2003), along with corresponding post-test verification procedures. The stiffness after yielding of the flexural reinforcement in the south and in the north directions were 1.29 kips/in. (0.23 kN/mm) and 1.22 kips/in. (0.21 kN/mm) respectively.
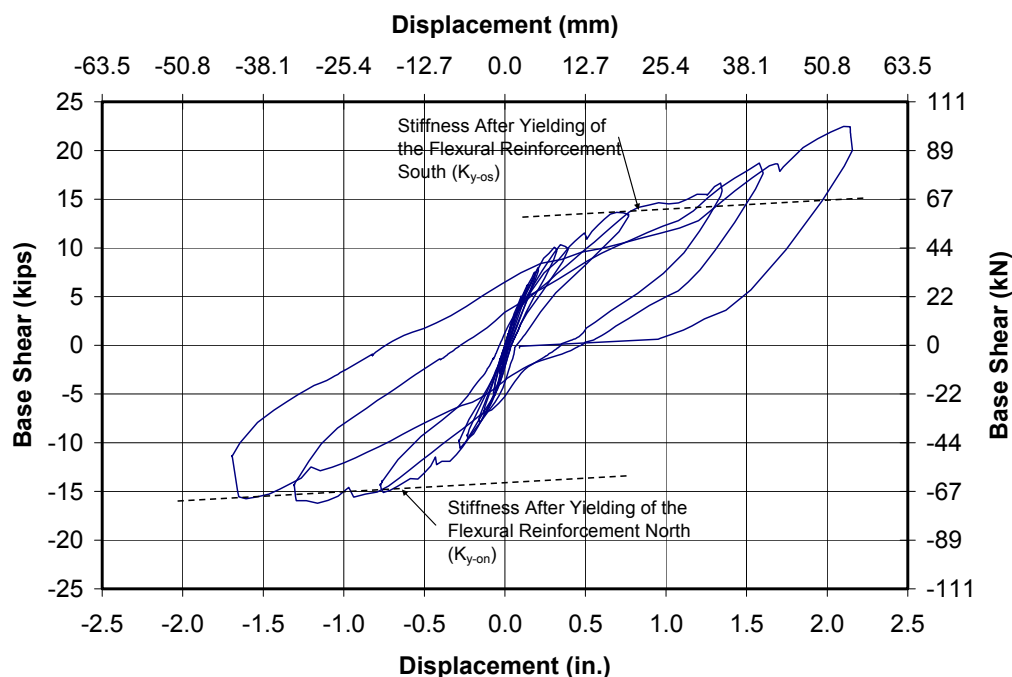
Figure 6.4 Stiffnesses after yielding of the flexural reinforcement for Shear Wall Specimen 13

The maximum selected displacements in the south and north directions for this specimen were 2.15 in. (54.6 mm) and 1.65 in. (41.9 mm) respectively (Figure 6.5). The corresponding displacement ductilities were 4.8 and 4.0 respectively, and the drift ratios were 1.4% and 1.1% respectively (Figure 6.6).
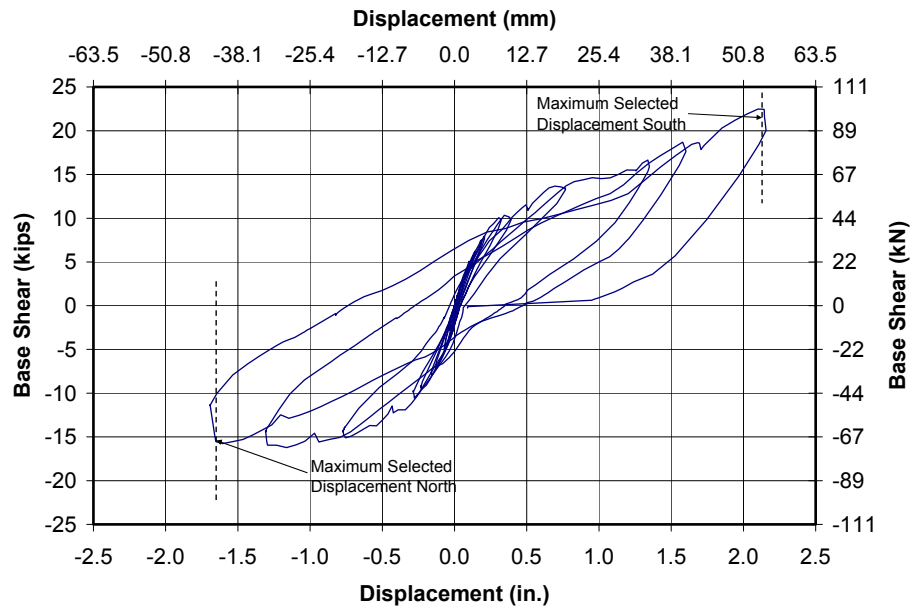
Figure 6.5 Maximum selected displacements for Shear Wall Specimen 13
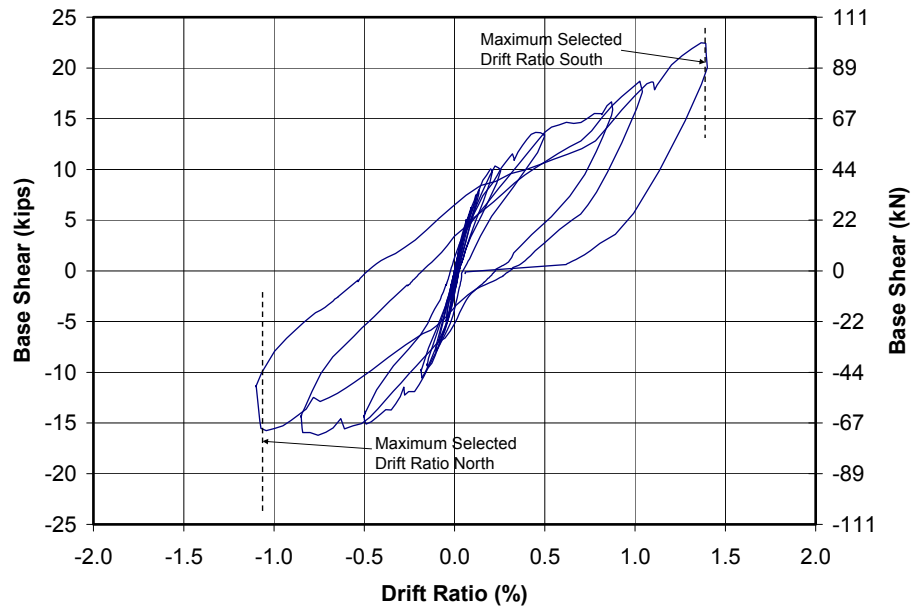
Figure 6.6 Maximum selected drift ratios for Shear Wall Specimen 13

6.1.2 Shear Wall Specimen 14a

In this specimen, a horizontal crack had already formed on the leveling bed mortar while connecting the dual actuators to the concrete loading beam before testing. In addition, this specimen was tested under monotonic reversed loads because the bar used as flexural reinforcement at the north end of the wall pulled out at the beginning of the test. The initial tangent stiffness of this specimen was 18 kips/in. (3.15 kN/mm). The load at which yielding of the flexural reinforcement was observed in the south direction was 6.6 (29.4 kN). The horizontal displacement at that load was 0.6 in. (15.2 mm), and the corresponding stiffness after flexural cracking was 11 kips/in. (1.9 kN/mm). The unloading stiffnesses after yielding of the flexural reinforcement of this specimen was 9.5 kips/in. (1.7 kN/mm), and the maximum observed displacement before unloading the specimen was 1.53 in. (38.9 mm). Figure 6.7 shows the stiffness after flexural cracking and the unloading stiffness after yielding of the flexural reinforcement for Shear Wall Specimen 14a.
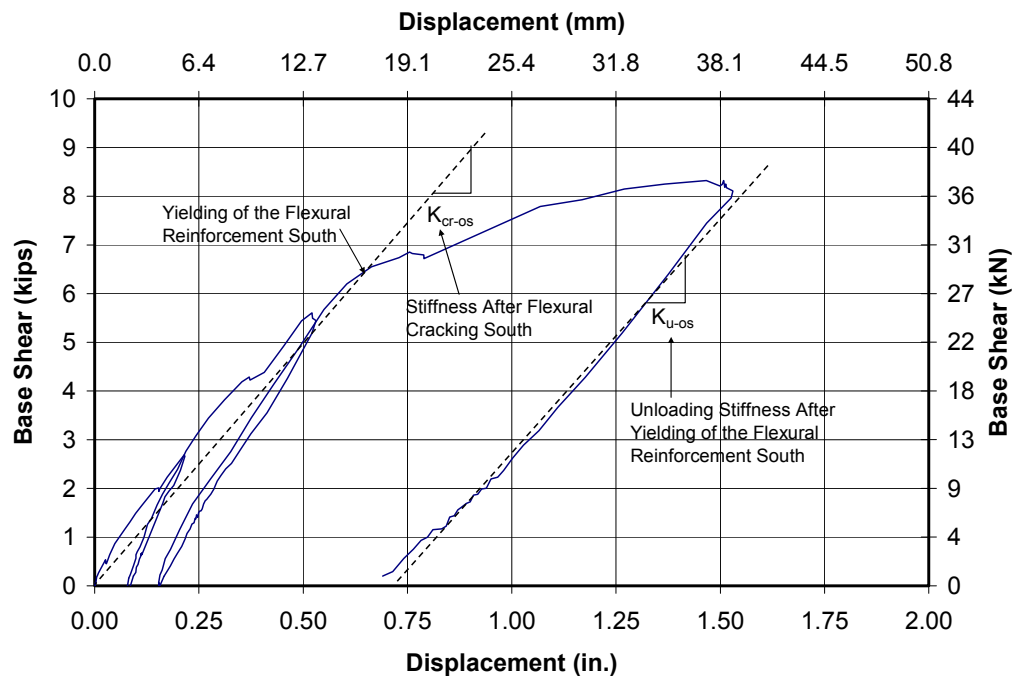
***Figure 6.7 Stiffnesses after flexural cracking and unlading stiffnesses after
yielding of the flexural reinforcement for Shear Wall Specimen 14a***

The stiffnesses after yielding of the flexural reinforcement shown with a
dashed line in Figure 6.8 was equal to 0.65 kips/in. (0.11 kN/mm).

Displacement (mm)

Stiffness After
Yielding of the
Flexural
Reinforcement
South (K_{y-os})
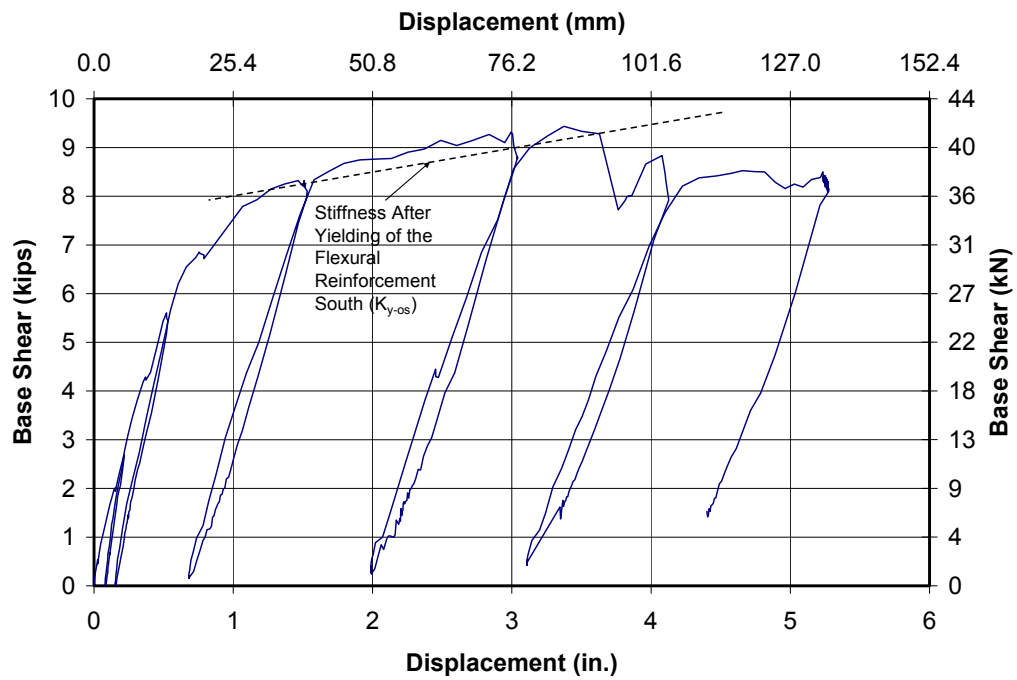
Figure 6.8 Stiffness after yielding of the flexural reinforcement for Shear Wall Specimen 14a

The maximum selected displacement for this specimen was 3 in. (mm). The corresponding displacement ductility was 5.0, and the drift ratio was 1.9%. Figure 6.9 shows the selected drift ratio for Shear Wall Specimen 14a.
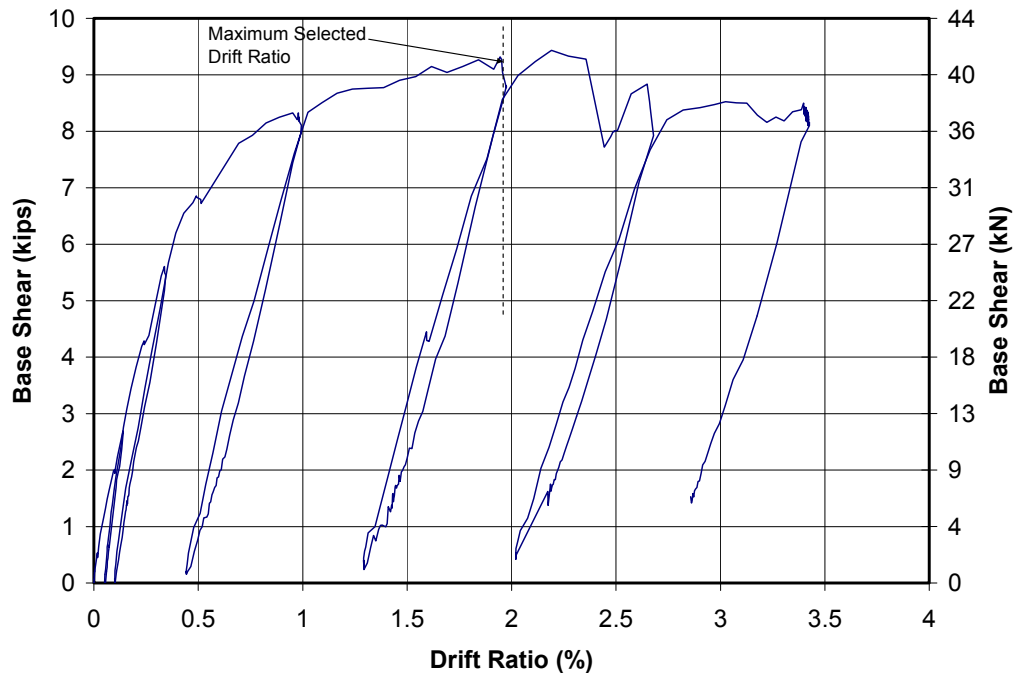
Figure 6.9 Maximum selected drift ratio for Shear Wall Specimen 14a

6.1.3   Shear Wall Specimen 14b

The initial tangent stiffness and the initial backbone stiffness for Shear Wall Specimen 14b were both 44 kips/in. (7.7 kN/mm). Yielding of the flexural reinforcement was first observed in this specimen when it was loaded in the south direction. The load at which yielding of the flexural reinforcement was observed in the south direction was 7 kips (31.1 kN). The horizontal displacement at that load was 0.56 in. (14.2 mm), and the corresponding stiffness after flexural cracking was 12.5 kips/in. (55.6 kN/mm). The maximum load at which yielding of the flexural reinforcement was observed in the north direction was 8.9 kips (39.6 kN). The horizontal displacement at that load was 0.62 in. (15.7 mm), and the corresponding stiffness after flexural cracking was 14.4 kips/in. (2.5 kN/mm).

Figure 6.10 shows the stiffnesses after flexural cracking in the south and north direction for Shear Wall Specimen 14b.
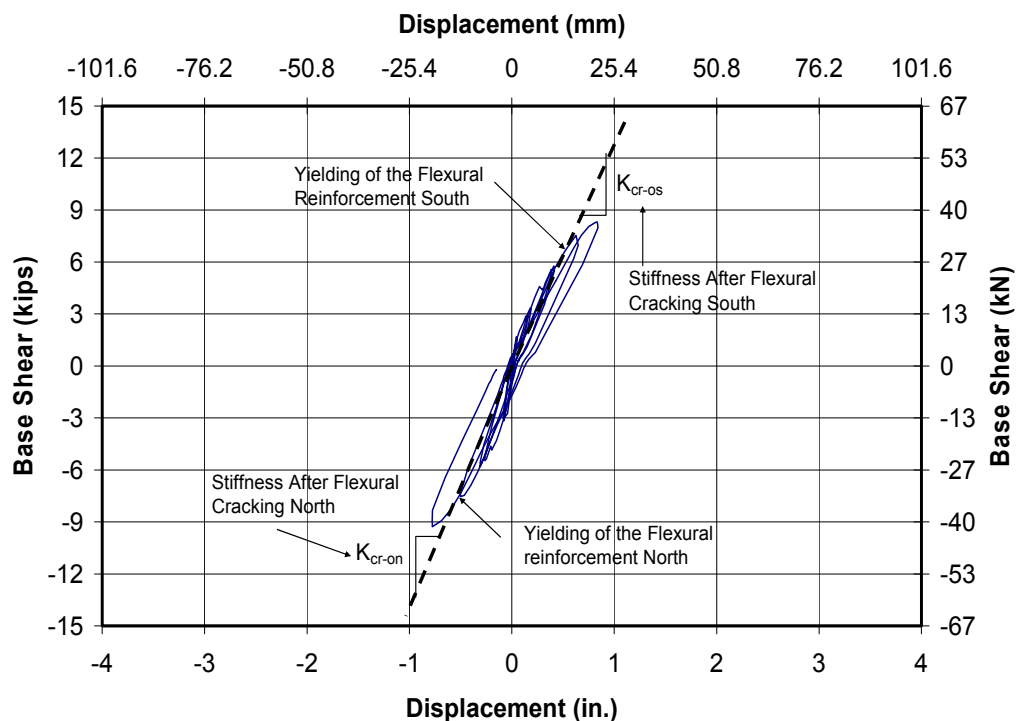
Figure 6.10 Stiffnesses after flexural cracking for Shear Wall Specimen 14b

The unloading stiffnesses after yielding of the flexural reinforcement of this specimen corresponding to the south and north directions were 12.5 kips/in. (2.2 kN/mm) and 12.8 kips/in. (2.24 kN/mm) respectively (Figure 6.11). The corresponding maximum displacements before unloading the specimen in the south and north directions were 0.65 in. (16.5 mm) and 0.78 in. (19.8 mm) respectively.
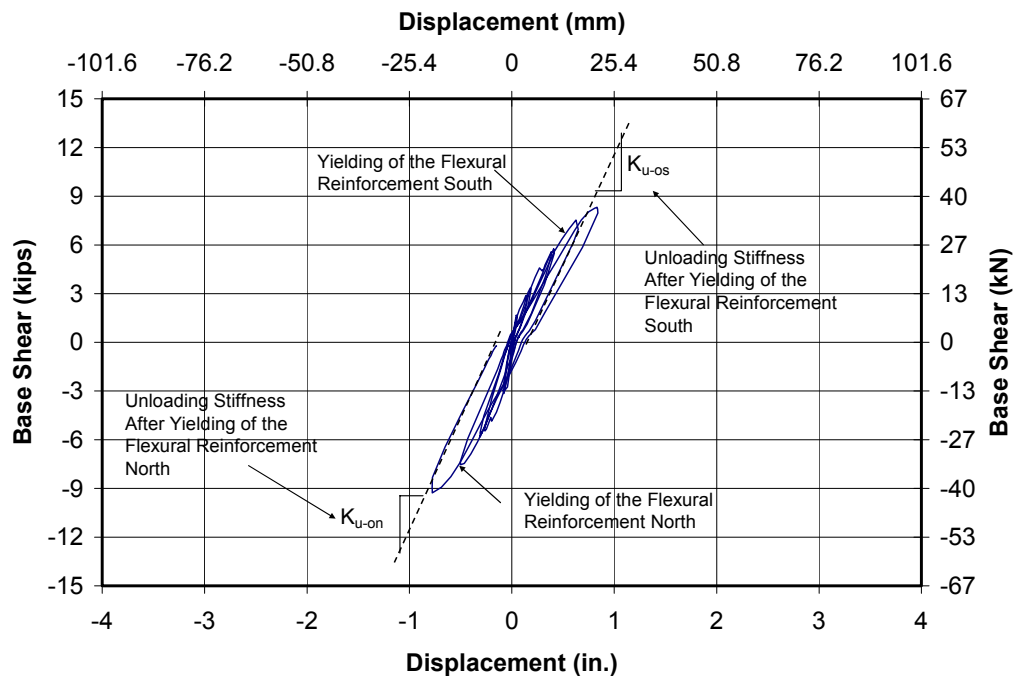
Figure 6.11 Unloading stiffnesses after yielding of the flexural reinforcement
for Shear Wall Specimen 14b

The stiffness after yielding of the flexural reinforcement for this specimen in the south and in the north directions were 0.65 kips/in. (0.11 kN/mm) and 1.1 kips/in. (0.19 kN/mm) respectively.
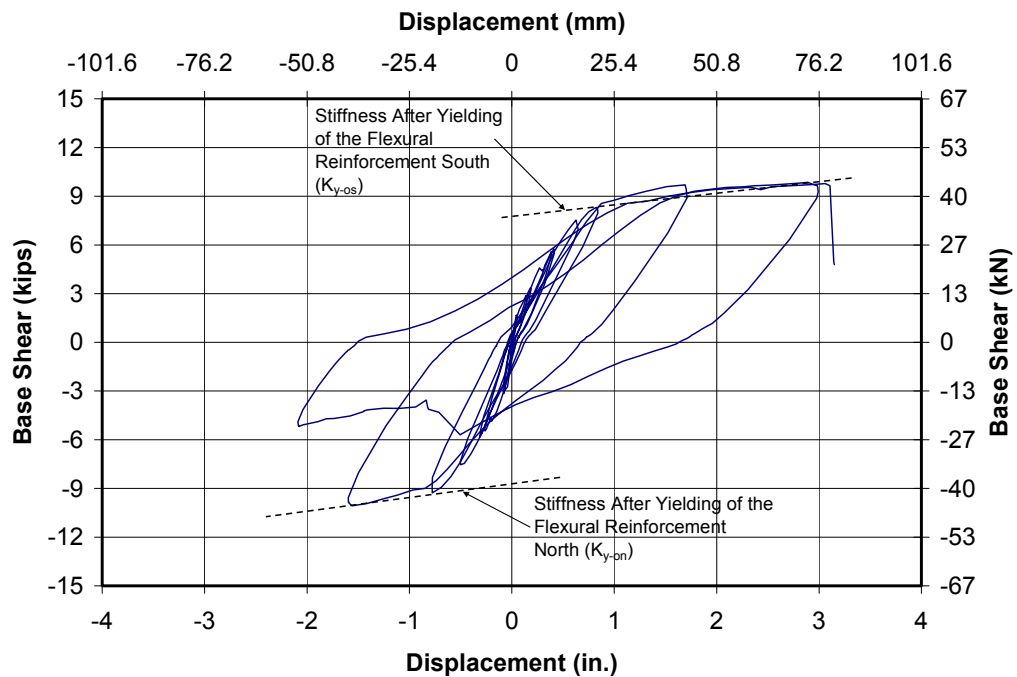
Displacement (mm)

Figure 6.12 Stiffnesses after yielding of the flexural reinforcement for Shear Wall Specimen 14b

The maximum selected displacements in the south and north directions for this specimen were 3.0 in. (76.2 mm) and 1.6 in. (40.6 mm) respectively. The corresponding displacement ductilities were 5.4 and 2.6 respectively, and the drift ratios were 1.9% and 1% respectively. Figure 6.13 shows the selected drift ratios in the south and north directions for Shear Wall Specimen 14b.
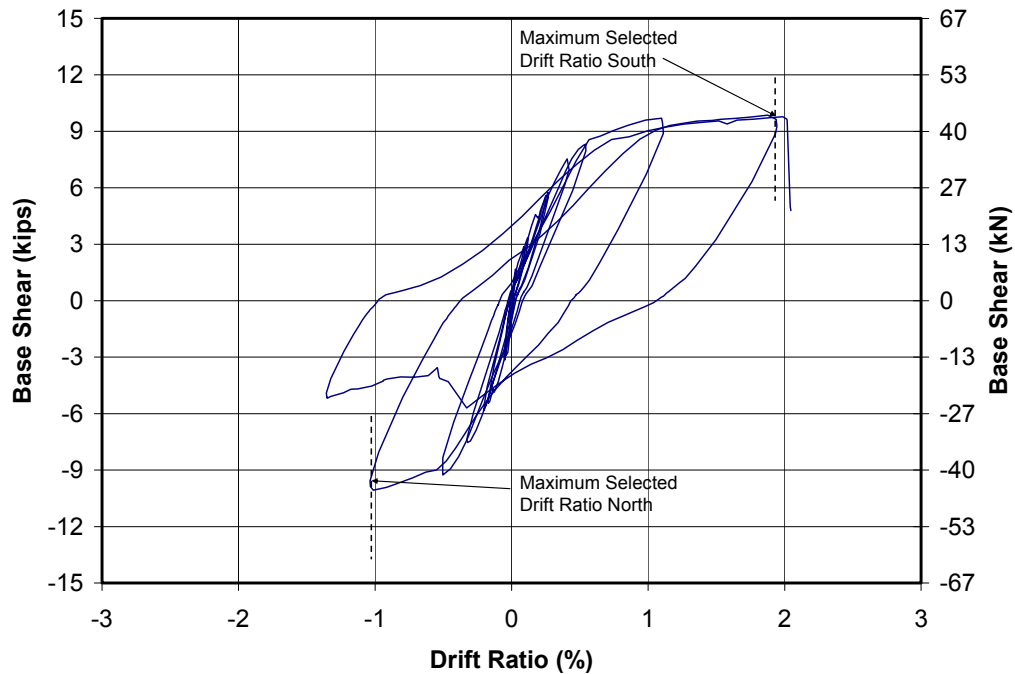
Figure 6.13 selected drift ratios for Shear Wall Specimen 14b

6.1.4   Shear Wall Specimen 15a

The initial tangent stiffness and the initial backbone stiffness for Shear Wall Specimen 15a were 215.7 kips/in. (37.8 kN/mm) and 183 kips/in. (31.9 kN/mm) respectively. Yielding of the flexural reinforcement was first observed in this specimen when the wall was loaded in the south direction. The load at which yielding of the flexural reinforcement was observed in the south direction was 23 kips (102.3 kN). The horizontal displacement at that load was 0.29 in. (7.4 mm), and the corresponding stiffness after flexural cracking was 92 kips/in. (16.1 kN/mm).   The maximum load at which yielding of the flexural reinforcement was observed in the north direction was 26 kips (115.7 kN). The horizontal displacement at that load was 0.26 in. (6.6 mm), and the corresponding stiffness after flexural cracking was 100 kips/in. (17.5 kN/mm). The unloading

105

stiffnesses after yielding of the flexural reinforcement for this specimen for the south and north directions were both 54.6 kips/in. (9.6 kN/mm). The maximum displacements before unloading the specimen in the south and north directions were 0.29 in. (7.4 mm) and 0.27 in. (6.9 mm) respectively. Figure 6.14 shows the stiffnesses after flexural cracking and the unloading stiffnesses after yielding of the flexural reinforcement in the south and north direction for Shear Wall Specimen 15a.
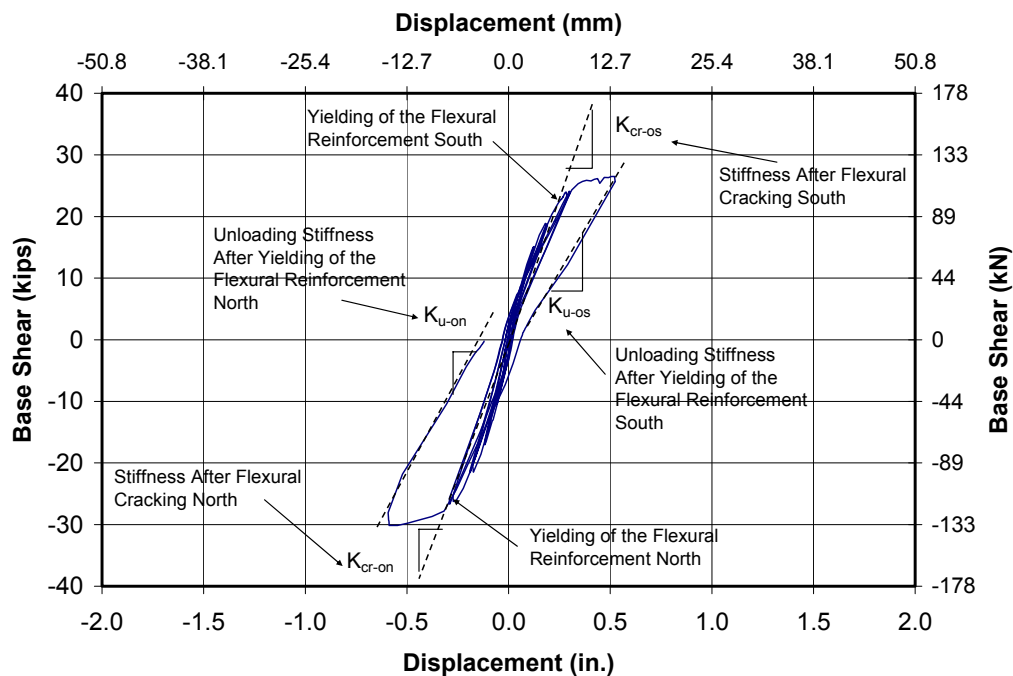
Figure 6.14 Stiffnesses after flexural cracking and unloading stiffnesses after yielding of the flexural reinforcement for Shear Wall Specimen 15a

The stiffness after yielding of the flexural reinforcement for this specimen in the south and in the north directions were 2.6 kips/in. (0.46 kN/mm) and 0.55 kips/in. (0.1 kN/mm) respectively (Figure 6.15).
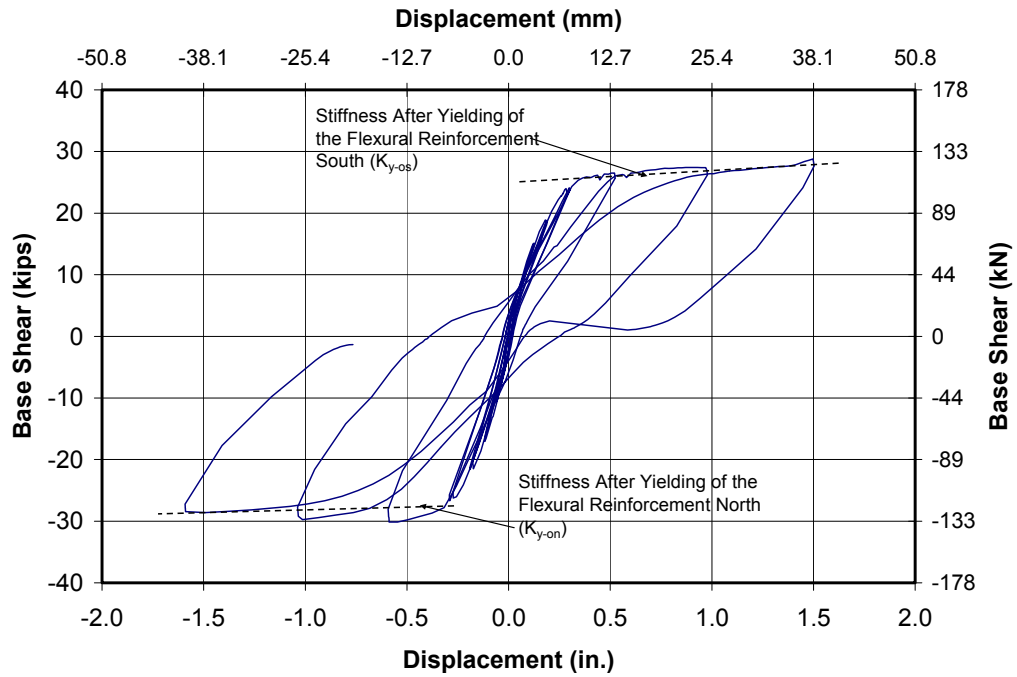
Figure 6.15 Stiffnesses after yielding of the flexural reinforcement for Shear Wall Specimen 15a

The maximum selected displacements for this specimen in the south and north directions were both equal to 1.5 in. (38.1 mm); the corresponding displacement ductilities were 6.0 and 5.8 respectively, and the drift ratios were both equal to 1.0% (Figure 6.16).
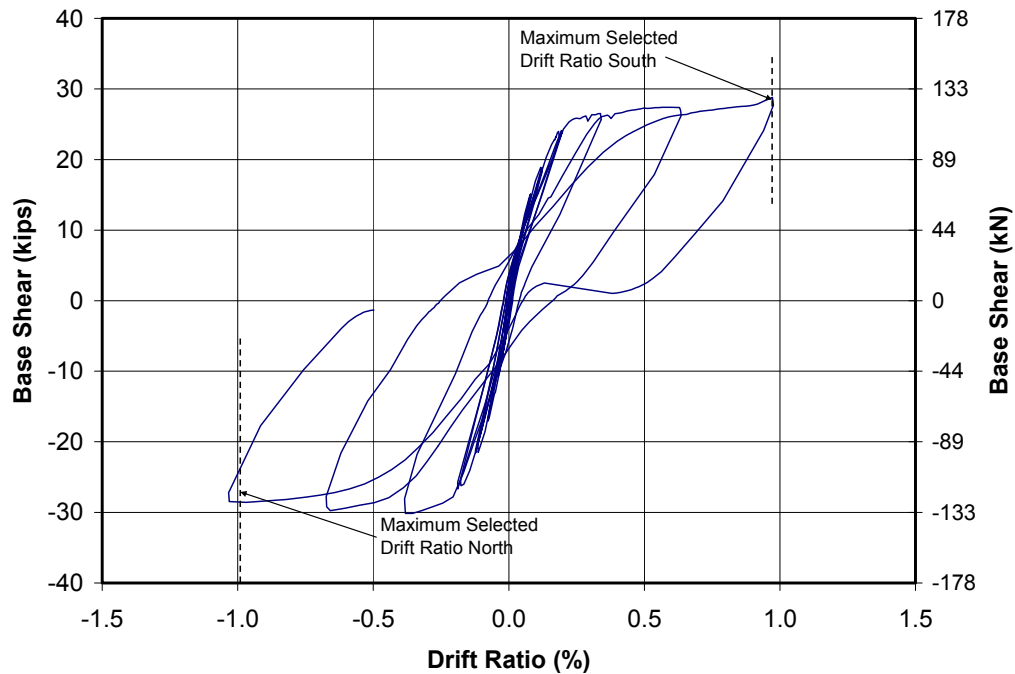
Figure 6.16 Maximum selected drift ratios for Shear Wall Specimen 15a

6.1.5   Shear Wall Specimen 15b

The initial tangent stiffness and the initial backbone stiffness for Shear Wall Specimen 15a were 218.7 kips/in. (38.3 kN/mm) and 190.1 kips/in. (33.3 kN/mm) respectively. Yielding of the flexural reinforcement was first observed in this specimen when it was loaded in the south direction. The load at which yielding of the flexural reinforcement was observed in the south direction was 22.9 kips (101.9 kN). The horizontal displacement at that load was 0.31 in. (7.9 mm), and the corresponding stiffness after flexural cracking was 73.9 kips/in. (12.9 kN/mm).   The maximum load at which yielding of the flexural reinforcement was observed in the north direction was 25.1 kips (111.6 kN). The horizontal displacement at that load was 0.31 in. (7.9 mm), and the corresponding stiffness after flexural cracking was 81 kips/in. (17.5 kN/mm). Figure 6.17 shows

the stiffnesses after flexural cracking in the south and north directions for this specimen.

Displacement (mm)
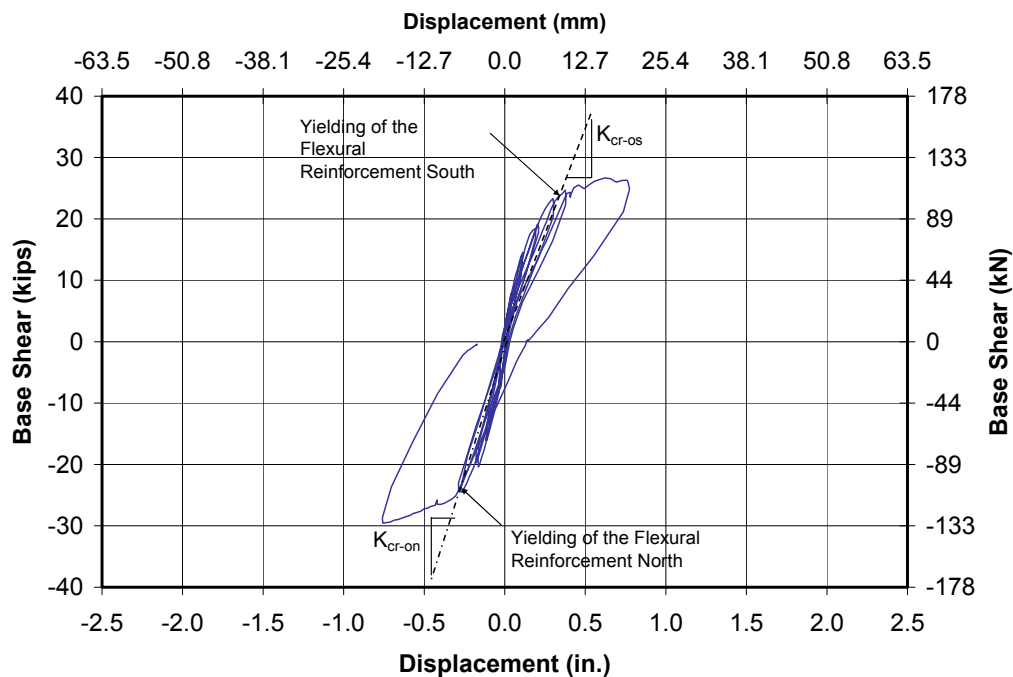
Figure 6.17 Stiffnesses after flexural cracking for Shear Wall Specimen 15a

The unloading stiffnesses after yielding of the flexural reinforcement for this specimen in the south and north directions were 62.9 kips/in. (11 kN/mm) and 36.7 kips/in. (6.4 kN/mm) respectively. The maximum displacements before unloading the specimen in the south and north directions were 0.38 in. (9.7 mm) and 0.76 in. (19.3 mm) respectively. Figure 6.18 shows the unloading stiffnesses after yielding of the flexural reinforcement in the south and north direction for Shear Wall Specimen 15b.
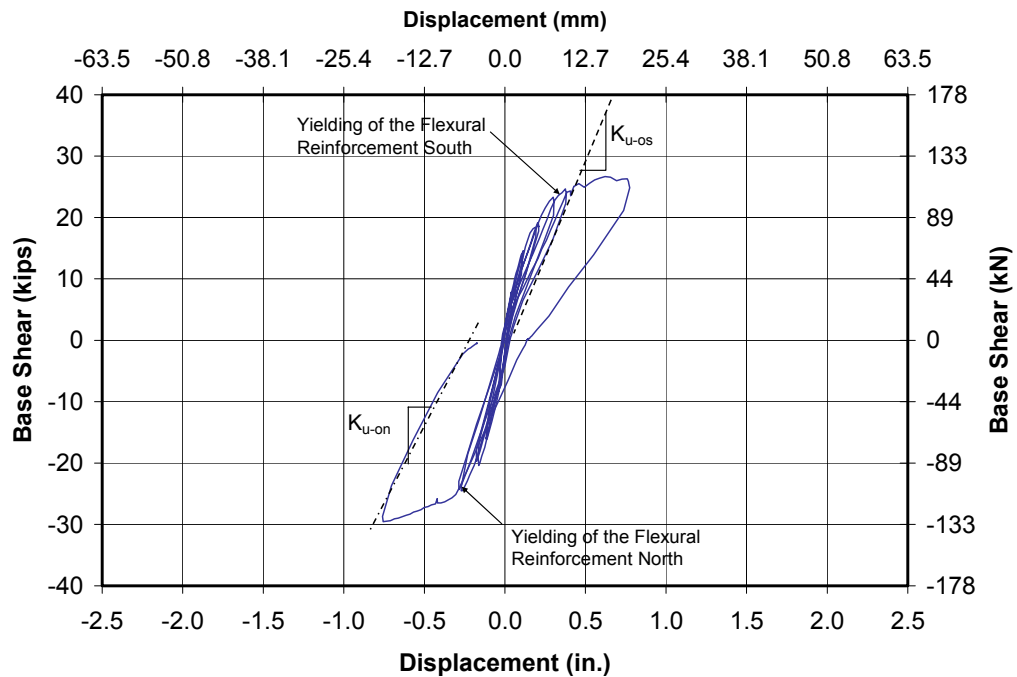
Figure 6.18 Unloading stiffnesses after yielding of the flexural reinforcement for Shear Wall Specimen 15a

The stiffness after yielding of the flexural reinforcement for this specimen in the south and in the north directions were 2.81 kips/in. (0.49 kN/mm) and 3.74 kips/in. (0.65 kN/mm) respectively (Figure 6.19). The last load cycle in the south and north directions were not included to calculate the stiffnesses after yielding of the flexural reinforcement because the selected horizontal displacements of this specimen were defined not considering those cycles.
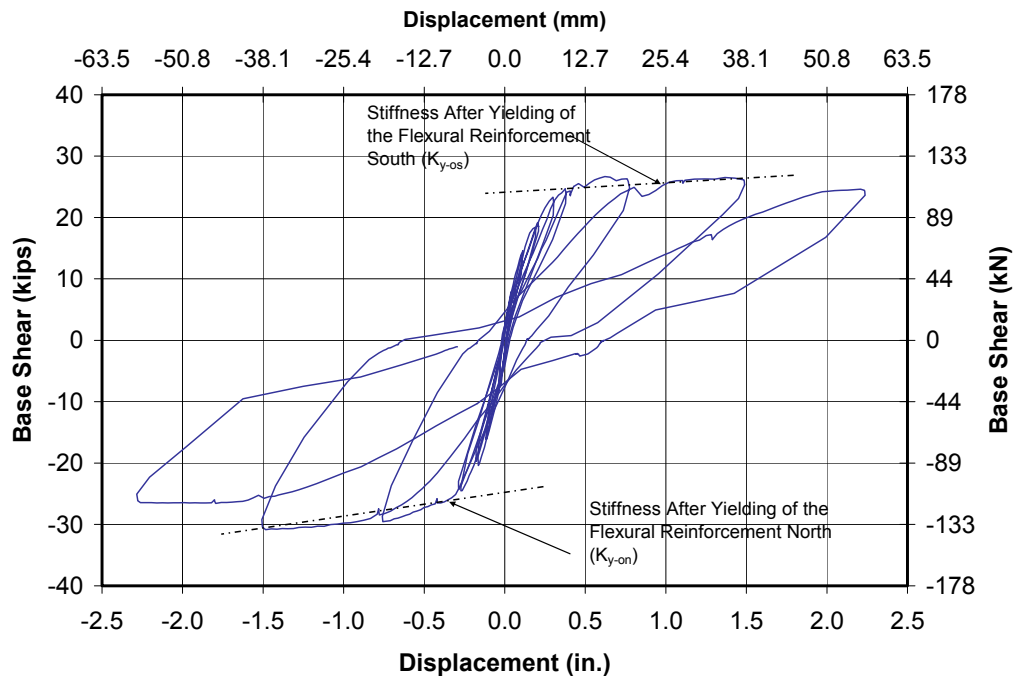
Figure 6.19 Stiffnesses after yielding of the flexural reinforcement for Shear Wall Specimen 15b

The maximum selected displacements for this specimen in the south and north directions were both equal to 1.5 in. (38.1 mm); the corresponding displacement ductilities were both equal to 4.8, and the drift ratios were both equal to 1.0%. Figure 6.20 shows the selected drift ratios in the south and north directions for Shear Wall Specimen 15b.
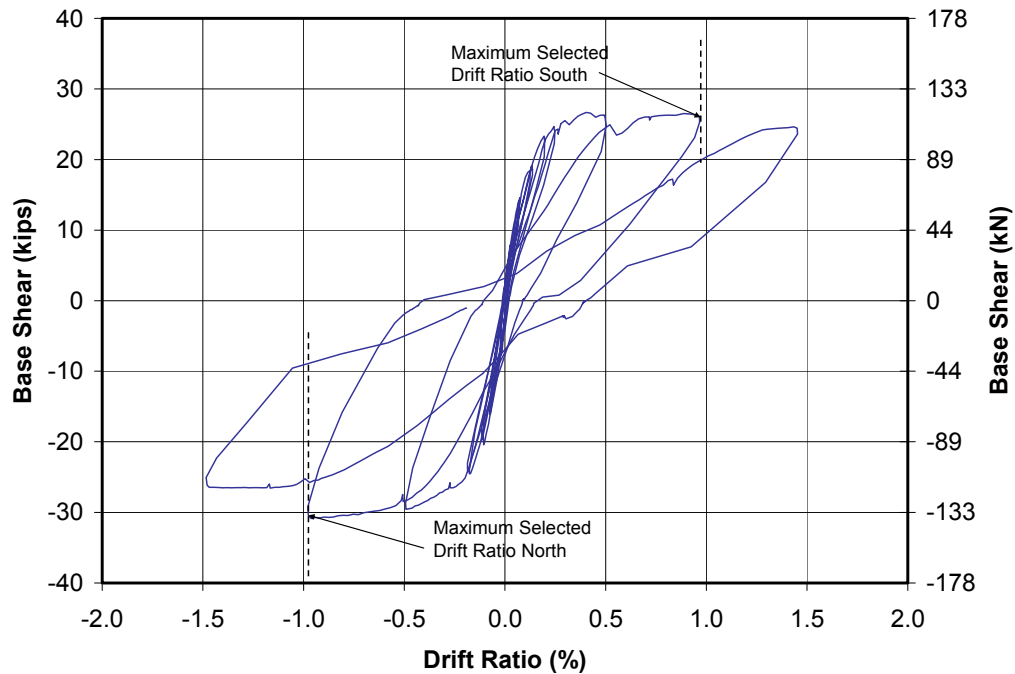
Figure 6.20 Selected drift ratios for Shear Wall Specimen 15b

6.1.6   Shear Wall Specimen 16

The initial tangent stiffness and the initial backbone stiffness for Shear Wall Specimen 16 were 139.6 kips/in. (24.4 kN/mm) and 109.9 kips/in. (19.2 kN/mm) respectively. Yielding of the flexural reinforcement was first observed in this specimen when it was loaded in the south direction. The load at which yielding of the flexural reinforcement was observed in the south direction was 26.2 kips (116.5 kN). The horizontal displacement at that load was 0.3 in. (7.6 mm), and the corresponding stiffness after flexural cracking was 87.3 kips/in. (15.3 kN/mm).   The maximum load at which yielding of the flexural reinforcement was observed in the north direction was 26.8 kips (119.2 kN). The horizontal displacement at that load was 0.36 in. (9.1 mm), and the corresponding stiffness after flexural cracking was 74.4 kips/in. (13 kN/mm). The unloading

stiffnesses after yielding of the flexural reinforcement for this specimen corresponding to the south and north directions were 64.1 kips/in. (11.2 kN/mm) and 53.7 kips/in. (9.4 kN/mm) respectively. The maximum displacements before unloading the specimen in the south and north directions were 0.5 in. (12.7 mm) and 0.63 in. (16 mm) respectively. Figure 6.21 shows the stiffnesses after flexural cracking and the unloading stiffnesses after yielding of the flexural reinforcement in the south and north direction for Shear Wall Specimen 16.
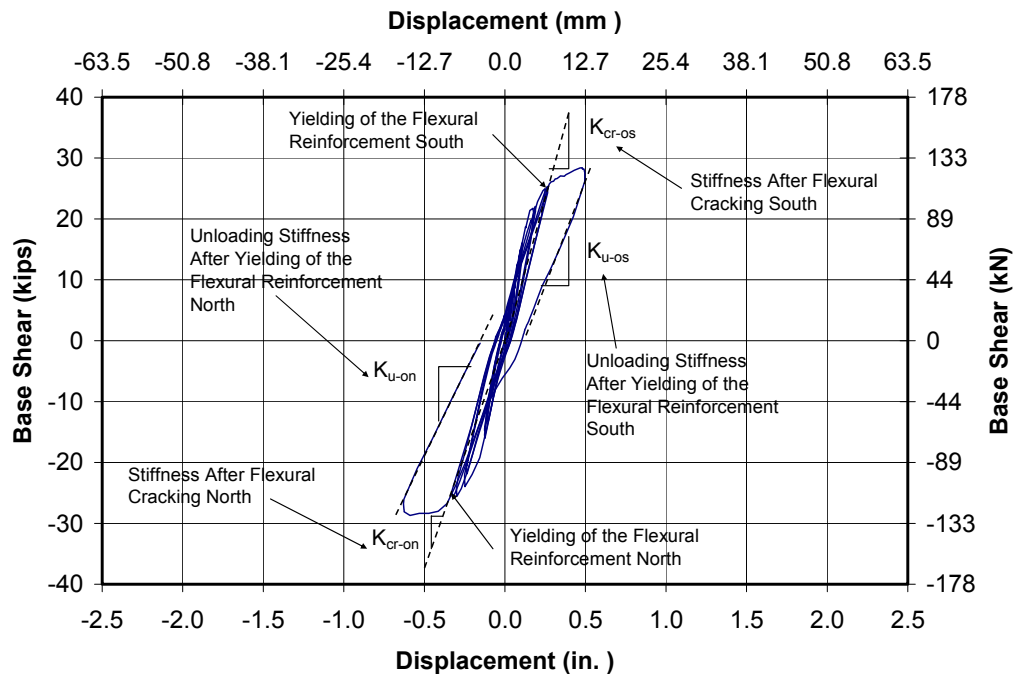
Figure 6.21 Stiffnesses after flexural cracking and unloading stiffnesses after yielding of the flexural reinforcement for Shear Wall Specimen 16

The stiffness after yielding of the flexural reinforcement for this specimen in the south and in the north directions were 3.17 kips/in. (0.56 kN/mm) and 3.8 kips/in. (0.67 kN/mm) respectively (Figure 6.22).
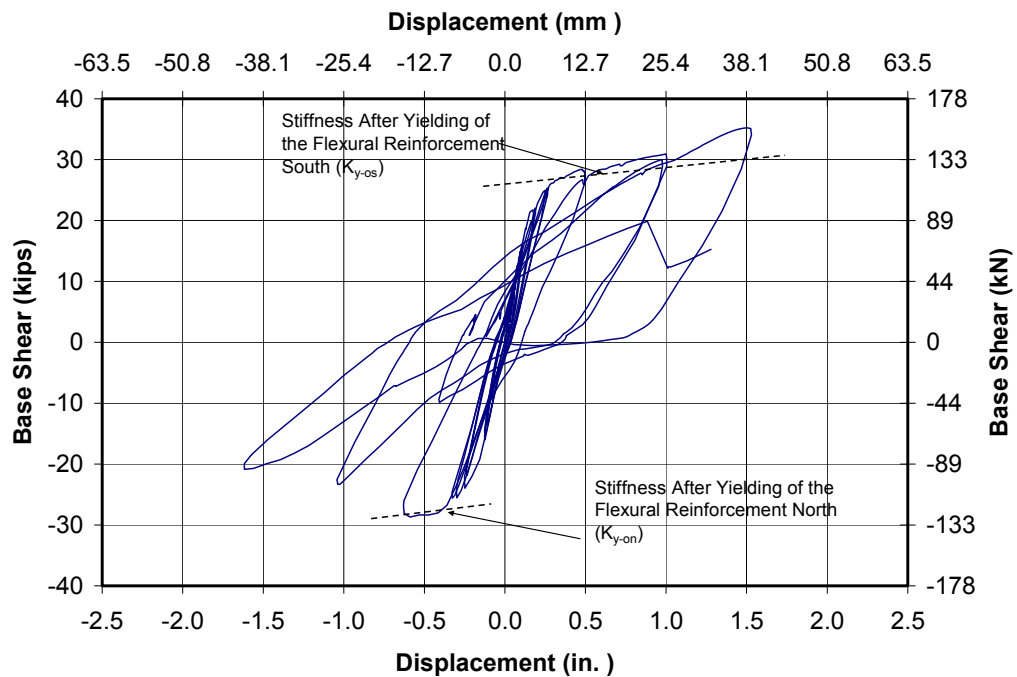
Figure 6.22 Stiffness after yielding of the flexural reinforcement in the south direction for Shear Wall Specimen 16

The maximum selected displacements for this specimen in the south and north directions were equal to 1.5 in. (38.1 mm) and 0.6 in. (15.2 mm); the corresponding displacement ductilities were equal to 5 and 1.7, and the drift ratios were equal to 1.0% and 0.4%. Figure 6.23 shows the selected drift ratios in the south and north directions for Shear Wall Specimen 15b
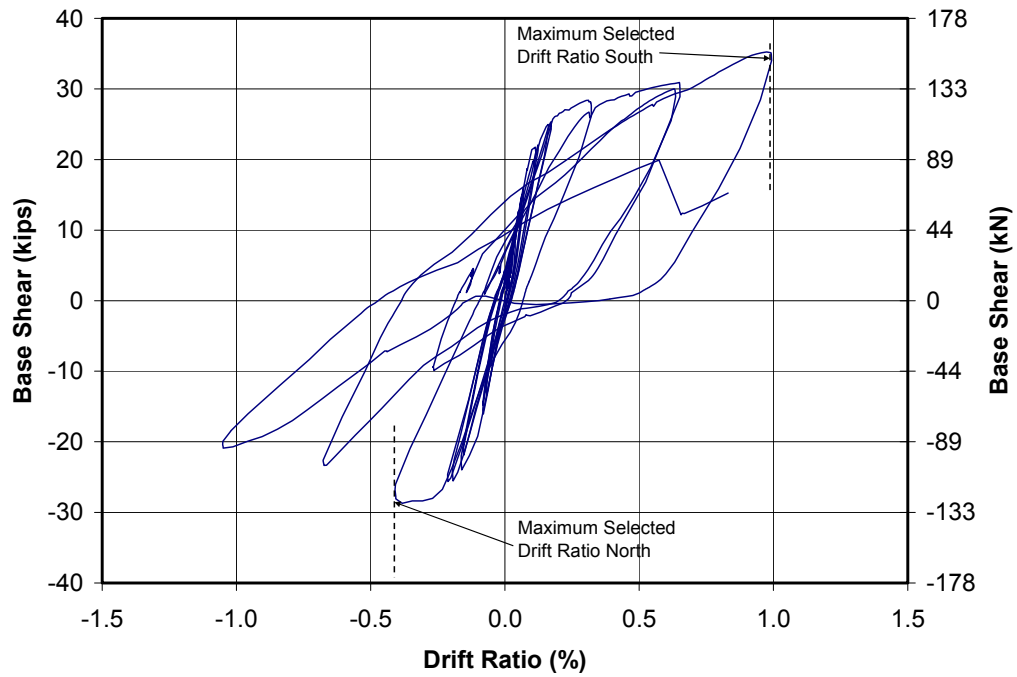
Figure 6.23 Selected drift ratios for Shear Wall Specimen 16

6.2   SUMMARY OF RESULTS FOR FLEXURE-DOMINATED SHEAR WALL SPECIMENS

The observed initial tangent stiffness (K_{ot-o}), initial backbone stiffness (K_{ob-o}), and the ratio of the initial backbone stiffness to initial tangent stiffness for each of the flexure-dominated specimens are presented in Table 6.1.

115

Table 6.1 Observed initial tangent and backbone stiffnesses for flexure-
dominated shear wall specimens

Specimen Number	K_{ot-o} Kips/in. (kN/mm)	K_{ob-o} Kips/in. (kN/mm)	K_{ob-o}/K_{ot-o}
13	61.6 (10.8)	63.4 (11.1)	1.03
14a	18.0 (3.2)	--	--
14b	44.0 (7.7)	44.0 (7.7)	1.00
15a	215.7 (37.8)	183.0 (32.0)	0.85
15b	218.7 (38.3)	190.1 (33.3)	0.87
16	139.6 (24.4)	109.9 (19.2)	0.79

The initial tangent stiffness for Shear Wall Specimen 14a was low compared with that of Shear Wall Specimen 14b (Table 6.1). This low value was related to the cracks in the leveling bed mortar caused while connecting the dual actuators to this specimen. The low value of the initial tangent and backbone stiffnesses of Shear Wall Specimen 16 compared with those of Shear Wall Specimens 15a and 15b (Table 6.1) can also be related to cracks on the leveling bed mortar caused while connecting the actuators to the specimen, to potential shrinkage cracks on that leveling bed mortar, or to variations in the properties of ASTM C270, Type S mortar by proportion, used as leveling bed mortar in each wall.

The observed secant stiffnesses after flexural cracking in the south (K_{cr-os}) and north (K_{cr-on}) directions, and the ratio of those observed secant stiffness after flexural cracking to initial tangent stiffness for each of the flexure-dominated specimens are presented in Table 6.2.

Table 6.2 Secant stiffnesses after flexural cracking for each flexure-dominated specimen

Specimen Number	K_{cr-os} Kips/in (kN/mm)	K_{cr-os}/K_{ot-o}	K_{cr-on} Kips/in (kN/mm)	K_{cr-on}/K_{ot-o}
13	24.9 (4.4)	0.40	26.0 (4.6)	0.42
14a	11.0 (1.9)	0.61	--	--
14b	12.5 (2.2)	0.28	14.4 (2.5)	0.33
15a	92.0 (16.1)	0.43	100.0 (17.5)	0.46
15b	73.9 (12.9)	0.34	81.0 (14.2)	0.37
16	87.3 (15.3)	0.63	74.4 (13.0)	0.53

Table 6.2 shows that the ratio of observed secant stiffness after flexural cracking to initial tangent stiffness varied from 0.28 to 0.61 when the specimens were loaded in the south direction, and from 0.33 to 0.53 when the specimens were loaded in the north direction. The unloading stiffnesses after web shear cracking in the south direction (K_{u-os}), and the ratio of those unloading stiffnesses to the initial tangent stiffness for each of the flexure-dominated specimens, are presented in Table 6.3. The unloading stiffnesses after web shear cracking in the north direction (K_{u-os}), and the ratio of those unloading stiffnesses to the initial tangent stiffness for each of the flexure-dominated specimens, are presented in Table 6.4.

Table 6.3 Unloading stiffnesses after yielding of the flexural reinforcement in the south direction for each flexure-dominated specimen

Specimen Number	K_{u-os} Kips/in (kN/mm)	K_{u-os}/K_{ot-o}	D_{u-os}/D_{ys}
13	18.6 (3.3)	0.30	1.71
14a	9.5 (1.7)	0.53	2.55
14b	12.5 (2.2)	0.28	1.16
15a	54.6 (9.6)	0.25	1.16
15b	62.9 (11.0)	0.29	1.23
16	64.1 (11.2)	0.46	1.67

117

Table 6.4 Unloading stiffnesses after yielding of the flexural reinforcement in the north direction for each flexure-dominated specimen

Specimen Number	$K_{u\text{-}on}$ Kips/in (kN/mm)	$K_{u\text{-}on}/K_{ot\text{-}o}$	$D_{u\text{-}on}/D_{yn}$
13	17.5 (3.1)	0.28	1.79
14a	--	--	--
14b	12.8 (2.2)	0.29	1.26
15a	54.6 (9.6)	0.25	1.04
15b	36.7 (6.4)	0.17	2.45
16	53.7 (9.4)	0.38	1.75

Table 6.3 shows that the ratio of the unloading stiffness after yielding of the flexural reinforcement varied from 0.25 to 0.53 when loading in the south direction, and Table 6.4 shows that that ratio varied from 0.17 to 0.38 when loading in the north direction. The observed stiffnesses after yielding of the flexural reinforcement in the south ($K_{y\text{-}os}$) and north ($K_{y\text{-}on}$) directions, and the ratio of those stiffnesses after yielding of the flexural reinforcement to initial tangent stiffness for each flexure-dominated specimen are presented in Table 6.5.

Table 6.5 Stiffnesses after yielding of the flexural reinforcement for each flexure-dominated specimen

Specimen Number	$K_{y\text{-}os}$ Kips/in (kN/mm)	$K_{y\text{-}os}/K_{ot\text{-}o}$	$K_{y\text{-}on}$ Kips/in (kN/mm)	$K_{y\text{-}on}/K_{ot\text{-}o}$
13	1.3 (0.23)	0.021	1.2 (0.21)	0.019
14a	0.7 (0.12)	0.039	--	--
14b	0.7 (0.12)	0.016	1.1 (0.19)	0.025
15a	2.6 (0.46)	0.012	0.6 (0.11)	0.003
15b	2.8 (0.49)	0.013	3.7 (0.65)	0.017
16	3.2 (0.56)	0.023	3.8 (0.67)	0.027

Table 6.5 shows that the ratio of observed stiffness after yielding of the flexural reinforcement to initial tangent stiffness varied from 0.012 to 0.039 when loading in the south direction, and from 0.013 to 0.039 when loading in the north direction.

118

In general, Shear Wall Specimen 14a and 16 presented the highest values of the ratios of the stiffness after flexural cracking to initial tangent stiffness (Table 6.2), of unloading stiffness to initial tangent stiffness (Table 6.3 and Table 6.4), and of stiffness after yielding of the flexural reinforcement to initial tangent stiffness (Table 6.5). The reason for those high values was the low value of the initial tangent stiffness observed for those specimens.

The maximum selected displacement ductilities and global drift ratios for each flexure-dominated specimen are presented in Table 6.6.

Table 6.6 Maximum selected displacement ductilities and drift ratios for each flexure-dominated specimen

Specimen Number	$\mu_{\Delta\text{-os}}$	$\mu_{\Delta\text{-on}}$	δ_{os} (%)	δ_{on} (%)
13	4.8	4.0	1.4	1.1
14a	5.0	--	1.9	--
14b	5.4	2.6	1.9	1.0
15a	6.0	5.8	1.0	1.0
15b	4.8	4.8	1.0	1.0
16	5.0	1.7	1.0	0.4

Table 6.6 shows that the maximum selected displacement ductilities and drift ratios varied from 4.8 to 6.9 and from 1.0% to 1.9% in the south direction respectively, and varied from 1.7 to 5.8 and from 0.4% to 1.1% in the north direction respectively. The selected displacement ductility and drift ratio in the north direction for Shear Wall Specimen 14b were low compared with those observed in the south direction. This difference can be attributed to the effect of the cyclic loading on the overall response of the wall, and to the large increment in the imposed displacement in consecutive load cycles during the test. The selected displacement ductility of 1.7 and drift ratio of 0.4% for Shear Wall Specimen 16 were low compared with the other corresponding observed values. The reasons for those low values were the following:

- cracking between the end vertical panel and the U blocks at the lower north corner of the wall damaged the north compressive toe early during the test (Figure 6.24); and

- additional axial load was applied inadvertently to this specimen during the test because the bottoming out of the rams connected to the load maintainer.

Figure 6.24 Vertical cracks at the north and south ends of Shear Wall Specimen 16 at the end of the test

A replica of this specimen was tested using Heli-fix® ties (Figure 6.25) between the vertical panel and the U blocks along the wall height and moving the flexural reinforcement away from the vertical joint between those U-blocks and the vertical panel. These changes eliminated the large vertical cracks observed in

Shear Wall Specimen 16 and improved the behavior of the compressive toe and the overall behavior of that specimen (Cancino 2003) (Figure 6.26).
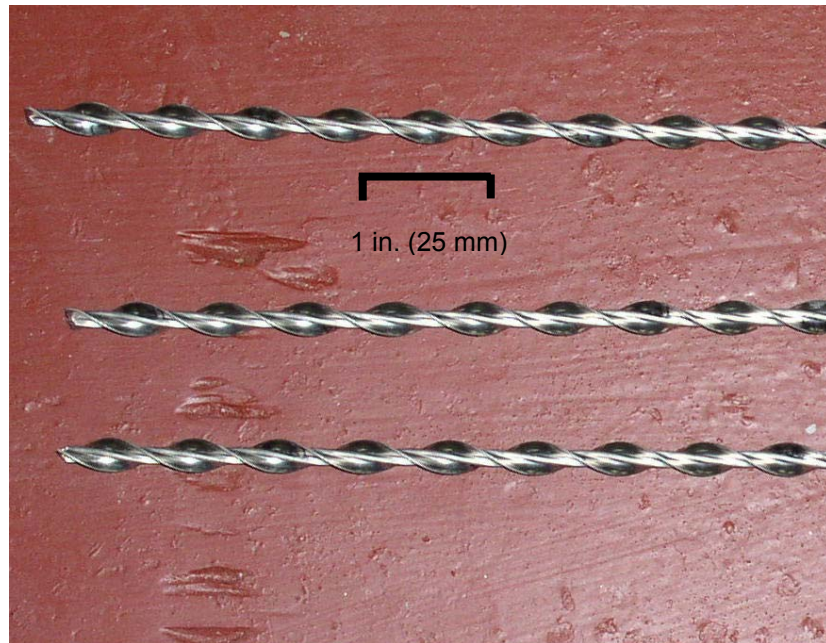
Figure 6.25 Heli-fix® ties

Figure 6.26 View of North compressive toe of Shear Wall Specimen 17

The behavior of the six flexure-dominated specimens at the end of the tests was in general governed by crushing of the compressive toe, that is, tests were in general stopped when severe damage was observed in any of the compressive toes of the walls. Figure 6.27 and Figure 6.26 show the compressive toes of Shear Wall Specimens 13 and 15a at the end of the test. If the compressive toe were improved by using Heli-fix[®] ties or walls with flanges, the overall hysteretic behavior of the AAC walls would be improved, and larger drift ratios and displacement ductility capacities would also be reached for AAC flexure-dominated walls.

Figure 6.27 North compressive toe of Shear Wall Specimen 13 at the end of the test

Figure 6.28 South compressive toe of Shear Wall specimen 15a at the end of the test

6.3   BEHAVIOR OF THE TWO-STORY ASSEMBLAGE SPECIMEN

Even though the two-story assemblage specimen was designed to behave also as a flexure-dominated specimen, its overall hysteretic behavior was influenced by web shear cracking in the lower story of both walls, and by sliding between those walls and the corresponding concrete foundations.   This is discussed further in Tanner (2003). In general the behavior of the specimen was defined by the list of events presented below:

- web-shear cracking in the lower story of both walls;
- yielding of the flexural reinforcement; and
- sliding between the walls and the underlying concrete base.

123

Although the intent of this dissertation is not to describe the behavior of the assemblage specimen in terms of those events, they are briefly explained to better understand the observed hysteretic behavior of that specimen. Details of these and other events are presented in Tanner (2003). Web shear cracking was observed in the assemblage specimen because the actual shear capacity of the AAC walls was lower than that expected. The initial predictions for web shear cracking were based on the tested strength of previously received Class 4 AAC material from Babb. ASTM C1006 splitting tensile strength tests performed on the assemblage material prior to testing of the assemblage gave a splitting tensile strength of 53 psi (0.36 MPa), significantly below the splitting tensile strength of 85 psi (0.58 MPa) observed from previous shipments of Class 4 AAC from the same manufacturer. The observed tensile strength of 53 psi (0.36 MPa) was not used in the initial prediction of assemblage strength because the moisture content at testing was 25%, above the maximum specified in ASTM C1386. After testing the assemblage, further tests of the assemblage material conducted at C1386 moisture contents, gave a compressive strength of 495 psi (3.4 MPa) and splitting tensile strength of 45 psi (0.31 MPa), both of which fall below the tested strengths of the prior Babb shipments of Class 4 AAC material. The tested compressive strength of 495 psi (3.4 MPa) was also below the minimum value specified in ASTM C1386 for Class 4 AAC. While this lower strength did not decrease the assemblage flexural capacity significantly, it did produce a proportional decrease in web shear cracking capacity, reducing it to (45 / 85), or 0.53 times the original prediction. Reasons for the non-complying material are not clear. Because of the non-complying material, the assemblage showed unexpected web shear cracking. This did not, however, appear to affect its flexural behavior. It may have slightly decreased the assemblage's drift and displacement ductility capacities. Sliding of the walls after yielding of the flexural reinforcement was related to the formation

of diagonal cracks around the dowels at the base of the wall (Figure 6.29). These diagonal cracks reduced the effectiveness of the dowel action and the overall sliding shear capacity of the walls of the assemblage specimen.

Figure 6.29 Diagonal cracks around the dowels of the assemblage specimen

The initial flexural capacity of the assemblage specimen was higher than predicted because of the contribution of the dowels to the flexural capacity. After the formation of diagonal cracks around the dowels, that contribution was eliminated, and the flexural capacity of the specimen was reduced to the originally predicted value. The strength degradation presented in Figure 6.30 and Figure 6.31 is also related to the shear cracking observed in the assemblage specimen. The overall hysteretic behavior of each wall of the assemblage specimen at the end of the test is presented in Figure 6.30 and Figure 6.31.
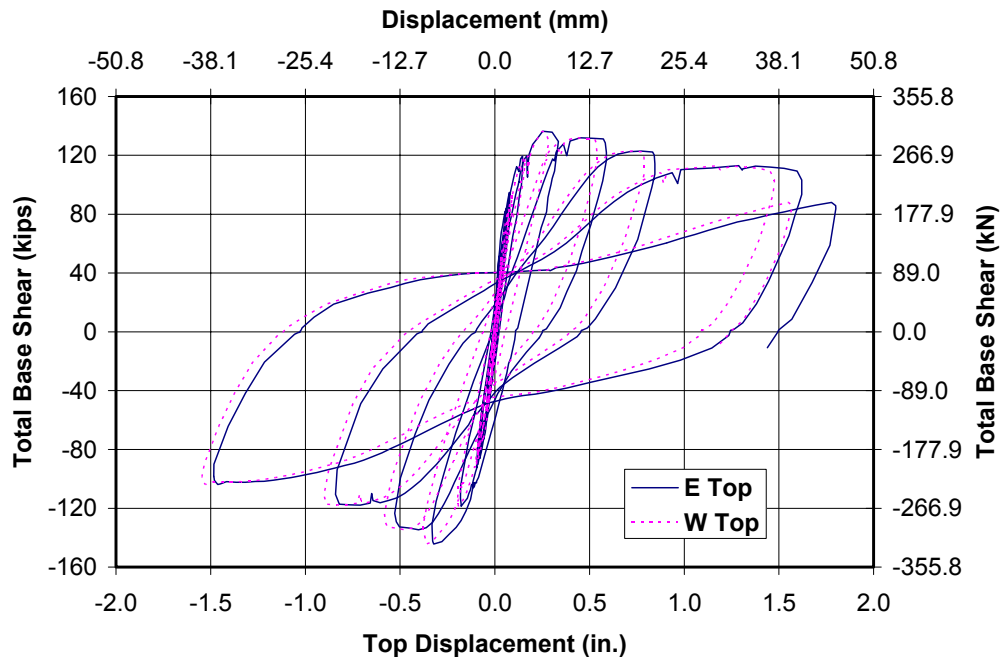
Figure 6.30 Overall hysteretic behavior of the assemblage specimen (including sliding at the base)
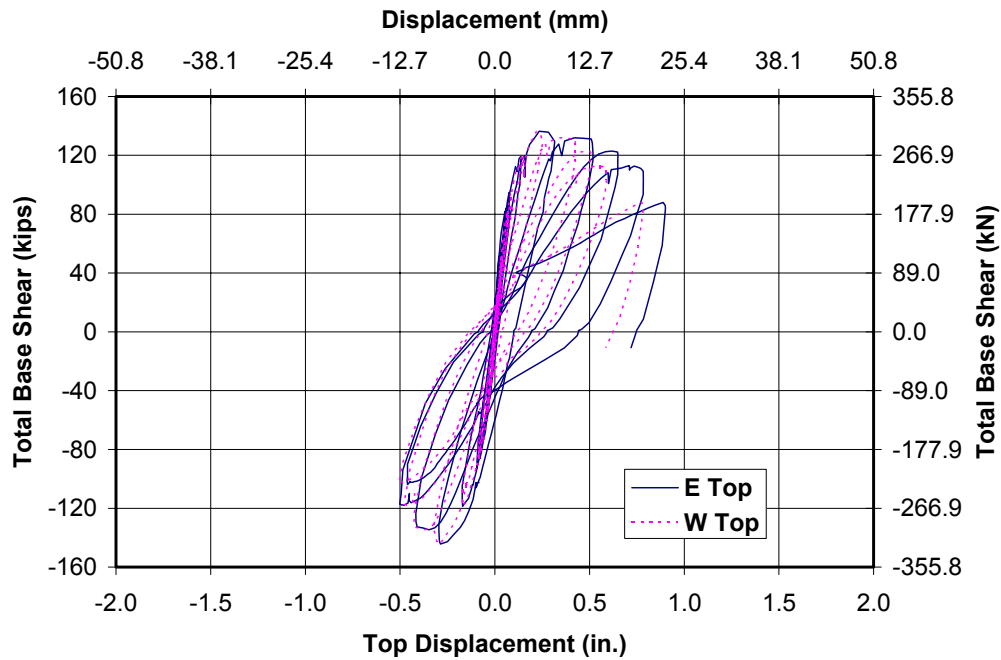
Figure 6.31 Overall hysteretic behavior of the assemblage specimen (corrected

for sliding at the base)

The observed displacements at yielding of the flexural reinforcement (Δ_y), the maximum observed displacements (Δ_m), and the maximum displacements corrected for sliding (Δ_{mc}) for each wall of the assemblage specimen are presented in Table 6.7.

Table 6.7 Maximum displacements for each wall of the assemblage specimen

Wall	Loading direction	Δ_y in. (mm)	Δ_m in. (mm)	Δ_{mc} in. (mm)
East	South	0.15 (3.8)	1.80 (45.7)	0.90 (22.9)
East	North	0.16 (4.1)	1.48 (37.6)	0.50 (12.7)
West	South	0.20 (5.1)	1.57 (39.9)	0.78 (19.8)
West	North	0.26 (6.6)	1.55 (39.4)	0.50 (12.7)

Displacements at yielding of the flexural reinforcement (Δ_y) as presented in Table 6.7 were based on the readings of the strain gages mounted on the flexural reinforcement of each wall. The strain gages were located 3 in. (76.2 mm), 6 in. (152.4 mm) and 9 in. (228.6 mm) from the bottom of the walls. Both displacements Δ_y for the east wall and the west wall in the south direction were based on the reading of the strain gages located 3 in. (76.2 mm) from the bottom. The displacement Δ_y for the west wall of 0.26 in. (6.6 mm) in the north direction, however was based on the reading of the strain gage located 9 in. (228.6 mm) from the bottom of the wall, because the other two strain gages did not work. A value of 0.2 in. (5.1 mm) was assumed as displacement at yielding of the flexural reinforcement for the west wall in the north direction. This value of 0.2 in. (5.1 mm) is equal to the displacement at yielding observed in the same wall in the south direction. The maximum displacements Δ_m and Δ_{mc} are the maximum displacements observed during tests; that is, the maximum displacements are not selected based on the criteria presented for the flexure-dominated specimens. The final maximum displacement ductilities calculated using the observed maximum displacements and those displacements corrected for sliding, are presented in Table 6.8.

Table 6.8 Maximum displacement ductilities for each wall of the assemblage specimen

Wall	Loading direction	μ_m	μ_{mc}
East	South	12.0	6.0
East	North	9.2	3.1
West	South	7.85	3.9
West	North	7.75	2.5

128

Table 6.8 shows that the maximum displacement ductilities calculated using the maximum observed displacements varied from 7.75 to 12.0, and those calculated correcting for sliding varied from 2.5 to 6.0. The overall hysteretic behavior of the assemblage specimen as a function of the drift ratios including and not including sliding are presented in Figure 6.32 and Figure 6.33 respectively.
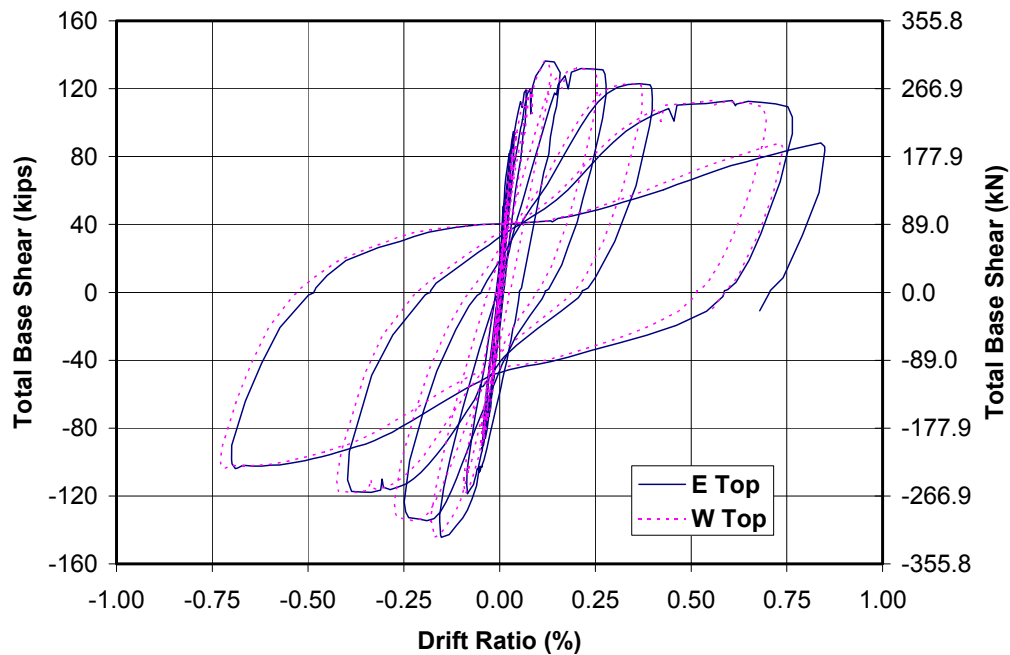
Figure 6.32 Overall hysteretic behavior of the assemblage as a function of drift ratio (including sliding at the base)
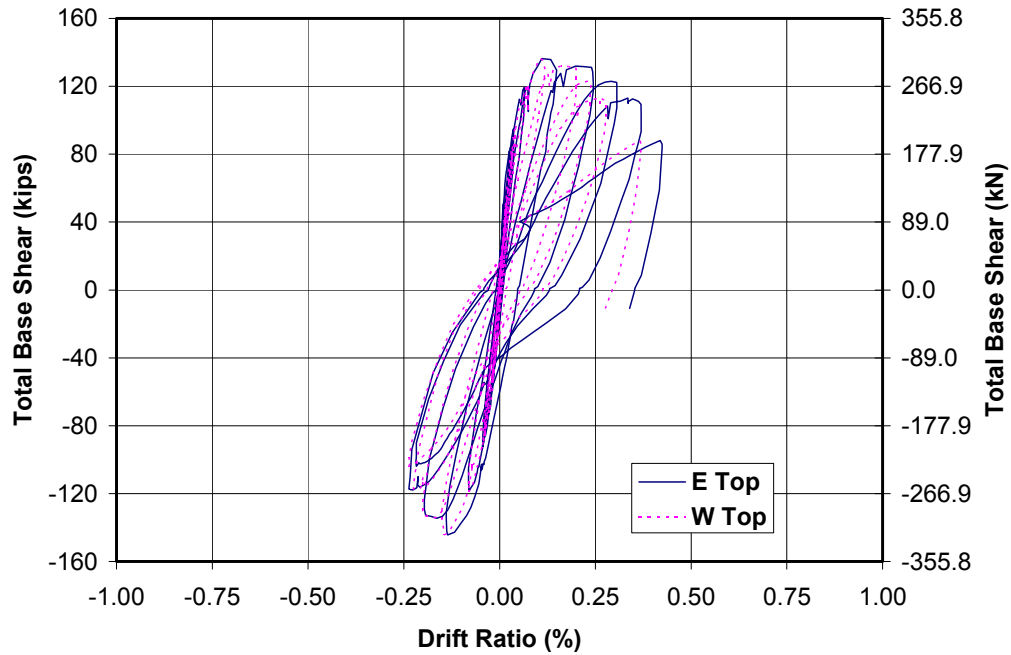
Figure 6.33 Overall hysteretic behavior of the assemblage as a function of drift ratio (corrected for sliding at the base)

The maximum drift ratios including sliding (δ_m) and the maximum drift ratios corrected for sliding (δ_{mc}) for each of the walls of the assemblage specimen are presented in Table 6.9.

Table 6.9 Maximum drift ratios for each wall of assemblage specimen

Wall	Loading direction	δ_m (%)	δ_{mc} (%)
East	South	0.85	0.42
East	North	0.70	0.24
West	South	0.74	0.37
West	North	0.73	0.24

130

Table 6.9 shows that the maximum drift ratios including sliding varied from 0.70% to 0.85%, and those excluding sliding varied from 0.24% to 0.42%. The behavior of the assemblage specimens at the end of the test was in general governed by large vertical cracks at the interfaces between the web and the flanges of the walls (Figure 6.34). These cracks formed because the flanges did not slide with the webs in the direction of loading. Crushing of the compressive toes of the walls of the assemblage specimen was not observed as it had been for the flexure-dominated shear wall specimens.

Figure 6.34 Vertical crack at the north end of east wall (base of first story wall)

6.4   SUMMARY OF RESULTS FOR THE TWO-STORY ASSEMBLAGE SPECIMEN

The overall hysteretic behavior of the assemblage specimen was defined by web shear cracking, yielding of the flexural reinforcement, and sliding shear. The observed strength degradation in the hysteresis loop was related to the formation of diagonal cracks around the dowels, which reduced both the sliding

shear capacity and the flexural capacity of the walls of the assemblage. Even though web shear cracking was observed in that specimen, the walls of the assemblage specimen reached displacement ductilities that were reasonably consistent with those observed in the flexure-dominated specimens. The maximum observed drift ratios were small compared with those observed for the flexure-dominated specimens. The major reasons were the large stiffness of the walls of the assemblage compared with that of the flexure-dominated specimens, and the presence of web shear cracking and sliding in the assemblage specimen. The behavior of the walls of the assemblage specimen showed that crushing of the compressive toe can be delayed or prevented by using walls with flanges.

CHAPTER 7

Development of Procedure to Select the Ductility Reduction Factor R_d for AAC structures

The seismic force-reduction factor (R) presented in this dissertation for flexure-dominated AAC structures can be defined as the product of a ductility reduction factor (R_d) and a system overstrength factor (Ω_{system}) as shown in Equation (7.1).

$$R = R_d \, \Omega_{system} \qquad\qquad \textbf{\textit{(7.1)}}$$

Equation (7.1) is consistent with that proposed in NEHRP (2000) for different structural systems, and also with that proposed in Uang (1991). Equation (7.1) shows that the value of the factor R for AAC structures depends on the selection of appropriate values of the factors R_d and Ω_{system} for those structures. In this chapter, a general procedure for selecting the ductility reduction factor (R_d) for AAC structures is presented. This procedure involved the selection and scaling of suites of earthquakes, selection and design of different AAC structures, selection of maximum displacement ductility and drift ratio capacities, and selection of nonlinear analysis program and corresponding analytical models, which are all presented in this chapter.

7.1 DESCRIPTION OF PROCEDURE TO SELECT THE DISPLACEMENT DUCTILITY FACTOR R_d

The following is a general description of the iterative procedure used to select the ductility reduction factor (R_d) for flexure-dominated AAC structures.

133

1) Select the type of AAC structure (for example, cantilever or coupled-wall structure).

2) Select the preliminary plan geometry of the AAC walls (thickness and plan length) based on architectural layout, other restrictions (such as manufacturer's limitations on different unit sizes), or both.

3) Select the structure's number of stories based on the architectural design, the maximum compressive strength of the AAC, or both.

4) Select a tributary width based on architectural plan distribution (for example, wall spacing).

5) Calculate the weights of different stories of the structure using the selected tributary width and the density of the materials (for example, density of AAC, reinforced concrete, or both).

6) Obtain the design spectrum according to the IBC 2000 using the intended geographic location of the structure.

7) Analyze the structure using the modal analysis procedure specified in the IBC 2000.

8) Calculate the elastic global drift ratio of the structure and compare it with the drift ratio capacity of 1% selected for AAC shear-wall structures (selection of drift ratio capacity is presented in Section 7.4). In this step, a value of ductility reduction factor R_d of one is used ($R_d = 1$). If the global drift ratio of the structure exceeds 1% then the wall length needs to be increased, its tributary width decreased, or both.

9) Assume that the flexural capacity of the walls and coupling beams if any, are equal to the bending moments obtained from the elastic analyses.

10) Select a suite of earthquakes representative of the design response spectrum.

11) Select an earthquake from the suite.

134

12) Select a value of R_d greater than unity. Redesign the structure for a reduced flexural capacity. For example, if R_d is selected as 2, then the required flexural capacity is reduced by a factor of 2.

13) Run a dynamic nonlinear analysis and calculate the drift ratio and displacement ductility demands. In this step, the earthquake selected in Step 11 is used with the design flexural capacity from step 12. If the drift ratio demand is equal to 1%, the value of R_d assumed is the critical value of R_d based on drift ratio, similarly, if the displacement ductility demand is equal to 3.5, the assumed value of R_d is the critical value based on displacement ductility.

14) Repeat for other earthquakes of the same suite, for other suites of earthquakes, and other AAC shear wall structures.

The procedure described above is used to select critical values of R_d based on drift ratio and displacement ductility capacities for AAC structures subjected to earthquake ground motions representing different seismic zones of the United States. The selection of the values of maximum drift ratio and displacement ductility capacities of 1% and 3.5 respectively are presented later in this chapter. The general procedure for selecting critical values of the factor R_d based on drift ratio and displacement ductility capacities is presented as flow charts in Figure 7.1 and Figure 7.2 respectively.
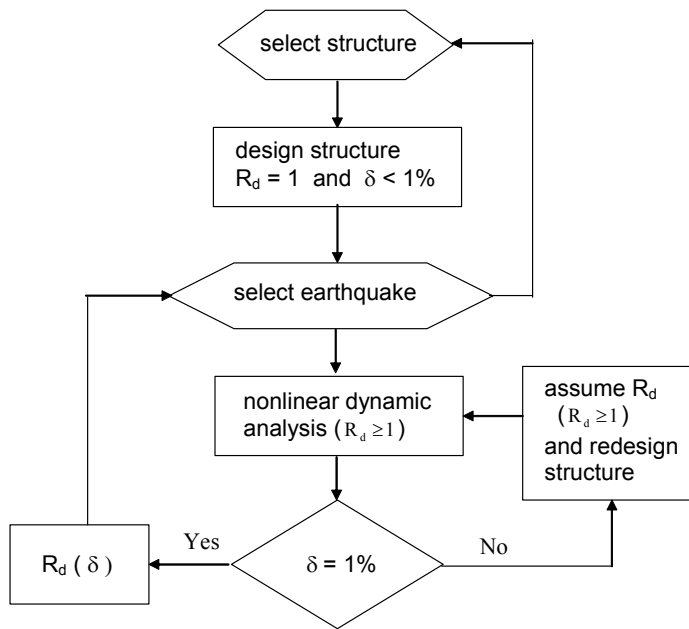
Figure 7.1 Procedure for selecting the factor R_d based on drift ratio
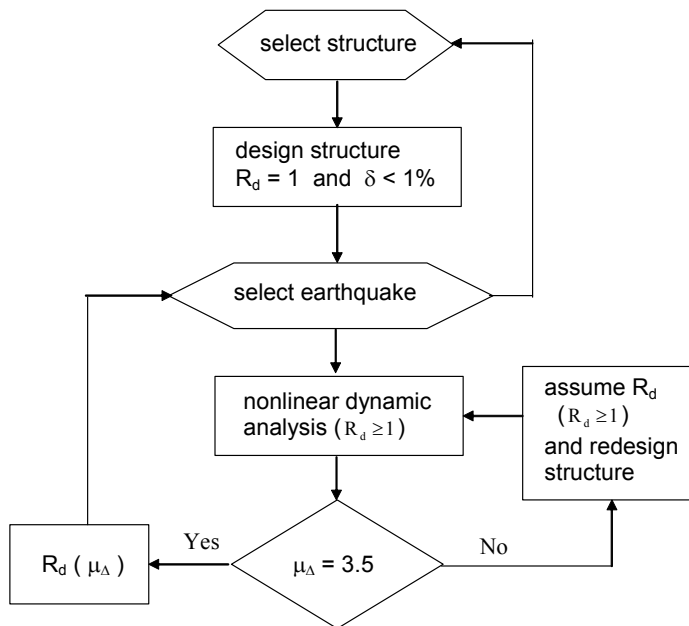
Figure 7.2 Procedure for selecting the factor R_d based on displacement

ductility

136

7.2   SELECTION AND SCALING OF SUITES OF EARTHQUAKES

Different suites of earthquake ground motions were selected based on areas with high potential for seismic activity. Zones in the central and eastern US were considered, and also zones in the western US. For the central and eastern US, three suites of earthquakes were selected: Charleston, SC; Carbondale, IL; and Memphis, TN. For the western US, two suites of earthquakes were selected: Los Angeles, CA; and Seattle WA. Each suite of earthquakes consists of ten earthquake ground motions.

7.2.1   Selection of Suite of Earthquakes for Central and Eastern US

Charleston, SC is a seismic region where earthquake ground motions of engineering interest are scarce. The use of synthetic earthquake ground motions representative of the seismicity of that region is a good alternative. A model created by Frankel *et al*. (1996) was used to develop synthetic ground motions representative of the B-C soil class interface of Charleston, SC. The suite of earthquakes for Charleston, SC used in this project was taken from that work, and corresponds to a 2% probability of exceedance in 50 years.

New Madrid is also a seismic zone where strong earthquake ground motions are scarce. Projects RR-1 and RR-2 of the Mid-America Earthquake Center (MAE) involved the development of uniform hazard spectra and synthetic ground motions for three major Mid-American cities: Carbondale, IL, Memphis, TN, and St. Louis, MO (Wen and Wu 1999). The ground motions used in this project for Carbondale, IL and Memphis, TN were taken from those projects RR-1 and RR-2. The selected suites are representative of the Soil Profile of Carbondale, IL and Memphis, TN, and correspond to a 2% probability of exceedance in 50 years

7.2.2 Selection of Suite of Earthquakes for Western US

The SAC Phase 2 Steel Project provided suites of earthquake ground motions for three United States cities: Boston, MA, Los Angeles, CA and Seattle, WA (Somerville *et al*. 1997). The suites of earthquakes for Los Angeles, CA and Seattle, WA used in this project were taken from that SAC project. The selected suites are representative of Soil Class D, and correspond to a 2% probability of exceedance in 50 years.

7.2.3 Scaling of Suites of Earthquakes

The selected five suites of earthquakes were scaled to represent the design seismic forces. Acceleration response spectra were calculated for each entire suite of earthquakes and compared with corresponding design spectra. For Charleston, Carbondale, and Memphis, acceleration response spectra were compared with corresponding IBC 2000 Site Class C design spectra and for Los Angeles and Seattle, with corresponding IBC 2000 Site Class D design spectra. Each entire suite was scaled using a single scaling factor calculated as follows:

1) Calculate the elastic response spectra for the suite of earthquakes.
2) Calculate the mean spectral accelerations of the response spectra for periods of 0.26 seconds and 0.62 seconds. In this step, periods of 0.26 seconds and 0.62 seconds are used because they represent the natural periods of the three-story and five-story AAC shear-wall structures studied.
3) Calculate a scaling factor for each period as the design spectral acceleration divided by the average spectral acceleration.
4) The final single scaling factor is the average of the two scaling factors calculated in Step 3. Two scaling factors, however, were used for the

suite of Charleston because of the large difference between the two scaling factors calculated in Step 3.

Table 7.1and Table 7.2 show examples of the procedure used to select the scaling factors for the suite of earthquakes of Los Angeles and Charleston respectively, and Table 7.3 shows the scaling factors selected for each of the suites of earthquakes studied.

Table 7.1 Procedure to select scaling factor for the suite of earthquakes of Los Angeles

Earthquake Name	Spectral Acceleration (cm/s^2) $T_n=0.26$ sec	Spectral Acceleration (cm/s^2) $T_n=0.62$ sec
La21	1797	2171
La24	829	2041
La25	1927	1853
La26	1788	2135
La27	1515	1504
La29	2539	1183
La33	2172	1686
La34	1937	1894
La35	2668	2198
La37	1008	1561
Average	1818	1823
Design Spectral Acceleration Site Class D	1145	1145
Scaling Factor	0.63	0.63
Single Scaling Factor	**0.63**	

139

Table 7.2 Procedure to select scaling factors for the suite of earthquakes of Charleston

Earthquake Name	Spectral Acceleration (cm/s^2) T_n=0.26 sec	Spectral Acceleration (cm/s^2) T_n=0.62 sec
acc-401-1	1098	324
acc-402-1	1330	509
acc-403-1	1317	591
acc-404-1	1216	889
acc-405-1	1476	676
acc-406-1	1515	515
acc-407-1	1183	391
acc-408-1	1779	644
acc-409-1	1030	545
acc-410-1	1045	442
Average	1299	553
Design Spectral Acceleration Site Class C	1053	641
Scaling Factor	0.81	1.16
Single Scaling Factor	--	

Table 7.3 Scaling factors for each of the suite of earthquakes studied

Suite of Earthquakes	Site Class	Scaling Factor T_n=0.26 sec	Scaling Factor T_n=0.62 sec	Single Scaling Factor
Los Angeles	D	0.63	0.63	0.63
Seattle	D	0.55	0.47	0.51
Carbondale	C	0.60	0.58	0.59
Memphis	C	0.92	0.77	0.84
Charleston	C	0.81	1.16	--

Figure 7.3 shows the Los Angeles response spectra without any scaling factor and the corresponding design spectrum for IBC 2000 Site Class D. Figure 7.4 shows the Los Angeles response spectra scaled by a factor of 0.63 and the design spectrum for IBC 2000 Site Class D.
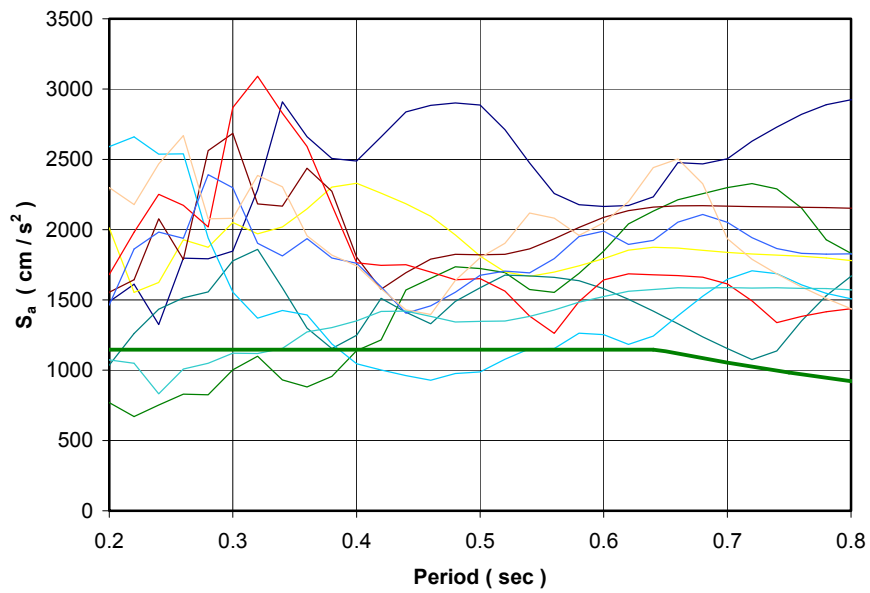
Figure 7.3 Response spectra without any scaling factor and Site Class D design spectrum for Los Angeles
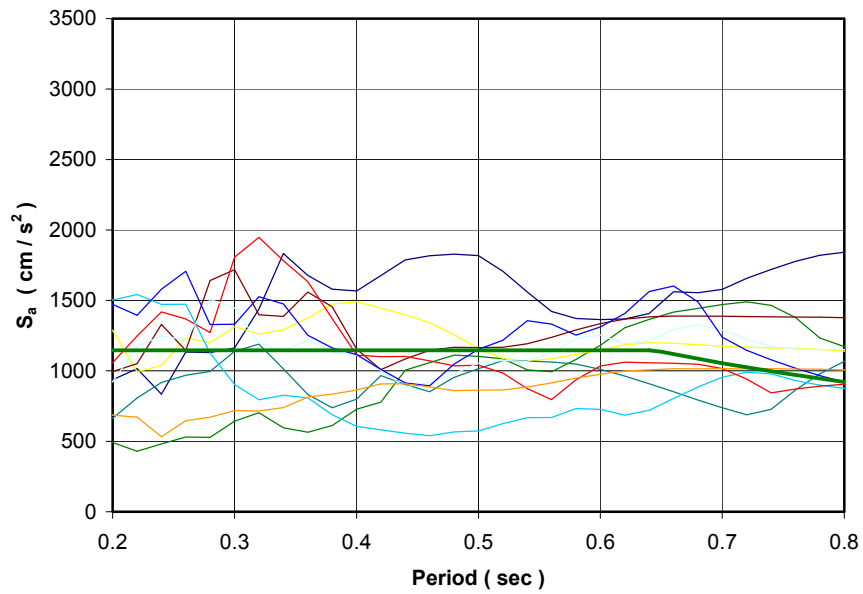
Figure 7.4 Response spectra scaled by a factor of 0.63 and Site Class D design spectrum for Los Angeles

141

Figure 7.5 shows the Seattle response spectra scaled by a factor of 0.51 and the design spectrum for IBC 2000 Site Class D. Figure 7.6 shows the Carbondale response spectra scaled by a factor of 0.59 and the design spectrum for IBC 2000 Site Class C. Figure 7.7 shows the Memphis response spectra scaled by a factor of 0.84 and the design spectrum for IBC 2000 Site Class C. Figure 7.8 shows the Charleston response spectra scaled by a factor of 0.81 and the design spectrum for IBC 2000 Site Class C. Figure 7.9 shows the Charleston response spectra scaled by a factor of 1.16 and the design spectrum for IBC 2000 Site Class C.
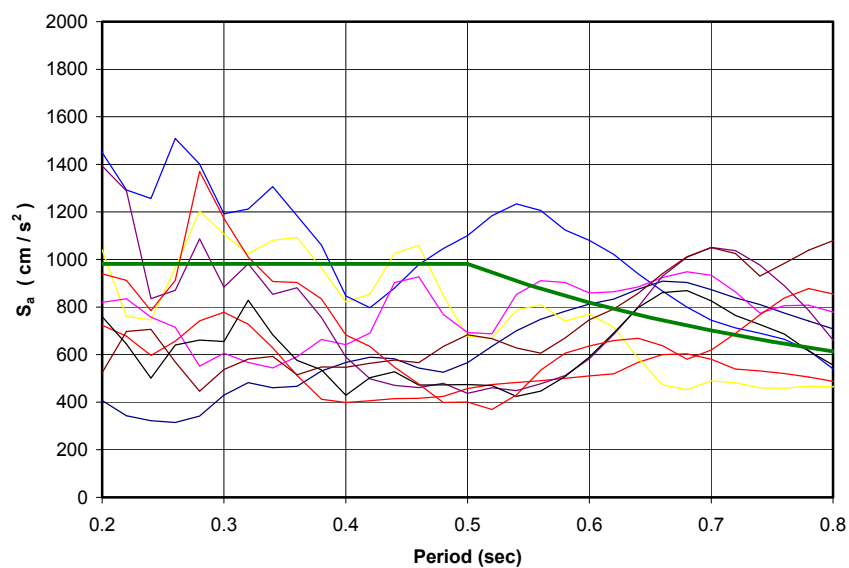
Figure 7.5 Response spectra scaled by a factor of 0.51 and Site Class D design spectrum for Seattle
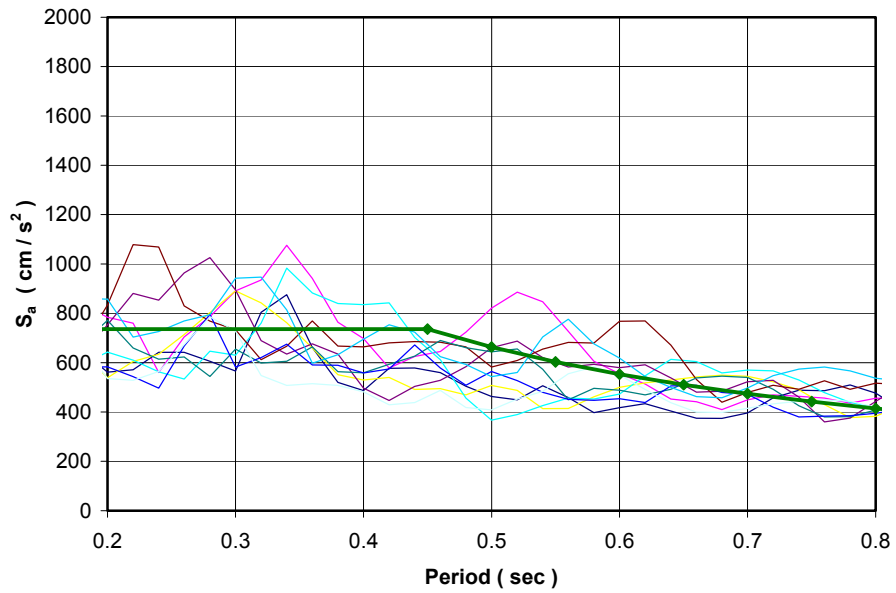
Figure 7.6 Response spectra scaled by a factor of 0.59 and Site Class C design spectrum for Carbondale
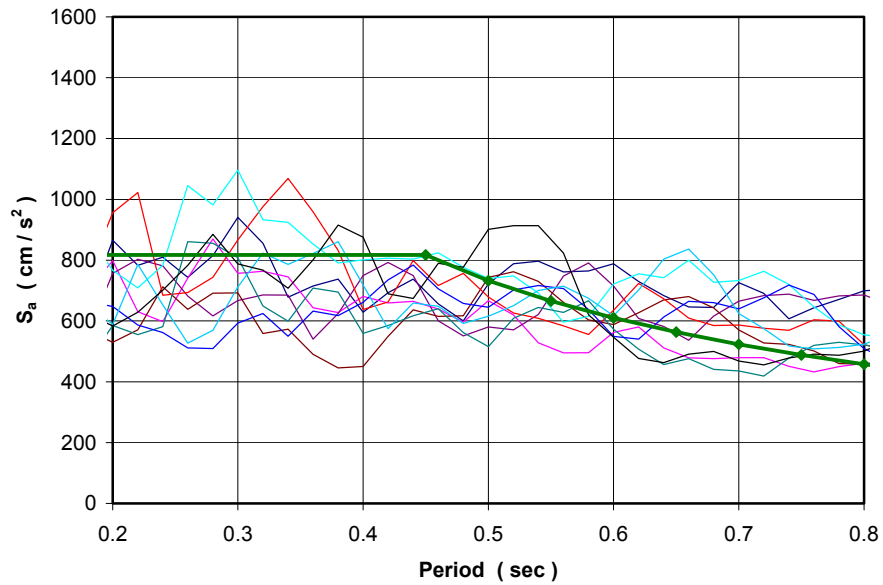
Figure 7.7 Response spectra scaled by a factor of 0.84 and Site Class C design spectrum for Memphis

143
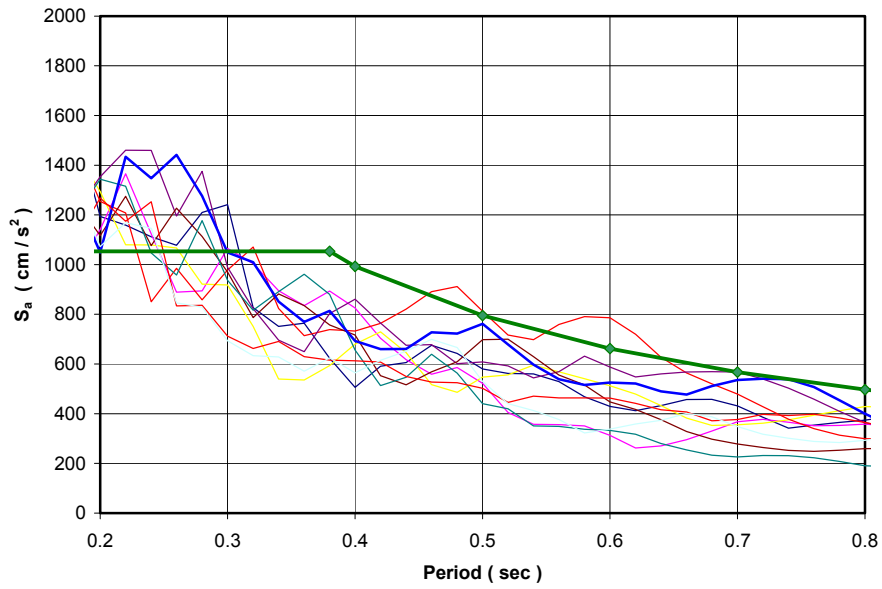
Figure 7.8 Response spectra scaled by a factor of 0.81 and Site Class C design spectrum for Charleston
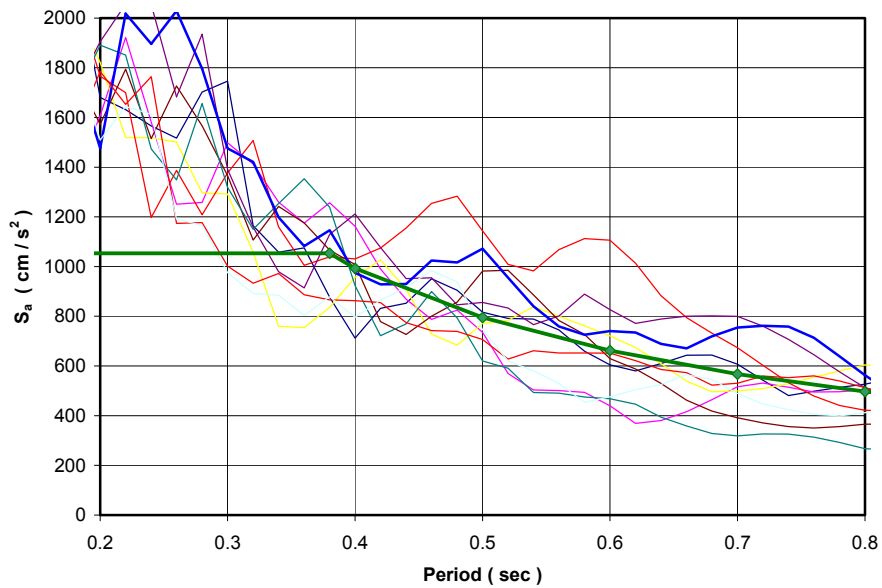
Figure 7.9 Response spectra scaled by a factor of 1.16 and Site Class C design spectrum for Charleston

144

7.3 SELECTION AND DESIGN OF AAC STRUCTURES

Four AAC structures were selected for evaluation under earthquake ground motions from different seismically active regions of the United States. The four structures were selected as AAC shear-wall structures because shear walls are the major structural elements resisting seismic forces. The AAC structures selected were a three and a five-story cantilever-wall structure (Figure 7.10), and a three and a five-story coupled-wall structure (Figure 7.11 and Figure 7.12 respectively). Typical wall dimensions of 240 in. (6.1 m) long, 120 in. (3 m) high and 10 in. (0.25 m) thick were used in every story of each structure. The coupled-wall structures consisted of two cantilever walls connected by coupling beams at every story. All coupling beams were 48 in. (1.2 m) long, 40 in. (1 m) wide and 10 in. (0.2 m) thick. Slabs were made of AAC planks 10 in. (0.25 m) thick.
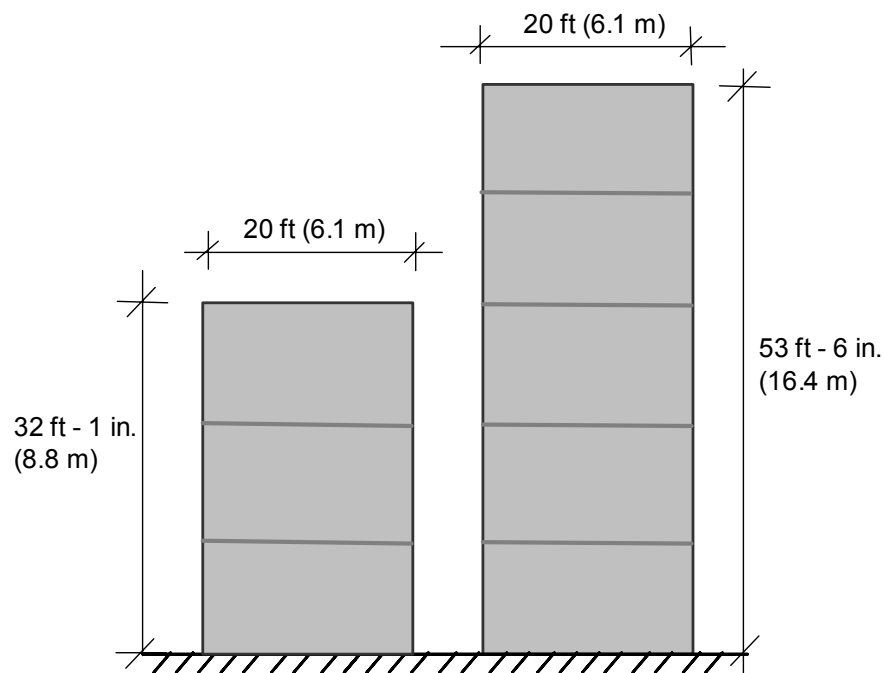
Figure 7.10 Selected cantilever wall structures
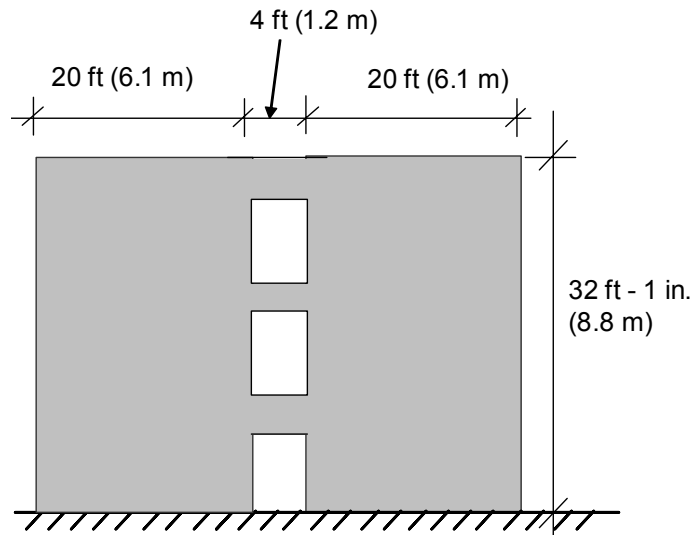
Figure 7.11 Selected three-story coupled-wall structure
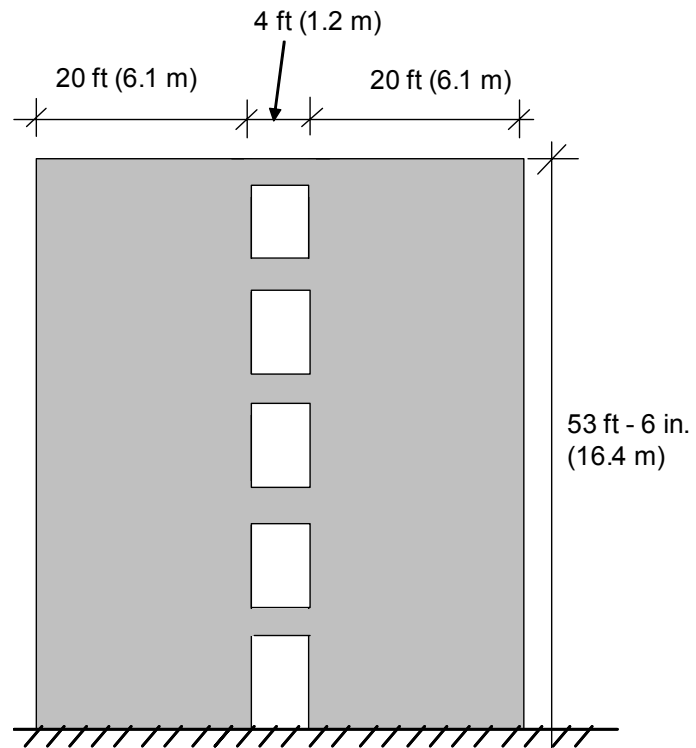
Figure 7.12 Selected five-story coupled-wall structure

146

Each AAC structure was analyzed and designed following the steps described in the procedure to select the factor R_d. The structures were modeled as planar structures. A tributary width of 240 in. (6.1 m) was assumed to calculate the weights of each story. Table 7.4 shows the story weights calculated for each of the selected structures. In that table, ST-1W-3S and ST-1W-5S are the three and five-story cantilever structures, and ST-2W-3S and ST-2W-5S are the three and five-story coupled-wall structures.

Table 7.4 Story weights for each of the selected structures

Structure	Story 1 kips (kN)	Story 2 kips (kN)	Story 3 kips (kN)	Story 4 kips (kN)	Story 5 kips (kN)
ST-1W-3S	34.7 (154)	34.7 (154)	29.0 (129)	--	--
ST-1W-5S	34.7 (154)	34.7 (154)	34.7 (154)	34.7 (154)	29.0 (129)
ST-2W-3S	76.4 (340)	76.4 (340)	63.7 (283)	--	--
ST-2W-5S	76.4 (340)	76.4 (340)	76.4 (340)	76.4 (340)	63.7 (283)

Design spectra for the seismic regions studied were calculated using site classes consistent with the suite of earthquakes selected (Figure 7.3 to Figure 7.9). Elastic analyses were carried out using the program SAP2000, with a reduced initial stiffness consistent with that used in the nonlinear analyses as presented in Section 7.5. Table 7.5 shows the natural period (T_n), base shear, and bending moment at base of the walls calculated from the modal analysis procedure for each of the four selected structures. Five modes were included in the modal analyses for the five-story structures, and three for the three-story structures.

147

Table 7.5 Natural period, base shear and bending moment at the base of the
walls calculated for each selected structure

Structure	Location	Site Class	T_n sec	Base Shear kips (kN)	Bending Moment Kip-in. (kN-m)
ST-1W-3S	Los Angeles	D	0.26	89 (396)	26788 (3027)
ST-1W-3S	Seattle	D	0.26	77 (342)	22957 (2594)
ST-1W-3S	Carbondale	C	0.26	58 (258)	17226 (1947)
ST-1W-3S	Memphis	C	0.26	64 (285)	19122 (2161)
ST-1W-3S	Charleston	C	0.26	83 (369)	24650 (2785)
ST-1W-5S	Los Angeles	D	0.62	143 (636)	67547 (7633)
ST-1W-5S	Seattle	D	0.62	101 (449)	46632 (5269)
ST-1W-5S	Carbondale	C	0.62	70 (311)	31564 (3567)
ST-1W-5S	Memphis	C	0.62	77 (342)	34839 (3937)
ST-1W-5S	Charleston	C	0.62	87 (387)	37898 (4283)
ST-2W-3S	Los Angeles	D	0.26	99 (440)	27400 (3096)
ST-2W-3S	Seattle	D	0.26	85 (378)	23482 (2653)
ST-2W-3S	Carbondale	C	0.26	64 (285)	17620 (1991)
ST-2W-3S	Memphis	C	0.26	71 (316)	19560 (2210)
ST-2W-3S	Charleston	C	0.26	92 (409)	25215 (2849)
ST-2W-5S	Los Angeles	D	0.61	159 (707)	66201 (7481)
ST-2W-5S	Seattle	D	0.61	114 (507)	46741 (5281)
ST-2W-5S	Carbondale	C	0.61	79 (351)	31641 (3575)
ST-2W-5S	Memphis	C	0.61	87 (387)	34924 (3946)
ST-2W-5S	Charleston	C	0.61	97 (431)	37999 (4294)

Flexural capacities of walls and coupling beams are assumed equal to the bending moments obtained from the elastic modal analyses as described in the procedure to select the factor R_d. Actual bar sizes for flexural reinforcement were not selected, to avoid introducing element overstrength. That issue is considered later in the selection of the system overstrength factor (Ω_{system}).

7.4   SELECTION OF MAXIMUM DRIFT RATIO AND DISPLACEMENT DUCTILITY CAPACITIES FOR AAC STRUCTURES

The proposed procedure for selecting the ductility reduction factor (R_d) is based on a maximum drift ratio and displacement ductility capacity. The drift

ratio capacity is considered to limit damage and differential movement in AAC shear-wall structures, and the displacement ductility capacity is considered to control the amount of inelastic deformation in those structures. The main objective on selecting drift and ductility capacities is to provide reasonable limits to avoid collapse of AAC shear-wall structures.

The maximum drift ratio and displacement ductility capacities were based on those drift ratios and displacement ductilities observed for each of the AAC flexure-dominated specimens presented in Chapter 6. The aspect ratio and total axial load applied (N) for each of those flexure-dominated specimens is presented in Table 7.6.

Table 7.6 Aspect ratio and total axial load applied for each of the flexure-dominated specimens

Specimen	Aspect Ratio	Total Axial Load kips (kN)	$N / (t\, L_w\, f_{AAC}')$ (%)
13	2.14	25 (111.2)	7.5
14a	2.75	5 (22.2)	1.5
14b	2.75	5 (22.2)	1.5
15a	1.38	25 (111.2)	3.8
15b	1.38	25 (111.2)	3.8
16	1.38	25 (111.2)	3.8

In the above table, f_{AAC}' is the specified compressive strength of the AAC for the specimens, equal to 580 psi (4 MPa), t is the thickness of the wall, and L_w is the length of the wall. Column 4 of Table 7.6 represents the normalized axial load for each of the flexure-dominated specimens. Table 7.6 shows that the aspect ratio of the flexure-dominated specimens varied from 1.38 to 2.75 and the normalized axial force from 1.5% to 7.5%. The aspect ratio and normalized axial force variations represent in general those expected in potential walls of AAC shear-wall structures up to five stories high.

149

A value of maximum drift ratio capacity of 1% was proposed to avoid collapse of AAC shear-wall structures. This value corresponds to the minimum observed selected drift ratio of the flexure-dominated specimens (Table 7.7). The maximum drift ratio of 0.4% for Shear Wall Specimen 16 was not considered because this low value of drift ratio was associated with failure of the joint between the vertical panel and the U blocks which can be eliminated using Heli-fix ties[®], walls with flanges, or both. This value of 1% was not based on a lower fractile because of the large dispersion observed in the selected drift ratios for each flexure-dominated specimen.

A value of maximum displacement ductility capacity of 3.5 was proposed to avoid collapse of AAC structures. This value corresponds to the 10% lower fractile of the selected displacement ductilities of the flexure-dominated specimens (Table 7.7). The maximum displacement ductility of 1.67 for Shear Wall Specimen 16 was not considered for the same reasons presented in the selection of the maximum drift ratio capacity.

Table 7.7 Maximum drift ratios and displacement ductilities for the flexure-dominated specimens not including those of Shear Wall Specimen 16 in the north direction

Specimen Number	$\mu_{\Delta\text{-os}}$	$\mu_{\Delta\text{-on}}$	δ_{os} (%)	δ_{on} (%)
13	4.8	4.0	1.4	1.1
14a	5.0	--	1.9	--
14b	5.4	2.6	1.9	1.0
15a	6.0	5.8	1.0	1.0
15b	4.8	4.8	1.0	1.0
16	5.0	--	1.0	--
Average	4.8	Average	1.2	
COV	0.20	COV	0.32	
10% Lower Fractile	3.6	10% Lower Fractile	0.7	

150

7.5   NONLINEAR ANALYSES

The procedure described above to select the ductility reduction factor (R_d) for AAC structures includes the evaluation of the seismic performance of AAC shear-wall structures under different earthquake ground motions. This evaluation can be carried out using computer analysis programs, specifically nonlinear analyses programs. In this dissertation, the nonlinear analysis program CANNY 99 (CANNY 99) was selected to evaluate the performance of the four AAC shear-wall structures subjected to the different suites of earthquakes.

7.5.1   Model for Nonlinear Walls

Structures in the program CANNY 99 are idealized as rigid nodes connected by line elements and springs. All structural elements are treated as massless line elements represented by their centroidal axes, with mass concentrated at the nodes or at the center of gravity of floors. The idealized wall element of CANNY 99 considers the wall as a line element located at the wall centerline. The wall element is idealized using two nonlinear flexural springs, two rigid links, one nonlinear shear spring and one axial spring Figure 7.13. The nonlinear flexural springs are located at the top and bottom of the wall centerline. Therefore, all nonlinearity is concentrated at the wall ends (lumped nonlinearity).

rigid link

node

nonlinear flexural spring

axial spring

nonlinear shear spring

Actual wall element   Idealized wall element of CANNY 99
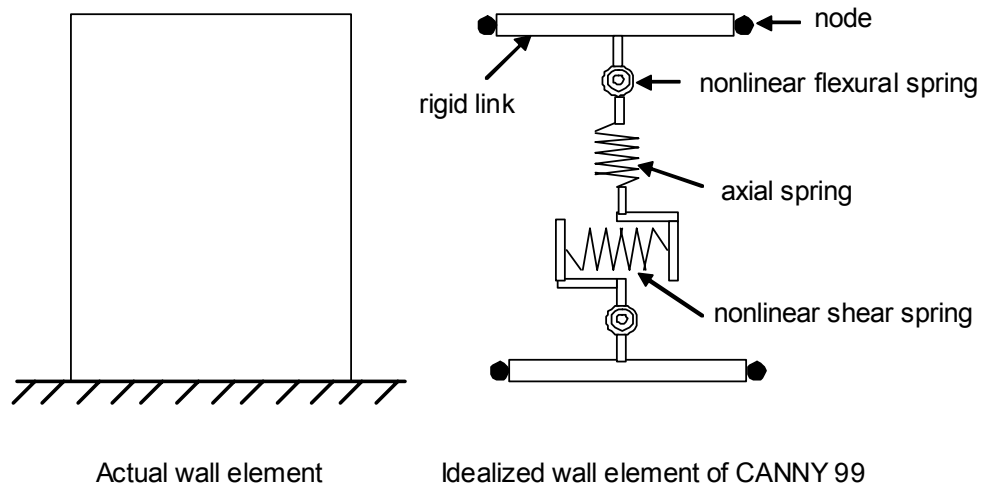
Figure 7.13 Actual wall element and idealized wall element of CANNY 99

The five and three-story cantilever-wall structures were modeled using five and three idealized wall elements respectively. Each wall of the five-story coupled wall structure was modeled using five idealized wall elements, and each wall of the three-story coupled-wall structure was modeled using three idealized wall elements.

7.5.2   Hysteretic Models for Nonlinear Behavior of Walls

The hysteretic model selected to represent the behavior of the nonlinear flexural and shear springs was the CANNY CA7 model (CANNY 99) which uses user-input hysteretic parameters to define the loading and unloading branches, degradation of strength and stiffness, and pinching of the hysteretic loops. The behavior of the nonlinear flexural spring is defined by a moment-rotation curve, and that of the nonlinear shear spring, by a force-displacement curve. The behavior of the axial spring was defined by the elastic model EL1. Bilinear curves were selected instead of trilinear curves to describe the loading branches of

152

both nonlinear flexural (Figure 7.14) and shear (Figure 7.16) springs, for the reasons presented below:

1) under moderate earthquakes, the flexural cracking capacity of an AAC wall, given by the bond tensile strength of the leveling bed mortar, can be exceeded. Therefore, cracks would form at the joint between the foundation and the AAC units;

2) under strong wind loads acting perpendicular to the plane of an AAC wall, the out-of-plane flexural capacity of an AAC wall can be exceeded. Therefore, cracks would form at the base of the wall;

3) shrinkage cracks can form in the leveling bed mortar; and

4) the bilinear curve is simple, for example, calculation of bending moment at flexural cracking is not needed.

The loading branches of the nonlinear flexural spring are presented in Figure 7.14. In that figure, M_y is the bending moment at yielding of the flexural reinforcement, K_{of} is the initial flexural stiffness, and K_y is the flexural stiffness after yielding of the flexural spring. The complete hysteretic behavior for the nonlinear flexural spring is presented in Figure 7.15.
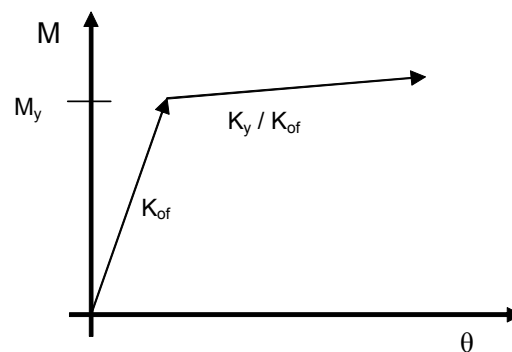
Figure 7.14 Loading branches of the nonlinear flexural spring
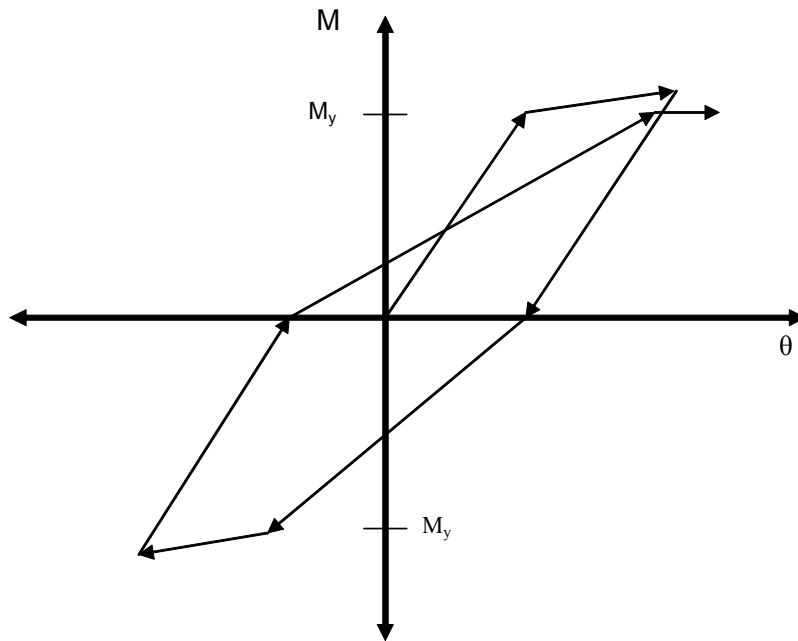
Figure 7.15 Complete hysteretic behavior for the nonlinear flexural spring

The loading branches of the nonlinear shear spring are presented in Figure 7.16. In that figure V_{AAC} is the shear force that causes shear cracking in the wall, K_{os} is the initial shear stiffness, and K_{AAC} is the stiffness after shear cracking. The complete hysteretic behavior for that shear spring is presented in Figure 7.17
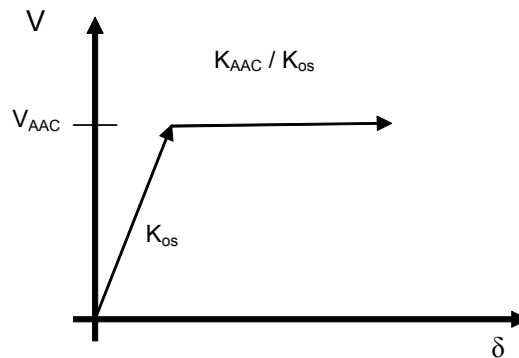
Figure 7.16 Loading branches of the nonlinear shear spring
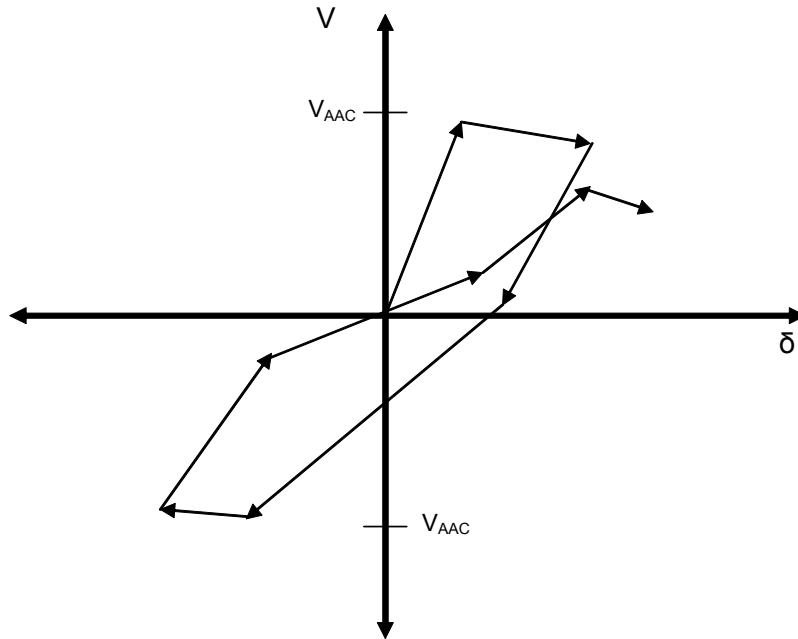
Figure 7.17 Complete hysteretic behavior for the nonlinear shear spring

7.5.3 Hysteretic parameters for the nonlinear flexural spring

For a cantilever wall with a force applied at the top, the predicted initial stiffness of the load-displacement curve including both flexural and shear deformations is given by Equation (7.2).

$$K_T = \frac{1}{\dfrac{H^3}{3\,E_{AAC}\,I} + \dfrac{H}{G_{AAC}\,A}} \qquad\qquad (7.2)$$

In Equation (7.2), H is the wall height, E_{AAC} is the modulus of elasticity of the AAC, G_{AAC} is the shear modulus of the AAC, I is the moment of inertia of the wall, and A is the cross-sectional area of the wall. Although axial load changes the initial flexural stiffness of a wall, this change is not included because the

155

program CANNY 99 only uses a constant moment of inertia during the analyses to define the stiffnesses of the walls. The initial stiffness of the flexural spring is, however, selected based on the observed performance of flexure-dominated shear wall specimens which had axial loads consistent with typical AAC structures up to five stories high. Two initial stiffnesses were calculated for each of the flexure-dominated specimens; one was calculated using the uncracked transformed moment of inertia (K_{pt}), and the other using the gross moment of inertia of the wall (K_{gp}). In both cases the gross area of the wall, a value of E_{AAC} of 310 ksi (2137 MPa), and a value of G_{AAC} of 129 ksi (889 MPa) were used (Table 7.8). The assumed value of E_{AAC} of 310 ksi (2137 MPa) is 5% higher than that proposed in the Draft Design Provisions (Argudo 2003 and Tanner 2003) for the AAC Class 4 used in the flexure-dominated specimens. The value of G_{AAC} of 129 ksi (889 MPa) was calculated using a Poisson's ratio of 0.2 as recommended in RILEM (1993).

Table 7.8 Calculated initial stiffnesses for each flexure-dominated specimen

Specimen Number	K_{tp} Kips/in. (kN/mm)	K_{gp} Kips/in. (kN/mm)	K_{ot-o} Kips/in. (kN/mm)	K_{ot-o}/K_{tp}	K_{ot-o}/K_{gp}
13	59.3 (10.4)	54.7 (9.6)	61.6 (10.8)	1.04	1.13
14a	40.2 (7.0)	33.6 (5.9)	18.0 (3.2)	0.45	0.54
14b	40.2 (7.0)	33.6 (5.9)	44.0 (7.7)	1.09	1.31
15a	227.6 (39.9)	208.6 (36.5)	215.7 (37.8)	0.95	1.03
15b	227.6 (39.9)	208.6 (36.5)	218.7 (38.3)	0.96	1.05
16	227.6 (39.9)	208.6 (36.5)	139.6 (24.4)	0.61	0.67

The ratios of observed initial tangent stiffnesses (K_{ot-o}) to the calculated initial stiffnesses for each of the flexure-dominated specimens are also presented in Table 7.8. The low values of the ratios (K_{ot-o}/K_{tp}) and (K_{ot-o}/K_{gp}) presented in that table for Shear Wall Specimens 14a and 16 are related to the low values of

the initial tangent stiffness observed for those specimens. The reasons for those low values are presented in Chapter 6.

The gross moment of inertia of the wall is used as a reference to select the different hysteretic parameters for the flexural spring because is easy to calculate, and because early in the design the flexural reinforcement of the wall it is not known.

7.5.3.1   Initial Stiffness of the Flexural Spring

The initial stiffness of the bilinear moment-rotation curve of the flexural spring is defined in CANNY 99 by the moment of inertia of the wall and the modulus of elasticity of the AAC. The ratios of the observed secant stiffness after flexural cracking to the calculated initial stiffness in the south and north directions for each of the flexure-dominated specimens are presented in Table 7.9.

Table 7.9 Ratios of observed secant stiffness after flexural cracking to calculated initial stiffness for each flexure-dominated specimen

Specimen Number	K_{cr-os} Kips/in (kN/mm)	K_{cr-os}/K_{gp}	K_{cr-on} Kips/in (kN/mm)	K_{cr-on}/K_{gp}
13	24.9 (4.4)	0.46	26.0 (4.6)	0.48
14a	11.0 (1.9)	0.33	--	--
14b	12.5 (2.2)	0.37	14.4 (2.5)	0.43
15a	92.0 (16.1)	0.44	100.0 (17.5)	0.48
15b	73.9 (12.9)	0.35	81.0 (14.2)	0.39
16	87.3 (15.3)	0.42	74.4 (13.0)	0.36
	Average	0.40	Average	0.43
	COV	0.13	COV	0.13

Based on the average values of the ratios K_{cr-os}/K_{gp} and K_{cr-on}/K_{gp} of 0.40 and 0.43 respectively presented in Table 7.9, a reduced initial stiffness of the nonlinear flexural spring defined using the modulus of elasticity of AAC and a moment of inertia equal to 40% of the gross moment of inertia is proposed for AAC walls.

7.5.3.2 *Unloading stiffness of the flexural spring*

The unloading stiffness after yielding of the flexural reinforcement (K_u) is defined in CANNY 99 by Equation (7.3). In that equation, θ is the hysteretic parameter that controls the amount of reduction of the unloading stiffness after yielding of the flexural spring, F_y is the load in the wall at yielding of the flexural reinforcement, and F_m and d_m are the maximum load and corresponding horizontal displacement in the wall in a given cycle after yielding of the flexural reinforcement.

$$K_u = \frac{\theta\, F_y + F_m}{\dfrac{\theta\, F_y}{K_T} + d_m} \qquad\qquad (7.3)$$

The maximum displacement (d_m) in any load cycle after yielding can be calculated as shown in Equation (7.4). In that equation, μ is the displacement ductility corresponding to that displacement d_m.

$$d_m = \mu\, \frac{F_y}{K_T} \qquad\qquad (7.4)$$

Substituting Equation (7.4) into Equation (7.3), the unloading stiffness of the flexural spring (K_u) is defined as shown in Equation (7.5).

$$K_u = \left[\frac{\theta\, F_y + F_m}{\theta\, F_y + \mu\, F_y}\right] K_T \qquad\qquad (7.5)$$

Table 7.10 shows the variation of the ratio unloading stiffness to initial stiffness (K_u/K_T) for different values of θ and μ assuming a value of F_y of 1 and a

value of F_m of 1.02. A value of F_m of 1.02 assumes a total flexural overstrength in an AAC wall of 2%.

Table 7.10 Variation of the ratio unloading stiffness to initial stiffness for different values of θ and μ

θ	μ	K_u/K_T
1	1	1.00
1	1.6	0.77
1	2	0.67
1	3	0.50
2	1	1.00
2	1.6	0.80
2	2	0.75
2	3	0.60

The ratio of the observed unloading stiffness after yielding of the flexural reinforcement to calculated initial stiffness in the south and north directions for each of the flexure-dominated specimens are presented in Table 7.11 and Table 7.12 respectively.

Table 7.11 Ratio of the observed unloading stiffness after yielding of the flexural reinforcement to calculated initial stiffness in the south direction for the flexure-dominated specimens

Specimen Number	K_{u-os} Kips/in (kN/mm)	K_{u-os}/K_{gp}	D_{u-os}/D_{ys}
13	18.6 (3.3)	0.34	1.71
14a	9.5 (1.7)	0.28	2.55
14b	12.5 (2.2)	0.37	1.16
15a	54.6 (9.6)	0.26	1.16
15b	62.9 (11.0)	0.30	1.23
16	64.1 (11.2)	0.31	1.67
	Average	0.31	1.58
	COV	0.13	0.34

159

Table 7.12 Ratio of the observed unloading stiffness after yielding of the flexural reinforcement to calculated initial stiffness in the north direction for the flexure-dominated specimens

Specimen Number	$K_{u\text{-}on}$ Kips/in (kN/mm)	$K_{u\text{-}on}/K_{gp}$	$D_{u\text{-}on}/D_{yn}$
13	17.5 (3.1)	0.32	1.79
14a	--	--	--
14b	12.8 (2.2)	0.38	1.26
15a	54.6 (9.6)	0.26	1.04
15b	36.7 (6.4)	0.18	2.45
16	53.7 (9.4)	0.26	1.75
	Average	0.28	1.66
	COV	0.28	0.33

Based on the average values of the ratios $K_{u\text{-}os}/K_{gp}$ and $K_{u\text{-}on}/K_{gp}$ of 0.31 and 0.28 presented in Table 7.11 and Table 7.12 respectively, an unloading stiffness after yielding of the flexural reinforcement equal to 30% of the calculated initial stiffness (K_{gp}) is proposed for AAC walls. Table 7.10 shows that using a value of θ of 1 and a value of μ of 1.6, the unloading stiffness (K_u) is equal to 77% of the initial stiffness (K_T). Because that initial stiffness K_T is defined as a reduced initial stiffness equal to 40% of K_{gp}, the unloading stiffness is equal to 30% of K_{gp}. The value of μ of 1.6 corresponded to the mean values of the ratios $D_{u\text{-}os}/D_{ys}$ and $D_{u\text{-}on}/D_{ys}$ presented in Table 7.11 and Table 7.12 respectively.

7.5.3.3   Stiffness after yielding of the flexural spring

The stiffness after yielding of the nonlinear flexural spring (K_y) is defined in CANNY 99 as a function of the initial stiffness (K_{of}) of that spring. The ratio of the observed stiffnesses after yielding of the flexural reinforcement to calculated initial stiffness in the south and north directions for each of the flexure-dominated specimens are presented Table 7.13.

160

Table 7.13 Ratios observed stiffness after yielding of the flexural reinforcement
to calculated initial stiffness for each of the flexure-dominated specimens

Specimen Number	$K_{y\text{-}os}$ Kips/in (kN/mm)	$K_{y\text{-}os}/K_{gp}$	$K_{y\text{-}on}$ Kips/in (kN/mm)	$K_{y\text{-}on}/K_{gp}$
13	1.3 (0.23)	0.024	1.2 (0.21)	0.023
14a	0.7 (0.12)	0.047	--	--
14b	0.7 (0.12)	0.019	1.1 (0.19)	0.033
15a	2.6 (0.46)	0.012	0.6 (0.11)	0.003
15b	2.8 (0.49)	0.014	3.7 (0.65)	0.018
16	3.2 (0.56)	0.015	3.8 (0.67)	0.018
	Average	0.022	Average	0.019
	COV	0.60	COV	0.58

Based on the average values of the ratios $K_{y\text{-}os}/K_{gp}$ and $K_{y\text{-}on}/K_{gp}$ of 0.022 and 0.019 respectively presented in Table 7.13, a value of the stiffness after yielding of the flexural reinforcement equal to 2% of K_{gp} is proposed for AAC walls. The stiffnesses after yielding of the flexural reinforcement presented in Table 7.13 are base on observed load-displacement curves rather than moment-rotation curves. Therefore, the stiffness after yielding of the nonlinear flexural spring (K_y) for the four selected AAC structures were back-calculated using the proposed stiffness after yielding equal to 2% of K_{gp} and the iterative procedure described below:

1) assume a value of the stiffness after yielding of the nonlinear flexural spring (K_y);

2) for a particular cantilever AAC wall with a load applied at the top, run a static nonlinear analysis, making sure that under the applied load the flexural capacity of the wall is exceeded;

3) calculate the stiffness after yielding of the flexural reinforcement of the wall as a function of the predicted initial stiffness (K_{gp});

4) if the stiffness calculated in Step 3 is equal to the proposed value of 2% of K_{gp}, then the assumed value of Step 1 is correct;

5) if the stiffness calculated in Step 3 is smaller or greater than the proposed value of 2% of K_{gp}, then increase or decrease the assumed stiffness after yielding of the flexural spring respectively, return to Step 1, and repeat.

In general, a value of the stiffness after yielding of the flexural spring of 2% of the initial stiffness (K_{of}) does not corresponds to a stiffness after yielding of the flexural reinforcement of 2% of the predicted initial stiffness (K_{gp}). For a given plan geometry of an AAC wall, the back-calculated stiffness after yielding of the moment-rotation curve of the nonlinear flexural spring depends on the number of idealized wall elements used to define a single AAC wall. The stiffness after yielding of the flexural spring would be different if the same wall were modeled using one or more than one element.

7.5.4 Summary of the hysteretic parameters for the flexural spring

The hysteretic behavior of the nonlinear flexural spring for the idealized wall element was defined as follows:

1) the initial stiffness (K_{of}) is defined using the modulus of elasticity of the AAC and a reduced moment of inertia equal to 40% of the gross moment of inertia of the AAC wall;

2) The stiffness after yielding (K_y) is back-calculated using the proposed stiffness after yielding of the flexural reinforcement of 2% of the initial stiffness (K_{gp}) calculated using the gross properties of the cross section of the AAC wall;

3) the unloading stiffness (K_u) is defined using the hysteretic parameter θ equal to 1; and

4) strength degradation and pinching are not included because they were not observed in all the flexure-dominated specimens up to a displacement ductility of 3 and a global drift ratio of 1%, and because the proposed unloading stiffnesses after yielding of the flexural reinforcement for each of the flexure-dominated specimens were calculated fitting a straight line on the observed unloading curve.

7.5.5 Hysteretic parameters for the nonlinear shear spring

A initial stiffness was calculated for each of the shear-dominated specimens using the gross properties of the cross section, a value of E_{AAC} of 310 ksi (2137 MPa), and a value of G_{AAC} of 129 ksi (889 MPa) as presented in Table 7.14.

Table 7.14 Calculated initial stiffnesses for each shear-dominated specimen

Specimen Number	K_{gp} Kips/in. (kN/mm)	K_{ot-o} Kips/in. (kN/mm)	K_{ot-o}/K_{gp}
1	853.8 (149.5)	678.6 (118.8)	0.80
3	853.8 (149.5)	732.1 (128.2)	0.86
4	853.8 (149.5)	591.8 (103.6)	0.69
5	853.8 (149.5)	771.8 (135.1)	0.90
7	311.1 (54.5)	300.0 (52.5)	0.96
9	117.4 (20.6)	143.0 (25.0)	1.21
11	17.5 (3.1)	34.9 (6.1)	1.99

The gross properties of the cross section are used to select the different hysteretic parameters for the shear spring because of the same reasons presented for the selection of the parameters for the nonlinear flexural spring. The low values of the ratio (K_{ot-o}/K_{gp}) presented in Table 7.14 for Shear Wall specimens 1 and 4 can be related to cracking in the leveling bed mortar as discussed in Chapter 5. The high value of the ratio (K_{ot-o}/K_{gp}) for Shear Wall Specimen 9 is inconsistent with those observed in the other flexure-dominated specimens. The

high value of the observed initial stiffness is however consistent with the high value of the bond tensile strength observed in that specimen with respect to those values reported for the remaining specimens (Tanner 2003).

7.5.5.1 Initial stiffness of the shear spring

The ratio of the observed secant stiffness after flexural cracking to calculated initial tangent stiffness in the south and north directions for each of the shear-dominated specimens are presented in Table 7.15.

Table 7.15 Ratios observed secant stiffness after flexural cracking to calculated initial stiffness for each of the shear-dominated specimens

Specimen Number	K_{cr-os} Kips/in (kN/mm)	K_{cr-os}/K_{gp}	K_{cr-on} Kips/in (kN/mm)	K_{cr-on}/K_{gp}
1	208.8 (36.6)	0.24	252.6 (44.2)	0.30
3	519.5 (91.0)	0.61	580.7 (101.7)	0.68
4	409.3 (71.7)	0.48	430.8 (75.4)	0.50
5	564.5 (98.8)	0.66	674.4 (118.1)	0.79
7	97.8 (17.1)	0.31	94.0 (16.5)	0.30
9	33.4 (5.8)	0.28	50.2 (8.8)	0.43
11	8.08 (1.4)	0.46	--	--
	Average	0.44	Average	0.50
	COV	0.37	COV	0.40

A reduced initial stiffness of the nonlinear shear spring defined using the shear modulus of the AAC and a reduced cross sectional area equal to 40% of the gross area is proposed for AAC walls. This reduced area is based on the average values of the ratios K_{cr-os}/K_{gp} and K_{cr-on}/K_{gp} of 0.44 and 0.50 respectively presented in Table 7.15 and those observed in Table 7.9 for the flexure-dominated specimens.

7.5.5.2 *Unloading stiffness of the shear spring*

The ratio of the observed unloading stiffness after web shear cracking to calculated initial stiffness in the south and north directions for each of the shear-dominated specimens are presented in Table 7.16 and

Table 7.17 respectively.

Table 7.16 Ratio of the observed unloading stiffness after web shear cracking to calculated initial stiffness in the south direction for the shear-dominated specimens

Specimen Number	$K_{u\text{-}os}$ Kips/in (kN/mm)	$K_{u\text{-}os}/K_{gp}$	$D_{u\text{-}os}/D_{ws1}$
1	175.3 (30.7)	0.20	--
3	534.4 (93.6)	0.63	1.16
4	377.7 (66.1)	0.44	1.04
5	460.2 (80.6)	0.54	1.45
7	98.8 (17.3)	0.32	1.10
9	33.9 (5.9)	0.29	1.02
11	--	--	--
	Average	0.40	1.15
	COV	0.40	0.15

Table 7.17 Ratio of the observed unloading stiffness after web shear cracking to calculated initial stiffness in the north direction for the shear-dominated specimens

Specimen Number	$K_{u\text{-}on}$ Kips/in (kN/mm)	$K_{u\text{-}on}/K_{gp}$	$D_{u\text{-}on}/D_{wn1}$
13	209.4 (36.7)	0.24	--
14a	546.7 (95.7)	0.64	1.07
14b	359.4 (62.9)	0.42	1.04
15a	546.8 (95.7)	0.64	1.40
15b	99.9 (17.5)	0.32	1.03
16	26.2 (4.6)	0.22	1.44
	Average	0.41	1.20
	COV	0.45	0.15

Based on the average values of the ratios K_{u-os}/K_{gp} and K_{u-on}/K_{gp} of 0.40 and 0.41 presented in Table 7.11 and Table 7.12 respectively, an unloading stiffness after web shear cracking equal to 40% of the predicted initial stiffness (K_{gp}) is proposed for the unloading branch of the nonlinear flexural spring. Table 7.18 shows the variation of the ratio unloading stiffness to initial stiffness of the wall for different values of the displacement ductility (μ) assuming a value of θ of 1, a value of F_y of 1, and a value of F_m of 1.02.

Table 7.18 variation of the ratio unloading stiffness to initial stiffness for different values of μ assuming a value of θ of 1, F_y of 1 and F_m of 1.02

θ	μ	K_u/K_T
1	1	1
1	1.15	0.93
1	1.20	0.91
1	1.25	0.89

Table 7.18 shows that using a value of θ of 1 and a value of μ of 1.15, the unloading stiffness (K_u) is equal to 93% of the initial stiffness (K_T), and using a value θ of 1 and a value of μ of 1.2, the unloading stiffness (K_u) is equal to 91% of that initial stiffness (K_T). Because the initial stiffness K_T is defined using a reduced initial stiffness equal to 40% of K_{gp}, the unloading stiffnesses are equal to 37% and 36% of K_{gp} respectively. The value of μ of 1.15 and 1.20 corresponded to the mean values of the ratios D_{u-os}/D_{ys} and D_{u-on}/D_{ys} presented in Table 7.11 and Table 7.12 respectively.

7.5.5.3 *Stiffness after web shear cracking of the shear spring*

Because degradation of the shear strength of an AAC wall from cycle to cycle is included in the hysteretic behavior of the nonlinear shear spring, a stiffness after web shear cracking of the load-displacement curve of the shear

spring equal to 1% of the initial stiffness (K_{gp}) is proposed. The trend of the stiffness after web shear cracking is defined by the shear degradation in the wall from cycle to cycle. The stiffness after web shear cracking of the nonlinear shear spring (K_{AAC}) was back-calculated using the proposed stiffness after web shear cracking of 1% of K_{gp} using a similar procedure as that used to define the stiffness after yielding of the flexural spring (K_y).

7.5.5.4   *Strength degradation of the shear spring*

The strength degradation in the program CANNY 99 is defined as a function of two independent hysteretic parameters. The first parameter (λ_e) is related to the energy dissipated in the wall and the second (λ_u) to the displacement ductility in the wall (CANNY 99). For simplicity, the proposed strength degradation of the wall was based only on the second hysteretic parameter (λ_u); that is, the first hysteretic parameter was assumed equal to zero. The proposed strength degradation in any cycle is given by Equation (7.6).

$$F' = F_{max} \left[1 - \lambda_u \left(1 - \frac{1}{\mu} \right) \right]$$

(7.6)

In Equation (7.6), F_{max} is the maximum load in the wall in a cycle "n" after web shear cracking and F' is the reduced load in the following cycle "n+1". Table 7.19 shows the variation of the parameter λ_u as a function of different assumed strength ratios (F'_{max}/F_{max}) and different assumed displacement ductilities (μ). The displacement ductility for the shear spring is defined as the displacement in a cycle "n" divided by the displacement at web shear cracking.

Table 7.19 variation of the parameter λ_u as a function of different values of the

ratio (F'_{max}/F_{max}) and displacement ductilities (μ)

F'_{max}/F_{max}	μ	λ_u
0.90	1.5	0.30
0.85	1.5	0.45
0.80	1.5	0.60
0.90	1.6	0.27
0.85	1.6	0.40
0.80	1.6	0.53

The strength ratio after web shear cracking and the ratio of the horizontal displacement at the maximum applied load in the corresponding next cycle after web shear cracking to horizontal displacement at web shear cracking in the south and north directions for each of the shear-dominated specimens are presented in Table 7.20.

Table 7.20 Strength ratios after web shear cracking and corresponding

displacement ratios for each of the shear-dominated specimens

Specimen Number	F_{ws2}/F_{ws1}	D_{ws2}/D_{ws1}	F_{wn2}/F_{wn1}	D_{wn2}/D_{wn1}
1	0.49	1.20	0.82	1.63
3	1.02	1.37	1.22	2.00
4	1.14	1.41	1.01	1.28
5	1.15	2.36	1.15	2.20
7	1.03	1.44	0.89	1.46
9	0.81	1.31	0.36	1.43
11	--	--	--	--
Average	0.94	1.52	0.91	1.67
COV	0.27	0.28	0.19	0.23

Based on the average values of the ratios F_{ws2}/F_{ws1} and F_{wn2}/F_{wn1} of 0.94 and 0.91 respectively presented in Table 7.20, a value of strength degradation ratio (F'_{max}/F_{max}) equal to 0.9 is proposed. Table 7.19 shows that for a value of λ_u

168

of 3 and a displacement ductility of 1.5, the strength ratio is equal to 0.90. Therefore, a hysteretic parameter λ_u of 0.30 is selected to define the strength degradation of the shear spring.

7.5.6 Summary of the hysteretic parameters for the shear spring

The hysteretic behavior of the nonlinear shear spring for the idealized wall element was defined as follows:

1) The initial stiffness (K_{os}) is defined using the shear modulus of the AAC and a reduced cross-sectional area equal to 40% of the gross area of the wall;

2) The stiffness after web shear cracking (K_{AAC}) is back-calculated using the proposed stiffness after web shear cracking equal to 1% of the initial stiffness (K_{gp}) calculated using the gross properties of the AAC wall;

3) the unloading stiffness (K_u) is defined using a hysteretic parameter θ equal to 1.

4) degradation of the shear strength of the wall is defined using a hysteretic parameter λ_u equal to 0.30.

5) pinching of the hysteretic loops is not included because this phenomenon was not observed in all the shear-dominated specimens, and because the proposed unloading stiffnesses after web shear cracking for each of the shear-dominated specimens were calculated fitting a straight line on the observed unloading curve.

7.5.7 Numerical Integration of the Equation of Motion

The dynamic response of the structure is determined in the program CANNY 99 by the Newmark's method. This numerical integration method is used with the assumption that the variation of the acceleration over a time step is

169

constant and equal to the average acceleration; this is defined in that method by values of the parameters β and γ of 0.25 and 0.5 respectively. The Newmark's method with the assumption of constant acceleration is unconditionally stable, that is, the numerical procedure leads to a bounded solution regardless of the time step length. The accuracy of the results, however depends on the time step selected; as the time step is smaller, the solution is more accurate. The time step length was selected as described in the following procedure:

1. Run a dynamic nonlinear analysis with a reasonable small time step;
2. Repeat the analysis with a shorter time step and compare the results;
3. Iterate until two consecutive solutions are within the desired tolerance.

Damping in the program CANNY 99 is described as a viscous damping defined by a linear combination of the mass and stiffness matrices as shown in Equation (7.7).

$$[C] = a_m[M] + a_K[K] \qquad\qquad (7.7)$$

In Equation (7.7), a_m and a_k are the damping coefficients proportional to the mass matrix and time-varying stiffness matrix respectively. Those coefficients can be calculated as a function of the assumed damping ratio for the first mode (ξ_1) and the natural frequency of that mode (ω_1) as shown in Equation (7.8) and Equation (7.9) respectively. The damping ratio for any higher mode n (ξ_n) is defined as a function of those parameters a_m, a_k and the circular frequency of that mode (ω_n), and is by Equation (7.10).

$$a_m = \xi_1\, \omega_1 \qquad\qquad\qquad (7.8)$$

$$a_k = \frac{\xi_1}{\omega_1} \qquad\qquad\qquad (7.9)$$

$$\xi_n = \frac{a_m}{2\,\omega_n} + \frac{a_k}{2}\,\omega_n \qquad\qquad (7.10)$$

Equation (7.10) shows that ξ_n increases as ω_n increases. That is, for higher modes the damping ratio ξ_n is greater than the value of the damping ratio ξ_1 selected for the first mode, which was assumed for all structures as 5% of the critical damping. To select the constants a_m and a_k, equivalent viscous damping of 5% was used; damping was assumed to have a local minimum at ω_1 as shown in Figure 7.18; and the initial stiffness was used. Equivalent viscous damping of 5% was selected to be consistent with the value prescribed in the IBC 2000 design spectra.
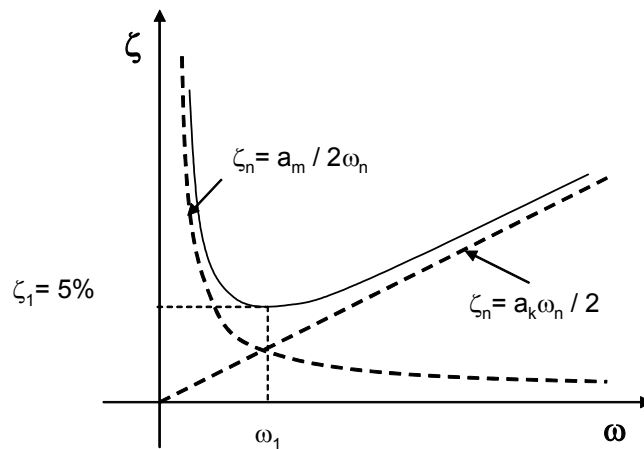
Figure 7.18 Selection of damping constants a_m and a_k assuming a local minimum at ω_1

171

7.5.8 Observed versus Calculated Load-Displacement Curves for the Flexure-Dominated Specimens

Observed load-displacement curves were compared against analytical load-displacement curves for each of the flexure-dominated specimens. The analytical curves were calculated using the parameters selected for the nonlinear flexural and shear springs, and the geometry and layout of each of those specimens. Nonlinear static analyses were carried out using target displacements consistent with those observed in the flexure-dominated specimens at the time the specimens were unloaded after yielding of the flexural reinforcement. Figure 7.19 through Figure 7.24 show observed versus calculated load-displacement curves for each of the flexure-dominated specimens. In those figures, observed curves are shown in solid lines and calculated curves in dashed lines.
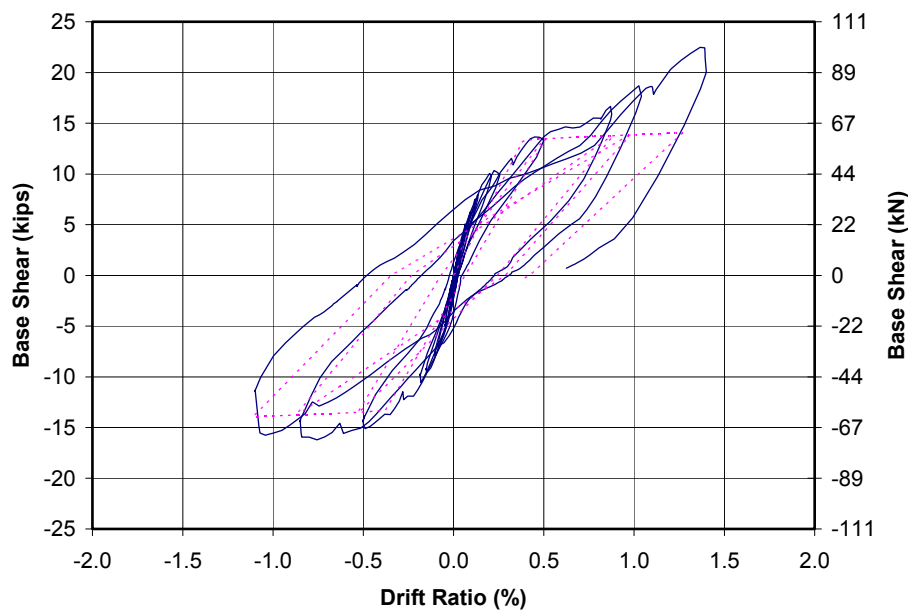
Figure 7.19 Observed versus calculated curves for Shear Wall Specimen 13
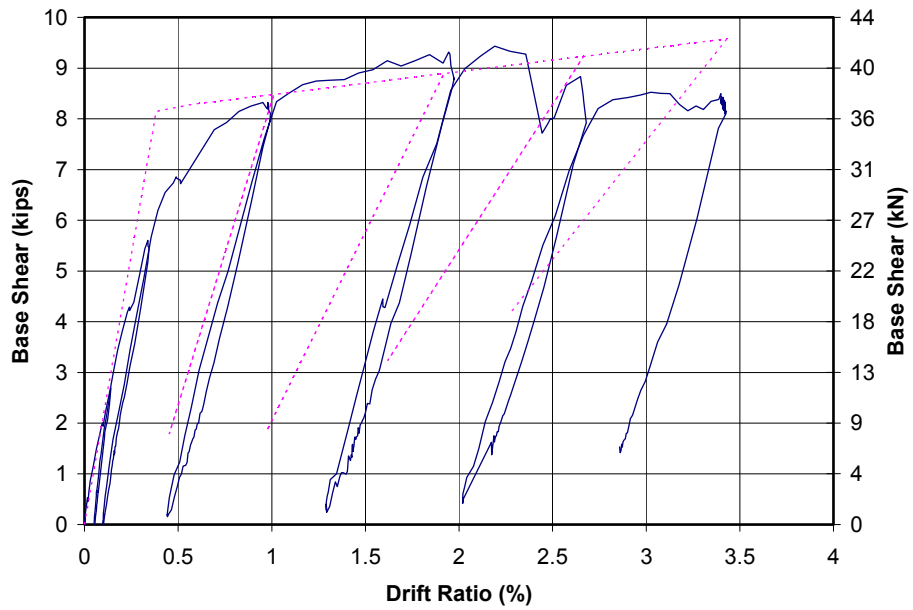
Figure 7.20 Observed versus calculated curves for Shear Wall Specimen 14a
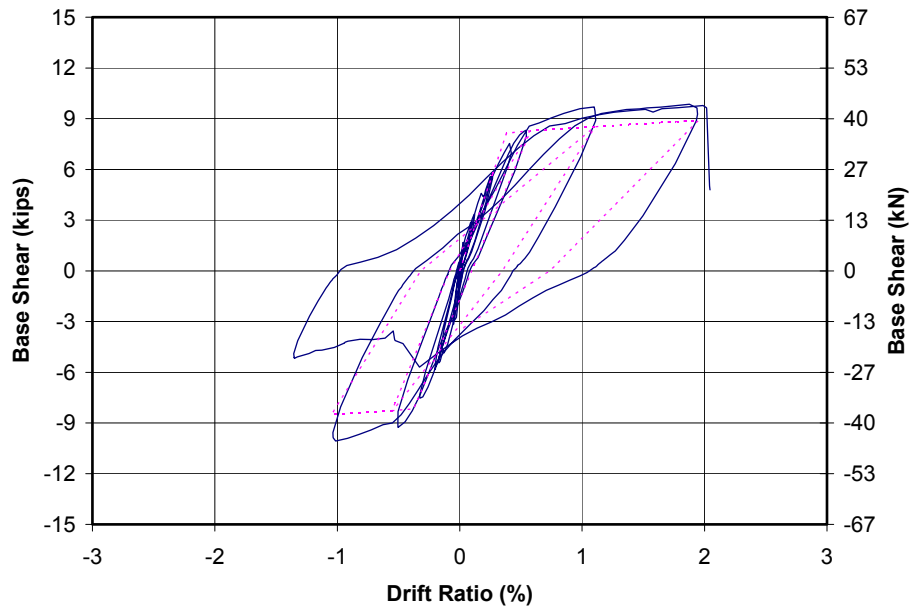
Figure 7.21 Observed versus calculated curves for Shear Wall Specimen 14b
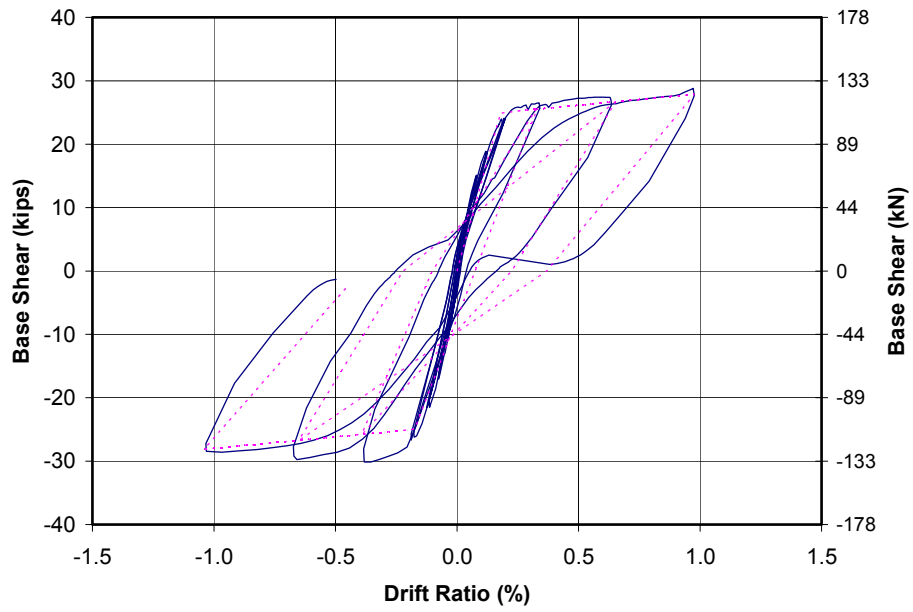
Figure 7.22 Observed versus calculated curves for Shear Wall Specimen 15a
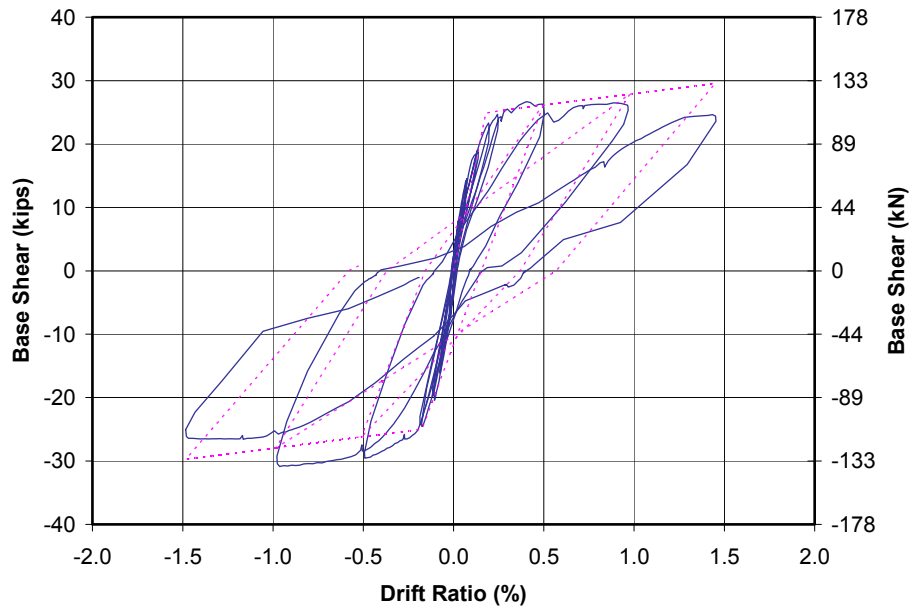
Figure 7.23 Observed versus calculated curves for Shear Wall Specimen 15b

174
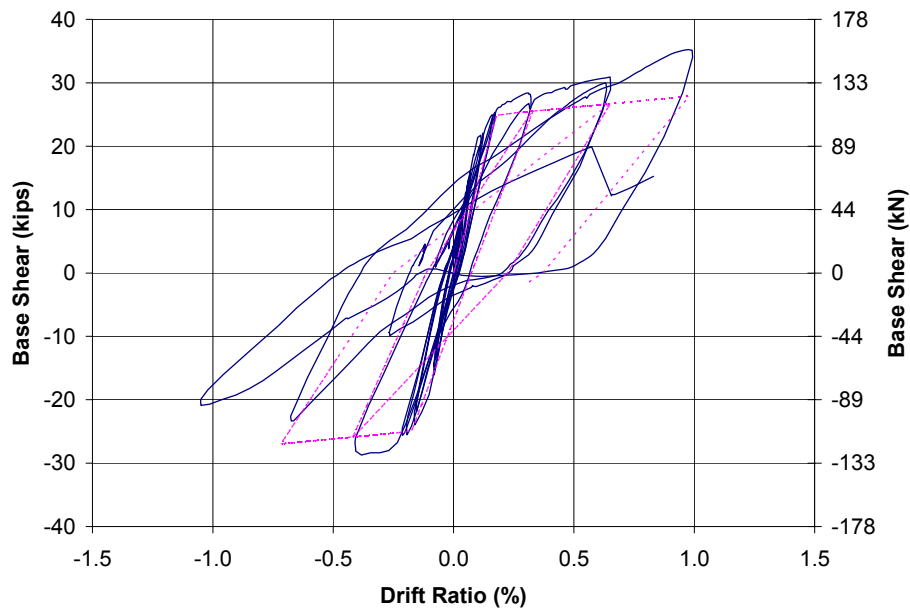
Figure 7.24 Observed versus calculated curves for Shear Wall Specimen 16

Figure 7.19 though Figure 7.24 show in general a good agreement between observed and calculated behavior for the flexure-dominated specimens up to a drift ratio of 1%. For values of drift ratio above 1%, calculated unloading stiffnesses after yielding of the flexural reinforcement are in general smaller than those observed.

7.5.9 Sensitivity Study

A sensitivity study was carried out to see if the nonlinear response of flexure-dominated AAC walls is sensitive to changes in the proposed hysteretic parameters selected. The effect of each parameter on the nonlinear response was studied by changing one parameter and keeping the others constant. The parameters studied were the reduced initial stiffness, yielding stiffness, and unloading stiffness. The AAC structure selected for this study was ST-1W-5S. This structure was selected because it was thought that it would be subjected to

175

the largest drift ratio and displacement ductility demands among the four structures selected in this dissertation. Nonlinear dynamic analyses were carried out using three different earthquakes selected randomly from the suites of Carbondale (carb-1), Charleston (acc401-1), and Los Angeles (la25). Because the results of the sensitivity analysis showed that drift ratio and displacement ductilities were not sensitive to the changes in the parameters studied, no further earthquakes were studied. Results of the sensitivity analysis focused on drift ratio and displacement ductility demands because these are the most important variables governing the selection of the factor R_d.

7.5.9.1 Initial Stiffness

The reduced initial stiffnesses selected were taken as 35%, 40%, and 45% of the calculated initial stiffness (K_{gp}). Table 7.21 shows the values of drift ratio and displacement ductility demands obtained for the different earthquakes and selected reduced initial stiffnesses.

Table 7.21 Drift ratio and displacement ductility demands for different selected initial stiffnesses

Earthquake	K/K_{gp}	δ (%)	δ / δ_{-40}	μ_Δ	$\mu_\Delta / \mu_{\Delta-40}$
carb-1	0.35	0.41	1.03	1.75	0.90
carb-1	0.40	0.40	1.00	1.95	1.00
carb-1	0.45	0.38	0.95	1.95	1.00
acc402-1	0.35	0.53	1.04	1.79	0.93
acc402-1	0.40	0.51	1.00	1.92	1.00
acc402-1	0.45	0.45	0.88	2.06	1.07
la25	0.35	1.32	1.08	2.93	0.87
la25	0.40	1.22	1.00	3.38	1.00
a25	0.45	1.15	0.94	3.46	1.02

Table 7.21 shows that as the ratio (K/K_{gp}) increases, the maximum displacement ductility demand increases. In contrast, as that ratio increases, the

176

drift ratio demand decreases. The reason is that as the reduced initial stiffness increases, the yielding displacement decreases more than the corresponding maximum displacement. The reduction in drift ratio demand can be associated directly with the increase in the initial stiffness. Table 7.21 also shows the variation in the ratio of the drift ratio demand for different reduced stiffness to that associated to 40% of K_{gp}, and the variation of the ratio of displacement ductility demand for different reduced initial stiffnesses to that associated to 40% of K_{gp}. Those variations presented in Table 7.21 show that the drift ratio and displacement ductility demands are not really sensitive to the changes in the initial stiffness studied.

7.5.9.2 *Stiffness after Yielding*

The stiffnesses after yielding of the flexural reinforcement selected were taken as 1%, 2%, and 3% of the calculated initial stiffness (K_{gp}). Table 7.22 shows the values of drift ratio and displacement ductility demands obtained for the different earthquakes and selected stiffnesses after yielding of the flexural reinforcement.

Table 7.22 Drift ratio and displacement ductility demands for different selected stiffnesses after yielding of the flexural reinforcement

177

Earthquake	K/K_{gp}	δ (%)	μ_Δ
carb-1	0.01	0.40	1.95
carb-1	0.02	0.40	1.94
carb-1	0.03	0.40	1.93
acc402-1	0.01	0.51	1.92
acc402-1	0.02	0.51	1.99
acc402-1	0.03	0.51	1.98
la25	0.01	1.28	3.38
la25	0.02	1.26	3.33
a25	0.03	1.25	3.30

Table 7.22 shows that for the earthquakes studied the drift ratio and displacement ductility demands are not sensitive to the changes in the stiffness after yielding studied. A reason for this is that the stiffnesses after yielding studied are small compared with the reduced initial stiffness of the AAC structure.

7.5.9.3 Unloading Stiffness

The unloading stiffnesses after yielding of the flexural reinforcement selected were selected using three different values of the unloading parameter θ, taken as 1, 2, and 3. Table 7.23 shows the values of drift ratio and displacement ductility demands obtained for the different earthquakes and selected unloading stiffnesses after yielding of the flexural reinforcement.

Table 7.23 Drift ratio and displacement ductility demands for different selected unloading stiffness

Earthquake	θ	δ (%)	μ_Δ
carb-1	1	0.40	1.95
carb-1	2	0.37	1.80
carb-1	3	0.35	1.70
acc402-1	1	0.51	1.98
acc402-1	2	0.49	1.98
acc402-1	3	0.48	1.92
la25	1	1.28	3.38
la25	2	1.28	3.37
a25	3	1.28	3.38

Table 7.23 shows that in general, as the selected unloading hysteretic parameter increases (unloading stiffness increases), the drift ratio and displacement ductility demands decrease. This reduction in the response can be associated to the increase in that unloading stiffness, that is, the structure becomes stiffer in the unloading branch, and the hysteretic damping associated to that unloading stiffness (area enclose in a hysteresis loop) larger. Table 7.23 also shows that the larger drift ratio and displacement ductility demand were always associated to the selected value of θ of 1. Values less than 1 were not included in this study because a value of 1 is the smallest number that can be assigned to θ (CANNY 99).

7.6   EXAMPLE OF PROCEDURE USED TO SELECT THE DUCTILITY REDUCTION FACTOR R_d

Below is an example of the procedure used to select critical values of the ductility reduction factor R_d based on drift ratio and displacement ductility capacities. The structure selected was the five-story cantilever-wall structure

presented in Section 7.3. This example is presented following the step numbers presented in Section 7.1.

1) Select the type of AAC structure. The AAC structure selected in this example was a cantilever-wall structure.

2) Select the preliminary plan geometry of the AAC wall. Typical wall dimensions of 240 in. (6.1 m) long and 10 in. (0.25 m) thick were used in every story of the structure

3) Select the structure's number of stories. A five-story structure was selected. Each story was 120 in. (3 m) high. The total height of the structure including the slabs was 645 in. (16.4 m).

4) Select a tributary width. The tributary width selected was 20 ft (6.1 m).

5) Calculate the weights of different stories of the structure. The story weights of Floors 1 to 4 were 34.7 kips (154 kN) and that of Floor 5 was 29 kips (129 kN).

6) Obtain the design spectrum according to the IBC 2000 using the intended geographic location of the structure. It was assumed that the structure would be built in Carbondale, IL on IBC 2000 Site Class C. The corresponding design spectrum is presented in Figure 7.6.

7) Analyze the structure using the modal analysis procedure specified in the IBC 2000. The structure was analyzed using the program SAP2000.

8) Calculate the elastic global drift ratio of the structure and compare it with the drift ratio capacity of 1% selected for AAC shear-wall structures. The global drift ratio of the five-story cantilever-wall structure, defined as the horizontal displacement at the top divided by the total height of the structure, was equal to 0.46%. This global drift ratio was calculated using a reduced initial stiffness defined using a moment of inertia equal to 40% of the gross moment of inertia of the wall, and a cross-sectional area equal

to 40% of the gross area of the wall. The modulus of elasticity of AAC was assumed equal to 310 ksi (2137 MPa), and the shear modulus of the AAC equal to 129 ksi (889 MPa).

9) Assume that the flexural capacity of the walls is equal to the bending moments obtained from the elastic analyses (R_d = 1). The bending moment at the base of the cantilever wall was equal to 31564 kips-in. (3567 kN-m) and the base shear was equal to 70 kips (311 kN). The flexural capacity of the cantilever wall was assumed equal to that bending moment at the base of the wall.

10) Select a suite of earthquakes representative of the design response spectrum. The suite of earthquakes selected was that corresponding to Carbondale, IL. The scaled response spectra for that suite are presented in Figure 7.6.

11) Select an earthquake from the suite. The first earthquake of the suite named "carb-1" was selected. Earthquakes named "carb-2" to "carb-10" were selected later.

12) Select a value of R_d greater than unity. A value of R_d of 1 was selected first. Values of R_d of 2, 3 and 4 were selected for further iterations.

13) Run a dynamic nonlinear analysis and calculate the drift ratio and displacement ductility demands. Figure 7.25 shows curves of global drift ratio demands corresponding to the assumed values of the factor R_d for the suite of earthquakes of Carbondale. A horizontal dotted line was added to that figure to represent the drift ratio capacity of 1%. Figure 7.26 shows curves of displacement ductility demands corresponding to the assumed values of the factor R_d for the suite of earthquakes of Carbondale. A horizontal dotted line was added to that figure to represent the displacement ductility capacity of 3.5. The displacement ductility demand

181

was calculated as the maximum horizontal displacement at the top of the wall calculated during the entire nonlinear analysis divided by the corresponding displacement at yielding of the flexural reinforcement. In the analyses is assumed that the shear capacity is greater than the shear demand in the structure.

14) Repeat for other earthquakes of the same suite, for other suites of earthquakes, and other AAC shear wall structures. This procedure was repeated for the selected structure and suites of earthquakes.
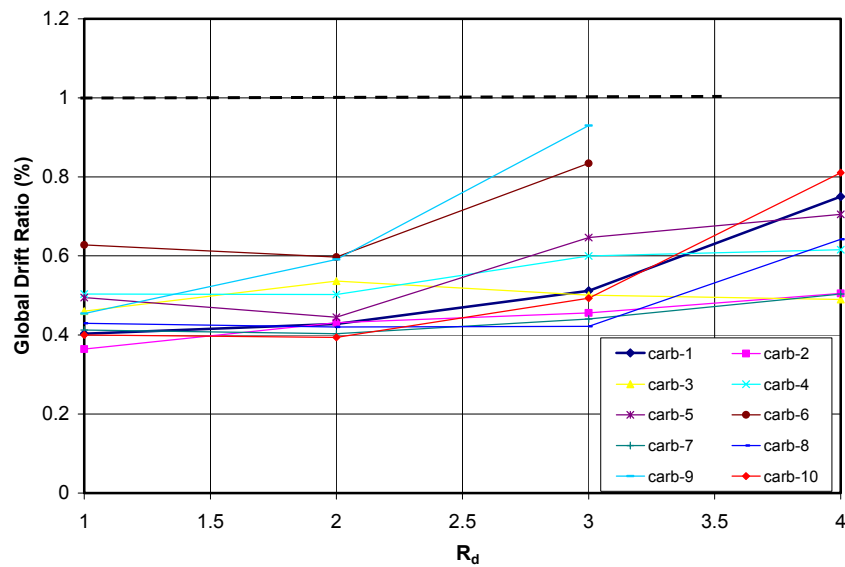
Figure 7.25 Curves of global drift ratio demands for the suite of earthquakes of Carbondale
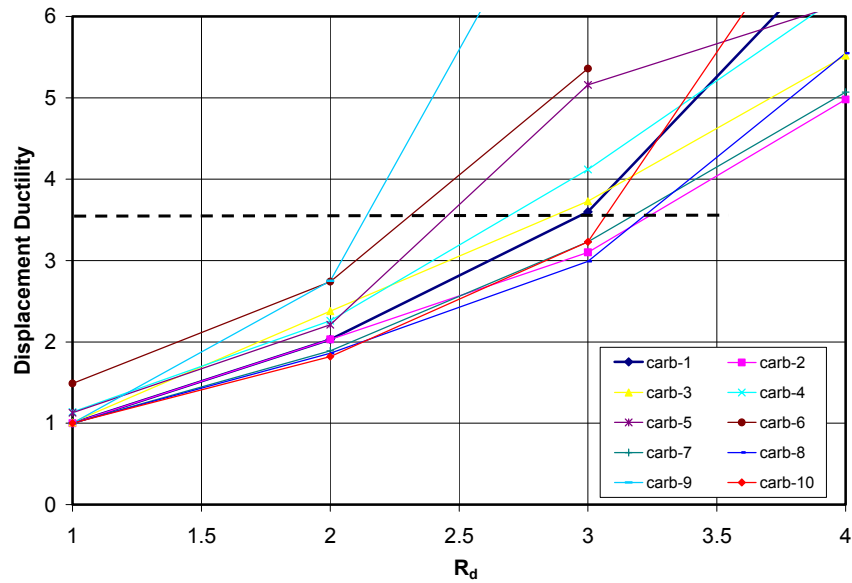
Figure 7.26 Curves of displacement ductility demands for the suite of earthquakes of Carbondale

The critical values of R_d based on drift ratio capacity are defined by the intersection of each drift ratio curve and the horizontal line representing the drift ratio capacity of 1% (Figure 7.25). Similarly, critical values of R_d based on displacement ductility are defined by the intersection of each displacement ductility curve and the horizontal line representing the displacement ductility capacity of 3.5 (Figure 7.26). Critical values of R_d based on drift ratio capacity for the suite of earthquakes of Carbondale are greater than three ($R_d>3$) for all the earthquakes studied (Figure 7.25). Critical values of R_d based on displacement ductility for the suite of earthquake of Carbondale are presented in Table 7.24.

183

Table 7.24 Critical values of Rd based on displacement ductility capacity for
the suite of earthquakes of Carbondale

Earthquake	R_d	Earthquake	R_d
carb-1	2.94	carb-6	2.29
carb-2	3.21	carb-7	3.15
carb-3	2.83	carb-8	3.20
carb-4	2.67	carb-9	2.13
carb-5	2.44	carb-10	3.06
		Average	2.80
		COV	0.14

The selected average value of the critical values of R_d based on displacement ductility capacity was equal to 2.80 (Table 7.24).

184

CHAPTER 8

Proposed Values of R and C$_d$ Factors for AAC-Shear Wall Structures

In this chapter, values of the seismic force-reduction factor (R) and displacement amplification factor (C$_d$) are proposed for flexure-dominated AAC shear-wall structures. Those proposed values depend on values of the factors R$_d$, Ω_{system}, and C$_{du}$, which are proposed in the following sections.

8.1 PROPOSED VALUE OF THE FACTOR R$_d$ FOR FLEXURE-DOMINATED AAC SHEAR-WALL STRUCTURES

The procedure described in Section 7.1 for selecting values of the ductility reduction factor (R$_d$) was carried out for the four selected structures using the suites of earthquakes representative of Charleston, Carbondale, Memphis, Los Angeles, and Seattle. In most cases values of R$_d$ of 1, 2, 3 and 4 were assumed in the proposed procedure. If the drift ratio or the displacement ductility demands changed significantly between two consecutive values of R$_d$, a new value of R$_d$ equal to the average of those values was assumed, for example values of R$_d$ of 2.5 and 3.5. Linear interpolation was used among those values to calculate critical values of R$_d$, (values of R$_d$ that make the global drift ratio and displacement ductility demands equal to the maximum global drift ratio and displacement ductility capacities). A mean value of the factor R$_d$ was selected for each different structure and suite of earthquakes, as the minimum value between the average critical values of R$_d$ based on global drift ratio and displacement ductility capacities as presented in the example of Section 7.6. In all cases the critical value of R$_d$ based on displacement ductility was smaller than that based on global drift ratio. In few cases during the nonlinear analyses, the global drift ratio

demand for a value of R_d of 1 was greater than the global drift ratio capacity of 1%. Therefore, for those particular cases, values of R_d based on that global drift ratio were not selected. Table 8.1 presents the selected mean values of R_d based on displacement ductility for the different structures and suites of earthquakes, and the corresponding coefficient of variation (COV).

Table 8.1 Selected mean values of R_d based on drift ratio and displacement ductility capacities for different structures and suites of earthquakes

Suite of Earthquakes	Structure	Mean R_d	COV	Structure	Mean R_d	COV
Los Angeles	ST-1W-5S	2.37	0.29	ST-2W-5S	2.48	0.30
Seattle	ST-1W-5S	2.67	0.28	ST-2W-5S	2.92	0.26
Carbondale	ST-1W-5S	2.80	0.15	ST-2W-5S	3.07	0.15
Memphis	ST-1W-5S	2.46	0.15	ST-2W-5S	2.66	0.17
Charleston	ST-1W-5S	2.93	0.19	ST-2W-5S	2.96	0.13
Los Angeles	ST-1W-3S	1.95	0.22	ST-2W-3S	2.19	0.22
Seattle	ST-1W-3S	2.15	0.39	ST-2W-3S	2.52	0.31
Carbondale	ST-1W-3S	2.26	0.15	ST-2W-3S	2.4	0.14
Memphis	ST-1W-3S	2.20	0.14	ST-2W-3S	2.43	0.14
Charleston	ST-1W-3S	2.96	0.11	ST-2W-3S	3.19	0.12
				Average	2.58	
				COV	0.14	
				10% lower fractile	2.13	

The mean values of R_d presented in Table 8.1, for the three and five-story cantilever-wall structures were smaller than those corresponding to the three and five-story coupled wall structures. The reason is that the maximum inelastic displacement and displacement ductility demands for the cantilever-wall structures were greater than those corresponding to the coupled-wall structures. Mean values of R_d for the three-story structures were smaller than those corresponding to the five-story structures. This can be related to the following:

- in the short period range, the nonlinear response of the structure increases rapidly; and

- the large dispersion among the spectral accelerations and the design spectral acceleration observed for a period of 0.26 seconds compared with that observed for a period of 0.62 seconds in the suites of earthquakes studied.

Based on the 10% lower fractile value of the mean values of R_d. presented in Table 8.1, a value of R_d of 2 is proposed for flexure-dominated AAC shear-wall structures. The approach adopted here was to select a value of R_d that would result in structural failure (exceedance of drift or ductility capacities) less than 10% of the time under suites of earthquakes representing in average the design spectra.

8.2   PROPOSED VALUE OF THE OVERSTRENGTH FACTOR (Ω_o)

The system overstrength factor (Ω_{system}) is the product of independent overstrength factors (NEHRP 2000 and Uang 91) defined as follows: (1) development of sequential plastic hinges in redundant structures; (2) material strengths higher than those specified in design; (3) strength reduction factors; (4) specified sections and reinforcement patterns greater than those required in design; (5) nonstructural elements; and (6) variation of lateral forces.

Independent overstrength factors are proposed for AAC shear-wall structures as follows: (1) Assume that plastic hinges at the base of the walls would form at the same time; that is, the redundancy factor would be equal to 1; (2) Assume actual yield strength of the flexural reinforcement 10% higher than that specified in design; (3) Assume a strength reduction factor for flexural design of walls equal to 0.9. This corresponds to an independent overstrength factor of

187

1.1; (4) Assume a selected amount of flexural reinforcement 10% greater than that required in design. (5) Ignore participation of nonstructural elements; (6) The minimum design seismic forces specified in the IBC 2000 for the four selected structures were at least 20% greater than those obtained from the elastic modal spectral analysis (Table 8.2). Two probable reasons are: (1) the static analysis is a simplification of the modal spectral analysis; and (2) cracked properties of the walls were used in all modal spectral analyses. Table 8.2 shows the minimum base shear prescribed in the IBC 2000 and that calculated using the modal analysis with the reduced initial stiffness for the tree and five-story cantilever-wall structures. Values of minimum base shear for the coupled-wall structures were similar to those presented for the cantilever-wall structures.

Table 8.2 Minimum IBC 2000 design base shear and base shear from elastic modal analysis for the three and five-story cantilever structures

Structure	Location	Site Class	IBC 2000 Minimum Base Shear V_{min} kips (kN)	Base Shear Used Analyses V_{used} kips (kN)	V_{min}/V_{used}
ST-1W-3S	Los Angeles	D	114 (507)	89 (396)	1.28
ST-1W-3S	Seattle	D	98 (436)	77 (342)	1.27
ST-1W-3S	Carbondale	C	74 (329)	58 (258)	1.27
ST-1W-3S	Memphis	C	81 (360)	64 (285)	1.27
ST-1W-3S	Charleston	C	98 (436)	83 (369)	1.18
ST-1W-5S	Los Angeles	D	194 (863)	143 (636)	1.31
ST-1W-5S	Seattle	D	124 (552)	101 (449)	1.22
ST-1W-5S	Carbondale	C	92 (409)	70 (311)	1.31
ST-1W-5S	Memphis	C	106 (471)	77 (342)	1.37
ST-1W-5S	Charleston	C	117 (520)	87 (387)	1.34

The product of the above independent overstrength factors is equal to 1.6. A value of system overstrength factor (Ω_{system}) of 1.5 is proposed for AAC shear-wall structures.

8.3 PROPOSED VALUE OF THE FACTOR R FOR FLEXURE-DOMINATED AAC SHEAR-WALL STRUCTURES

The factor (R) is the product of the ductility reduction factor (R_d) and the system overstrength factor (Ω_{system}). Using the proposed ductility reduction factor (R_d) of 2 and the system overstrength factor (Ω_{system}) of 1.5, a value of the seismic force-reduction factor (R) of 3 is proposed for flexure-dominated AAC shear-wall structures. This value of R of 3 is equal to the value of R for detailed plain concrete shear walls, and is 20% greater than the value of R for ordinary reinforced and detailed plain masonry shear walls prescribed in the IBC 2000.

8.4 PROPOSED VALUE OF THE FACTOR C_d FOR FLEXURE-DOMINATED AAC SHEAR-WALL STRUCTURES

The value of the displacement amplification factor C_d is defined as the maximum nonlinear displacement during an earthquake (D_{max}), divided by the elastic displacement (D_s) calculated using reduced seismic design forces (NEHRP 2000) as presented in Figure 8.1.

189
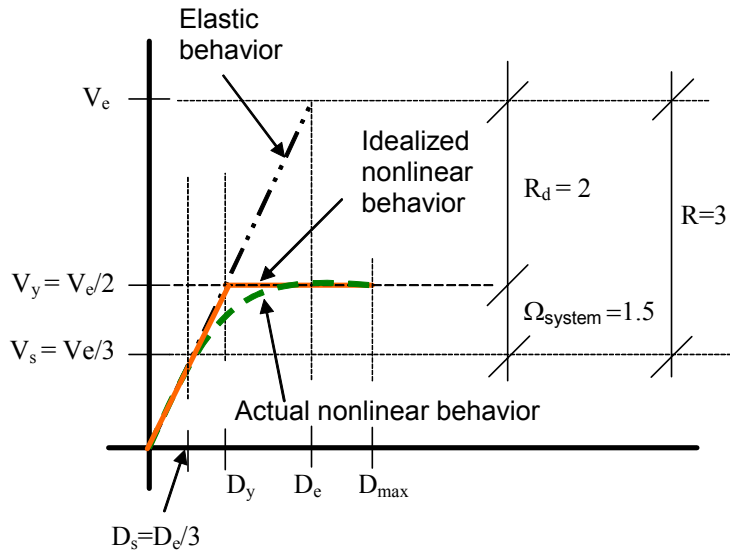
Figure 8.1 Maximum inelastic displacement and elastic displacements
associated with a value of the factor R of 3

In Figure 8.1, V_e is the elastic design lateral force associated with a value of R of 1; V_y is the lateral force at which significant yield is observed in the structural system; and D_e and D_y are the elastic displacements calculated using V_e and V_y respectively. The factor C_d can be calculated as shown in Equation (7.1).

$$C_d = \frac{D_{max}}{D_y} \Omega_{system} \qquad\qquad (8.1)$$

Setting the ratio D_{max}/D_y equal to the amplification parameter C_{du}, the displacement amplification factor (C_d) is given by Equation (8.2).

$$C_d = C_{du}\, \Omega_{system} \qquad\qquad (8.2)$$

Equation (8.2) shows that the factor C_d depends on the selection of the amplification factor (C_{du}) and the system overstrength factor (Ω_{system}). Using the results of the dynamic nonlinear analyses carried out with a value of R_d of 2, mean critical values of C_{du} were calculated for each different AAC structure and suite of earthquakes studied. Each critical value of C_{du} was defined as the maximum nonlinear displacement divided by the elastic displacement calculated using reduced seismic forces (R_d=2). The mean critical values of the factor C_{du} for the different structures and suites of earthquakes are presented in Table 8.3.

Table 8.3 Mean critical values of the factor C_{du} for different structures and suites of earthquakes

Suite of Earthquakes	Structure	Mean C_{du}	COV	Structure	Mean C_{du}	COV
Los Angeles	ST-1W-5S	2.77	0.46	ST-2W-5S	2.49	0.48
Seattle	ST-1W-5S	2.31	0.34	ST-2W-5S	2.14	0.26
Carbondale	ST-1W-5S	2.08	0.16	ST-2W-5S	1.95	0.09
Memphis	ST-1W-5S	2.27	0.19	ST-2W-5S	2.09	0.17
Charleston	ST-1W-5S	2.08	0.23	ST-2W-5S	1.93	0.19
Los Angeles	ST-1W-3S	3.01	0.42	ST-2W-3S	2.96	0.46
Seattle	ST-1W-3S	2.11	0.46	ST-2W-3S	2.42	0.57
Carbondale	ST-1W-3S	2.58	0.22	ST-2W-3S	2.89	0.37
Memphis	ST-1W-3S	2.35	0.24	ST-2W-3S	2.34	0.30
Charleston	ST-1W-3S	1.91	0.10	ST-2W-3S	1.85	0.11
				Average	2.32	
				COV	0.16	
				10% lower fractile	1.86	
				10% Upper fractile	2.79	

The 10% lower fractile, average, and 10% upper fractile values of the calculated mean critical values of C_{du} were equal to 1.86, 2.32, and 2.79

191

respectively. A value of C_{du} of 2 was selected as amplification factor for flexure-dominated AAC shear wall structures. Using this proposed value of C_{du} of 2, and the proposed value of Ω_{system} of 1.5, a value of C_d of 3 was proposed for the seismic design of flexure-dominated AAC shear wall structures in the United States.

The value of R of 3 proposed for the seismic design of flexure-dominated AAC shear-wall structures was based on a 10% lower fractile value to be conservative in selecting the final design seismic forces. The value of C_d, however, should be based on a upper fractile value to be conservative in the estimation of the maximum inelastic displacements. If the factor C_{du} is based on the 10% upper fractile value of 2.79 and on the value of Ω_{system} of 1.5, then the value of C_d would be greater than the proposed value of R of 3. A value of C_d of 3 is proposed for the seismic design of flexure-dominated AAC shear-wall structures to be consistent with the relationship between the values of R and C_d for other structural systems in the IBC 2000 (for example, values of R are in most cases greater than or equal to those values of C_d).

8.5   CONCLUDING REMARKS ABOUT THE FACTOR R

The values of the factor R prescribed in the IBC 2000 correspond to different structural systems. The permissible range of structural systems is restricted based on the IBC 2000 seismic design categories, which depend on the geographic location of the structure, the seismic use group, and the underlying soil. For masonry structures, for example, special reinforced masonry shear walls are required in Seismic Design Category D and higher. Seismic design categories also are associated with prescriptive detailing requirements and restrictions on permitted types of seismic analysis for different structural systems.

The current approach of linking the particular structural systems to seismic design categories can result in the design of a structural system whose available displacement ductility is less than that implied by the system's R value. For example, long, one-story masonry shear walls are incapable of developing flexural ductilities regardless of their detailing. If a designer uses the relatively high R value permitted by the special detailing that is mandated by the applicable seismic design category, the actual seismic forces may well be underestimated. For this reason, it is more logical to link R to the probable available displacement ductility, rather than the level of detailing. This is a trend in current efforts towards a more rational use of the R factor.

A value of the factor R of 3 is proposed in this dissertation for the seismic design of flexure-dominated AAC shear-wall structures, and a value of R of 1.5 is proposed for the seismic design of shear-dominated AAC shear-wall structures based on the value of Ω_{system} of 1.5. The latter value implies essentially elastic behavior.

CHAPTER 9

Summary, Conclusions and Recommendations

9.1 SUMMARY

The research presented in this dissertation consists of the development of a rational procedure to select values of the force-reduction factor (R) and the displacement-amplification factor (C_d) for the seismic design of flexure-dominated AAC structures in the United States. The proposed procedure involves a combination of the experimental results from fourteen AAC shear wall specimens, and the analytical results of numerical simulations of the performance of AAC shear wall structures subjected to earthquake ground motions. It is rational within the limitation imposed by a period-independent value of R.

A series of eight shear-dominated and six flexure-dominated AAC shear wall specimens were tested under quasi-static reversed cyclic loads. The specimens were designed and tested using different panels and block orientations, reinforcement layouts, aspect ratios, and axial loads that represent a variety of AAC shear walls. The shear-dominated and flexure-dominated specimens provided experimental data to develop hysteretic models that represent the shear behavior as governed by web shear cracking, and flexural behavior of AAC shear walls subjected to earthquake ground motions. The flexural-dominated specimens also provided information to define appropriate values of the drift ratio and displacement ductility capacities for AAC shear walls. Even though web shear cracking was observed in walls of the assemblage specimen, these walls reached displacement ductilities that were reasonably consistent with those observed in the flexure-dominated specimens. The maximum observed drift ratios were small compared with those observed for the flexure-dominated specimens. The major

reasons were the large stiffness of the walls of the assemblage compared with that of the flexure-dominated specimens, and the presence of web shear cracking and sliding in the assemblage specimen. The behavior of the walls of the assemblage specimen showed that crushing of the compressive toe can be improved or eliminated by using walls with flanges.

The force-reduction factor (R) was defined as the product of the ductility reduction factor (R_d) and the system overstrength factor (Ω_{system}). A procedure was developed to calculate critical values of R_d for flexure-dominated AAC structures based on drift ratio and displacement ductility capacities.   This procedure involved the selection and design of AAC shear wall structures, selection of suites of earthquakes representing seismic zones of the United States, selection of drift ratio and displacement ductility capacities for those structures, and the development of hysteretic models to predict the performance of flexure-dominated AAC shear wall structures under earthquakes.

Four AAC structures were selected and designed to calculate critical values of R_d. The structures were selected as AAC shear wall structures because shear walls are the major structural elements resisting seismic forces.

The suite of earthquake ground motions were selected based on areas with high potential for seismic activity. For the central and eastern zones of the United States, three suites of earthquakes were selected: Charleston, SC; Carbondale, IL; and Memphis, TN. For the western zone of the United States, two suites of earthquakes were selected: Los Angeles, CA; and Seattle, WA. The five suites of earthquakes were scaled to represent in average the design seismic forces defined by corresponding design spectra.

Drift ratio and displacement ductility capacities were included in the procedure to select R_d to provide reasonable limits to avoid collapse of AAC shear wall structures under earthquakes. The drift ratio capacity was considered

to limit damage and differential movement, and the displacement ductility capacity to control the amount of inelastic deformation in AAC shear wall structures. Using the experimental results of the six flexure-dominated specimens, values of the drift ratio and displacement ductility capacities of 1% and 3.5 were selected for flexure-dominated AAC shear wall structures, respectively. Those values were based on lower characteristic values of the observed drift ratios and displacement ductilities of the flexure-dominated specimens.

Dynamic nonlinear dynamic analyses were carried out using the program CANNY 99. The idealized wall element used in the analyses was defined mainly by two nonlinear flexural springs, and one nonlinear shear spring. The hysteretic parameters for those nonlinear springs were based on average values observed in the six flexure-dominated specimens.

A value of R_d of 2 was selected for flexure-dominated AAC shear-wall structures based on the 10% lower fractile value of the mean critical values of R_d. The approach adopted was to select a value of R_d that would result in exceedance of drift or ductility capacities less than 10% of the time under suites of earthquakes representing in average the design spectra.

The system overstrength factor (Ω_{system}) was defined as the product of six independent overstrength factors defined as follows: (1) development of sequential plastic hinges in redundant structures; (2) material strengths higher than those required in design; (3) strength reduction factors; (4) specified sections and reinforcement greater than those required in design; (5) nonstructural elements, and (6) variation of lateral loads. These independent overstrength factors were evaluated for the case of cantilever and coupled-wall structures, and a value of system overstrength factor (Ω_{system}) of 1.5 was proposed for flexure-dominated AAC shear wall structures.

196

Based on the proposed ductility reduction factor (R_d) of 2, and the proposed value of system overstrength factor (Ω_{system}) of 1.5, a value of R of 3 was proposed for the seismic design of flexure-dominated AAC shear wall structures in the United Sates. A value of R of 1.5 is proposed for the seismic design of shear-dominated AAC shear-wall structures based on the value of Ω_{system} of 1.5. The latter value of R implies essentially elastic behavior.

The displacement-amplification factor was defined as the product of an amplification factor (C_{du}) and the system overstrength factor (Ω_{system}). A value of C_{du} of 2 was selected as amplification factor for flexure-dominated AAC shear wall structures. Using this proposed value of C_{du} of 2, and the proposed value of Ω_{system} of 1.5, a value of C_d of 3 was proposed for the seismic design of flexure-dominated AAC shear wall structures in the United States. The value of C_{du} of 2 was proposed to be consistent with IBC 2000 values of R and C_d for other structural systems.

9.2 CONCLUSIONS

Based on a combination of the experimental results of fourteen AAC shear wall specimens and a two-story assemblage, and analytical results on the performance of AAC shear wall structures, the following conclusions are presented:

- A rational procedure was developed to select values of the force-reduction factor (R) and the displacement-amplification factor (C_d) for the seismic design of flexure-dominated AAC shear wall structures in the United States.

- The value of the factor (R) was proposed equal to 3 for flexure-dominated shear-wall structures, and was proposed equal to 1.5 for shear-dominated AAC shear-wall structures. The value of the factor (C_d) was proposed equal to

197

3. Those values of R and C_d are intended to be proposed for eventual incorporation in ASCE 7.

- The seismic force-reduction factor (R) proposed for flexure-dominated AAC shear wall structures was governed by the critical values of R_d based on displacement ductility capacity.

- The average value of the mean critical values of R_d for the five-story structures was about 10% higher than that average value for the three-story structures studied. This difference showed that the value of R depends on the natural period of the structure. For the AAC shear wall structures studied here, however, the value of R was not that sensitive to the period of the structure.

- The displacement-amplification factor (C_d) proposed for flexure-dominated AAC shear wall structures was based on a lower characteristic value of structural response slightly below the mean. That value of C_d was selected to be consistent with the relationship between the values of R and C_d proposed for other structural systems in the IBC 2000.

- Behavior of the flexural-dominated specimens showed that flexure-dominated AAC shear walls are structural elements capable of dissipate a satisfactory amount of energy through inelastic deformation. The hysteretic behavior of the those specimens was in general predictable and stable up to values of drift ratio and displacement ductility of 1% and 3.5, respectively.

- The observed behavior of the walls of the assemblage specimen showed that the behavior of the compressive toe of AAC shear walls under lateral loads was improved by the presence of wall flanges.

9.3 RECOMMENDATIONS FOR PRACTICAL APPLICATIONS AND FUTURE RESEARCH

- The process developed here for selecting R and C_d factors could be used in any geographic location, and in the context of any design code. In applying this process to a geographic location outside United States (for example, Mexico), the suites of earthquakes should include those applicable to Mexico. In the design context of other codes (for example, Mexican codes), the trial structure should be designed according to those codes, and the code-dependant factors analogous to R and C_d should be included correctly in the evaluation of response.

- Upper characteristic values of response might arguably be used to establish C_d for AAC shear-wall structures, and other structural systems as well. This should be examined globally for all structural systems.

- Additional experimental research would be necessary to further study the behavior of AAC shear walls with flanges, and the effect of Heli-fix® ties on the behavior of the compressive toes, and on the overall behavior of the walls. Testing would focus on defining the required number, diameter and spacing of the Heli-fix® to connect wall flanges or U-blocks to AAC walls to enhance the behavior of the compressive toe of those walls.

APPENDIX A

Testing Program for Two-Story Assemblage Specimen

Phase II of the experimental program consisted of testing a two-story, full-scale assemblage specimen with AAC shear walls and untopped AAC floor diaphragms. The specimen was subject to reversed cyclic loads applied at each floor level. In this appendix, the objectives, test setup, loading equipment, loading history and instrumentation of that assemblage are presented.

9.4 OBJECTIVES OF TESTING PROGRAM (PHASE II)

The objectives of the assemblage were to verify that a system of squat walls designed to fail in a flexure-dominated mode would indeed fail in flexure; to verify proposed design provisions for AAC shear walls; to verify that lateral load could be transferred through AAC floor diaphragms; to verify proposed design procedures for such diaphragms; and to verify the proposed analytical models for the flexure-dominated specimens.

9.5 DESCRIPTION OF SPECIMEN

The Two-Story AAC Assemblage Specimen consisted of two flanged walls connected by floor slabs, and is shown in isometric view in Figure 2. The walls were constructed with vertical AAC panels, and the floor slabs were constructed with untopped AAC floor panels. The following sections describe the details of the Two-Story AAC Assemblage Specimen and justify the decisions

made in construction. Additional plan views and elevations of the specimen are presented in Appendix A.
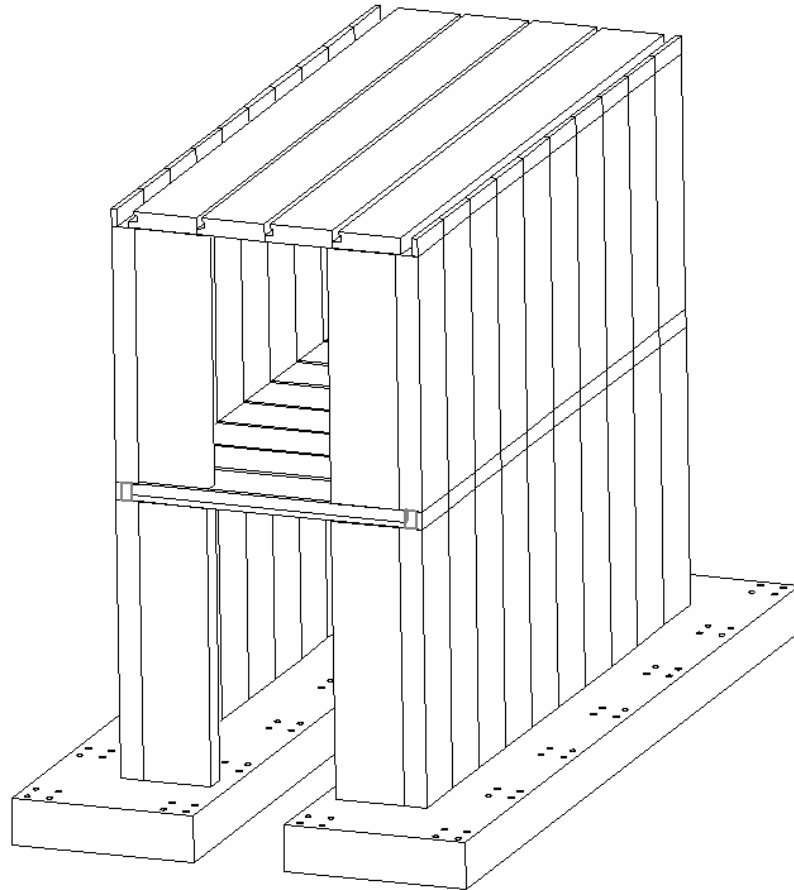
Figure 2: Isometric View of Two-story AAC Assemblage Specimen

9.5.1 Wall Configuration

The plan dimensions of the assemblage were 20 ft (6.1 m) long by 9.33 ft (2.8 m) wide (Figure 3). These dimensions were governed by laboratory space restrictions. Another potential configuration would have been using 12 ft. (3.7 m) walls and a distance of 17.33 ft. (5.1 m) between the wall ends. The wall length

of 20 ft. (6.1 m) was selected in order to meet the design goal of forcing flexural behavior in a squat wall. The maximum width was determined by laboratory space restrictions. Flanged walls were selected because this is a very common layout in actual construction. Flanges are usually present in the form of returns at wall corners, or even as extended elements. Flanged walls were also selected because it was thought that flanges would increase the crushing resistance and stability of the unconfined compression toes of the AAC shear walls. In a real building, the in-plane behavior of walls is affected by some tributary width of the perpendicular walls. In addition, the flanges add stability to the compression toe and provide out-of-plane support for the entire system. The flanges represent the contributing portions of the walls perpendicular to the direction of loading. The flange length was selected as 30 in. (0.76 m) to allow access to the interior of the specimen.

30 in.

Applied lateral load

240 in.

112 in.
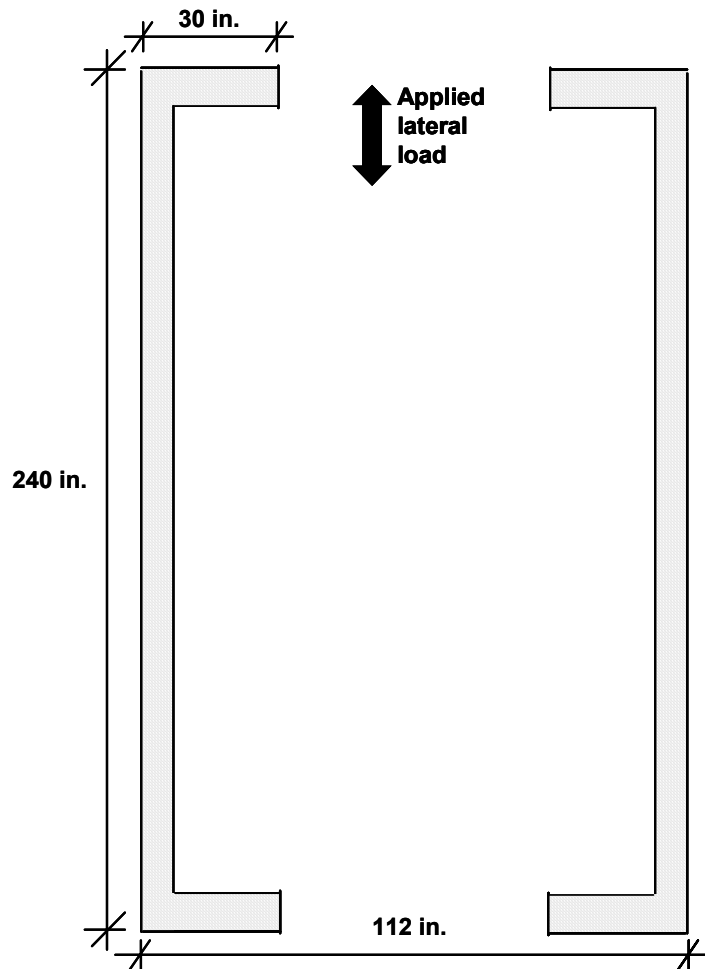
Figure 3: Plan layout of shear walls in the AAC assemblage

The walls were connected by an untopped AAC diaphragm at each floor level. Diaphragm details are presented in Sections 9.5.3 and 9.5.4.

9.5.2   AAC Layout and Web-to-flange Connection at Corners

Potential options for AAC units were horizontal panels, modular blocks and vertical panels. Vertical panels were selected for the assemblage because these are potentially the most vulnerable configuration, based on the observed behavior of single-story, lineal AAC shear walls (Chapter 9).

The purpose of the web-to-flange connections at the corners was to transfer shear between the flange and web. This connection is necessary if the flanges are to provide out-of-plane stability and it also permits the flange and web to work together to slightly increase the nominal flexural capacity. Since vertical panels are manufactured so that cores are placed between head joints only, vertical reinforcement was placed between the last two vertical panels in the web. To transfer shear from between the web and flange, two 8 mm Heli-fix® spiral anchors were used at intervals of 2 ft (0.6 m). A picture and a cross-sectional view of one of the 16 in. (0.41 m) long ties used in the assemblage specimen are shown in Figure 5 and Figure 6. The final wall layout, including web-to-flange connections, is presented in Figure 126.

Heli-fix spiral

Vertical reinforcement
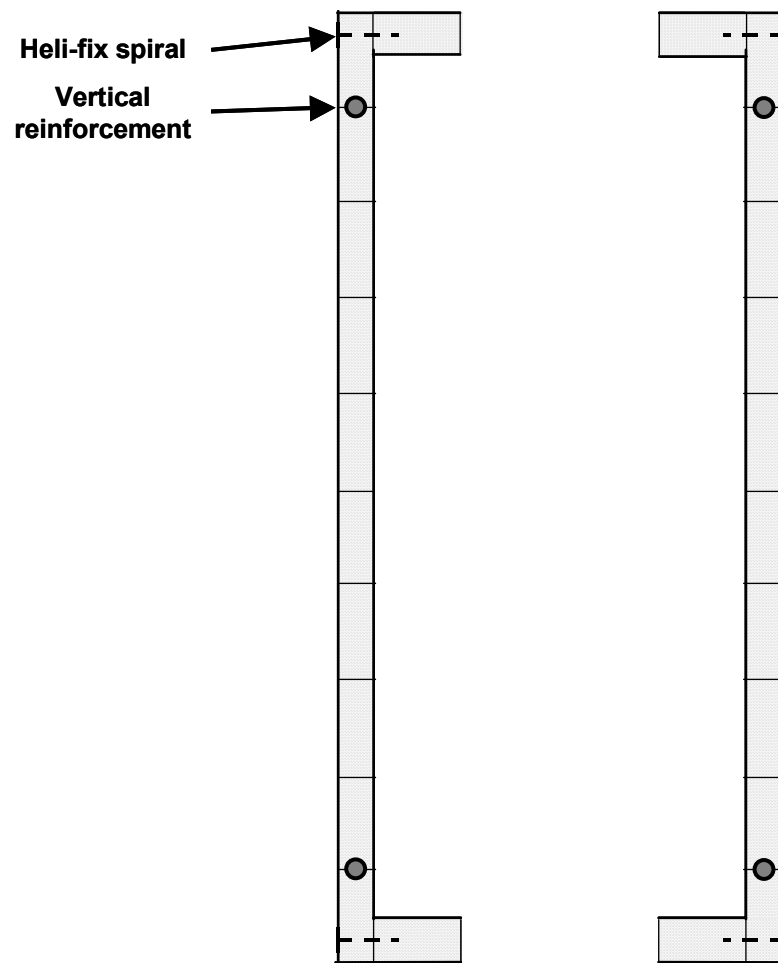
Figure 126: Connection detail for web-to-flange connection
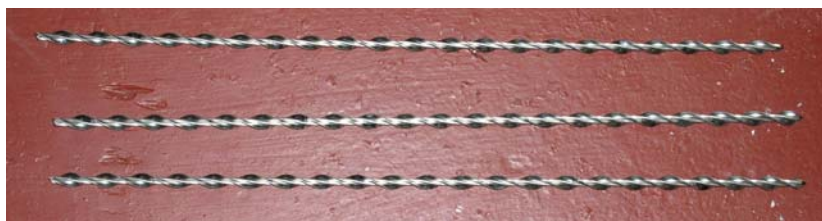
Figure 5: Heli-fix spiral anchor
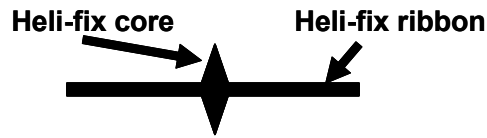
Figure 6:   Cross-section of Heli-fix spiral anchor

9.5.3   Floor System

A maximum potential diaphragm width was 16 ft (4.9 m); for this case the maximum wall length would be reduced to 12 ft (3.7 m).   The 20 ft (6.1 m) assemblage was selected to meet the design goal of forcing flexural behavior in a squat wall.

Typical AAC floor systems are panels with reinforcement placed in grouted keys.   The panels may be oriented either parallel or perpendicular to the applied load.   Plan and elevation views of floor panels oriented perpendicular to the walls are presented in Figure 129 and Figure 130.   In Figure 129, a "Detail A" is identified, that same detail is referred to elsewhere (for example Figure 130 and Figure 134).   The reinforcement in the grouted keys is anchored into the bond beam (see Detail A in Figure 134).
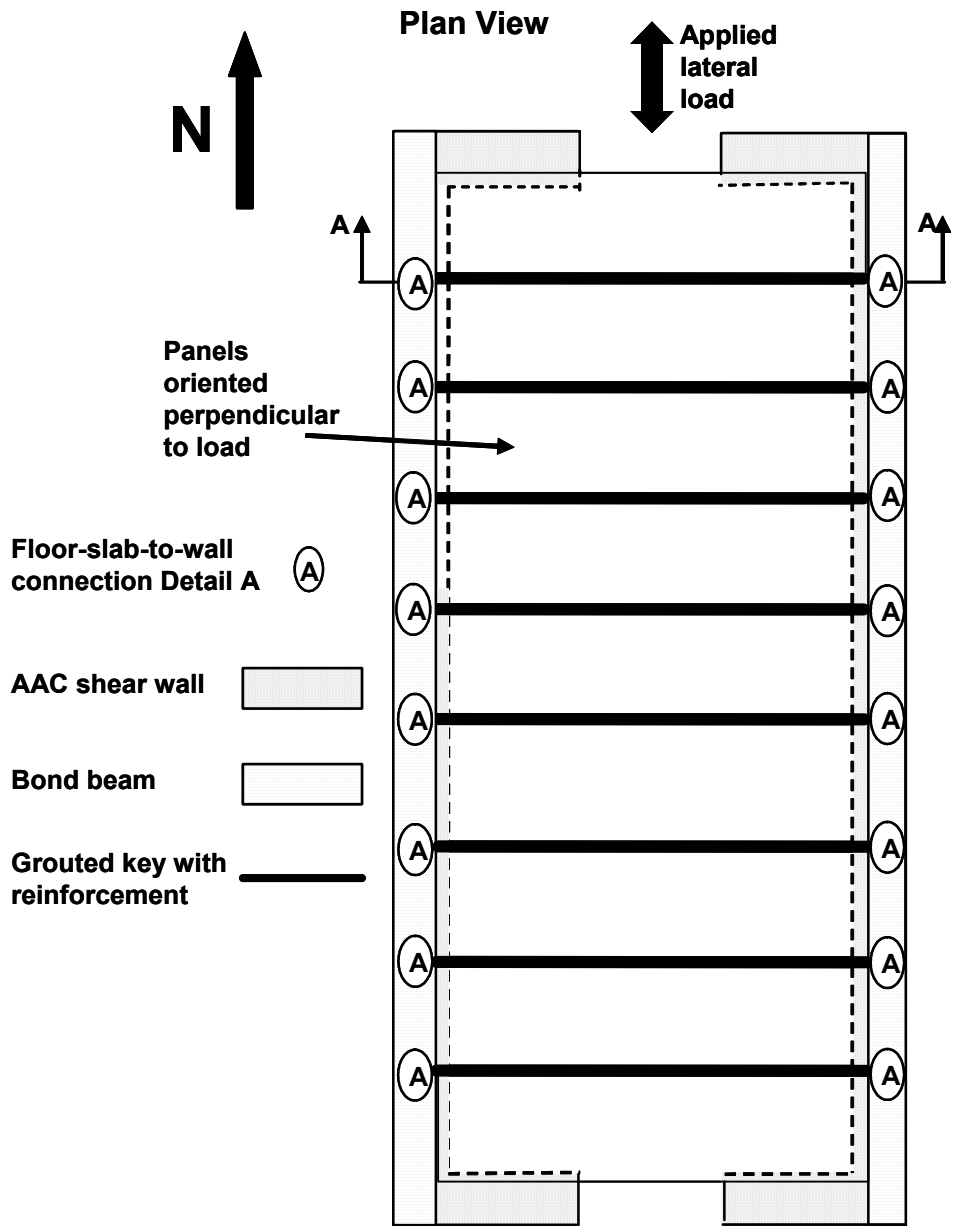
Figure 129: Floor plan for panels oriented perpendicular to applied load

207
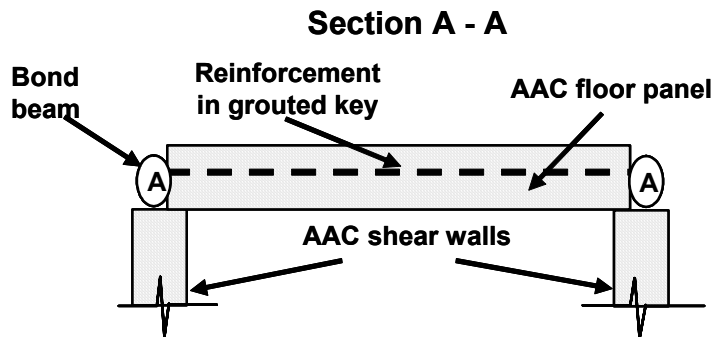
Section A - A

Figure 130: Elevation of Section A-A, floor slab-shear wall connection (panels oriented perpendicular to the direction of loading)

In a real structure, seismic lateral loads can act in any plan direction. Therefore, for testing purposes, lateral load transfer should be verified for panels parallel and perpendicular to the direction of loading. Floor panels oriented perpendicular to the direction of the loading were selected in the first elevated floor level (Figure 129 and Figure 130), and floor panels oriented parallel to the applied load were selected for the second elevated floor level.

Plan view and elevations of the second floor are presented in Figure 131 through Figure 137. The interior panels of the second floor that did not rest entirely on the wall flanges were shored during construction. Bond beams were constructed in both the north-south and east-west directions. The grouted key reinforcement was anchored into the two east-west bond beams. Connection Details A and B are presented in Figure 134 and Figure 137 of Section 9.5.4. Specimen details and dimensions are presented in Appendix A. Shear transfer was expected to be critical in the second-floor slab, due to the lack of continuous reinforcement perpendicular to the applied lateral load.

Figure 131: Floor slab for second story (panels oriented parallel to the direction of loading)

Section B - B

N-S bond
beam

AAC floor panel
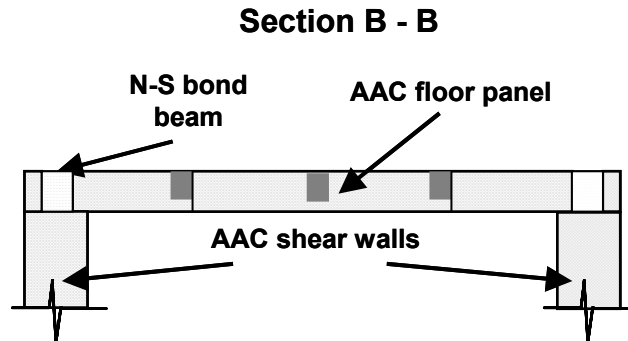
AAC shear walls

Figure 132: Elevation of Section B-B, second story floor slab-shear wall connection (panels oriented parallel to the direction of loading)

Section C - C

E-W
Bond
Beam

Reinforcement
in grouted key

AAC floor
panel

E-W
Bond
Beam

B

B

AAC shear wall
flanges
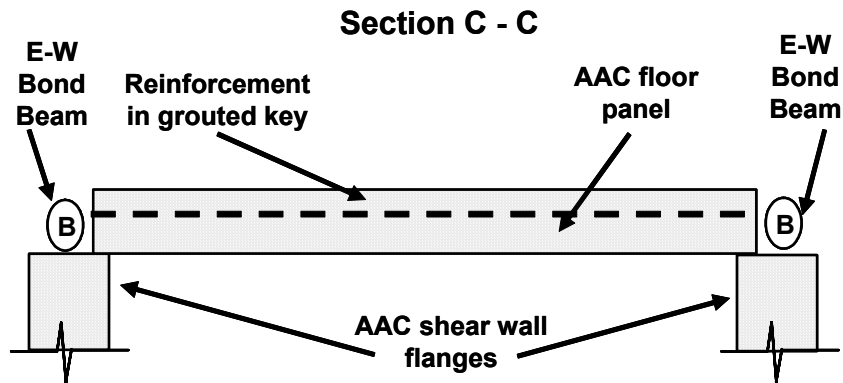
Figure 133: Section through connections between second-story floor slab, with longitudinal reinforcement, and bond beam (section rotated so floor is horizontal)

9.5.4 Connections between Wall and Floor Slab

Detail A, a connection between the bond beam and floor panels defined in Figure 129 and Figure 130, is shown in Figure 134. The reinforcement in the grouted key consists of a standard 90 degree hook bent around the longitudinal reinforcement and oriented in a vertical plane.

210

In cases where a vertical reinforcing bar was present in Detail A, (Figure 135) the detail was modified as shown in Figure 136. Detail B, a connection between the floor panels defined in Figure 131 and Figure 132, is shown in Figure 137.
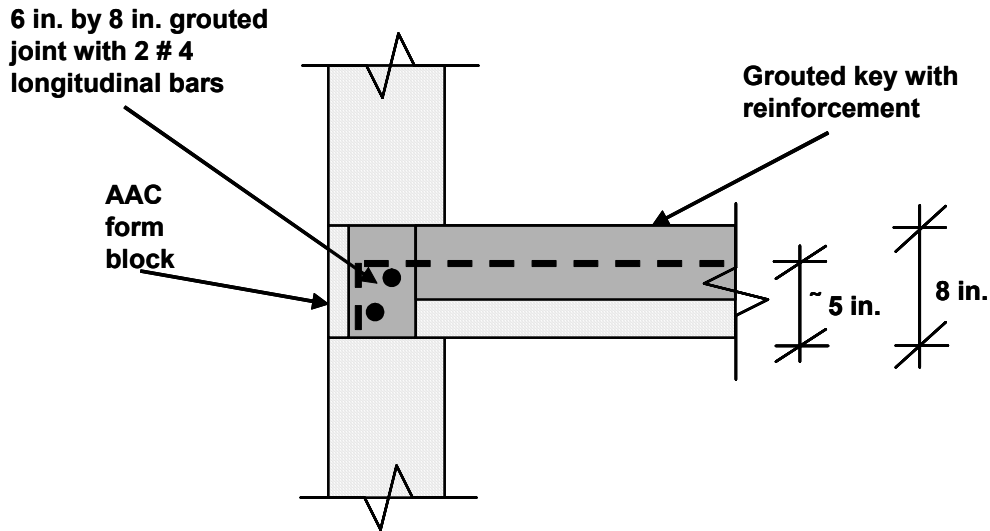
Figure 134: Detail A, anchorage of reinforcement in grouted keys for panels oriented perpendicular to the direction of loading

Figure 135: Photograph of Detail A, at intersection with vertical bar
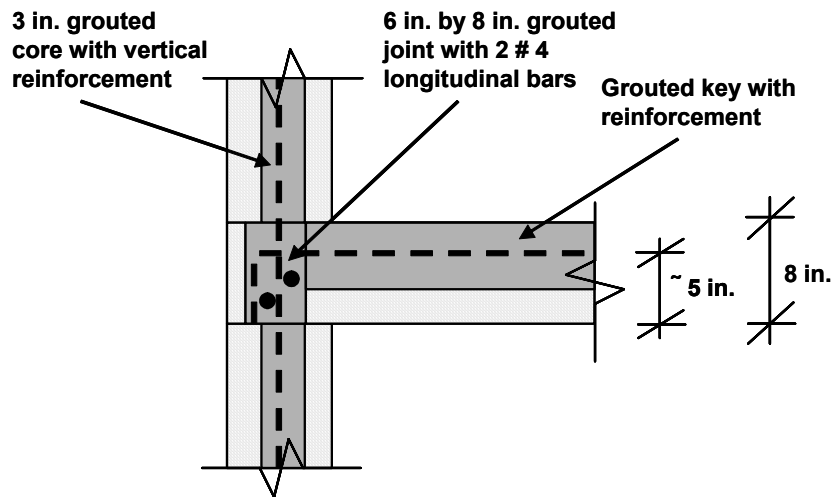
Figure 136: Detail A, at intersection with vertical bar
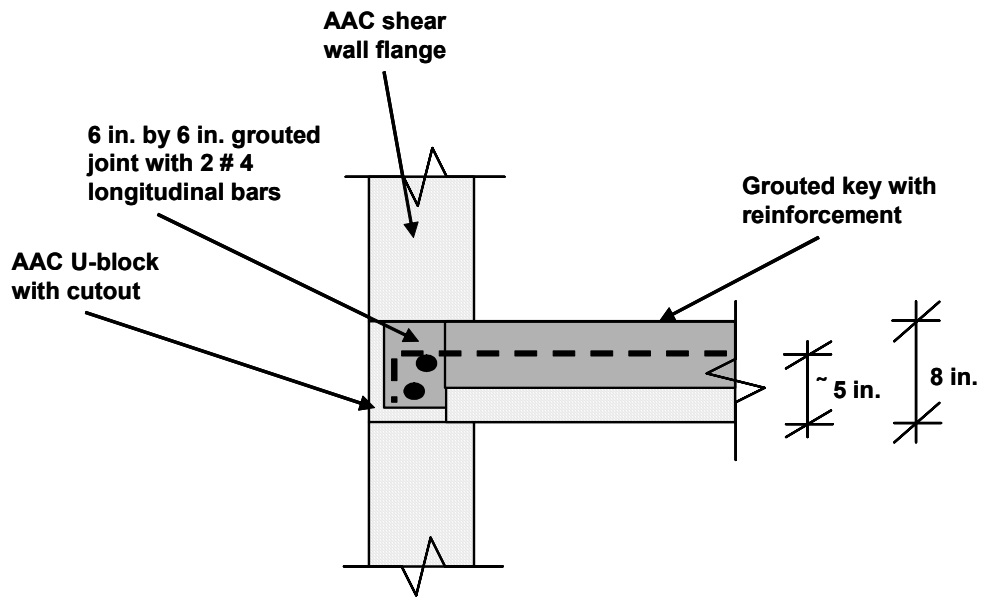
Figure 137: Detail B, anchorage of reinforcement in grouted keys for panels oriented parallel to the direction of loading

9.5.5 Lateral Load Transfer in Floor Slab for Panels Oriented Perpendicular to Direction of Loading

In a building subject to seismic loading, concentrated inertial forces are generated in areas of concentrated mass, usually the floor slabs. Forces generated in floor slabs must be transferred to shear walls. Lateral load applied perpendicular to the panels was designed to be transferred through dowel action of perpendicular reinforcement in grouted keys. Based on dowel action, the capacity of a connection between a floor slab and a shear wall is 35.6 kips (158 kN), which is 1.4 times the load corresponding to nominal flexural capacity.

9.5.6 Connections between Wall and Floor Slab for Panels Oriented Parallel to Direction of Loading

Lateral load generated in the floor slab must be transferred to the base of the structure through the shear walls. Shear transfer is critical in the case of panels oriented parallel to the direction of load, due to the lack of continuous reinforcement perpendicular to the applied load. This shear transfer can occur through adhesion between the panels and through a truss mechanism. These methods are discussed independently in the following sections.

9.5.6.1 Shear transfer through adhesion between joints

The second story of the Two-story Assemblage Specimen was designed based on shear transfer through adhesion. The critical sections in the second story floor slab are Section D-D and Section E-E, since no steel is oriented perpendicular to these paths (Figure 138). In panel-to-panel connections, Section D-D, the adhesion depends on both the thin-bed mortar and grouted key adhesion (Figure 139). In panel-to-bond beam connections the adhesion depends primarily on grout and a small section of thin-bed mortar (Figure 140).
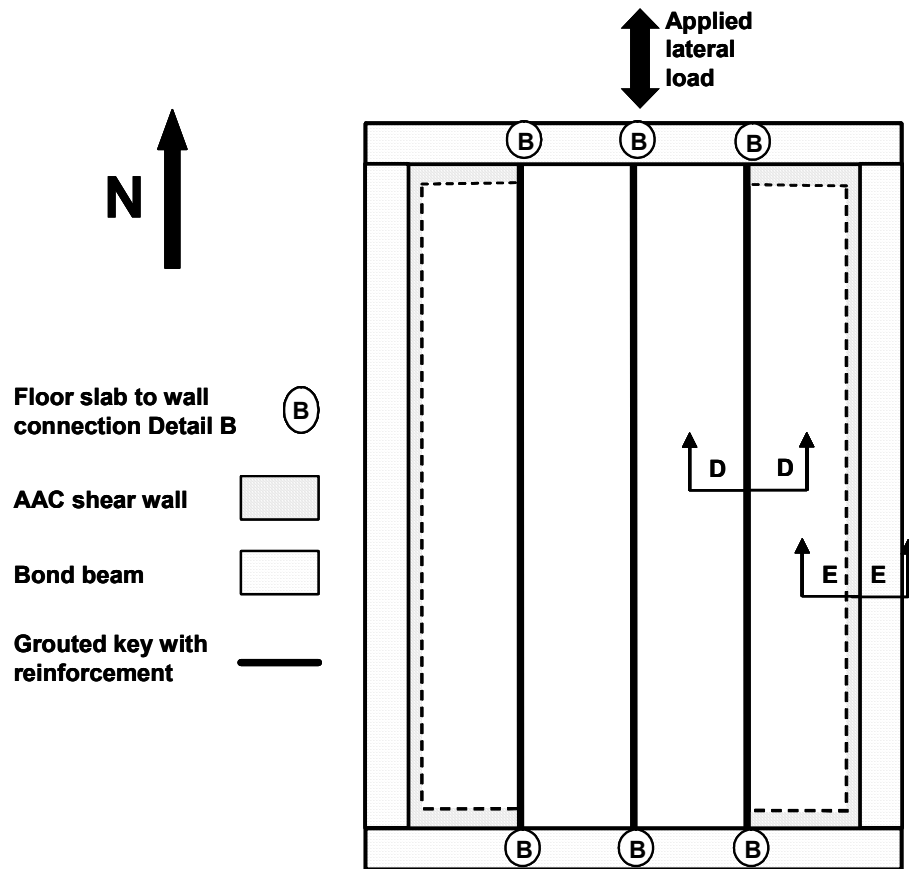
Figure 138: Plan view of second story floor panels

The panel-to-panel joints were constructed by applying thin-bed mortar at the panel joint below the grouted key and clamping adjacent panels. The grouted key was cleaned with compressed air and pre-wetted prior to placing grout. The grout was vibrated during placement. The same construction process is proposed for all panel-to-panel joints. Based on the average shear strengths and the corresponding lengths of grout and thin-bed mortar, the shear capacity is 60.5 kips (270 kN) for each joint, 2.4 times the predicted load at each joint for the nominal flexural capacity.

Section D - D
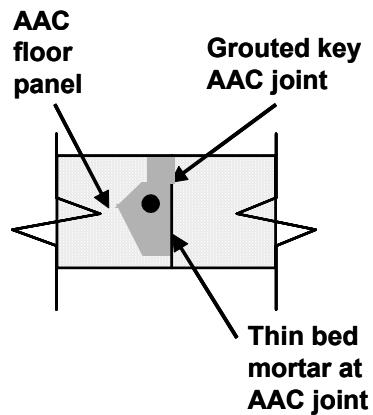
Figure 139: Elevation of Section D-D, panel-panel connection

The joints between panels and bond beams were constructed by applying thin-bed mortar at the bed joint between panels and the slab. In some cases a gap existed between the top of the vertical panel and the floor panel due to differences in the height of the leveling bed, which caused different heights at the top of panels. For this reason, the thin-bed mortar area was conservatively neglected. The bond beam was cleaned with compressed air and pre-wetted prior to placing grout. The grout was vibrated during placement. The same construction process is proposed for all panel-to-bond beam joints. Based on the average shear strength of grout and AAC the shear capacity is 69.1 kips (310 kN) for each joint, 2.8 times the load in each joint at the nominal flexural capacity.

Section E - E
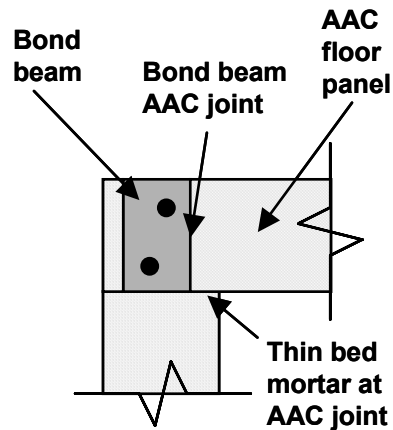
Figure 140: Elevation of Section E-E, panel-bond beam connection

If a failure occurred in the second-story slab, load could no longer be applied to the second story and the shear walls could not have been tested to failure. Due to the lack of redundancy in the system combined with the brittle nature of an adhesion failure, reinforcement was used across the joint. A plan view of deformed reinforcing bars oriented along a diagonal is shown in Figure 141.   In this configuration the deformed reinforcement works efficiently in tension. Strain gages were applied to the bars to indicate the tensile force, which is related to the shear resistance through geometry. AAC panels were modified to permit this by cutting with a masonry blade on a rotary saw (Figure 142).
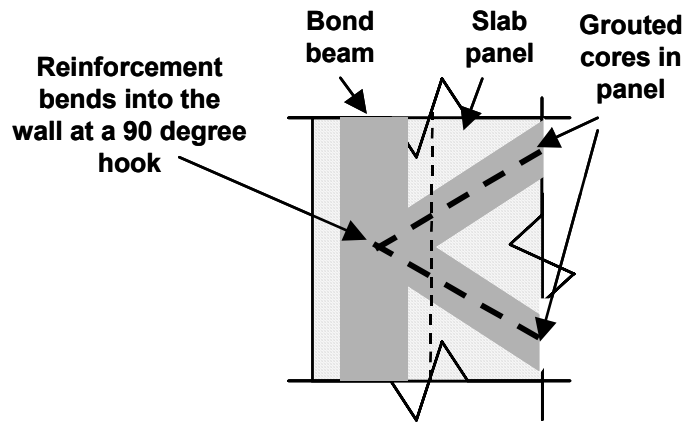
*Figure 141: Incorporation of diagonal steel across joint parallel to the
direction of load in Two-story Assemblage Specimen*

*Figure 142: Picture of diagonal reinforcement across the joint parallel to the
direction of load in Two-story Assemblage Specimen*

9.5.6.2   Shear transfer through truss mechanism

Shear transfer may also be applied through a truss mechanism, which
follows the principles of a strut-and-tie model.   Compression is transferred
through the panels in the form of struts. The reinforcement in the grouted keys

serves as tension ties, which must be tied into the bond beam by 90-degree standard hooks bent around the longitudinal reinforcement in the tension ties and oriented in a vertical plane.

The strut-and-tie model used to design the diaphragm (Figure 143) has a capacity of 77.1 kips (343 kN), 1.5 times the load in the diaphragm at nominal flexural capacity. This model is discussed in Section 9.4.6.
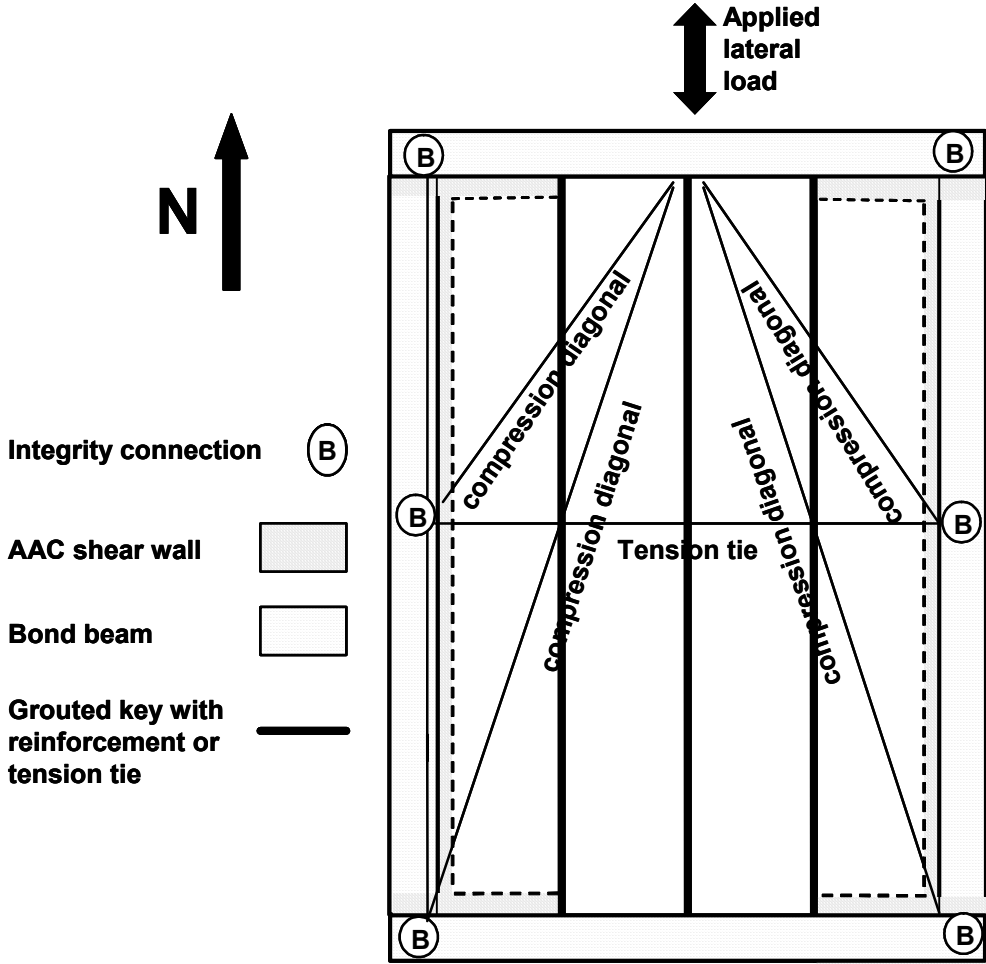
Figure 143: Truss mechanism for transferring lateral load parallel to the orientation of the panels

9.5.7 Connection between First- and Second-Story Wall

The first- and second-story walls were connected through the vertical reinforcement and the bond beam. If the surface of the grouted joint at the floor slab level was rough, a leveling bed was used between the joint and the AAC shear wall. The vertical reinforcement was spliced in the second-story wall above the first-story floor slab (Figure 134, Figure 136 and Figure 137).

9.5.8 Longitudinal Reinforcement in the Two-story AAC Assemblage Specimen

The in-plane behavior of an AAC shear wall depends on its plan configuration, reinforcement, and axial load. The selected reinforcement and location affects the shear force that causes yielding of the flexural reinforcement, the nominal flexural capacity, and the sliding shear capacity. Flexural reinforcement shown in Figure 144 was selected so that the wall behavior would be governed by flexure rather than shear.

The nominal flexural capacity was determined using the proposed flexural design provisions (Argudo 2003). The expected flexural capacity was 1.25 times the nominal flexural capacity, because of material overstrength and strain hardening. The nominal flexural capacities were converted to nominal base shear capacities based on the relationship between moment and shear found using the vertical distribution of lateral forces proposed in Section 9.6.3. A tested compressive strength of 1025 psi (7.07 MPa) found in previous Class 4 material from Babb was used in the calculations. Elasto-plastic behavior of the steel was assumed, with a yield strength of 75 ksi (517 MPa), based on mill test reports for the vertical reinforcement used in the AAC shear wall specimens.

220

The design web-shear capacity using the appropriate strength-reduction factors (φ) from ACI 318-02 was greater than the nominal flexural capacity with 1 #4 bar at 2 ft. (0.7 m) from the ends of the wall for the design axial load of 30 kips (133 kN) per shear wall. The capacity as governed by web-shear cracking was based on equations proposed and calibrated at The University of Texas at Austin, and described in Chapter 8 of this dissertation. The tested splitting tensile strength for the Babb units in the previous shipment, 88 psi (0.61 MPa), was used for this prediction.

Three additional #5 dowels were placed at the base and at the first elevated floor slab to increase the design sliding-shear capacity (Figure 144).
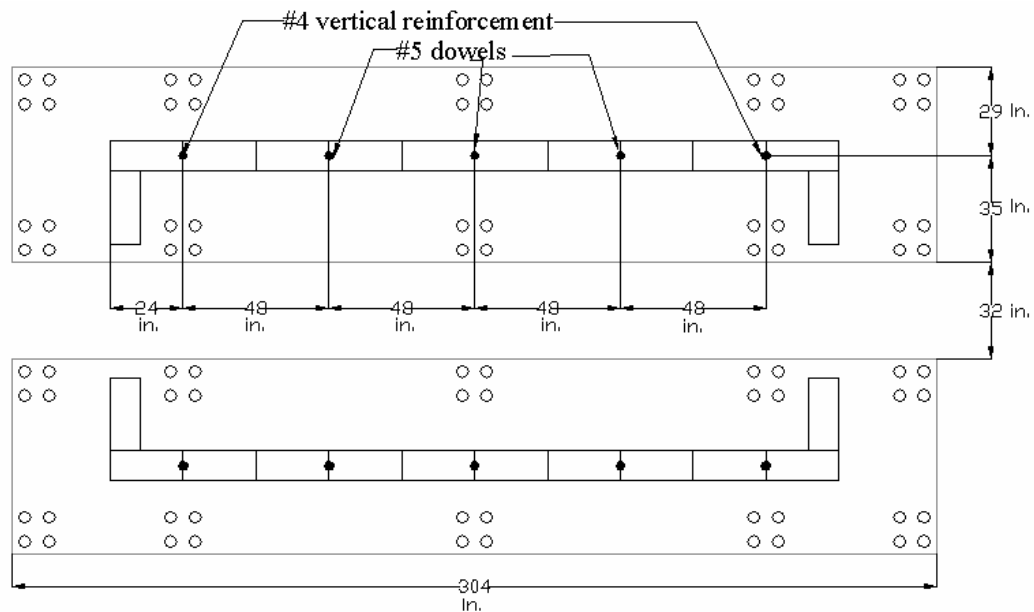
Figure 144: Plan view of base beams

9.6   Test Setup

9.6.1   Base Beam

Individual rectangular concrete base beams, reinforced and post-tensioned, were cast as foundations for each wall. The foundation size, 304 in. (7.7 m) by 64 in. (1.6 m) by 16 in. (0.41 m), was dictated by the geometry of the lab tie-downs. For a 20 ft. (6.1 m) long wall, using tie-downs only at the ends of the wall will result in large stresses, which may induce cracking of the slab. The foundations and tie-down holes are shown in Figure 144.

9.6.2   Application of Lateral Load

The lateral load was applied to the floor slabs through reinforced concrete loading beams attached to the slabs.   The loading beams themselves were longitudinally post-tensioned. Two loading beams, one above and one below each floor slab, were clamped together by vertical rods. The loading beams were 16 in. (400 mm) by 20 in. (500 mm) by 256 in. (6.5 m). The lateral load was applied through the frictional resistance between the concrete loading beam and the AAC floor slab. The required clamping force was based on the predicted maximum lateral load. The size of the loading beam and location of vertical post-tensioning rods were determined using a linear elastic finite element model. Principal tensile stresses were determined to avoid cracking either the loading beams or AAC floor slab. Plan and elevation details for the loading beam–floor slab connection are shown in Figure 145 and Figure 146. In the case of panels oriented parallel to the direction of loading, the panels could not carry the weight of the loading beam. A loading slab spanning the entire width of the floor slab and resting directly on the top of the shear walls was selected to transfer the load to the shear walls, and to carry the weight of the lower loading beam.   Since these sections were half the height of the loading beams in the first story, additional

222

vertical rods were used to distribute the clamping force.   An elevation of this
system is shown in Figure 147.
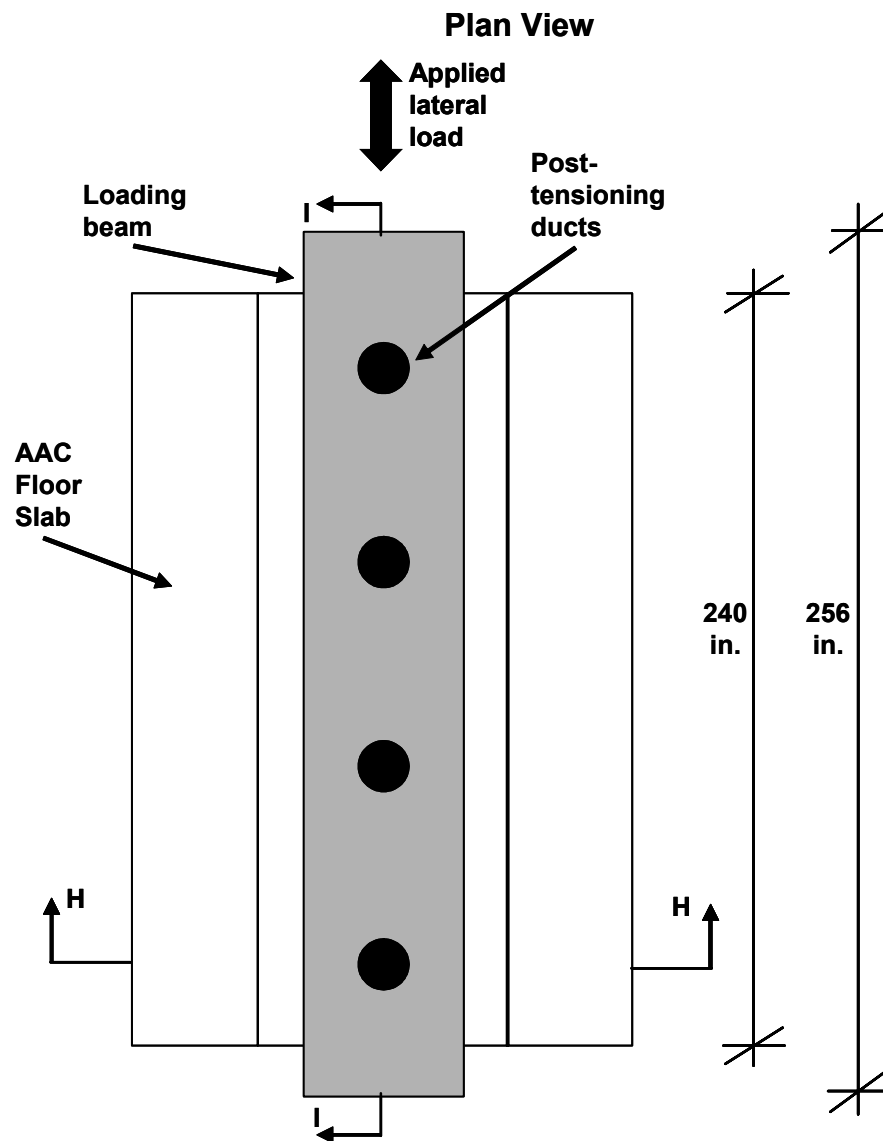
Plan View

Figure 145: Plan view of loading beam attachment to the floor slab

223
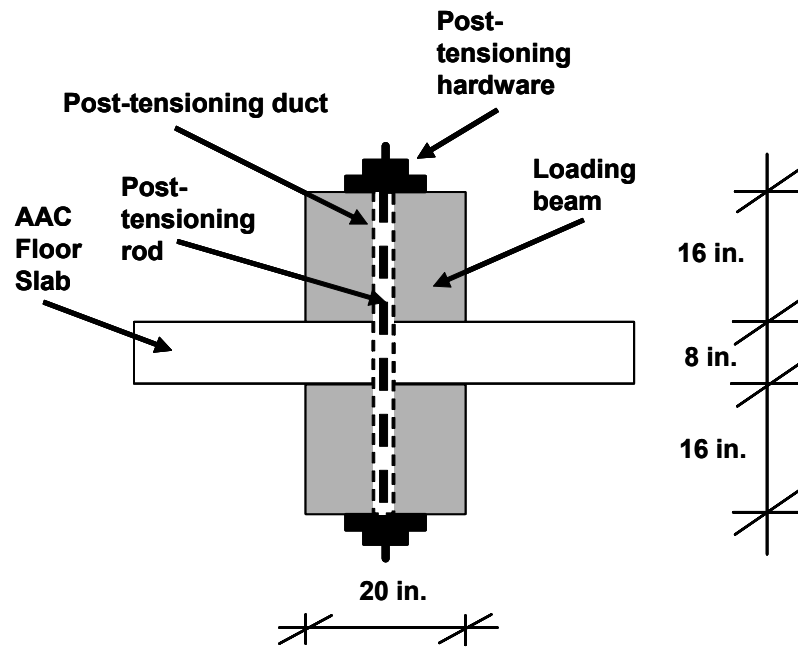
Figure 146: Elevation of Section H-H, loading beam attachment to the floor slab
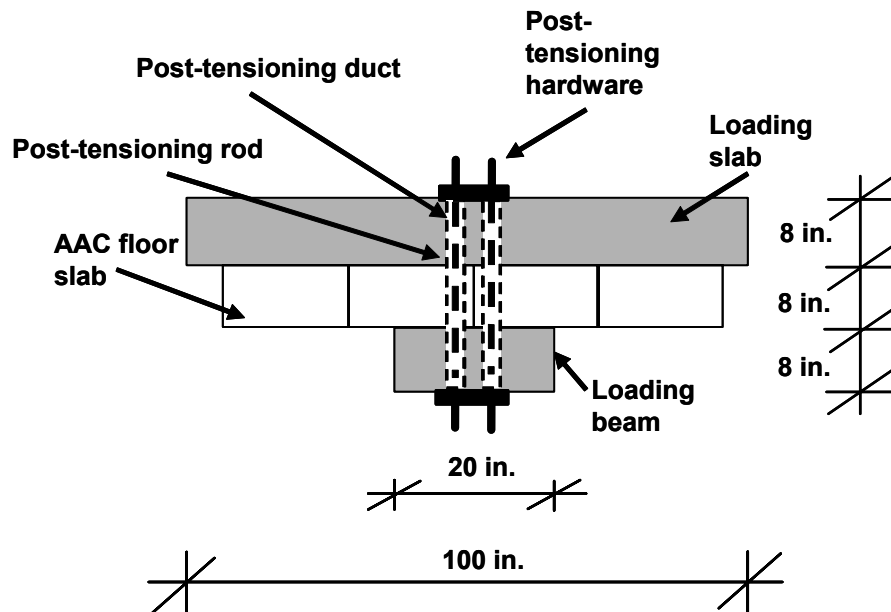
Figure 147: Modification of Section H-H for loading slab

The loading beams were also post-tensioned longitudinally.   The connection between the rams and loading beam is shown in Figure 148.   The vertical post-tensioning rods are omitted for clarity. For panels oriented parallel to the direction of loading, the loading slab and loading beam contained two internal post-tensioning ducts.   Although the risk for cracking due to non-concentric loading is increased, the calculated stresses are below the cracking load. This system is shown in Figure 149.

225

Steel plates

W-Section

Loading beam

AAC floor slab

Internal post-tensioning duct with rod
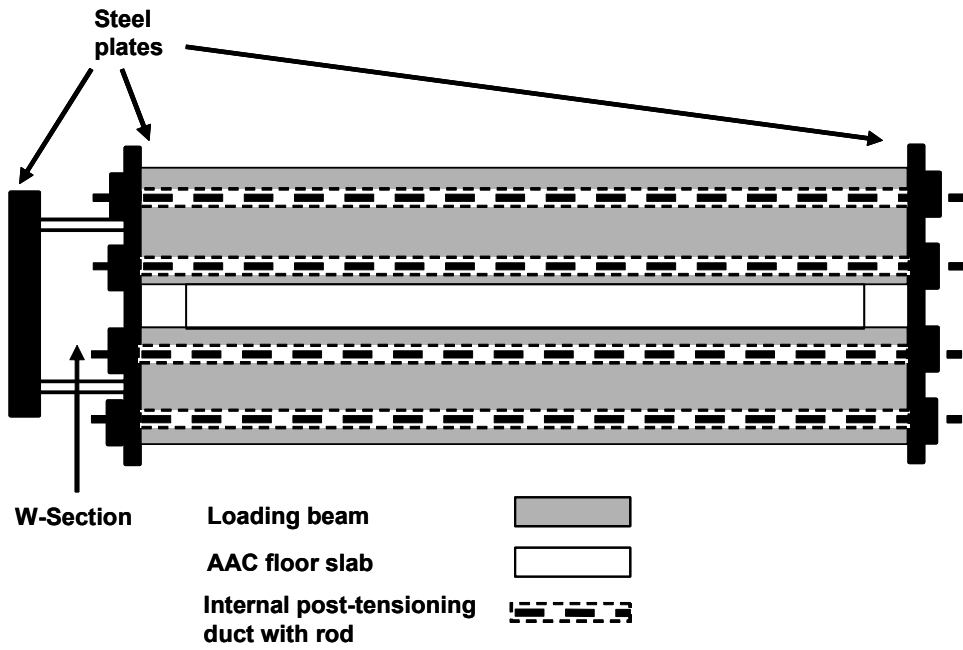
Figure 148: Elevation of Section I-I, loading beam-ram connection

Steel plates

W Section

Loading beam

AAC floor slab

Internal post-tensioning duct with rod
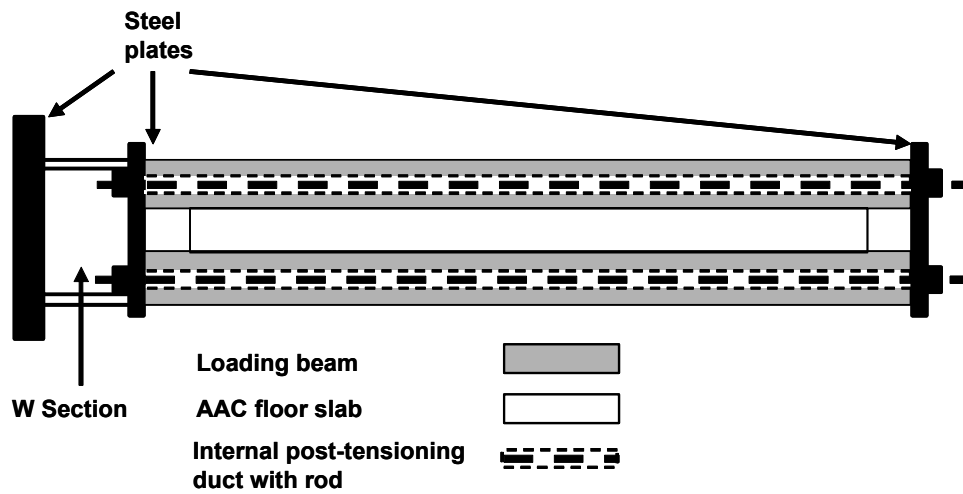
Figure 149: Modification of Section I-I for loading slab

226

During construction of the concrete loading slab, the cross-section was concave down. To transfer gravity loads to the wall, shims were placed between the exterior edges of the concrete loading slab and the bond beam (Figure 150). The center of the loading slab was bearing on the AAC slab, while the edges of the loading slab were bearing the grouted beam through the action of the shims. Based on this configuration part of the loading slab weight was transferred to the shear walls and another part was transferred through the AAC floor slab. Due to the gaps present in Figure 150 the clamping force from the slab is only transferred at the center of the slab. A free body diagram of the clamping force transferred to the floor system is shown in Figure 151. The lateral load is expected to be transferred to the AAC floor slab at this location. It is improbable that lateral load was transferred through friction from the weight of the loading slab. Even if this were true, the lateral load transfer would be limited by the low coefficient of friction between the plastic shims and the concrete loading slab.
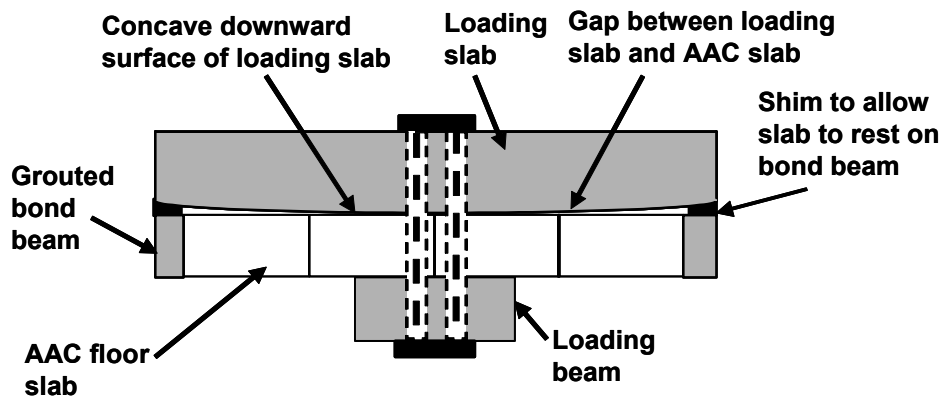
Figure 150: Cross-section of as built upper loading slab including shims

227

Vertical clamping force from loading slab is transferred only at points of contact

Grouted bond beam
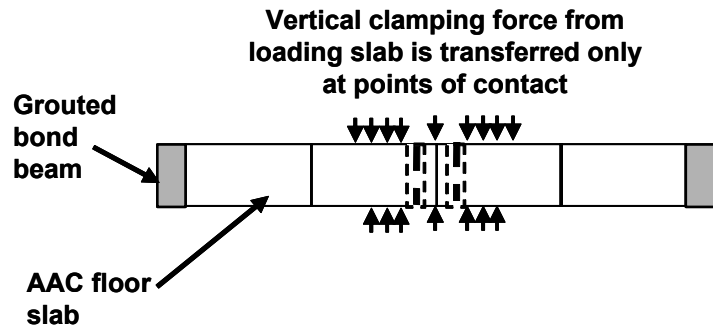
AAC floor slab

Figure 151: Free-body diagram of clamping force on AAC floor slab

9.6.3   Vertical Distribution of Lateral Load

The vertical distribution of seismic lateral load over the height of the building could take many forms. For design of the assemblage specimen, two specific distributions are considered, a triangular distribution and a uniform distribution (equal load at each floor). Those distributions are shown in Figure 152 and Figure 153 respectively.

228
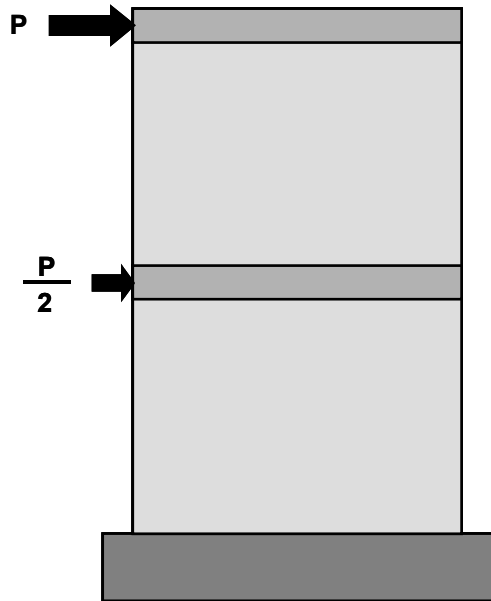
Figure 152: Vertical distribution of lateral forces for triangular load distribution
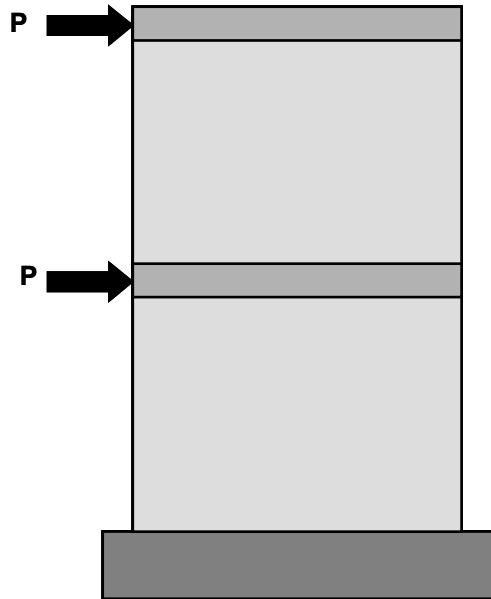
Figure 153: Vertical distribution of lateral forces for uniform load distribution

The triangular load distribution follows the IBC 2000 equivalent lateral force procedure for low-rise buildings. The uniform vertical load distribution applies equal loads to each story and produces a smaller moment at the base than a triangular distribution corresponding to the same base shear. Both load distributions simulate first-mode behavior, which is dominant in a symmetrical two-story building.

To estimate the most reasonable vertical distribution of lateral loads, several non-linear analyses were performed using CANNY99 (CANNY99). A single wall with the geometry and reinforcement was modeled using the observed behavior of Shear Wall Specimen 13, the first flexure-dominated AAC shear wall tested at UT Austin. The wall was subject to ground motion records from California earthquakes (PEER 2002). For these ground motions, the structure

remained elastic; the earthquakes were then scaled up to force yielding of the flexural reinforcement. The ratio of the maximum moment in the structure (M_{max}) to the moment at yielding of the flexural reinforcement (M_{yield}) is also presented in Table 0.1. The forces generated at each level as a function of time for the Arleta 1 ground motion are presented in Figure 154. Prior to flexural yielding at the base of the wall, the force generated at the second story was larger than the forge generated at the second story. After flexural yielding at the base of the wall, the forces in each story are nearly equal. To quantify these values the ratio of second-story forces (F_2) to first-story forces (F_1) was calculated at times corresponding to the generation of maximum base shear in the structure. Results are presented in Table 0.1. The average ratio of forces was 1.1 and the COV was 11%. The Canoga Park 2 ground motion resulted in a large negative base shear at the very end of the analysis. This anomalous result was associated with second-mode behavior and the next largest negative base shear was used for the analysis.

Figure 154: Lateral loads in the first and second elevated levels as a function of time for the Arleta 1 record

Table 0.1: Ratio of lateral force at second elevated force to force at first elevated level for maximum positive and negative peaks of base shear
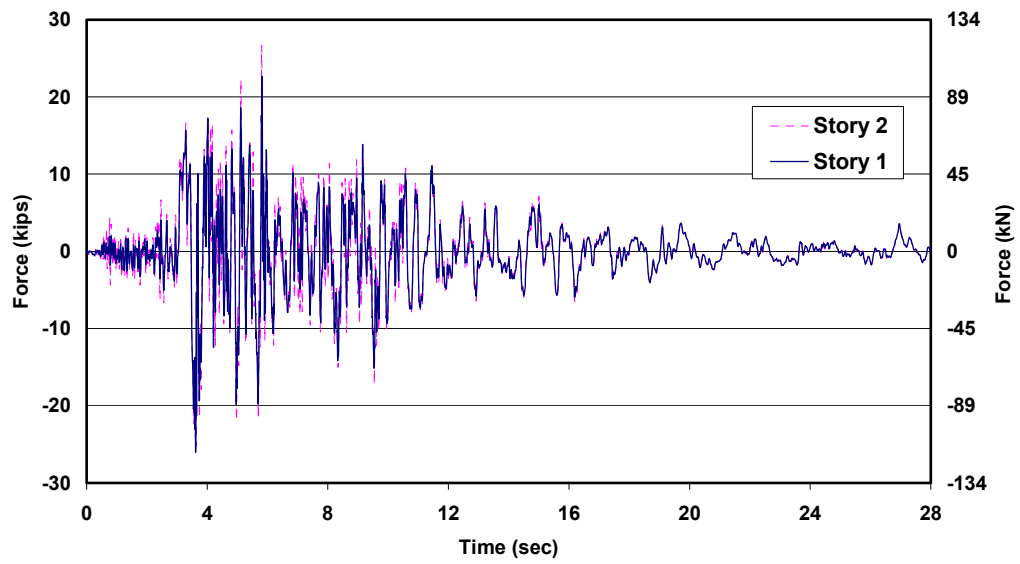
Location (Date)	Station	Record	M_{max}/M_{yield}	Positive F_2/F_1	Negative F_2/F_1
Corralitos 1 (1989)	57007	CLS000	1.164	1.22	1.05
Corralitos 2 (1989)	57007	CLS090	1.206	1.08	1.01
Gilroy #1 2 (1989)	47379	GO1000	1.004	1.05	1.11
Gilroy #1 1 (1989)	47379	GO1090	1.029	1.40	1.01
Canoga Park 1 (1994)	90053	CNP106	1.003	1.07	0.87
Canoga Park 2 (1994)	90053	CNP196	1.123	1.13	0.88
Arleta 1 (1994)	24087	ARL090	1.007	1.14	1.17
Arleta 2 (1994)	24087	ARL360	1.017	1.09	1.05
Canyon Country 1 (1994)	90057	LOS000	1.003	1.27	1.04
Canyon Country 2 (1994)	90057	LOS270	1.003	1.04	1.11
Mendocino (1992)	89005	CMP000	1.006	0.971	0.90
Mendocino (1992)	89005	CMP090	1.006	0.997	0.95

A more rigorous approach was used to verify the ratio of forces in the second story to forces in the first story during the duration of the earthquake ground motion. A minimum value of base shear was selected, V_{min}. For any point in the time history analysis when the total base shear exceeded the minimum selected base shear (V_{min}) the ratio of forces in each story was determined. The average of all of the ratios of forces after yielding of the flexural reinforcement was calculated along with the COV for these data points. As the minimum base shear increased, the average ratio of forces approaches 1.1 and the COV decreases. The results of the ratio of forces versus V_{min} are presented in Figure 155 and Figure 157 for Northridge and Loma Prieta earthquakes respectively. The COV's that correspond to these ratios of forces are plotted in Figure 156 and Figure 158. This information is also presented in tabular format in Table 0.2 and Table 0.3. These findings indicate that the ratio of forces is approximately 1.1 for the peak base shear and for values approaching the peak base shear.
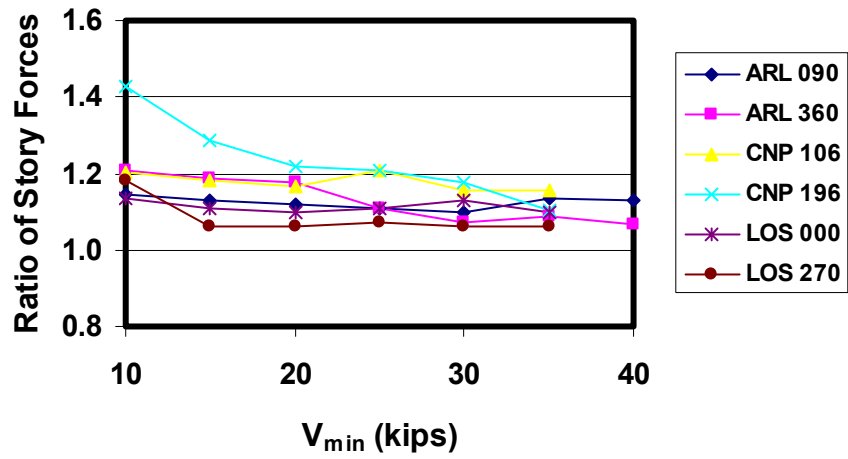
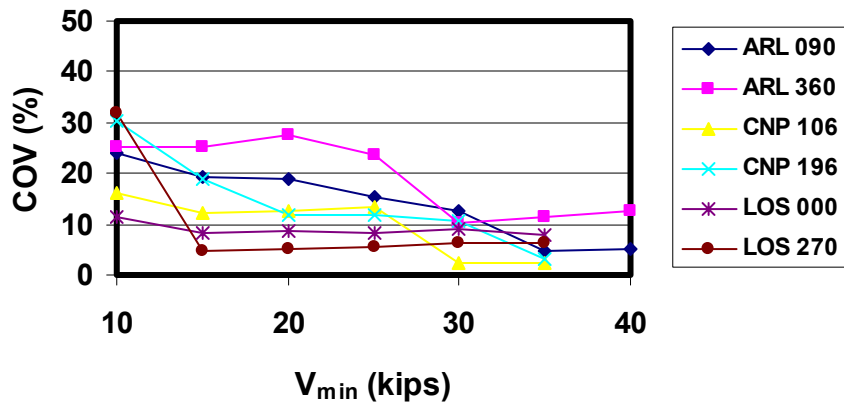*Figure 155: Ratio of forces versus V$_{min}$ for Northridge records*

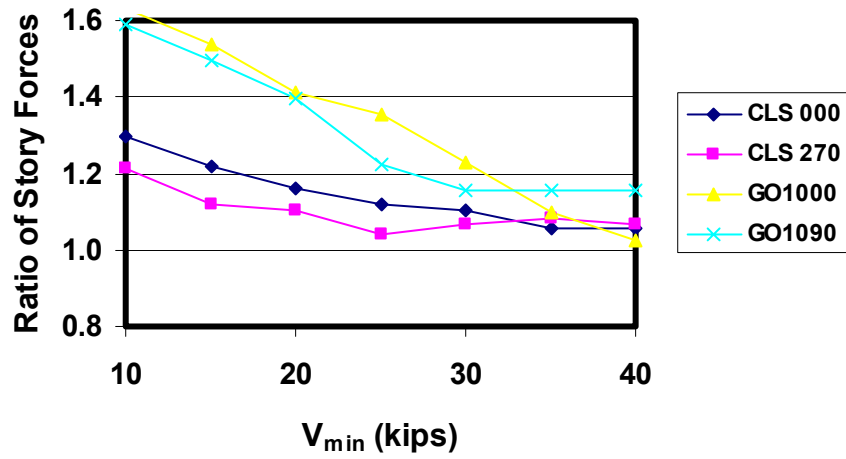*Figure 156: Corresponding COV's for ratio of forces versus V$_{min}$ for Northridge records*

Figure 157: Ratio of forces versus V_min for Loma Prieta records
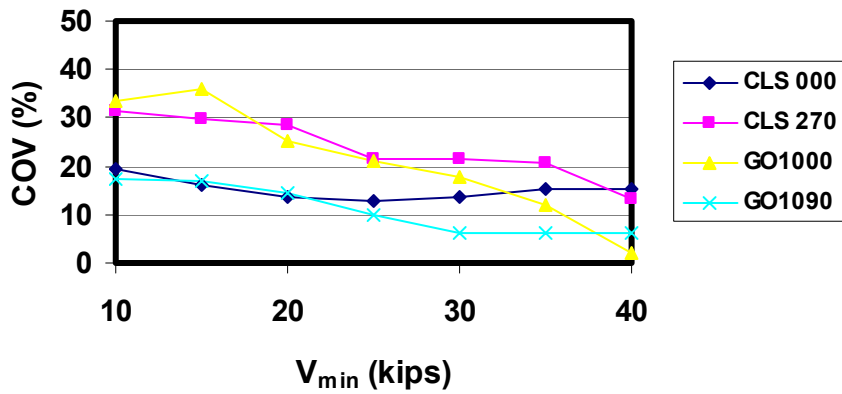
Figure 158: Corresponding COV's for ratio of forces versus V_min for Loma Prieta records

Table 0.2: Ratio of forces versus V_{min}, for different records

V_{min}	ARL 90	ARL 360	CNP 106	CNP 196	LOS 000	LOS 270	CLS. 000	CLS 270	GO 1000	GO 1090
10	1.15	1.21	1.20	1.43	1.13	1.18	1.30	1.21	1.63	1.59
15	1.13	1.19	1.18	1.29	1.11	1.08	1.22	1.12	1.54	1.50
20	1.12	1.18	1.17	1.22	1.10	1.07	1.16	1.10	1.41	1.39
25	1.11	1.11	1.21	1.21	1.11	1.06	1.12	1.04	1.35	1.22
30	1.10	1.07	1.16	1.18	1.13	1.05	1.10	1.07	1.23	1.16
35	1.14	1.09	1.16	1.10	1.10	1.05	1.06	1.08	1.10	1.16
40	1.13	1.06				1.06	1.06	1.07	1.02	1.16

Table 0.3: Corresponding COV's for ratio of forces versus V_{min}, for different records

V_{min}	ARL 90	ARL 360	CNP 106	CNP 196	LOS 000	LOS 270	CLS. 000	CLS 270	GO 1000	GO 1090
10	24.2	25.0	16.0	30.3	11.5	27.70	19.5	31.4	33.4	17.4
15	19.3	25.4	12.1	19.0	8.2	8.10	15.9	29.9	35.9	16.9
20	19.1	27.5	12.7	11.9	8.6	6.30	13.6	28.4	25.2	14.4
25	15.4	23.4	13.3	11.9	8.3	5.20	13.0	21.6	20.9	10.1
30	12.7	10.3	2.2	10.5	9.1	5.40	13.5	21.5	18.0	6.0
35	4.9	11.4	2.2	3.3	7.9	5.70	15.1	20.8	11.8	6.0
40	5.3	12.8				6.30	15.1	13.2	2.0	6.0

Based on both of these analyses, equal lateral loads were applied at each floor of the assemblage specimen. This is justified since ratio of forces of 1.1 is nearly equal to the ratio of one for a uniform distribution. The ratio is significantly lower than two which corresponds to the ratio of forces for a triangular distribution. The selected vertical distribution of forces subjected both orientations of floor panels to the same lateral load. This load was applied manually through a hydraulic actuator using identical rams at each story. The loading equipment used in the shear wall specimens was used in the assemblage tests.

9.6.4   Overview of Assemblage Specimen

The Two-story Assemblage Specimen was constructed between June and July 2002 and was tested on August 12, 2002. A picture of the in-plane walls including the rams is presented in Figure 159. A picture of the flanges and loading beams is shown in Figure 160.

Figure 159 Elevation view of assemblage specimen (North-South direction)

Figure 160 Elevation view of assemblage specimen (East-West direction)

9.7   LOADING HISTORY

The planned in-plane loading history for the shear wall specimens, shown in Figure 161, consisted of a series of reversed cycles to monotonically increasing maximum load. Lateral loads were manually controlled using a hydraulic actuator. The predetermined target values (PV) were based on the predicted load to produce significant changes in the behavior of the specimen such as flexural cracking and yielding of the flexural reinforcement. After yielding of the flexural

reinforcement load was applied by controlling the displacements, a minimum of one cycle at each displacement level was applied. The proposed loading history is shown in Figure 161.

Figure 161: Proposed loading history
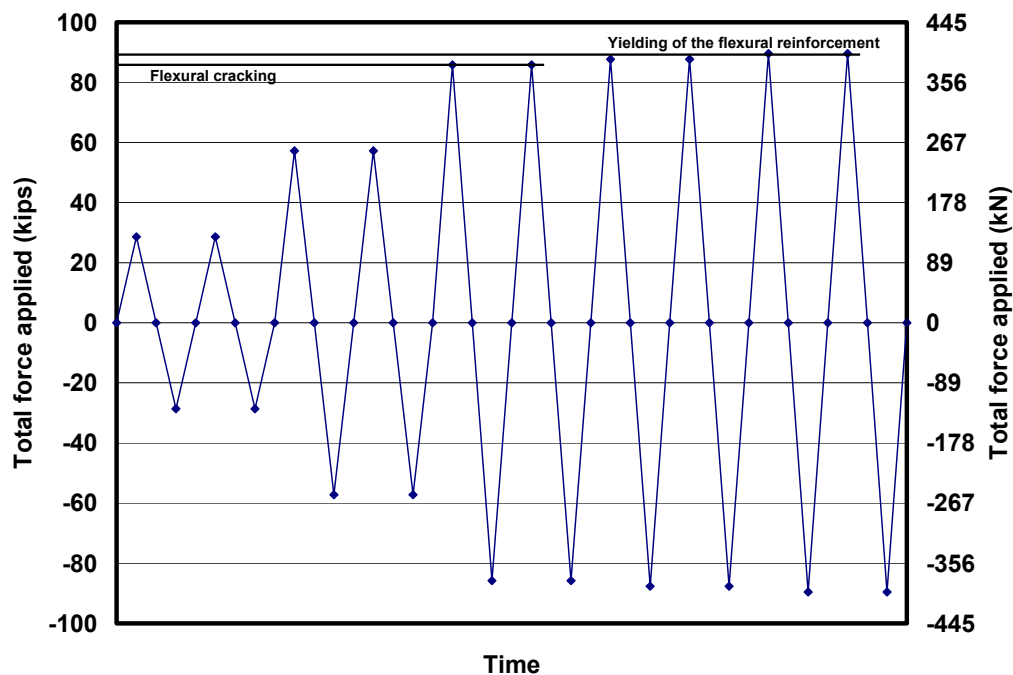
9.8   AXIAL LOAD

Axial load on the assemblage specimen comes from the weight of the assemblage itself and the loading equipment. The total axial load per wall is 30.2 kips (133 kN).

9.9   TRANSVERSE STABILITY

The flanges were also intended to enhance the out-of-plane stability of the assemblage specimen by increasing the stiffness of the assemblage about its weak axis.

9.10 INSTRUMENTATION

The purpose of instrumentation was to determine the behavior of the assemblage. This instrumentation was selected to measure global and local behavior of the assemblage.

9.10.1 Global Behavior

The global behavior of the assemblage specimen is characterized by its overall force-displacement behavior in the direction of loading. The horizontal displacement of each wall was measured at each floor level using string potentiometers. The applied load was measured using the same pin load cells as in the shear wall tests. Pressure transducers were used to verify those load-cell readings.

9.10.2 Local Behavior

The local behavior of the assemblage was described in terms of the deformation patterns of individual components. The following measurements were recorded for both stories of the east and west shear wall:

- vertical displacement of wall;
- vertical displacement through mid-height of wall;
- diagonal deformation of wall;
- horizontal deformation along transverse length of floor slab; and
- slip between elements.

The vertical deformations were measured using string potentiometers mounted to the wall. The diagonal deformations indicate the shear deformation in each wall, using string potentiometers mounted to wooden blocks mounted to the specimen (Figure 162). The displacement of each slab was measured to determine abnormal deformation patterns or indicate slip between floor panels on the second elevated slab. Possible slip between adjacent elements was measured

using a linear potentiometer mounted between the adjacent elements. This was done to detect any relative movement between the loading beam and the floor slabs, between the base of the wall and the foundation, and between the foundation and the laboratory floor. For other locations slip was determined manually observing any offset in a line drawn perpendicular to the interface between adjacent elements (Figure 163 through Figure 165). Slip was monitored during the tests; if the line was no longer continuous, the slip was quantified based on manual readings. This technique was used where slip was not probable, or was possible along several planes:

- vertical panel connections;
- bond beam-wall connection;
- floor slab panel joints; and
- loading beam-floor slab joints.
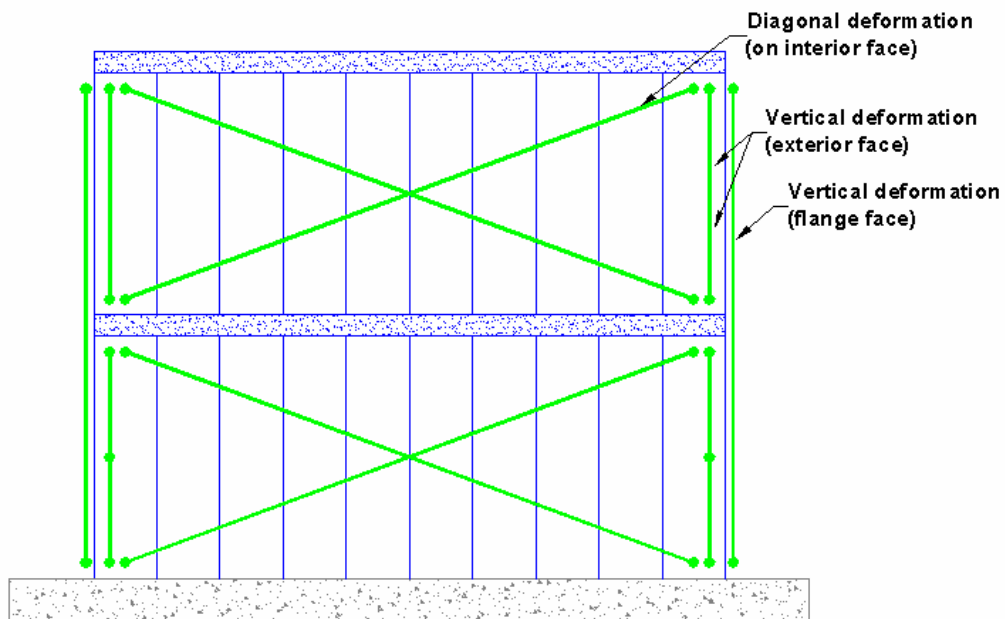
Figure 162: Displacement transducers to measure vertical and diagonal deformation in each shear wall

241
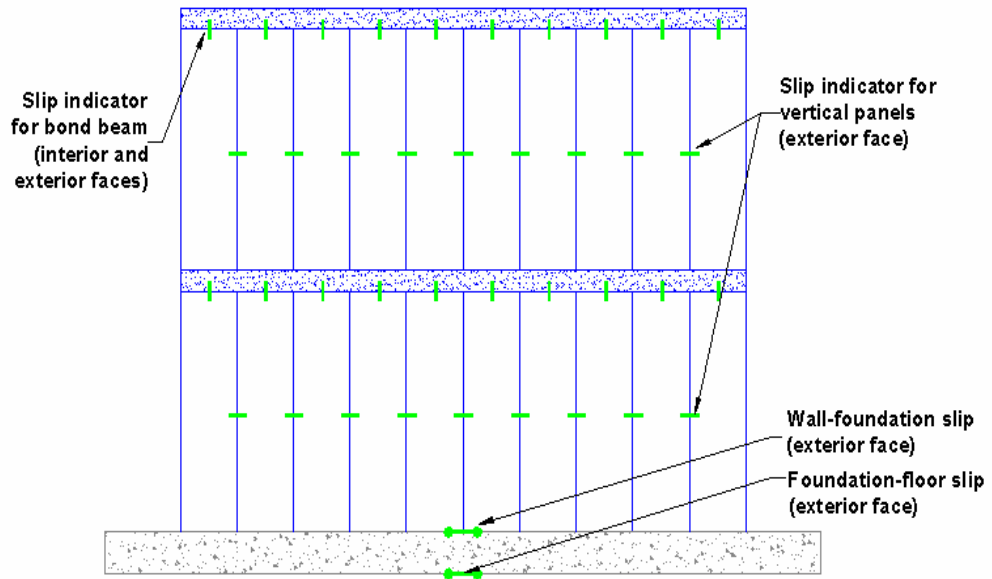
Figure 163: Measurement of relative slip for wall elevation
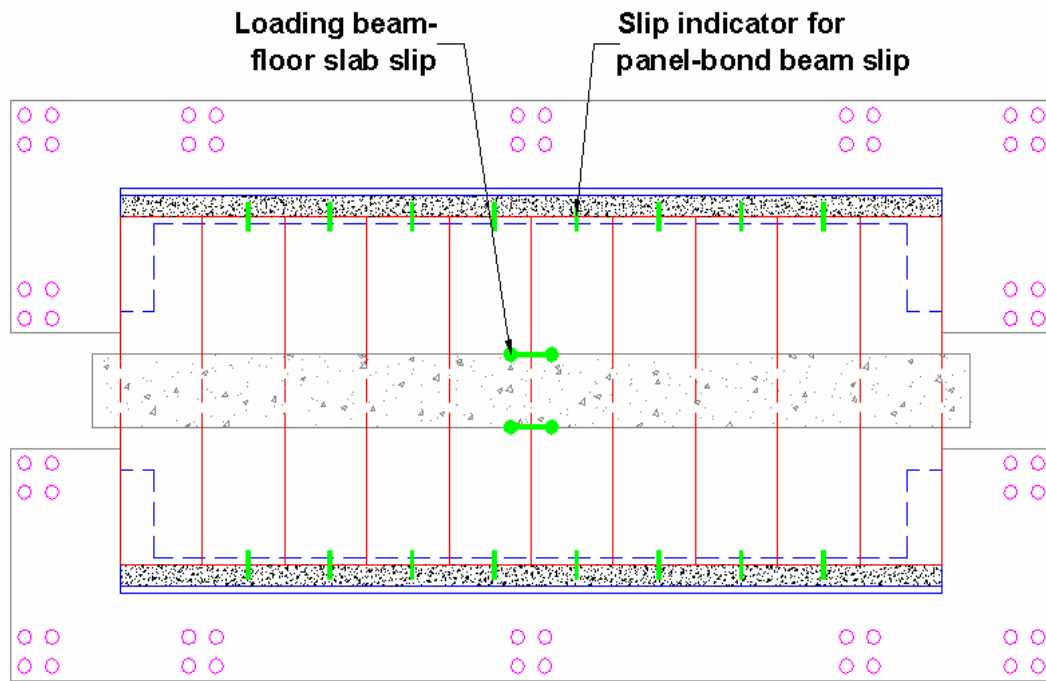
Figure 164: Measurement of relative slip at first story
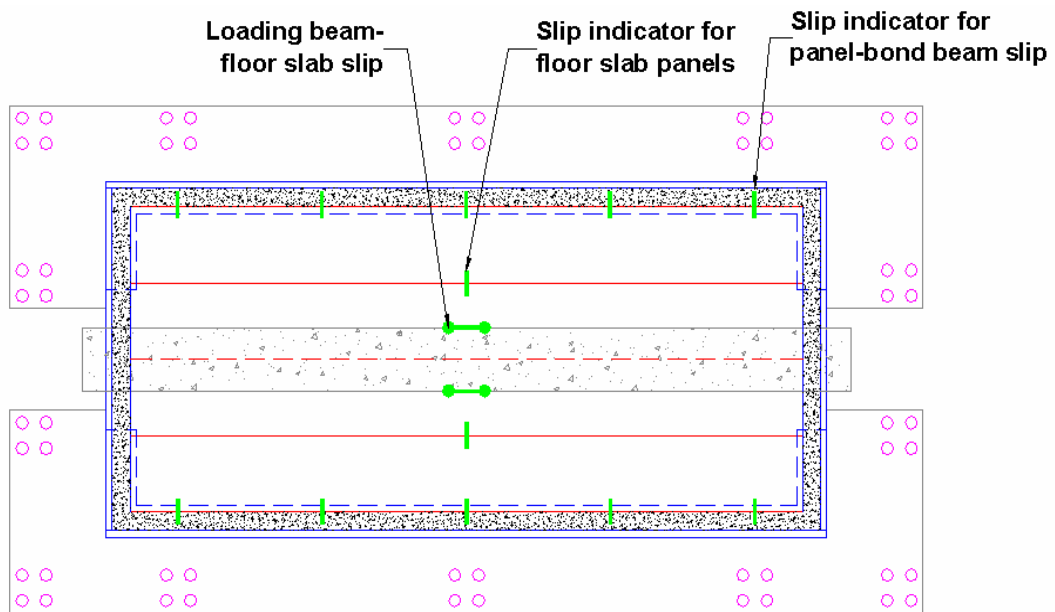
Figure 165: Measurement of relative slip at second story

9.10.3 Data Acquisition

Data were acquired in real time using a HP 3852 scanner. Analog-to-digital conversion was carried out by a National Instruments card in a Windows-based microcomputer, running under Measure, a National Instruments add-on for the Microsoft Excel spreadsheet program. Once in Excel format, data were plotted conventionally.

APPENDIX B

CANNY 99 Input File Examples

This appendix includes input files examples for the dynamic nonlinear analyses for each of the AAC structures studied in this dissertation

Example 1

Dynamic nonlinear analysis for the five-story cantilever wall structure

five-story cantilever wall structure
Wall length 20 ft
frame-floor numbering system used
July, 2002

title: 2-D dynamic analysis
units: kip, in, sec

//control data, unit (kip, in)
2D analysis in X-direction
gravity acceleration = 386.4
required modes = 5
loading direction in 0 degree

output for overall responses at floor levels
output for node displacement, velocity and acceleration
output for all panel response
output for extreme responses
output step interval = 1

/*overall iteration instructions
overall iteration limit = 20

absolute convergent tolerance= 0.001 for force
absolute convergent tolerance= 0.01 for moment

relative convergent tolerance= 0.001 to structural weight
terminate when iteration failed

/*element iteration instructions
element iteration limit = 20
panel unbalance tolerance = 0.001 0.001

/* dynamic control data
integration step = 2
start time = 0, end time = 23
Beta-value 0.25
Gamma-value 0.5
damping coefficient 0.5 to [M]
damping coefficient 0.005 to [K]
scale factor 0.3937, TX input file = \\earthquakes\charleston\acc401\acc401-1.dat
scale factor 1, TY input file =
scale factor 1, TZ input file =
scale factor 1, RZ input file =
//

//floor level, unit (kip, in)
6F Z=645
5F Z=515
4F Z=385
3F Z=255
2F Z=125
1F Z=0
//

//frame location, unit (kip, in)
Y1:0, X1:0, X2:240
//

//node location, unit (kip, in)
Y1 X1 1F~6F
Y1 X2 1F~6F
//

//supernode, unit (kip, in)
R6 6F TX : G(120,0) W=29

R5 5F TX : G(120,0) W=34.7
R4 4F TX : G(120 0) W=34.7
R3 3F TX : G(120 0) W=34.7
R2 2F TX : G(120 0) W=34.7
//
//node DOFs, unit (kip, in)
Y1 X1 1F prescribed TX TZ RY
Y1 X2 1F prescribed TX TZ RY
//

//shear panel data, unit (kip, in)
Y1 X1-X2 1-2F rigid BU600 TU600 SU200 AU300
Y1 X1-X2 2-3F rigid BU600 TU600 SU200 AU300
Y1 X1-X2 3-4F rigid BU600 TU600 SU200 AU300
Y1 X1-X2 4-5F rigid BU600 TU600 SU200 AU300
Y1 X1-X2 5-6F rigid BU600 TU600 SU200 AU300
//

//HD, unit (kip, in)
/* stiffness and hysteresis parameters
U600 CA7 310 4608000 C(0 0) Y(18949 18949) A(1 1) B(0.0046 0.0046) P(0 1 0
0 0 0 0)
U200 CA7 119 800 C(0 0) Y(250 250) A(1 1) B(0.01 0.01) P(0 1 0 0.45 0 0 0)
U300 EL1 310 2400
//

Example 2
Dynamic nonlinear analysis for the three-story cantilever wall structure

three-story cantilever wall structure
Wall length 20 ft
frame-floor numbering system used
July, 2002

title: 2-D dynamic analysis
units: kip, in, sec

//control data, unit (kip, in)
2D analysis in X-direction

247

gravity acceleration = 386.4
required modes = 3

output for overall responses at floor levels
output for node displacement, velocity and acceleration
output for all panel response
output for extreme responses
output step interval = 1

/*overall iteration instructions
overall iteration limit = 20

absolute convergent tolerance= 0.001 for force
absolute convergent tolerance= 0.01 for moment
relative convergent tolerance= 0.001 to structural weight
terminate when iteration failed

/*element iteration instructions
element iteration limit = 20
panel unbalance tolerance = 0.001 0.001

/* dynamic control data
integration step = 2
start time = 0, end time = 23
Beta-value 0.25
Gamma-value 0.5
damping coefficient 1.15 to [M]
damping coefficient 0.0022 to [K]
scale factor 0.3937, TX input file = \\earthquakes\charleston\acc401\acc401-1.dat
scale factor 1, TY input file =
scale factor 1, TZ input file =
scale factor 1, RZ input file =
//

//floor level, unit (kip, in)
4F Z=385
3F Z=255
2F Z=125
1F Z=0
//

//frame location, unit (kip, in)
Y1:0, X1:0, X2:240
//

//node location, unit (kip, in)
Y1 X1 1F~4F
Y1 X2 1F~4F
//

//supernode, unit (kip, in)
R4 4F TX : G(120 0) W=29
R3 3F TX : G(120 0) W=34.7
R2 2F TX : G(120 0) W=34.7
//

//node DOFs, unit (kip, in)
Y1 X1 1F prescribed TX TZ RY
Y1 X2 1F prescribed TX TZ RY
//

//shear panel data, unit (kip, in)
Y1 X1-X2 1-2F rigid BU600 TU600 SU200 AU300
Y1 X1-X2 2-3F rigid BU600 TU600 SU200 AU300
Y1 X1-X2 3-4F rigid BU600 TU600 SU200 AU300
//

//HD, unit (kip, in)
/* stiffness and hysteresis parameters
U600 CA7 310 4608000 C(0 0) Y(24650 24650) A(1 1) B(0.01 0.01) P(0 1 0 0 0 0 0)
U200 CA7 119 800 C(0 0) Y(250 250) A(1 1) B(0.01 0.01) P(0 1 0 0.45 0 0 0)
U300 EL1 310 2400
//

Example 3
Dynamic nonlinear analysis for the five-story coupled- wall structure

five-stories coupled-wall structure
Coupling beams (10" X 40in. X 48in.)

length of walls 20 ft
frame-floor numbering system used
July , 2002

title: 2-D dynamic analysis
units: kip, in, sec

//control data, unit (kip, in)
2D analysis in X-direction
gravity acceleration = 386.4
required modes = 5

output for overall responses at floor levels
output for node displacement, velocity and acceleration
output for all panel response
output for all beam response
output for extreme responses
output step interval = 1

/*overall iteration instructions
overall iteration limit = 20

absolute convergent tolerance= 0.001 for force
absolute convergent tolerance= 0.01 for moment
relative convergent tolerance= 0.001 to structural weight
terminate when iteration failed

/*element iteration instructions
element iteration limit = 20
panel unbalance tolerance = 0.001 0.001
beam unbalance tolerance = 0.001 0.001

/* dynamic control data
integration step = 2
start time = 0, end time = 22
Beta-value 0.25
Gamma-value 0.5
damping coefficient 0.518 to [M]
damping coefficient 0.0048 to [K]
scale factor 0.3937, TX input file = \\earthquakes\charleston\acc401\acc401-1.dat

scale factor 1, TY input file =
scale factor 1, TZ input file =
scale factor 1, RZ input file =
//

//floor level, unit (kip, in)
6F Z=645
5F Z=515
4F Z=385
3F Z=255
2F Z=125
1F Z=0
//

//frame location, unit (kip, in)
Y1:0, X1:0, X2:10, X3:58, X4:68
//

//node location, unit (kip, in)
Y1 X1 1F~6F
Y1 X2 1F~6F
Y1 X3 1F~6F
Y1 X4 1F~6F
//

//supernode, unit (kip, in)
R6 6F TX : G(264,0) W=63.7
R5 5F TX : G(264,0) W=76.4
R4 4F TX : G(264,0) W=76.4
R3 3F TX : G(264,0) W=76.4
R2 2F TX : G(264,0) W=76.4
//

//node DOFs, unit (kip, in)
Y1 X1 1F prescribed TX TZ RY
Y1 X2 1F prescribed TX TZ RY
Y1 X3 1F prescribed TX TZ RY
Y1 X4 1F prescribed TX TZ RY

/* Y1 X1 1F eliminate TY RX RZ

251

/* Y1 X2 1F eliminate TY RX RZ
//

//shear panel data, unit (kip, in)
Y1 X1-X2 1-2F rigid BU600 TU600 SU200 AU300
Y1 X1-X2 2-3F rigid BU600 TU600 SU200 AU300
Y1 X1-X2 3-4F rigid BU600 TU600 SU200 AU300
Y1 X1-X2 4-5F rigid BU600 TU600 SU200 AU300
Y1 X1-X2 5-6F rigid BU600 TU600 SU200 AU300
Y1 X3-X4 1-2F rigid BU600 TU600 SU200 AU300
Y1 X3-X4 2-3F rigid BU600 TU600 SU200 AU300
Y1 X3-X4 3-4F rigid BU600 TU600 SU200 AU300
Y1 X3-X4 4-5F rigid BU600 TU600 SU200 AU300
Y1 X3-X4 5-6F rigid BU600 TU600 SU200 AU300
//

//beam data, unit (kip, in)
Y1 X2-X3 2F LU700 RU700 SU800 AU900 r(0,0)
Y1 X2-X3 3F LU700 RU700 SU800 AU900 r(0,0)
Y1 X2-X3 4F LU700 RU700 SU800 AU900 r(0,0)
Y1 X2-X3 5F LU700 RU700 SU800 AU900 r(0,0)
Y1 X2-X3 6F LU700 RU700 SU800 AU900 r(0,0)
//

//HD, unit (kip, in)
/* panels stiffness and hysteresis parameters
U600 CA7 310 4608000 C(0 0) Y(37999 37999) A(1 1) B(0.0046 0.0046) P(0 1 0
0 0 0 0)
U200 CA7 119 800 C(0 0) Y(250 250) A(1 1) B(0.01 0.01) P(0 1 0 0.45 0 0 0)
U300 EL1 310 2400
/*
/* beams stiffness and hysteresis parameters
U700 CA7 310 21333 C(0 0) Y(1144 1144) A(1 1) B(0.01 0.01) P(0 4 0 0 0 0 0)
U800 CA7 119 333 C(0 0) Y(250 250) A(1 1) B(0.01 0.01) P(0 4 0 0.45 0 0 0)
U900 EL1 310 400
//

Example 4
Dynamic nonlinear analysis for the three-story coupled- wall structure

252

three-story coupled wall structure
Coupling beams (10" X 40in. X 48in.)
length of walls 20 ft
frame-floor numbering system used
July , 2002

title: 2-D dynamic analysis
units: kip, in, sec

//control data, unit (kip, in)
2D analysis in X-direction
gravity acceleration = 386.4
required modes = 3

output for overall responses at floor levels
output for node displacement, velocity and acceleration
output for all panel response
output for all beam response
output for extreme responses
output step interval = 1

/*overall iteration instructions
overall iteration limit = 20

absolute convergent tolerance= 0.001 for force
absolute convergent tolerance= 0.01 for moment
relative convergent tolerance= 0.001 to structural weight
terminate when iteration failed

/*element iteration instructions
element iteration limit = 20
panel unbalance tolerance = 0.001 0.001
beam unbalance tolerance = 0.001 0.001

/* dynamic control data
integration step = 2
start time = 0, end time = 22
Beta-value 0.25
Gamma-value 0.5

253

damping coefficient 1.16 to [M]
damping coefficient 0.0022 to [K]
scale factor 0.3937, TX input file = \\earthquakes\charleston\acc401\acc401-1.dat
scale factor 1, TY input file =
scale factor 1, TZ input file =
scale factor 1, RZ input file =
//

//floor level, unit (kip, in)
4F Z=385
3F Z=255
2F Z=125
1F Z=0
//

//frame location, unit (kip, in)
Y1:0, X1:0, X2:10, X3:58, X4:68
//

//node location, unit (kip, in)
Y1 X1 1F~4F
Y1 X2 1F~4F
Y1 X3 1F~4F
Y1 X4 1F~4F
//

//supernode, unit (kip, in)
R4 4F TX : G(264,0) W=63.7
R3 3F TX : G(264,0) W=76.4
R2 2F TX : G(264,0) W=76.4
//

//node DOFs, unit (kip, in)
Y1 X1 1F prescribed TX TZ RY
Y1 X2 1F prescribed TX TZ RY
Y1 X3 1F prescribed TX TZ RY
Y1 X4 1F prescribed TX TZ RY

/* Y1 X1 1F eliminate TY RX RZ
/* Y1 X2 1F eliminate TY RX RZ

254

//

//shear panel data, unit (kip, in)
Y1 X1-X2 1-2F rigid BU600 TU600 SU200 AU300
Y1 X1-X2 2-3F rigid BU600 TU600 SU200 AU300
Y1 X1-X2 3-4F rigid BU600 TU600 SU200 AU300
Y1 X3-X4 1-2F rigid BU600 TU600 SU200 AU300
Y1 X3-X4 2-3F rigid BU600 TU600 SU200 AU300
Y1 X3-X4 3-4F rigid BU600 TU600 SU200 AU300
//

//beam data, unit (kip, in)
Y1 X2-X3 2F LU700 RU700 SU800 AU900 r(0,0)
Y1 X2-X3 3F LU700 RU700 SU800 AU900 r(0,0)
Y1 X2-X3 4F LU700 RU700 SU800 AU900 r(0,0)
//

//HD, unit (kip, in)
/* panels stiffness and hysteresis parameters
U600 CA7 310 4608000 C(0 0) Y(25215 25215) A(1 1) B(0.01 0.01) P(0 1 0 0 0 0 0)
U200 CA7 119 800 C(0 0) Y(250 250) A(1 1) B(0.01 0.01) P(0 1 0 0.45 0 0 0)
U300 EL1 310 2400
/*
/* beams stiffness and hysteresis parameters
U700 CA7 310 21333 C(0 0) Y(1144 1144) A(1 1) B(0.01 0.01) P(0 4 0 0 0 0 0)
U800 CA7 119 333 C(0 0) Y(250 250) A(1 1) B(0.01 0.01) P(0 4 0 0.45 0 0 0)
U900 EL1 310 400
//

REFERENCES

1. Al-Shalen and Attiogbe 1997: Al-Shaleh, M. and Attiogbe, E. K., "Flexural strength characteristics of non-load bearing masonry walls in Kuwait," *Materials and Structures* 30 (June), pp. 277-283, 1997.

2. Argudo 2003: Argudo, J., "Design Provisions for reinforced AAC panels," M.S. thesis, Dept. of Civil Engineering, The University of Texas at Austin, December 2003.

3. ASTM A 193-B7 (2001): *Standard Specification for Alloy-Steel and Stainless Steel Bolting Materials for High Temperature Service,* American Society for Testing and Materials, West Conshohocken, PA, 2001.

4. ASTM C 476 (2002): *Standard Specification for Grout for Masonry,* American Society for Testing and Materials, West Conshohocken, PA, 2002.

5. ASTM C 1006 (2001): *Standard Test Methods for Splitting Tensile Strength of Masonry Units,* American Society for Testing and Materials, West Conshohocken, PA, 2001.

6. ASTM C 1386 (1998): *Standard Specification for Precast Autoclaved Aerated Concrete (PAAC) Wall Construction Units,* American Society for Testing and Materials, West Conshohocken, PA, 1998.

7. ASTM C 1452 (2000): *Standard Specification for Reinforced Autoclaved Aerated Concrete Elements,* American Society for Testing and Materials, West Conshohocken, PA, 2000.

8. Brightman 2000:   Brightman, M., "AAC Shear Wall Specimens: Development of Test Setup and Preliminary Results,*"* M.S. Thesis, Dept. of Civil Engineering, The University of Texas at Austin, May 2000.

9. Cancino 2003: Cancino, U., "Study of Low-strength AAC Shear Walls," M.S. thesis, Dept. of Civil Engineering, The University of Texas at Austin, December 2003.

10. CANNY 99:   A 3-Dimensional Nonlinear Static / Dynamic Structural Analysis Program, CANNY Structural, Vancouver, Canada, 1999

11. de Vekey *et al*. 1986: de Vekey, R. C., N. J. Bright., K. R. Luckin., and S. K. Arora., "Research results on autoclaved aerated concrete blockwork," *The Structural Engineer* 64a (11), pp. 332-340.

12. Frankel *et al*. 1996: Frankel A., Muller, D., Barnhard, T., Perkins, D., Leyendecker, E. V., Dickman, N., Hanson, S., and Hopper, M., "National Seismic Hazard Maps," Documentation: U.S., Geological Survey, *Open-File Report 96-532*, June 1996, 100 p.

13. IBC 2000: *International Building Code, 2000 Edition*, International Code Council, Falls Church, VA, 2000.

14. Lai and Biggs 1980: Lai, S. –P. and Biggs, J. M., "Inelastic Response Spectra for Aseismic Building Design," *Journal of the Structural Division*, American Society of Civil Engineers, Vol. 106, No. ST6, pp. 1295-1310, New York, N.Y., 1980.

15. Miranda and Bertero 1994: Miranda, E. and Bertero, V., "Evaluation of Strength Reduction Factors for Earthquake-Resistant Design," *Earthquake Spectra*, Earthquake Engineering Research Institute, Vol. 10, No. 2, pp. 357-379, Oakland, CA, 1994.

16. Nassar and Krawinkler 1991: Nassar, A. A. and Krawinkler, H., "Seismic Demands for SDOF and MDOF Systems," *Report No. 95*, The John A. Blume Earthquake Engineering Center, Stanford University, Stanford, CA, 1991.

17. NEHRP 2000: *Recommended Provisions for Seismic Regulations for New Buildings and Other Structures, 2000 Edition, Part 2: Commentary,* Building Seismic Safety Council, Washington, D.C.

18. PEER 2002: Pacific Earthquake Engineering Research Center Strong Motion Database. http://peer.berkeley.edu/smcat.

19. Riddell *et al*. 1989: Riddell, R., Hidalgo, P. and Cruz, E. "Response Modification Factors for Earthquake Resistant Design of Short Period Structures," *Earthquake Spectra*, Earthquake Engineering Research Institute, Vol. 5, No. 3, pp. 571-590, Oakland, CA, 1989.

20. RILEM 1993: *Autoclaved Aerated Concrete: Properties, Testing and Design*, RILEM Recommended Practice, RILEM Technical Committees 78-MCA and 51-ALC, E & FN Spon, London.

21. SAP2000: SAP2000 Nonlinear V7.10, 1999, Computers and Structures, Inc., Berkeley, California.

22. Somerville *et al*. 1997: Somerville, P., Smith, N., Puntamurthula, S., and Sun, J., "Development of ground motion time histories for phase 2 of the FEMA/SAC steel project," SAC *Background Document SAC/DB-97/04*, SAC Joint Venture, Richmond, CA, 1997.

23. Tanner 2003:   Tanner, J. E., "Design Provisions for Autoclaved Aerated Concrete (AAC) Structural Systems," Ph.D. dissertation, Dept. of Civil Engineering, The University of Texas at Austin, May 2003.

24. Uang 1991: Uang C-M, "Establishing R (or R_w) and C_d Factors for Building Seismic Provisions," *Journal of Structural Engineering*, vol 117, no.1, pp. 19-28, American Society of Civil Engineers, New York, N.Y., 1991.

25. Weng and Wu 1999:   Wen, Y.K. and Wu, C.L., "Generation of Ground Motions for Mid-American Cities," "Projects RR-1 and RR-2," Mid-America Earthquake Center, University of Illinois at Urbana-Champaign, 1999.

VITA

Jorge Luis Varela Rivera was born in Merida Yucatan, Mexico on August 25, 1967. He received his Bachelor of Science in Civil Engineering from University Autonomous of Yucatan in 1990. He worked from 1989 to 1994 for "Constructora Bosca del Ste", a construction firm in Merida, Mexico. In August of 1994 he entered into the graduate program in structural engineering at University National Autonomous of Mexico. After he received his Master in Engineering in February of 1997, he went to The University of Texas as a visiting student. From August of 1997 to June of 1998, he worked for University Autonomous of Yucatan, teaching undergraduate classes, and working as a forensic engineer. In August 1998, he enrolled into the graduate program at The University of Texas at Austin. He has recently accepted a job as an assistant professor with The University Autonomous of Yucatan.

Permanent address: Calle 61b No. 216
                      Fracc. Yucalpeten
                      Merida Yucatan, Mexico
                      C.P. 97248

This dissertation was typed by the author.

259